

INFILLED REINFORCED CONCRETE FRAME PERFORMANCE UNDER
SEISMIC ACTIONS

A THESIS SUBMITTED TO
THE GRADUATE SCHOOL OF NATURAL AND APPLIED SCIENCES
OF
MIDDLE EAST TECHNICAL UNIVERSITY

BY

İSMAİL OZAN DEMİREL

IN PARTIAL FULFILLMENT OF THE REQUIREMENTS
FOR
THE DEGREE OF DOCTOR OF PHILOSOPHY
IN
CIVIL ENGINEERING

MAY 2023

Approval of the thesis:

**INFILLED REINFORCED CONCRETE FRAME PERFORMANCE
UNDER SEISMIC ACTIONS**

submitted by **İSMAİL OZAN DEMİREL** in partial fulfillment of the requirements
for the degree of **Doctor of Philosophy in Civil Engineering, Middle East
Technical University** by,

Prof. Dr. Halil Kalıpçılar
Dean, Graduate School of **Natural and Applied Sciences** _____

Prof. Dr. Erdem Canbay
Head of the Department, **Civil Engineering** _____

Prof. Dr. Ahmet Yakut
Supervisor, **Civil Engineering, METU** _____

Examining Committee Members:

Prof. Dr. Polat Gülkan
Civil Engineering, Başkent University _____

Prof. Dr. Ahmet Yakut
Civil Engineering, METU _____

Prof. Dr. Barış Binici
Civil Engineering, METU _____

Prof. Dr. Sabahattin Aykaç
Civil Engineering, Gazi University _____

Prof. Dr. Erdem Canbay
Civil Engineering, METU _____

Date: 11.05.2023

I hereby declare that all information in this document has been obtained and presented in accordance with academic rules and ethical conduct. I also declare that, as required by these rules and conduct, I have fully cited and referenced all material and results that are not original to this work.

Name, Last name : İsmail Ozan Demirel

Signature :

ABSTRACT

INFILLED REINFORCED CONCRETE FRAME PERFORMANCE UNDER SEISMIC ACTIONS

Demirel, İsmail Ozan
Doctor of Philosophy, Civil Engineering
Supervisor : Prof. Dr. Ahmet Yakut

May 2023, 263 pages

A comprehensive experimental campaign was conducted at METU Uğur Ersoy Structural Mechanics Laboratory to investigate the seismic response of infilled reinforced concrete frames. A total of 22 half-scaled frame tests were conducted on identical, single-story, single-bay frame specimens infilled with hollow clay bricks and aerated concrete blocks. Retrofit techniques such as isolation joints, steel mesh overlays, sliding joints and horizontal steel ties were investigated. Frame specimens under constant vertical load were subjected to cyclic in-plane, monolithic out-of-plane and simultaneous in-plane and out-of-plane loading conditions using servo-controlled hydraulic jacks and airbags. Particular attention was devoted to the definition of lateral drift-based performance limits for infill walls, identification of in-plane wall damage on the out-of-plane capacity and the performance of retrofit techniques applied to infill walls to enhance earthquake resistance.

Keywords: Infill Wall, Reinforced Concrete Frame, Experimental Study, Seismic Performance, Retrofit

ÖZ

DOLGU DUVARLI BETONARME ÇERÇEVELERİN DEPREM ETKİSİ ALTINDA PERFORMANSI

Demirel, İsmail Ozan
Doktora, İnşaat Mühendisliği
Tez Yöneticisi: Prof. Dr. Ahmet Yakut

Mayıs 2023, 263 sayfa

Dolgu duvarlı betonarme çerçevelerin sismik davranışını incelemek için ODTÜ Uğur Ersoy Yapısal Mekaniği Laboratuvarı'nda kapsamlı bir deneysel çalışma yürütülmüştür. Boşluklu tuğla ve gaz beton bloklarla doldurulmuş özdeş, yarı ölçekli, tek katlı, tek bölmeli betonarme çerçeve numuneleri üzerinde toplam 22 adet çerçeve testi yapılmıştır. İzolasyon derzleri, çelik hasırla yüzey kaplama, kayar derzler ve yatay çelik bağlar gibi güçlendirme teknikleri denenmiştir. Sabit düşey yük altındaki çerçeve numuneleri, servo kontrollü hidrolik krikolar ve hava yastıkları kullanılarak döngüsel düzlem içi, monolitik düzlem dışı ve eşzamanlı düzlem içi ve dışı yükleme koşullarına tabi tutulmuştur. Dolgu duvarlar için yanal ötelenmeye bağlı performans limitleri tanımlanmış, düzlem içi duvar hasarının düzlem dışı kapasite üzerindeki etkisi araştırılmış ve deprem dayanımını iyileştirmek için dolgu duvarlara uygulanan güçlendirme tekniklerinin performansları karşılaştırılmıştır.

Anahtar Kelimeler: Dolgu Duvar, Betonarme Çerçeve, Deneysel Çalışma, Deprem Performansı, Güçlendirme

the life was shattered and without love
I found you in the nobility of a belief
I loved you in a beauty of a fight
that fight hasn't finished yet
and it will continue
until the earth's surface will be the surface of love

all the masters of life have said love
to love a beauty with passion
and be able to fight for that beauty
and here are almond flowers on your face
smiling soil and spring in your hair
are you that fight in which I loved you?
or are you the beauty of that love?

I found you in the nobility of a belief
I loved you in a beauty of a fight
they trimmed our branches thousand times
they broke thousand times
we are blooming again, we are yielding fruit again
they choked the time with fear thousand times
they killed it thousand times
we are at birth again we are in joy
that fight hasn't finished yet
and it will continue
until the earth's surface will be the surface of love

since the first rivers which we passed
our feet became the feet of waters
our hands are hands of rock and soil
we were growing in the mornings thirsty
on your towers with ceremonies
we sang songs with the same chord
same sound, same heart
we gave the purple color to the mountains
our youth hadn't been so ravaged yet
neither to the sorrow of deaths in sunset
nor to the joy of births in dawn

our call is only to you, Oh nature!
you, creating gravediggers with a hand
and running with midwives in other hand
although we live the beauty of you
that fight hasn't finished yet
and it will continue
until the earth's surface will be the surface of love

palaces, thrones will collapse
and blood will keep silent someday
tyranny will finish
even violets will blossom on us
and lilacs will smile
from today to the future
only will remain those who go to tomorrow
and those who fight for tomorrows

again will rise the poems
again will rain the feelings
and heart
is on top of the images.
Oh those who say everything has finished
those who eat intimidation on the table of fear
neither flowers which resist on fields
nor the angers which grow huge in cities
haven't said farewell yet
that fight hasn't finished yet
and it will continue
until the earth's surface will be the surface of love

Adnan Yücel

*For those who go to tomorrow
and those who fight for tomorrows*

ACKNOWLEDGMENTS

The experimental work of this study was conducted in the Uğur Ersoy Structural Mechanics Laboratory of METU. I spent days and nights designing and fabricating the test setup for in-plane and out-of-plane testing of infilled frame specimens. I worked in casting specimens, constructing infill walls, conducting material tests, attaching and wiring measurement devices, conducting tests not to mention post-processing the experimental data, and publishing the results. I drew every detail of the test setup in 3D, checked the compatibility and capacity of different parts, visited the industrial estate at least once a week to purchase the required materials and delivered expenditure order forms for every purchase. After spending so much time and effort, finally, I was connected with the test setup to the extent that I found myself washing it with a brush before the tests!

On top of all my efforts, I truly believe that it was not my contribution that made this research possible. It was the long-lasting order, harmony and tradition of METU Uğur Ersoy Lab where many distinguished scholars and qualified workers have contributed for so many years. It has been an honor and pleasure to be part of this community.

During my research, I had the unique opportunity to meet and collaborate with several great people. Yet I owe my academic experience in METU to two individuals. I want to thank Prof. Güney Özcebe, who picked me up for a teaching assistant position in the structural mechanics division and my advisor Prof. Ahmet Yakut who made the unfortunate decision of picking me up as a doctoral student. I want to express my deepest appreciation to him for the knowledge and sincere guidance he gracefully offered me throughout the years and for his rock-solid patience during the course of this study.

I am also thankful to Prof. Barış Binici, who gave me the opportunity to become actively involved in the laboratory. His critical and constructive suggestions were of

great value for the development of my research. The guidance and contribution of Prof. Erdem Canbay to my experimental studies were also gratefully acknowledged. I had the opportunity to work with Prof. Polat Gülkan which was one of the most rewarding experiences of my research. I thank Prof. Sabahattin Aykaç for his positive attitude toward me. The tender love and care of Dr. Erhan Karaesmen and Dr. Ergin Karaesmen couple were invaluable. Research unoriented small talks, which reminded me that the academy is not only about research, was as important if not more important than research-related discussions.

Finding words strong enough to thank Dr. Alper Aldemir is not easy. We started our academic journey together as teaching assistants assigned to office K2-105 where we spent eight years full of joyful memories. He always supported me in my academic as well as personal life. He is like a brother to me. Despite his heavy workload, he was kind enough to deal with my problems and push me to focus on my studies. Working and spending time with him was a pleasure. His desire to help people around him is simply matchless.

Hasan Metin was one of the most influential figures in my research. Actively working in the lab since 1964, he is truly a legend. He encapsulates the values that made the lab great such as work ethics, solidarity, know-how and respect. He taught me the right way to do labor work and advised me on the viability of my testing setup designs. He was my best company in and out of campus.

I was fortunate to have collaborated with a skillful and knowledgeable laboratory crew who supported my experimental endeavors. I am most grateful to individuals including but not limited to Murat Demirel, Osman Keskin, Barış Esen, Musa Şahin, Salim Azak, Cuma Yıldırım and Burhan Alam for their sincere support.

The financial support of the European Commission within the project INSYSME “INnovative SYStems for earthquake resistant Masonry Enclosures in RC buildings”, grant FP7-SME-2013-2-GA606229, 2013-2016 and the Scientific and Technological Research Council of Türkiye (113M557) within the project

CONCERT-Japan “Connecting and Coordinating European Research and Technology Development with Japan”, 2012-2015 and by Turkish Autoclaved Aerated Concrete Association (TGÜB) is acknowledged.

I am also thankful to several colleagues and friends who crossed my path at office K2-105 of the structural mechanics building, including Andaç Lüleç, Gizem Mestav, Taylan Solmaz, Emre Özkök, Erşan Erdoğan, Riccardo Milanese, Erhan Budak, İlkay İhsan Önal, Cem Sonat, Baran Çobanoğlu, Beyazıt Bestami Aydın, Deniz Üçer, Lana Todorovic, Selin Aktaş and at office K6-111 of earthquake studies building including Koray Kadaş, Levent Mazılıgüney, Uğur Akpınar, Vesile Hatun Akansel, Feyza Soysal and Batu Türksönmez. I want to thank Veysel Çam and Nazile Tekin for the strong fresh Turkish teas they brewed and for always being considerate in providing an excellent environment for studying in the offices.

Final thanks go to my family and my kids, İdil and Deniz, for their pure and warm love, which hardened me against failures, reminding me of Samuel Beckett’s quote: “Ever tried, ever failed, no matter, try again, fail again, fail better.”

TABLE OF CONTENTS

ABSTRACT.....	v
ÖZ	vi
ACKNOWLEDGMENTS	x
TABLE OF CONTENTS.....	xiii
LIST OF TABLES	xvii
LIST OF FIGURES	xviii
LIST OF ABBREVIATIONS	xxiii
LIST OF SYMBOLS	xxiv
CHAPTERS	
1 INTRODUCTION	1
1.1 Background	3
1.2 Motivation.....	8
1.3 Objective and Scope.....	15
1.4 Organization of Thesis	18
2 LITERATURE REVIEW	21
2.1 Chronological Summary of Previous Research	21
2.2 Database on Previous Infilled Frame Tests.....	29
2.3 Retrofit Techniques for Infill Walls.....	37
2.4 Code Approaches on Design and Assessment of Infill Walls	44
2.5 Analytical Strut Modeling of Infill Walls	49
3 EXPERIMENTAL PROGRAM	55
3.1 RC Frame Specimen	55
3.1.1 Design	55
3.1.2 Scaling.....	59
3.1.3 Construction	61
3.2 Masonry Infill Walls	64
3.2.1 HCB Infill (CB)	66

3.2.2	HCB Infill with Plaster (CBP).....	66
3.2.3	HCB Infill with Steel Mesh Reinforcement (CBMR).....	67
3.2.4	HCB Infill with Continuous Horizontal Steel Ties (TieC).....	69
3.2.5	HCB Infill with Staggered Horizontal Steel Ties (TieS).....	70
3.2.6	LB Infill with Plaster (LBP).....	71
3.2.7	ACB Infill (AB).....	72
3.2.8	ACB Infill with Isolation Joint (ABI)	73
3.2.9	ACB Infill with Fiber Mesh Reinforced Plaster (ABRP).....	74
3.3	Experimental Study	75
3.3.1	Test Setup	76
3.3.2	Instrumentation.....	81
3.3.3	Loading Protocol	86
4	MATERIAL CHARACTERIZATION	89
4.1	Material Tests	90
4.1.1	Concrete.....	90
4.1.2	Reinforcing Steel Bars.....	92
4.1.3	Brick Units.....	94
4.1.4	Mortar	96
4.1.5	Mesh Reinforcement	99
4.1.6	Tie Wire.....	100
4.1.7	Horizontal Steel Ties	101
4.1.8	Summary of Material Tests	101
4.2	Masonry Prism Tests	103
4.2.1	Uniaxial Compression Test	105
4.2.2	Diagonal Tension Test.....	108
4.2.3	Sliding Shear Test.....	110
4.2.4	Bending Test.....	112
4.2.5	Influence of Plaster and Mesh Reinforcement	114
5	EXPERIMENTAL RESULTS	115
5.1	Assumptions and Corrections in Processing Raw Data	115

5.1.1	Correction for Lateral Component of Vertical Jacks	115
5.1.2	Curve Fitting for Hysteresis Loops	118
5.1.3	Calculation of Member End Rotations and Curvatures	120
5.2	In-plane Cyclic Loading Test Results	122
5.2.1	Bare Frame (BF)	122
5.2.2	HCB Infilled Frame Specimen (CB).....	124
5.2.3	HCB Infilled Frame Specimen with Plaster (CBP)	128
5.2.4	HCB Infilled Frame with Steel Mesh Reinf. (CBMR)	131
5.2.5	HCB Infilled Frame with Continuous Steel Ties (TieC)	134
5.2.6	HCB Infilled Frame with Staggered Steel Ties (TieS)	137
5.2.7	LB Infilled Frame with Plaster (LBP)	140
5.2.8	ACB Infilled Frame (AB)	143
5.2.9	ACB Infilled Frame with Isolation Joint (ABI).....	147
5.2.10	ACB Infilled Frame with Fiber Mesh Reinf. Plaster (ABRP).150	
5.2.11	Summary of IP Damage Propagation	153
5.2.12	Summary of Measured Response	158
5.3	Out-of-Plane Monolithic Loading Test Results	169
5.3.1	Damage Propagation	171
5.3.2	Load-Displacement Response	174
5.3.3	OOP Response Summary	176
5.4	Simultaneous Bidirectional Loading Test Results	177
5.4.1	Damage Propagation	179
5.4.2	Load Displacement Response	182
5.4.3	Failure Envelope	183
6	PERFORMANCE ASSESSMENT.....	185
6.1	Introduction to Performance Assessment of Infill Walls.....	185
6.2	Previous Studies on the Seismic Performance of Infill Walls	186
6.3	A Methodology for Performance Assessment of Infill Walls.....	188
7	CONCLUSION	195
	REFERENCES	205

APPENDICES

A. Database of Previous Experimental Studies 239

B. Infill Damage vs Drift for Frame Specimens Tested under IP Load 248

CURRICULUM VITAE 257

LIST OF TABLES

TABLES

Table 1.1 Tested frame specimens	17
Table 2.1 Equivalent strut models proposed by various researchers	51
Table 3.1 Summary of scale factors for RC models (Harris & Sabnis, 1999).....	60
Table 3.2 Instrumentation of frame specimen tests	83
Table 4.1 Concrete specimen test results	91
Table 4.2 Mechanical properties of reinforcing bars	94
Table 4.3 Mortar test results	98
Table 4.4 Mechanical properties of tie wire	100
Table 4.5 Mechanical properties of steel tie and channel	101
Table 4.6 Average material strengths at frame test day	103
Table 4.7 Uniaxial compression test results for masonry prisms w/o plaster.....	107
Table 4.8 Diagonal tension test results for masonry prisms w/o plaster.....	109
Table 4.9 Bending test results for masonry beam prisms	113
Table 4.10 Comparison of CB, CBP and CBMR prism specimens.....	114
Table 5.1. RC frame specimens tested at IP direction	122
Table 5.2. Load displacement response parameters under IP loading	163
Table 5.3. Extracted load displacement response parameters of infill walls	164
Table 5.4. OOP monolithic tests	170
Table 5.5. Load displacement response parameters for OOP loading	175
Table 5.6. Biaxial infilled frame tests	178
Table 6.1. Definition of infill wall damage for different performance levels.....	187
Table 6.2. Mean IDR associated with damage states for solid infill walls	193
Table 7.1 Lateral drift at first bar yielding of the frame member	197
Table 7.2 IDR (%) for the major frame and wall damages for IP tests	199
Table 7.3. IDR (%) corresponding to proposed DLS's of tested infill walls.....	200

LIST OF FIGURES

FIGURES

Figure 1.1. Infill wall involvement to structural response under lateral loads	4
Figure 1.2. Out of plane failure modes of solid infill walls	5
Figure 1.3. IP failure modes of infilled frames (Šipoš et al, 2013)	6
Figure 1.4. The decisive role of infills, 2011 Van Earthquake ($M_w=7.2$)	11
Figure 1.5. Barış apartment complex in İzmir, 2020 Samos EQ ($M_w=6.9$)	12
Figure 1.6. Different damages on identical blocks, 1998 Ceyhan EQ ($M_w=6.2$)	13
Figure 1.7. OOP failure of infills, 2023 Kahramanmaras EQ ($M_w=7.7$).....	14
Figure 2.1. Failure mechanisms of infilled frames (Mehrabi, 1994).....	25
Figure 2.2. OOP capacity loss due to prior IP damage (Angel,1994)	26
Figure 2.3. Study program of infilled frames (Mosalam, 1996)	27
Figure 2.4. Simplified force-drift curve for infilled RC frames (Stavridis, 2009) ..	29
Figure 2.5. Documented parameters from selected previous experimental studies	32
Figure 2.6. Some variables of the created database (all publications)	33
Figure 2.7. Frame specimen properties in the database tested at IP direction only	35
Figure 2.8. Frame specimen properties in the database tested at OOP direction	36
Figure 2.9. Seismic retrofit of infilled frames	37
Figure 2.10. Non-interacting retrofit solutions.....	38
Figure 2.11. Mesh reinforcement of infill walls.....	39
Figure 2.12. Horizontal partition of infill walls with sliding joints.....	40
Figure 2.13. Surface overlay of infill walls	41
Figure 2.14. Vertical partition of infill walls.....	42
Figure 2.15. Bed joint reinforcement of infill walls	43
Figure 2.16. Energy dissipating infill systems	43
Figure 2.17. A sample detailing for flexible joints, TBEC (2018).....	45
Figure 2.18. Design procedure for infill walls for new construction in the EU	47
Figure 2.19. Design procedure for infill walls for new construction in the USA ...	48
Figure 2.20. Multiple strut models	52

Figure 2.21. Hysteresis models for equivalent strut models	52
Figure 2.22. Infill strut models accounting for IP-OOP interaction	53
Figure 3.1. Prototype Building.....	56
Figure 3.2. The specimen dimension and reinforcement (All units in mm)	57
Figure 3.3. Member sections and materials for bare frame specimen	58
Figure 3.4. Column and beam section capacities of bare frame specimen	59
Figure 3.5. Details of modular formwork designed to cast frame specimens.....	61
Figure 3.6. Construction stages of frame specimens	62
Figure 3.7. Concrete casting and sampling	63
Figure 3.8. Placement of frame specimens on the transfer slab.....	64
Figure 3.9. Construction of HCB infilled frame	66
Figure 3.10. Construction of HCB infilled frame with plaster	67
Figure 3.11. Construction sequence of CBMR specimen.....	68
Figure 3.12. Horizontal steel ties spanning full length between the columns	69
Figure 3.13. Continuous horizontal steel tie (TieC) application.....	70
Figure 3.14. Staggered horizontal steel tie (TieS) application.....	71
Figure 3.15. Construction sequence of LBP specimen	72
Figure 3.16. Construction details for AB specimen.....	73
Figure 3.17. Construction stages for ABI specimen	74
Figure 3.18. Construction sequence of ABRP specimen	75
Figure 3.19. In-plane testing setup.....	76
Figure 3.20. The vertical and horizontal loading assembly	77
Figure 3.21. Construction of transfer slab	78
Figure 3.22. Out-of-plane testing setup	79
Figure 3.23. Out-of-plane loading assembly details	80
Figure 3.24. Experimental setup for multi directional tests.....	81
Figure 3.25. Instrumentation labelling a) In-plane, b) Out-of-plane	84
Figure 3.26. Strain gauge attachment to longitudinal bars	85
Figure 3.27. LVDT attachment to frame specimen	86
Figure 3.28. In-plane loading protocol.....	87

Figure 4.1. Concrete sampling and testing	90
Figure 4.2. Uniaxial tensile testing of reinforcing bars	92
Figure 4.3. Stress-strain graph for reinforcing bars.....	93
Figure 4.4. Tested infill walls and utilized brick units	95
Figure 4.5. Compressive strength of the masonry units	96
Figure 4.6. Production and sampling of mortar.....	96
Figure 4.7. Flow tests conducted for mortar consistency	97
Figure 4.8. Tests on mortar specimens	97
Figure 4.9. Testing of mesh reinforcement a) Fiber (Todorovic 2019), b) Steel	99
Figure 4.10. Steel mesh reinforcement test results.....	100
Figure 4.11. Time based mortar compressive strength correction curve	102
Figure 4.12. Setup for masonry prism tests	105
Figure 4.13. Uniaxial compression testing of masonry prisms	105
Figure 4.14. Masonry prism uniaxial test setup details	106
Figure 4.15. Stress-strain curves of HCB prisms under uniaxial compression.....	108
Figure 4.16. Diagonal compression test	109
Figure 4.17. Stress-strain curves of HCB prisms under diagonal tension tests.....	110
Figure 4.18. Sliding shear test of masonry prisms	111
Figure 4.19. Mohr-Coulomb failure surface after sliding tests	112
Figure 4.20. Bending tests of masonry beam specimens.....	113
Figure 4.21. Failed diagonal tension specimens a) CB, b) CBP, c) CBMR.....	114
Figure 5.1. Base shear correction due to vertical jacks	116
Figure 5.2. Axial load correction on hysteresis responses of tested specimens	117
Figure 5.3. Equation fit for displacement cycle of CBMR specimen at 2% drift .	118
Figure 5.4. Equation fits to experimental hysteresis data.....	119
Figure 5.5. LVDT attachment locations	121
Figure 5.6. Load-displacement response of BF specimen.....	123
Figure 5.7. Propagation of column damage for BF	124
Figure 5.8. Load-displacement response of CB specimen	125
Figure 5.9. Sequence of damage propagation for CB	127

Figure 5.10. Propagation of damage for CB frame.....	128
Figure 5.11. Load-displacement response of CBP specimen	129
Figure 5.12. Sequence of damage propagation for CBP.....	130
Figure 5.13. Propagation of damage for CBP frame.....	131
Figure 5.14. Load-displacement response of CBMR specimen.....	132
Figure 5.15. Sequence of damage propagation for CBMR.....	133
Figure 5.16. Propagation of damage for CBMR frame.....	134
Figure 5.17. Load-displacement response of TieC specimen	135
Figure 5.18. Sequence of damage propagation for TieC	136
Figure 5.19. Propagation of damage for TieC frame	137
Figure 5.20. Load-displacement response of TieS specimen	138
Figure 5.21. Sequence of damage propagation for TieS.....	139
Figure 5.22. Propagation of damage for TieS frame.....	140
Figure 5.23. Load-displacement response of LBP specimen.....	141
Figure 5.24. Sequence of damage propagation for LBP	142
Figure 5.25. Propagation of column damage for LBP.....	143
Figure 5.26. OOP testing of damaged AB frame with vibration generator	144
Figure 5.27. Load-displacement response of AB specimen	145
Figure 5.28. Sequence of damage propagation for AB.....	146
Figure 5.29. Propagation of damage for AB frame.....	147
Figure 5.30. Load-displacement response of ABI specimen	148
Figure 5.31. Sequence of damage propagation for ABI	149
Figure 5.32. Propagation of damage for ABI frame	150
Figure 5.33. Load-displacement response of ABRP specimen.....	151
Figure 5.34. Sequence of damage propagation for ABRP.....	152
Figure 5.35. Propagation of damage for ABRP frame.....	153
Figure 5.36. Influence of brick stacking direction (Suzuki et al. 2017)	154
Figure 5.37. Ultimate IW damages under IP loading	158
Figure 5.38. Hysteretic response of tested RC frame specimens.....	159
Figure 5.39. Extracted hysteretic response of infill walls.....	160

Figure 5.40. Averaged backbone curves	162
Figure 5.41. Stiffness degradation of tested infilled frames.....	165
Figure 5.42. Energy dissipation of infill walls	165
Figure 5.43. Distribution of lateral force among IW and bounding frame.....	167
Figure 5.44. Distribution of energy dissipation among IW and bounding frame..	168
Figure 5.45. Front and back views of OOP test setup	169
Figure 5.46. OOP Instrumentation	170
Figure 5.47. Ultimate infill damages under OOP loading.....	171
Figure 5.48. Ultimate damage patterns of infills under OOP loading.....	172
Figure 5.49. OOP displacement profile of infills	173
Figure 5.50. Load displacement curves in OOP direction.....	175
Figure 5.51. Test setup for combined IP and OOP loading of infilled frames.....	178
Figure 5.52. Ultimate infill damages under combined loading	179
Figure 5.53. Ultimate damage patterns of infills under combined loading	180
Figure 5.54. OOP displacement profile under combined loading	181
Figure 5.55. OOP central displacement under increasing IP drift.....	182
Figure 5.56. IP and OOP interaction diagram	183
Figure 6.1. Definition of damage states for infill walls.....	189
Figure 6.2. Infill wall damages for proposed DLS's: push (+), pull (-)	193
Figure 6.3. Proposed DLS's on infilled frame backbone (2nd cycle).....	194

LIST OF ABBREVIATIONS

ABBREVIATIONS

ACB: Aerated concrete block

AB: ACB infilled wall

ABI: ACB infilled wall with isolation joints

ABRP: ACB infilled wall with fiber reinforced plaster

BF: Bare frame

C: Cyclic loading

CB: HCB infilled wall

CBP: HCB infilled wall with plaster

CBMR: HCB infilled and bilateral steel mesh reinforced wall with plaster

FRP: Fiber reinforced polymer

HC: Half cyclic loading

HCB: Hollow clay brick

IDR: Inter-story drift ratio

IP: In-plane

LB: Locking clay brick

LBP: LB infilled wall with plaster

LVDT: Linear variable displacement transducer

M: Monotonic loading

OOP: Out-of-plane

PsD: Pseudo-dynamic loading

RC: Reinforced concrete

ShkT: Shake table

TieC: HCB infilled wall with continuous horizontal steel ties

TieS: HCB infilled wall with staggered horizontal steel ties

LIST OF SYMBOLS

SYMBOLS

A_c : Area of column

d_y (δ_y): Yield displacement

d_u (δ_u): Ultimate displacement

$E_{w,h}$: Modulus of elasticity of wall in horizontal direction

$E_{w,v}$: Modulus of elasticity of wall in vertical direction

f_b : Compressive strength of brick unit in vertical direction

f_c : Cylindrical compressive strength of concrete

f_{ck} : Characteristic compressive strength of concrete

$f_{m,c}$: Compressive strength of joint mortar

$f_{m,t}$: Tensile strength of joint mortar

$f_{m,c,cylinder}$: Compressive strength of 75 mm diameter cylinder mortar sample

$f_{m,c,cube}$: Compressive strength of 50mm cube mortar sample

$f_{m,c,prism}$: Compressive strength of 40x40x160 mm³ prism mortar sample

$f_{m,t,prism}$: Flexural tensile strength of 40x40x160 mm³ prism mortar sample

$f_{p,c}$: Compressive strength of plaster

$f_{p,t}$: Tensile strength of plaster

f_{st} : Split tension strength of concrete

f_y : Yield stress of longitudinal bars

f_{yk} : Characteristic yield stress of reinforcing steel

f_{yw} : Yield stress of transverse bars

$f_{w,dt}$: Diagonal tension strength of infill wall

$f_{w,h}$: Compressive strength of infill wall in horizontal direction

$f_{w,v}$: Compressive strength of infill wall in vertical direction

G_w : Shear modulus of infill wall

N_c : Axial compressive load on column

T_R : Return period

CHAPTER 1

INTRODUCTION

Laying bricks to create a controlled internal environment is one of the oldest construction techniques in history. The primary load-bearing structural members were masonry walls, vaults, and domes until the 20th century. Although masonry structural systems were widely replaced by moment-resisting frames for multi-story buildings, providing a building envelope and partitioning the internal space is still commonly achieved by masonry walls placed within framing members. Low to medium-rise RC moment frames infilled with unreinforced masonry are typical construction practices in many areas of high seismicity worldwide, including Türkiye. Since infill walls are constructed after casting the frame skeleton, their structural role is practically limited to transferring lateral loads and their self-weight back to the structural framework. However, it is no secret that infill walls develop strong interaction with the bounding frames under seismic loading, resulting in a response significantly different from that of the frame acting alone.

Due to the no-tension-bearing interface between the wall and the frame, lateral in-plane deflection of the bounding frame concentrates compressive stresses along the diagonal of the infill wall. As a result, infill walls contribute to lateral resistance by forming diagonal compression struts that respond similarly to bracings. Several studies indicate that the infill wall interacting with the adjoining RC frame alters structural and dynamical properties such as stiffness, strength, energy dissipation capacity, and damping against seismic loadings (Brokken and Bertero 1981).

Controversial arguments have been set forth on the role of infill walls in modifying the seismic response of RC frames. Some researchers claim that infill walls are unaccounted for in the design, so they serve as a reserve capacity in terms of

increasing the stiffness and strength of the RC frames and providing better deformation control for the structure (Bennett et al. 1996; De Luca et al. 2014). Other researchers, on the other hand, claim that infill walls may jeopardize the seismic design philosophy for frame action due to the damage imposed on the boundary elements and infill driven irregularities (Arteta et al. 2019; Hermanns et al. 2014).

After infill wall contribution to lateral resistance was realized and formulated in 1960s, many researchers aimed to include infill walls in structural design. Yet, accounting for infill wall contribution in seismic response comes at a price due to the involvement of many uncertainties and complexities, such as:

- non-standardized construction practice of the infill walls
- complexity of the interaction between the wall and the bounding frame
- variability of the failure modes
- resistance of masonry to analytical modeling due to its anisotropic, heterogenous and brittle nature
- interaction of in-plane and out-of-plane damages
- influence of openings
- possible shear failure of frame members due to excessive shear induced by the compression strut.

Thus, ignoring the structural contribution of infill walls to avoid the complexities in the structural analysis and design was favored by the structural engineering community as a less painful solution.

However, disregarding infill wall-frame interaction in design, relying on the bare frame for seismic resistance, and perceiving infill wall contribution as a reserve capacity in case of a major seismic event also did not prove to be a reliable approach during past earthquakes. Improper arrangement of infill walls on the plan and in the elevation resulted in structural deficiencies such as undesired torsion, soft-story, short-column, and out-of-plane failures as illustrated by many other post-earthquake damage surveys (Sezen et al. 2003; Vicente et al. 2012) and experimental studies

(Dolšek and Fajfar 2001). Furthermore, ignoring infill walls in analytical models is not always safe as infills increase the lateral stiffness of the building, which may increase the earthquake demand of the structure by reducing the natural period.

All in all, the seismic response of infilled frames should be better identified, the positive and negative influence of infills should be accounted in structural design and retrofit measures that can enhance the resilience of infilled buildings against seismic actions should be developed.

This study presents an extensive experimental campaign conducted at the METU Uğur Ersoy Structural Mechanics Laboratory to investigate the seismic response of infilled RC frames. Particular attention was devoted to the definition of lateral drift based performance limits for infill walls, the investigation of the impact of in-plane wall damage on the out-of-plane capacity, and the retrofit techniques applied to infill walls to enhance their earthquake resistance. Half-scaled, single-story, single-bay ductile RC frame specimens designed according to contemporary design requirements were constructed and infilled with hollow clay bricks and aerated concrete blocks. Retrofit techniques such as isolation joints, mesh overlays, horizontal sliding joints, and horizontal steel ties were applied. After extensive characterization of the involved materials, infilled frame specimens were subjected to constant vertical, cyclic in-plane, monolithic out-of-plane and simultaneous in-and-out-of-plane loading conditions using servo-controlled hydraulic jacks and airbags. Experimental measurements were carefully investigated, reported, and discussed to enhance our understanding of the performance of infilled RC framed structures and the efficiency of retrofit techniques.

1.1 Background

Paulay and Priestley (1992) explained the interaction between the infill panel and the bounding frame as follows: “At low levels of in-plane lateral force, the frame and infill panel will act in a fully composite fashion, as a structural wall with boundary

elements. As lateral deformations increase, the behavior becomes more complex as a result of the frame attempting to deform in a flexural mode while the panel attempts to deform in a shear mode. The result is the separation between frame and panel that may occur at 50 to 70% of the ideal lateral shear capacity of the infill for reinforced concrete frames.” A masonry panel standing alone has very high lateral stiffness and low ductility, while a bare reinforced concrete frame is relatively ductile but has low stiffness. Separated by a no-tension bearing interface, individual responses of flexure dominant moment frame and shear dominant masonry wall cannot be superimposed to calculate the ultimate lateral response due to the complex interaction between them. Under lateral load, full contact is observed between the infill panel and the bounding frame in the loaded diagonal corners, whereas gaps form in the boundaries of the opposite diagonal. Load transfer along contact surfaces leads to the accumulation of compressive stresses along the loaded diagonal of the infill panel and the combined structural action becomes similar to that of a frame braced by an equivalent diagonal compression strut, as illustrated in Figure 1.1.

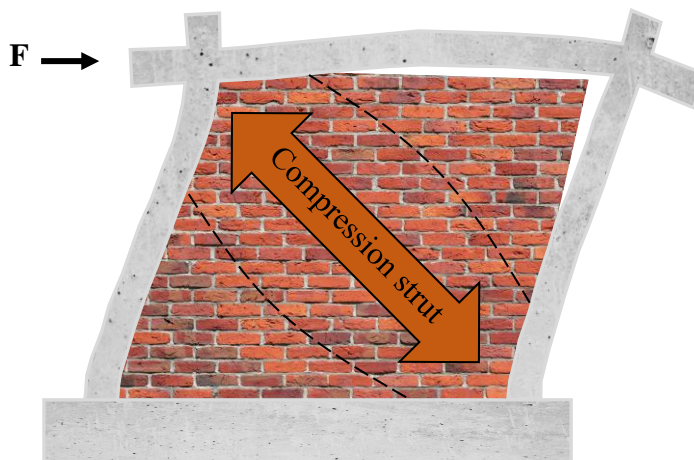


Figure 1.1. Infill wall involvement to structural response under lateral loads

Different approaches were developed to approximate the width of the equivalent strut in order to account for the infill panel contribution to the lateral response. Malcolm Holmes (1961), Paulay & Priestley (1992), and Richard Angel (1994) assumed constant values for the strut width as $1/3$, $1/4$ and $1/8$ of the diagonal

dimension of the infill, respectively. Others (R. Mainstone 1971; Smith and Carter 1969) developed complex expressions for equivalent strut width considering the relative stiffness of the infill to the frame. Although the equivalent strut concept beautifully simplifies the infill wall–frame interaction after the initial separation, earthquake driven lateral displacement reversals demanding non-linear cyclic response and deterioration of the infill resistance bring more unknowns into the equation.

The dynamic response of buildings under ground shaking results in accelerations and displacements at floor levels. The relative displacement of stories (i.e., inter-story drift) activates infill wall contribution to the in-plane (IP) resistance of the frames. In contrast, floor accelerations trigger inertial loads in the out-of-plane (OOP) direction of the infill walls. Various failure modes of infill and frame members are possible when the infilled frame is loaded normal and parallel to its plane.

Failure modes of solid infill walls when loaded normal to their planes (i.e., OOP direction) are illustrated in Figure 1.2. Out-of-plane response of the infill panel is characterized by plate bending in the elastic range. After the cracking of the infill, the non-linear response and the capacity are dominated by arching action. Slenderness, compressive strength, openings, and boundary conditions of the wall are the main parameters influencing out-of-plane behavior.

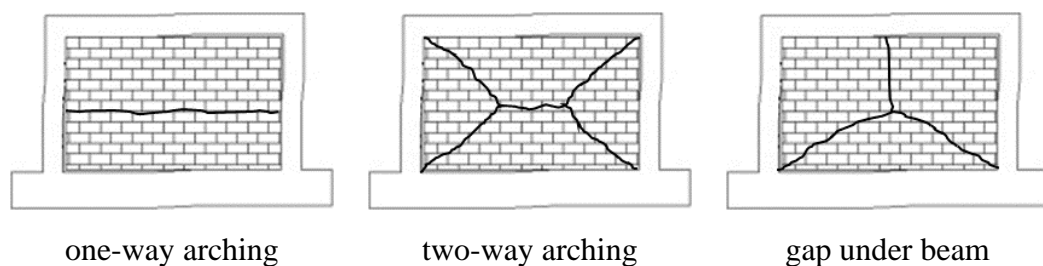


Figure 1.2. Out-of-plane failure modes of solid infill walls

The in-plane failure mode of the infill wall depends on the aspect ratio and compressive strength of the wall, mortar strength, location and size of window and door openings and lateral strength of the frame. Failure modes associated with in-

plane loading are illustrated in Figure 1.3. The strength associated with each possible failure mode should be considered in determining the governing mechanism. The damage pattern of frame members under in-plane loads depends on the ductility of the frame (i.e. detailing of the member ends and joints), concrete strength, vertical load on columns, and the strength of the infill wall.

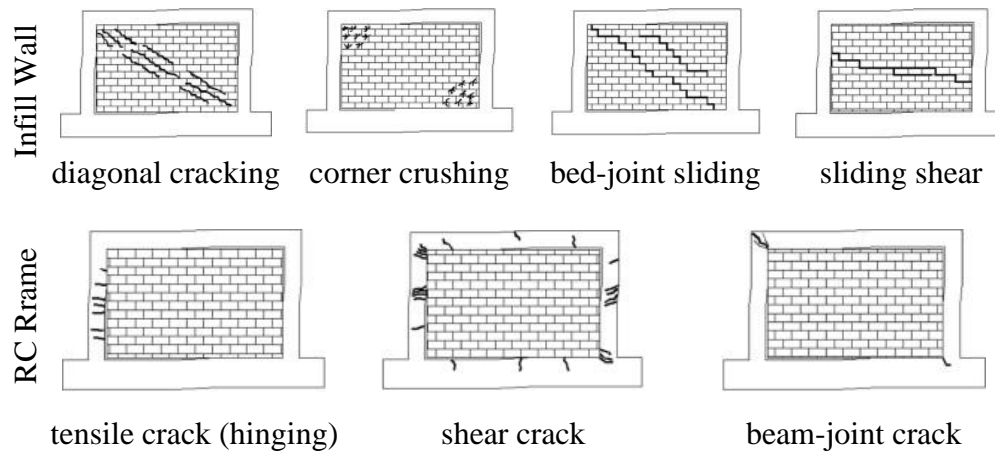


Figure 1.3. IP failure modes of infilled frames (Šipoš et al, 2013)

The main parameter characterizing the ultimate failure of the infilled frame is the relative strengths of the infill panel and the frame, as underlined by Mehrabi (1994). A non-ductile and weak RC frame infilled with strong masonry would possibly experience shear failure of frame members, whereas a ductile and strong RC frame infilled with weak masonry would undergo plastic hinging at member ends accompanied by one or a sequential combination of sliding, diagonal cracking, and corner crushing failure modes.

IP and OOP failure modes of infilled frames are also influenced by the nature of seismic excitations, where both directions of the infilled frames are loaded simultaneously so that IP damage affects OOP capacity and vice versa.

The fundamental criterion of seismic design is to provide life safety under the design level earthquake. Claiming that infill contribution diminishes and infilled frame response converges to bare frame in an extreme seismic event, infill wall influence on seismic demand and structural resistance has been neglected based on a single no-

collapse performance target. Practicing engineers were also reluctant to consider the infill contribution due to a lack of knowledge of the composite behavior of infilled frames and a lack of practicable methods for stiffness and strength prediction (Kwan 1982). In this regard, infill contribution has long been regarded as a reserve capacity and not considered in seismic design. On the other hand, in the displacement-based design approach, the damage state of members associated with different performance levels is concerned with varying levels of seismic action. The selection of performance objectives sets the acceptance criteria for the design. Expected performance levels should be linked to limiting values of measurable structural response parameters such as drift, rotation, strain or floor acceleration (R. D. Bertero and Bertero 2002). Knowing that infill walls contribute to seismic resistance, they should be included in the structural analysis. Limiting values of measurable response parameters should be defined for them that comply with the performance targets defined in seismic codes. Accurate modeling and seismic assessment strategies are crucial for developing efficient mitigation measures against seismic damages, casualties, and economic losses (Furtado and De Risi 2020).

In this way, recent experimental and analytical studies on infilled frames have been trying to figure out the different kinds of complexity that are part of infilled frame systems so that we can better understand how they react to earthquakes (Furtado and De Risi 2020). Along with complex and sophisticated numerical computer models, reliable and simple analysis methods for infilled frames are being developed (Asteris et al. 2013; Nicola et al. 2015). Numerous structural retrofit techniques aimed at infill walls were proposed and tested. Cyclic, pseudo-dynamic and shaking table tests of scaled and full-scale infilled frame specimens were conducted. The performance of infill panels is being considered in conjunction with the frame members for performance assessment studies. Seismic design and assessment guidelines are being updated to account for previously ignored infill panels.

1.2 Motivation

Capitalism is a system of accumulation that organizes production, distribution, and social reproduction to extract surplus value, as identified by Karl Marx (1867). Due to the capitalist development of the Turkish economy, uncontrolled migration from rural to urban regions started in the 1950s led to a lack of government control over urbanization. As a result, more than three-quarters of the Turkish population lives in metropolitan cities as of 2020, compared to one-quarter back in 1950. People rushing to urban cities compensated for their accommodation requirements through unauthorized and non-engineered masonry buildings named “gecekondü”, a building constructed overnight in Turkish. Following economic growth, 3 to 6-story RC framed buildings suffering proper seismic design emerged to encourage compact urban living and replace non-engineered masonry buildings.

Despite Turkey's long history of earthquakes, which resulted in the creation of various seismic zoning maps in 1945, 1947, 1963, 1972, 1996 (Özmen 2012) and building design codes in 1947, 1953, 1961, 1968, 1975, 1997, 2007 (Aydınöğlü 2007), the authorities were unable to implement an earthquake-resistant design practice, as addressed by Polat Gülkan (2000).

Populist and profit-oriented policies resulted in unrestrained and uncontrolled construction practices, especially before the devastating earthquakes hit the highly populated and industrialized Marmara region of Türkiye in 1999. A large proportion of residential and commercial buildings in Türkiye is made up of 3 to 7-story cast-in-situ RC beam-column frames with hollow brick infill walls (Bal et al. 2008). Buildings constructed before the 1999 Kocaeli earthquake ($M_w=7.4$) barely comply with the earthquake-resistant design requirements.

The common deficiencies of these buildings are:

- Poor concrete quality
- Use of plain bars for longitudinal and transverse reinforcement

- Lack of confinement (Widely spaced confinement steel without densification at member ends, lack of stirrups at beam-column joints, stirrups hooked 90°)
- Improper detailing (in hooks, connections, etc.)
- Beams stiffer and stronger than columns
- Structural irregularities (soft story, plan irregularities, discontinuity of members, lack of framing)
- Lap splices above floor slab with insufficient length
- Corrosion of reinforcement

The exterior cladding and interior partitions of the urban RC framed construction stereotype are made of infill walls constructed in contact with the bounding frame. Internal partition walls are commonly built with HCB or concrete masonry units of 10 to 13.5 cm, whereas thicker units of 16 to 20 cm are used for exterior walls. Two-layer construction of external walls accommodating insulation between the layers is popular in eastern regions where a colder climate dictates better heat isolation. Gaps at infill boundaries are filled with mortar and no special connectors aimed at transferring shear forces between the enclosures and the surrounding RC elements are provided.

In the absence of adequately designed and constructed RC frames, the contribution of infill walls to the lateral resistance of deficient buildings becomes more pronounced. If placed properly, infill walls influence the ultimate performance of deficient buildings by acting as the first line of defense against seismic loads, providing increased base shear capacity, dissipating energy, limiting story drifts, and reducing the ductility demand of structural members. Several researchers underlined the favorable influence of infill walls on seismic resistance. Khalid Mosalam (1996) stated that: “The performance shown by infilled frames is advantageous especially when the capacity and ductility of the frame itself is suspected to be inadequate. This is the case of frames mainly designed for gravity loads without attention to lateral loads when subjected to moderate or severe lateral loads due to earthquakes”. Bertero and Brokken (1983) claimed that: “The proper use of infill elements can be of great

practical value in strengthening and stiffening the usually very flexible moment resisting bare frame”. Calvi, Bolognini and Penna (2004) indicated that the common trend of neglecting infill on the response because of the fact that masonry panels crack and separate from the frame early in the response is disproved and it is shown that most of the energy dissipation takes place in the infills and damage in beams and columns tends to be low.

On the other hand, the majority of the casualties after sizable earthquakes in Türkiye are due to the collapse of low to medium-rise (i.e., 4 to 9 stories) RC framed buildings which might be triggered by the collapse of infill walls, as pointed out by Gaudio et al. (2019). Another possibility, as mentioned by Fardis et al. (1999), might be an improper arrangement of infills in the plan or the elevation leading to an unbalanced torsion or the concentration of inelastic deformation demands in ground story columns resulting in captive column and soft-story mechanisms.

During this study, the author was involved in several post-earthquake damage survey studies after destructive earthquakes in Türkiye as a member of the METU Earthquake Engineering Research Center (EERC), including 2011 Van-Erciş ($M_w=7.2$), 2011 Van-Edremit ($M_w=5.6$), 2020 Elazığ ($M_w=6.5$), 2020 Samos ($M_w=6.9$) and 2023 ($M_w=7.7$ and $M_w=7.6$) Kahramanmaraş earthquakes. During damage surveys of these service and design level earthquakes, the importance of the infill walls to the final performance of framed RC buildings was observed.

Figure 1.4 illustrates three six-story RC frame buildings infilled with hollow brick masonry exposed to various levels of infill damage in Ercis city after the 2011 Van Earthquake ($M_w=7.2$). Although the structural components remained intact with minor structural damage as expected for the experienced level of ground shaking (i.e. 0.1-0.2g), various losses occurred in the infill walls. The severity of infill damage influenced immediate usability, the time required for post-earthquake recovery, the cost of repair, and the impact on human lives, which are decisive factors in the ultimate seismic performance of buildings.



a) Light infill damage b) Moderate infill damage c) Heavy infill damage

Figure 1.4. The decisive role of infills, 2011 Van Earthquake ($M_w=7.2$)

A clear example of the benefit of infill walls in reducing soft-story failure risk after 2020 Samos Earthquake ($M_w=6.9$) is illustrated in Figure 1.5 (Demirel, Yakut, and Binici 2022). Eight-story apartment complex comprised of four identical RC buildings resting on deep soil deposit and exposed to 0.1g peak ground acceleration measured in Bayraklı district of İzmir city after the 2020 Samos Earthquake. Despite the amplification of long-distance seismic waves caused by local soil conditions, experienced spectral accelerations were at least 20% lower than the design values specified in the 1975 Turkish Earthquake Code (ABYBHY 1975) which was utilized for their design.

One of the four identical ground-floor buildings had a lot of infill walls around the outside and inside the plan so that the space could be used as meeting rooms and storage (Figure 1.5a). In the other three buildings, the ground floors had no infill walls due to architectural preference (Figure 1.5c). Three of the buildings without infill walls collapsed, resulting in nine fatalities. The one with the infill walls in the first story, on the other hand, experienced moderate infill wall damage without any significant structural damage (Figure 1.5e). The presence of infill walls determined the “to collapse or not to collapse” choice for the deficient buildings.



Figure 1.5. Barış apartment complex in İzmir, 2020 Samos EQ ($M_w=6.9$)

Another very similar example illustrating the decisive role of infill walls is from the Ceyhan district of Adana city after the 1998 Ceyhan Earthquake ($M_w=6.2$). The presence and absence of infill walls in the ground story caused different damages to the six-story RC apartment, which was made up of two identical and separated blocks (Figure 1.6). Bayülke (2003) stated that solid infill walls located at the ground story of the intact block prevented total failure even after the shear failure of RC columns. He also noted that infill walls could carry the vertical load redistributed after the shear failure of the columns.



Figure 1.6. Different damages on identical blocks, 1998 Ceyhan EQ ($M_w=6.2$)

Kahramanmaras earthquake sequence in 2023 ($M_w=7.7$ and $M_w=7.6$) affected 14 million people in southern Turkiye and created peak ground accelerations above 1.0g. More than 500.000 buildings were inspected as collapsed, needing urgent demolition or being heavily damaged by the Turkish authorities. Widespread infill wall damage in various intensities was observed in hundreds of thousands of buildings after the earthquake.

Failure of infill walls in the OOP direction can dictate the final performance of the building as falling hazard directly threatens life safety. Captured images during the damage survey (Figure 1.7) illustrate that OOP failure does not necessarily occur at elevations where maximum floor accelerations are expected (i.e., upper stories). Instead, the influence of prior IP damage is more effective and the failure results from IP and OOP interaction.



Figure 1.7. OOP failure of infills, 2023 Kahramanmaraş EQ ($M_w=7.7$)

Türkiye is one of the most seismically prone countries in the world. Millions of people living and working in residential, public and commercial buildings in urban cities such as İstanbul and İzmir face seismic risk. 93% of the RC frame structures in Türkiye use brick as the infill wall material (Ay, Azak, and Erberik 2016) and infill walls existing in Turkish deficient buildings pose an essential potential for feasible and efficient seismic upgrading. Developing and implementing viable and innovative improvement techniques for infill walls could prevent the collapse of the deficient building stock of Türkiye by improving and sustaining infill contribution to seismic resistance under strong earthquakes and reducing economic losses by mitigating damage to infills under moderate earthquakes.

1.3 Objective and Scope

This study investigates the seismic performance of RC frames infilled with solid masonry walls and proposes innovative retrofit techniques to improve seismic resistance. An experimental campaign was conducted at the METU Uğur Ersoy Structural Mechanics Laboratory to perform in-plane (IP), out-of-plane (OOP) and bidirectional testing of half-scaled, one-bay, one-story RC frame specimens. The tested frame specimen belongs to the first-story central-internal bay of the five-story prototype RC building designed for the first seismic zone and Z4 soil type according to the high ductility requirements of the Turkish Earthquake Code (2007).

Light masonry units typical to Turkish construction practice, such as hollow clay brick units and aerated concrete blocks, were utilized as infill wall material. Easy-to-apply systems to enhance seismic response relying on accessible materials and minimum expertise, such as isolation joints, mesh overlays, horizontal sliding joints and bed joint reinforcement, were proposed and tested.

A total of 22 frame tests carried out on identical half-scaled RC frame specimens are presented in Table 1.1. The abbreviations of the tested specimens in the table were based on the infill system being used. The first letter in the abbreviation indicates the infill material, where CB stands for Clay Brick, AB stands for Aerated concrete Block and LB stands for Locking Brick. The only exception is HCB infilled frame specimens with infill tie systems where TieC and TieS represent Continuous and Stepped tie configurations. P symbolizes the inclusion of Plaster on the infill surface. Finally, I and MR stand for Isolated and Mesh Reinforced infill walls. For specimens tested under combined loading, the numbers (i.e., 0.33 and 0.67) represent the ratio of the applied constant load to the load capacity in the OOP direction.

The vertical loading on the beam and columns was simulated by weight blocks and manually controlled hydraulic jacks. The axial load ratio of columns, corresponding to the axial load divided by the concrete compression capacity (i.e. $N_c/A_c f_c$), was arranged to 0.175 using the hydraulic jacks for all tests.

In-plane cyclic testing of ten undamaged frame specimens, nine infilled with solid masonry panels, was conducted using a servo-controlled horizontal hydraulic jack. The nonlinear behavior of the specimens under increasing lateral displacement reversals up to 4.0% drift was investigated. Lateral and vertical forces, lateral displacements, member end rotations, yielding of longitudinal reinforcement at member ends, and damage propagation in the RC frames and the infill walls were monitored.

Out-of-plane testing of six solid infill walls was conducted under monolithically increasing uniformly distributed pressure on the wall surface exerted by an airbag. Infill walls bounded by the RC frame specimen were pushed in the OOP direction up to failure by a controlled increase of air pressure inside the airbag. Lateral force, displacement profile, and crack propagation on the surface of the infill walls were monitored.

Finally, combined testing of six infilled frame specimens was conducted. Increasing cyclic displacement reversals were applied in the in-plane direction, while the predetermined constant pressure exerted by the airbag was sustained in the out-of-plane direction. Combined tests were executed until the failure of the infill wall took place in the OOP direction.

Table 1.1 Tested frame specimens

<i>Test No</i>	<i>Direction</i>	<i>Wall Unit*</i>	<i>Plaster</i>	<i>Retrofit</i>	<i>Abbreviation</i>	<i>Test Date</i>
1	IP	Bare	NA	No	BF	16-07-2014
2	IP	HCB	No	No	CB	09-05-2014
3	IP	HCB	Yes	No	CBP	01-06-2015
4	IP	HCB	Yes	Steel mesh overlay	CBMR	29-08-2014
5	IP	HCB	No	Infill-tie (cont.)	TieC	10-09-2014
6	IP	HCB	No	Infill-tie (staggered)	TieS	29-12-2014
7	IP	LB	Yes	Dry slip joints	LBP	29-12-2015
8	IP	ACB	No	No	AB	18-02-2015
9	IP	ACB	No	Isolation joint	ABI	28-11-2014
10	IP	ACB	Yes	Fiber mesh overlay	ABRP	02-04-2015
11	OOP	HCB	Yes	No	CBP	29-04-2016
12	OOP	HCB	No	No	CB	05-05-2016
13	OOP	LB	Yes	Dry slip joints	LBP	16-05-2016
14	OOP	HCB	Yes	Steel mesh overlay	CBMR	24-05-2016
15	OOP	HCB	No	Infill-tie (cont.)	TieC	25-07-2016
16	OOP	ACB	Yes	Fiber mesh overlay	ABRP	12-01-2017
17	IP+OOP	HCB	Yes	No	CBP_0.33	08-06-2016
18	IP+OOP	HCB	Yes	No	CBP_0.67	20-06-2016
19	IP+OOP	LB	Yes	Dry slip joints	LBP_0.33	01-07-2016
20	IP+OOP	HCB	No	Infill-tie (cont.)	TieC_0.33	08-12-2016
21	IP+OOP	ACB	Yes	Fiber mesh overlay	ABRP_0.33	03-02-2017
22	IP+OOP	HCB	Yes	Steel mesh overlay	CBMR_0.33	16-10-2019

* HCB: Hollow clay brick, ACB: Aerated concrete block, LB: Clay brick with dry lock

1.4 Organization of Thesis

Chapter 1 presents background information on the infilled frame response. The motivation behind the selection of the research topic is revealed by referring to the damage studies carried out after destructive earthquakes in Türkiye. Objectives and the methods to achieve the targeted goals of the research were mentioned. The scope and variables studied in the experimental study were explained. Finally, the organization of the thesis on a chapter basis was explored.

Chapter 2 presents a review of the most relevant experimental testing campaigns from the literature on the infilled frames subjected to in-plane, out-of-plane, and combined loading conditions. Selected influential doctoral studies conducted by Mehrabi (1994), Richard Angel (1994), Khalid Mosalam (1996) and Andreas Stavridis (2009) are summarized.

Also, a database of 214 carefully chosen publications containing important information about the experimental testing of infilled frames was developed (Appendix A). The documented variables include the author, year of publication, where the study was done, frame type, frame ductility, brick unit, concrete, and infill compressive strength, scale, number of bays and stories, aspect ratio, direction, and type of loading. A good perception of the scope and development of infill related research can be acquired by investigating the collected database. For a complete understanding of the subject, recent studies related to seismic retrofit solutions targeting masonry infill walls and current seismic code approaches on the design and assessment of infilled frames were reviewed. Finally, simple analytical modeling of infilled frames was summarized.

Chapter 3 presents the framework of the experimental work. A detailed description of the experimental program was provided, including test setup, loading protocols, instrumentation, scaling, frame specimen design, and construction details of tested infill wall systems.

Chapter 4 illustrates the characterization of the materials involved in the construction of frame specimens and masonry prism specimens, which are representative of tested infill wall systems.

Chapter 5 includes experimental results and discussions on the observed response of infilled frames under in-plane, out-of-plane and combined loading tests. Detailed descriptions of the progression of infill wall and RC frame damages, modes of failure, degradation of strength and stiffness, characteristics of hysteretic response, and energy dissipation for tested frames were illustrated.

Chapter 6 evaluates the performance assessment of infilled frames mainly focusing on the definition of infill wall performance levels and comparison of test results against performance limits defined in previous studies and the seismic codes.

In Chapter 7, the results and most important findings of the experimental campaign were summarized, and suggestions for future research were made.

CHAPTER 2

LITERATURE REVIEW

The seismic response of infilled frames has been investigated since the 1950s. Over the course of seven decades, numerous efforts were made to better understand, formulate, characterize, analyze, and enhance the infilled frame response. A wide range of parameters complicating the interaction between the infill panel and the bounding frame were revealed. Topics deemed appropriate to have a good overall perception of the infilled frame response were summarized in this chapter. The literature review is divided into five parts. First, the chronological progress of previous research on infilled frame responses was summarized. Second, a comprehensive database was created based on experimental studies related to infilled frames. Third, strengthening techniques proposed to enhance the seismic response of infilled frames were reviewed. Fourth, seismic guidelines for the design and assessment of infilled R.C. frames were investigated. Fifth, analytical strut modeling was reviewed.

2.1 Chronological Summary of Previous Research

The structural engineering community's interest in the infill wall contribution to the lateral resistance of moment frames dates back to the 1950s. The earliest studies relied on experimental evidence. Before the Old Dental Hospital in Johannesburg was demolished in 1952, Ockleston (1955) applied horizontal load at the roof level of a three-story high and one-bay wide identical RC frame building. The brick walls were left intact in one of the frames and removed from the other. The load capacity of the infilled frame was measured as five times that of the bare frame, and the infilled frame behaved considerably stiffer than the bare.

Polyakov (1960) was the first researcher to identify that compressive stresses transmitted within contact surfaces between the frame and the infill initiate diagonal strut formation in the panel. Following studies belonging to Holmes (1961), Smith and Carter (1969) and Mainstone (1971) were primarily concerned with the formulation of equivalent diagonal strut concepts to predict added strength and stiffness to the surrounding frame. The majority of the experimental studies in this era were based on monolithic testing of one-story, one-bay steel frames infilled with masonry panels. A summary of the pioneering experimental research for infilled frame response was given by Abdul-kadir (1974). Initial studies concerned with the experimental testing of RC frames were conducted by Yorulmaz and Sözen (1968) (1968) and Fiorato (1971) from the University of Illinois. The former ran 10 and the latter ran 26 monolithic tests on 1/8-scaled RC frames infilled with masonry walls. Controlled variables include number of stories, number of bays, reinforcement ratio of frame members, axial load on columns and presence of openings. In the later years, improved testing methods such as cyclic quasi-static testing (Brokken and Bertero 1981; Klingner and Bertero 1976; Mander et al. 1993; Zarnic and Tomazevic 1985), dynamic testing via a shaking table (Dawe and Seah 1989; Liauw and Kwan 1992; Moghaddam 1988), pseudo-dynamic testing (Khalid Mahmoud Aly Mosalam 1996; Negro and Verzeletti 1996), and out-of-plane testing using airbags (Adham 1985; Dawe and Seah 1989) were employed for better simulation of seismic action. Angel (1994) summarized the ongoing and planned research on infill behavior in American universities and institutions in the early 1990s. Parameters of interest in these studies include frame type, infill type, the interaction between in-plane and out-of-plane responses, and the development of repair methods.

Mallick and Severn (1967) made the earliest attempt to analyze infilled frames by finite element method, accounting for separation at the structural interface. It was not until the 1980s that efforts on non-linear modeling of the infilled frames emerged (Dhanasekar and Page 1986; Kwan 1982). The rapid increase in computing power during the 1990s and the first decade of the new century led to the development of analytical tools that shifted the focus of research on infilled frames from

experimental to analytical. Numerous approaches were developed, from simple compression strut models to sophisticated nonlinear finite element models. Parametric analyses on calibrated computer models were utilized to identify the influence of different factors on the seismic response of infilled frames. Armin Mehrabi's (1994) and Khalid Mosalam's (1996) works are valuable in this context.

After the introduction of the performance-based seismic engineering concepts, research has concentrated on the performance assessment and seismic retrofit of existing buildings infilled with masonry panels (Furtado and De Risi 2020; M. Griffith 2008). Several methods were proposed and supported by experimental research to enhance the seismic capacity of infilled frames (F. Da Porto et al. 2016; Furtado et al. 2020b). More recently,

- The database of previous experiments was utilized to characterize the lateral load-displacement response (Alwashali et al. 2018; Blasi et al. 2021; De Risi et al. 2018; Huang and Simonen 2018; Turgay et al. 2014).
- Drift based acceptable damage limits corresponding to different performance levels were defined (Felice Colangelo 2013; De Risi et al. 2018; X. Lu and Zha 2021; Morandi, Hak, and Magenes 2018b; Sassun et al. 2016).
- Fragility curves to estimate infill performance under different intensities of seismic action were derived (Cardone and Perrone 2015; Chiozzi and Miranda 2017; Gaudio et al. 2019).
- Probabilistic seismic loss estimation frameworks and functions were proposed (Gaudio et al. 2019; O'Reilly and Calvi 2021; Rossi et al. 2021; Sousa and Monteiro 2018).

In order to avoid infill wall induced irregularities, damages and losses experienced after sizable seismic actions (Baggio et al. 2007; Bennett et al. 1996), analysis and design provisions for infilled frames were introduced in seismic design codes of different countries (Kaushik, Rai, and Jain 2006). Recent developments in understanding the seismic response of infilled frames and the need for their inclusion

in seismic performance assessment were reflected in recent seismic guidelines such as NZSEE2017-C7 (2017) and ASC41-17 (2018).

From the vast amount of research on the infilled frame response, four important doctoral studies that tested infilled frames in the lab were chosen and summed up. Armin Mehrabi from the University of Colorado-Boulder did in-plane cyclic tests in 1994, Richard Angel from the University of Illinois-Urbana did out-of-plane monolithic tests with an airbag in 1994, Khalid Mosalam from Cornell University did pseudo-dynamic tests in 1996, and Andreas Stavridis from the University of California-San Diego did shake table tests on infilled frames in 2009.

Mehrabi (1994) identified possible failure mechanisms of infilled frames and used the plastic analysis method to approximate the ultimate capacities. He specifically investigated the influence of the relative strengths of the infill and the bounding frame, panel aspect ratio, and column axial load on the infilled frame response by conducting in-plane cyclic and monotonic testing of ductile and non-ductile 14 half-scaled RC specimens infilled either with weak hollow concrete blocks or strong solid concrete bricks. Four main failure mechanisms were identified in his doctoral study (Figure 2.1).

A frame infilled with a weak panel tends to exhibit a relatively ductile response governed by the sliding along the masonry bed joints over the height of the wall. Flexural yielding and shear cracking in the frame members are expected for ductile and non-ductile detailing of frame members, respectively. Flexural hinging could also be observed at beam ends if the strong column/weak beam principle is followed in design (Figure 2.1c). Alternatively, cracking could be concentrated at the infill's mid-height, enforcing a short column behavior and potentially resulting in shear failure of non-ductile columns (Figure 2.1a). Another possible mechanism is the diagonal cracking of the infill from the top windward column to the bottom leeward column. In case a strong infill is bound by a weak non-ductile frame, diagonal cracking is accompanied by shear failure of frame members leading to brittle failure. Otherwise, flexural hinging of frame members and corner crushing of infill might be

observed (Figure 2.1b). In the case of a strong frame and a strong infill, where the diagonal compression strut mechanism is fully developed and the infill's contribution to lateral resistance is maximized (Figure 2.1d), a final mechanism is likely characterized by corner crushing of infill.

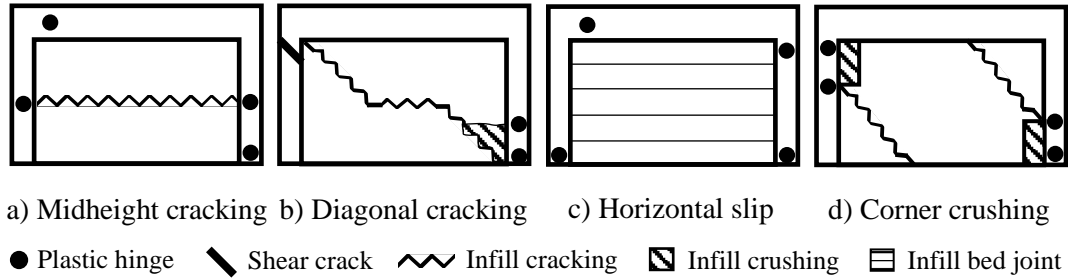


Figure 2.1. Failure mechanisms of infilled frames (Mehrabi, 1994)

Interpreting test results, Mehrabi concluded that “in the case of a weak infill, sliding shear was the dominant failure mode, where the frame and the wall actions were more or less independent and their strengths were additive. In the case of a strong infill, the lateral resistance was governed by the shear strength of the columns and the diagonal compression mechanism in the infill. In the case of a strong frame, the higher frame stiffness resulted in a more efficient compression strut mechanism and a higher resistance.” Mehrabi also illustrated that cyclic loads resulted in faster degradation of the post-peak resistance, which is more evident for strong infills.

Richard Angel (1994) investigated the OOP response of infill panels bounded by RC frames in his doctoral research. The experimental program consisted of testing eight full-scale infill panels constructed with unreinforced clay bricks or concrete masonry units placed within a single-story, single-bay ductile reinforced concrete frame. His research focused on the loss of OOP strength due to previous IP cracking. Frame specimens were initially loaded up to twice the cracking drift under IP cyclic load reversals by a hydraulic actuator and then pushed monotonically with an airbag in the OOP direction. The influence of frame to infill relative strengths, previous in-plane damage, strengthening techniques, slenderness (height-to-thickness) of the infill, mortar type, and wall unit type on the OOP capacity was revealed. Slenderness

ratio and infill wall compressive strength were identified as the most effective parameters influencing OOP stiffness and strength.

The observed out-of-plane failure modes of the infills varied between two distinct mechanisms: snap-through and crushing of the arch. The former was observed in slender members (i.e. $h/t > 20-30$, depending on the crushing strain of masonry). Excessive lateral deflection causes the arch to vanish after the attainment of the ultimate strength of the infill, followed by a rapid reduction in capacity. The latter occurs in infills with low slenderness ratios (i.e. $h/t < 20-30$, depending on the crushing strain of masonry). After the peak load is reached, the strength reduces slowly until the crushing strain is reached. Previous IP damage due to twice the IP cracking drift reduced the OOP strength of the slender infills by a factor as high as two, as illustrated below (Figure 2.2).

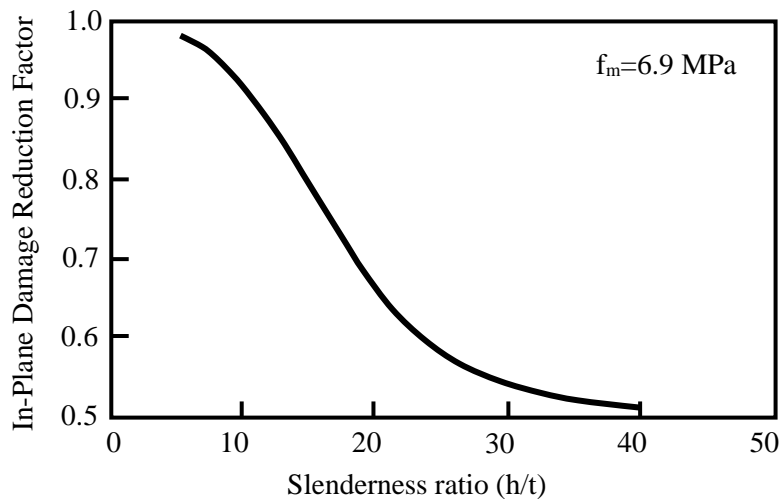


Figure 2.2. OOP capacity loss due to prior IP damage (Angel,1994)

The out-of-plane strength was increased by 2.5 and 5 times for slenderness ratios of 17 and 34, respectively, when wire meshes (12.7 mm apart and 1 mm in diameter) were attached to the panel faces on both sides with steel bolts spaced 400 mm apart. Finally, the out-of-plane strength of the infill panels was predicted with an analytical model based on the arching action of a strip of infill that spans between two fully restrained supports.

In his PhD study, Khalid Mosalam (1996) conducted quasistatic and pseudo-dynamic testing of six 1/3-scale steel frames infilled with ungrouted concrete masonry units. Key parameters investigated within the test program (Figure 2.3) include panel strength, openings on the panel, and the number of bays. Strain gages and LVDTs were utilized to identify the straining of the bounding steel frame, the directions of principal strains in infill walls, deformation of the infills along the diagonals, and interface movements (i.e., opening and closing of gaps, sliding).

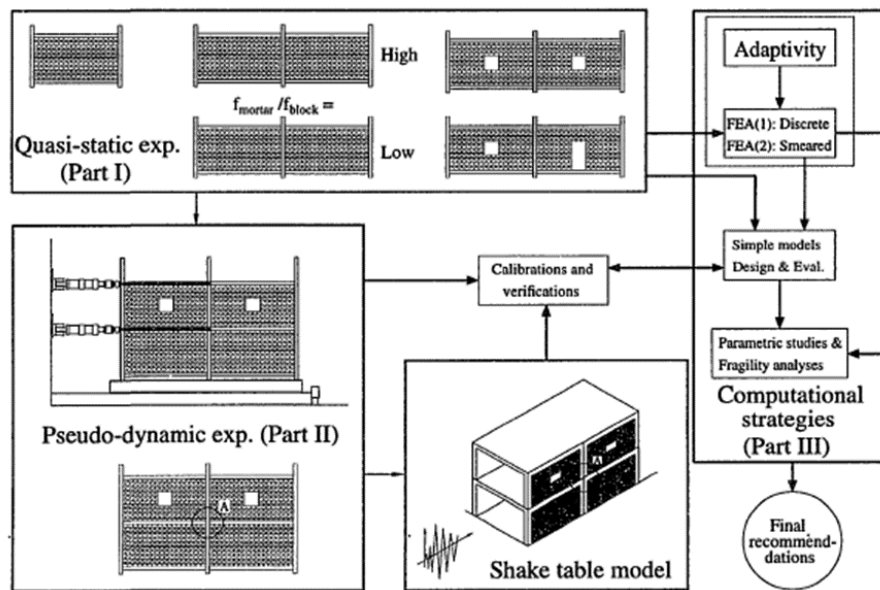


Figure 2.3. Study program of infilled frames (Mosalam, 1996)

Experimental results revealed that infills significantly alter the bending moment distribution in the frame members. The variation of bending moment is highly nonlinear and cracking dependent because of the continuous change of the contact length between the frame members and the infill. It was also pointed out that the observed damage to the infills correlates well with the dissipated hysteretic energy. After experimental testing, appropriate computational strategies such as micro-modeling, meso-modeling, and macro modeling were investigated for the analytical prediction of the infilled frame response. The latter was deemed appropriate for analysis and design purposes. The final part of the dissertation was devoted to the derivation of structural fragility curves for infilled frames. The inclusion of infill

walls to bare frames was deemed a feasible retrofit measure for limiting the lateral drifts.

Andreas Stavridis's doctoral research (Stavridis 2009) included a lot of analytical and experimental work to determine how RC frames filled with masonry respond to earthquakes. He conducted quasistatic tests on four 2/3-scale non-ductile, single frames infilled with solid clay bricks investigating three different configurations of openings. Additionally, he ran shake table testing of a 2/3-scale, three-story, two-bay non-ductile frame under increasing intensities of scaled ground motions. Cyclic tests revealed that the strength contribution of the perforated walls not only depends on the size but also the location of the opening. Utilizing the experimental data for validation of the proposed analytical finite element model, parametric analyses were conducted to identify the influence of the selected variables (i.e., the aspect ratio of infill panel, vertical load on columns, longitudinal reinforcement ratio, spacing and the transverse reinforcement) on the structural response. Stavridis revealed counter-intuitive results that two compressive struts tend to develop in both loading directions at angles close to 45° instead of a single diagonal strut. For single-story, single-bay infilled frames, formed struts act against the top of the windward column and the bottom of the leeward column forcing columns into shear failure. Regarding the inspected parameters, the vertical load on columns is influential as it increases the shear capacity of the columns, but the most significant parameter is the aspect ratio of the infill, which characterizes the failure mechanism and contribution to lateral resistance. Based on the findings of the parametric study, a simplified method is proposed to derive the backbone curve of infilled frames (Figure 2.4).

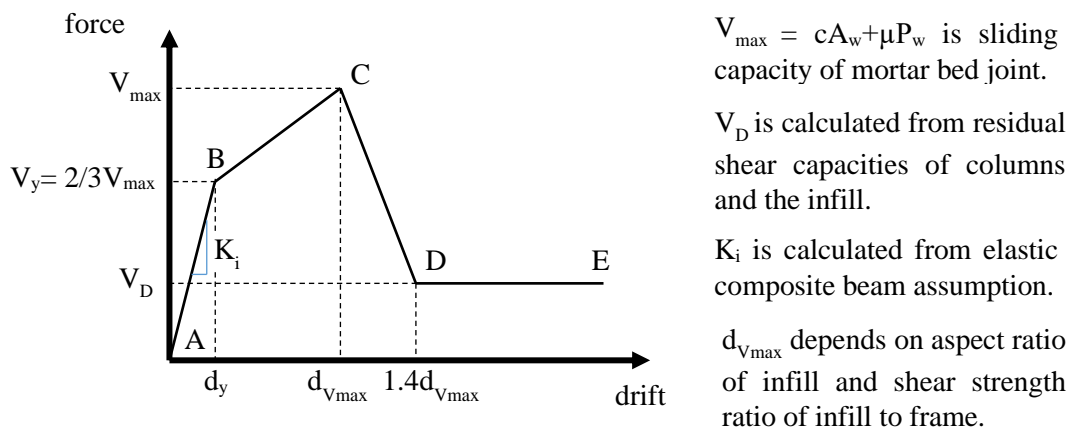


Figure 2.4. Simplified force-drift curve for infilled RC frames (Stavridis, 2009)

2.2 Database on Previous Infilled Frame Tests

A thorough literature review was done on the previous research on experimental testing of infilled frames. The major parameters of the tests and the tested specimens were documented. 214 publications, including dissertations, test reports, journal papers, and conference proceedings, were investigated. A list of publications illustrating essential information and major parameters of the investigated testing campaigns is provided in Appendix A. The publications are listed in chronological order, beginning with Ockleston's pioneering work in 1952 and continuing through January 2022.

A similar methodology utilized by Furtado et al. (2020) is followed to perform a systematic review. Firstly, references from journal papers focusing on a compilation of relevant studies were extracted considering the works of (Akin 2006; Turgay et al. 2014; Sassun et al. 2016; De Risi et al. 2018; Alwashali et al. 2018; Liberatore et al. 2018; Anić et al. 2020; Dorji et al. 2020a; Furtado et al. 2020b; Furtado and De Risi 2020; H. Huang and Burton 2020; Blasi et al. 2021; X. Lu and Yan 2021; Pradhan et al. 2021).

A reference list for each included publication was checked for other potentially relevant studies. An additional search was conducted using electronic databases

including Web of Knowledge, ASCE, Science Direct and Google Scholar using keywords related to subject.

Publications based on experimental testing of infilled frames and providing adequate information on the test campaign, material characterization, testing methodology, and test results were deemed eligible. Excluded are numerical studies and experimental studies on confined masonry walls. The gathered publications were organized with the Mendeley reference editor and read thoroughly to extract and record specific parameters (Figure 2.5). If a publication contains a series of frame tests, parameters pertaining to reference specimens (i.e., an undamaged frame infilled with a solid masonry wall without retrofit measures) were recorded. The following assumptions were made during data extraction:

- If test results for a reference specimen are published in different publications, only the one providing more details and information is accounted for. On the other hand, if a publication involves testing more than one reference specimen (i.e., not retrofitted and fully infilled frame specimens with different geometry, bay/story, wall material, etc.) and seeking details for each specimen that are available, all the reference specimens involved in the publication are included in the database.
- If scaling is not indicated but the specimen geometry is provided, the clear height of a full-scale solid wall is assumed to be around 2.5m to calculate the scaling of the specimen.
- If the bounding RC frame is said to be designed to a contemporary seismic design code, or although such a statement is absent but the provided detailing complies with seismic design rules such as stirrup densification at member ends, 135-degree bent hooks, etc. then the frame is accepted as ductile. If gravity design is implemented or seismic deficiencies are pronounced, then the frame is accepted as non-ductile.
- The material strengths corresponding to frame test days were relied upon whenever data is present. Unfortunately, there is always a time lag between

frame tests and corresponding material tests, especially for infill walls and mortar.

- For concrete compressive strength (f_c), if cube strength is provided, it is translated to cylinder strength by multiplying by 0.83. If characteristic concrete strength is given instead of material test results, mean compressive strength is calculated by multiplying f_{ck} with 1.3 as per ASCE41-17. If the compressive strength of structural members is given separately, column compressive strength is relied upon.
- The compressive strength of brick units in the vertical direction ($f_{b,v}$) is based on the gross area of the unit. A conversion is made in cases where the compressive strength for the net area and perforation ratio are given.
- The compressive strength of the infill wall ($f_{w,v}$) is based on the gross area of the wall cross-section in the vertical direction.
- If two different loading types were implemented on the reference specimen, more advanced testing method is documented (i.e., ShkT > PsD > C > M).
- The origin of the study is based on the country where the experimental campaign took place. If there is no mention of the testing lab, the country of the institution where the corresponding author works is used.
- Various loading devices and protocols were used for loading infills in the OOP direction. Some researchers utilized airbags (AirB) for uniform loading, whereas others make use of loading frames attached to hydraulic jacks capable of applying point loading (Pt) at various locations on the wall surface.
- There is no consensus on the loading protocol for coupled tests. The majority of the coupled testing campaigns involve OOP loading after testing the frame up to a prescribed IP drift level. Simultaneous application of IP and OOP loading is limited to dynamic shake table tests (ShkT) and a few studies (including this one) involving constant OOP loading plus cyclic IP loading.

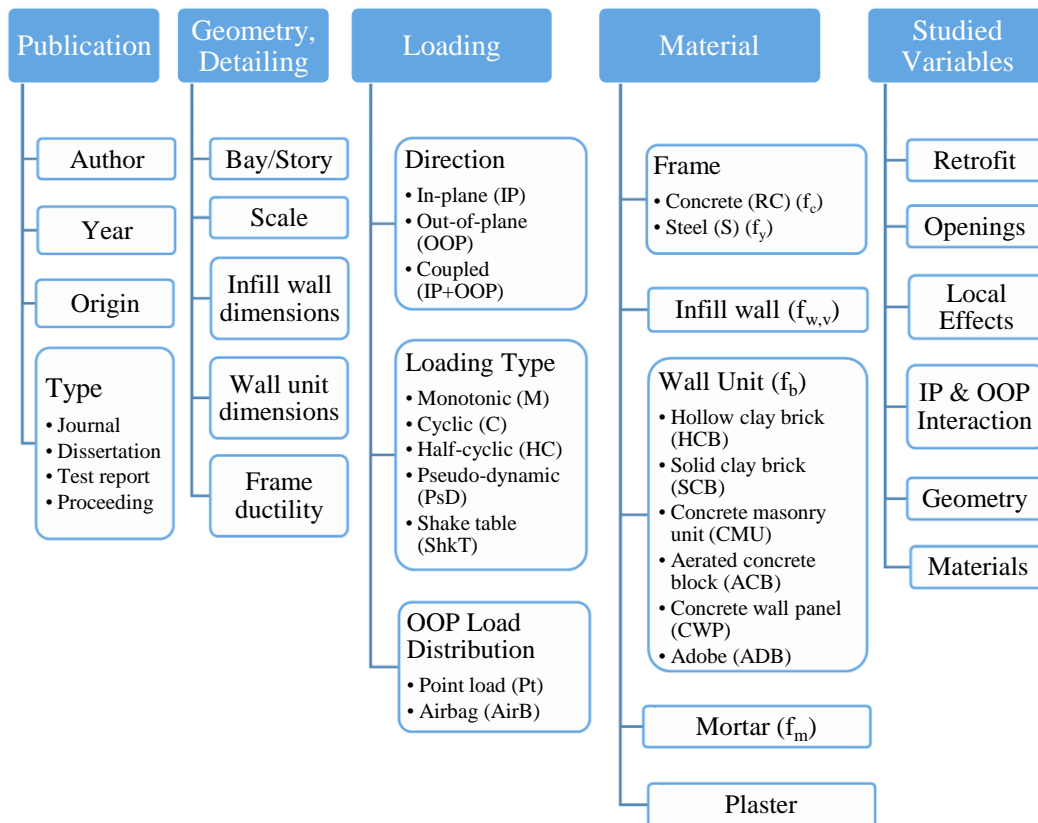


Figure 2.5. Documented parameters from selected previous experimental studies

Some variables such as publication year, origin of publication, loading direction and loading method of the collected database, are illustrated in Figure 2.6. The distribution of publication years graph reveals that 70% of the publications on experimental testing of infilled frames were conducted in the last 11 years. Nearly half of the research was conducted in Mediterranean countries such as Italy, Türkiye, Portugal, Greece, Croatia, etc., where infilled frame construction and earthquakes are popular. Most of the tests (i.e., 72%) were executed under IP-only loading conditions and using static testing methodologies such as monolithic and cyclic loading. Although seismic excitation is dynamic, due to its high cost and requirement of advanced technology, dynamic tests (i.e., shake table, pseudo-dynamic loading) were utilized in only 13% of all tests.

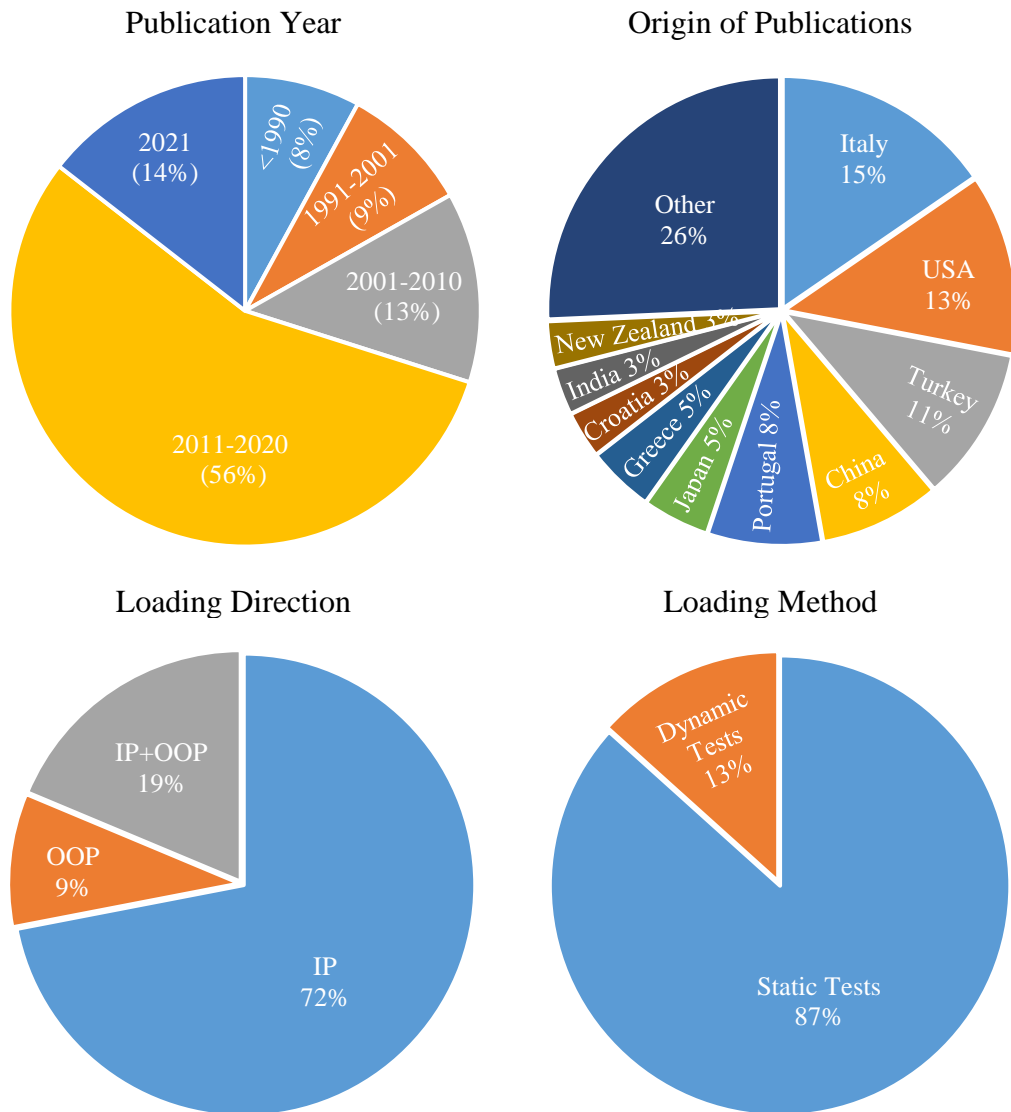


Figure 2.6. Some variables of the created database (all publications)

Figure 2.7 summarizes the distribution of selected parameters among IP only tests. It is understood that 79% of all in-plane tests were conducted on single bay, single story frames, and 77% of all in-plane tests were conducted under cyclic loading.

The distribution between deficient and code-compliant RC frames is even. Only one-fifth of tests were conducted on full-scaled test specimens. The compressive strength of tested RC frames and infill walls were 28.43MPa (standard deviation=8.94 MPa) and 8.12 MPa (standard deviation=7.60 MPa). A high standard deviation of infill

compressive strength indicates the high variability of masonry units and construction practices. Variation of the aspect ratio of tested infill walls varies evenly between 0.5 to 1.0. However, tests involving an aspect ratio less than 0.5 or higher than 1.0 comprise only 12% of all tests. Other variables investigated under in-plane loading include various retrofit techniques (isolation of infill, mesh overlays, FRP wrapping, creating horizontal slip surfaces, vertical segmentation, tie beams, etc.), openings, infill to frame strength, infill to frame connection details, infill pattern (soft story), frame ductility, tapered beam-column joints, presence of plaster and brick type.

Figure 2.8 summarizes how certain parameters are spread out among tests that use out-of-plane loading, such as OOP-only tests and coupled tests that use both IP and OOP loads. From the loading graph, it can be seen that there is no agreement on the loading devices and loading protocols for OOP tests. The total number of tests involving multi-point loading, airbag loading and dynamic loading is close. RC bounding frames were utilized in 92% of all OOP tests. Again, the vast majority (92%) of the tests were carried out on single-story, single-bay frames.

Compared to IP tests, the ratio of full-scaled testing is more common in OOP tests. Only 23% of IP tests were full-scaled, compared to 60% in OOP tests. The aspect ratio of the infill walls tested in the OOP direction is typically between 0.5 and 1.0, similar to the IP direction.

The standard deviation of the slenderness ratio, aspect ratio, and infill compressive strength is high. Other variables investigated under out-of-plane loading include prior in-plane damage, various retrofit techniques, boundary conditions (gaps under beam and column-infill interfaces), openings, workmanship, pre-compression on beam, number of leaves and connection between them, presence of plaster, and brick type.

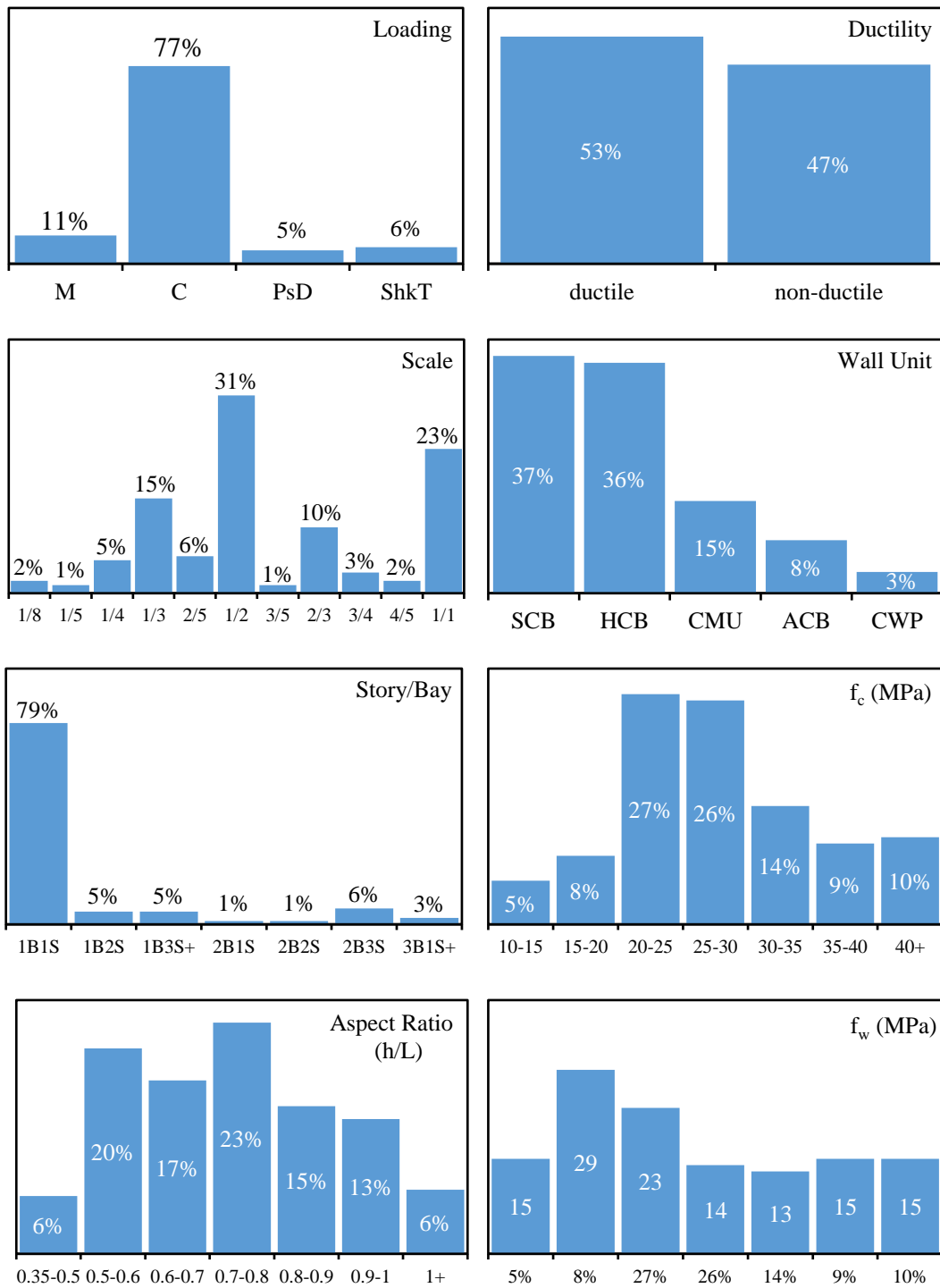


Figure 2.7. Frame specimen properties in the database tested at IP direction only

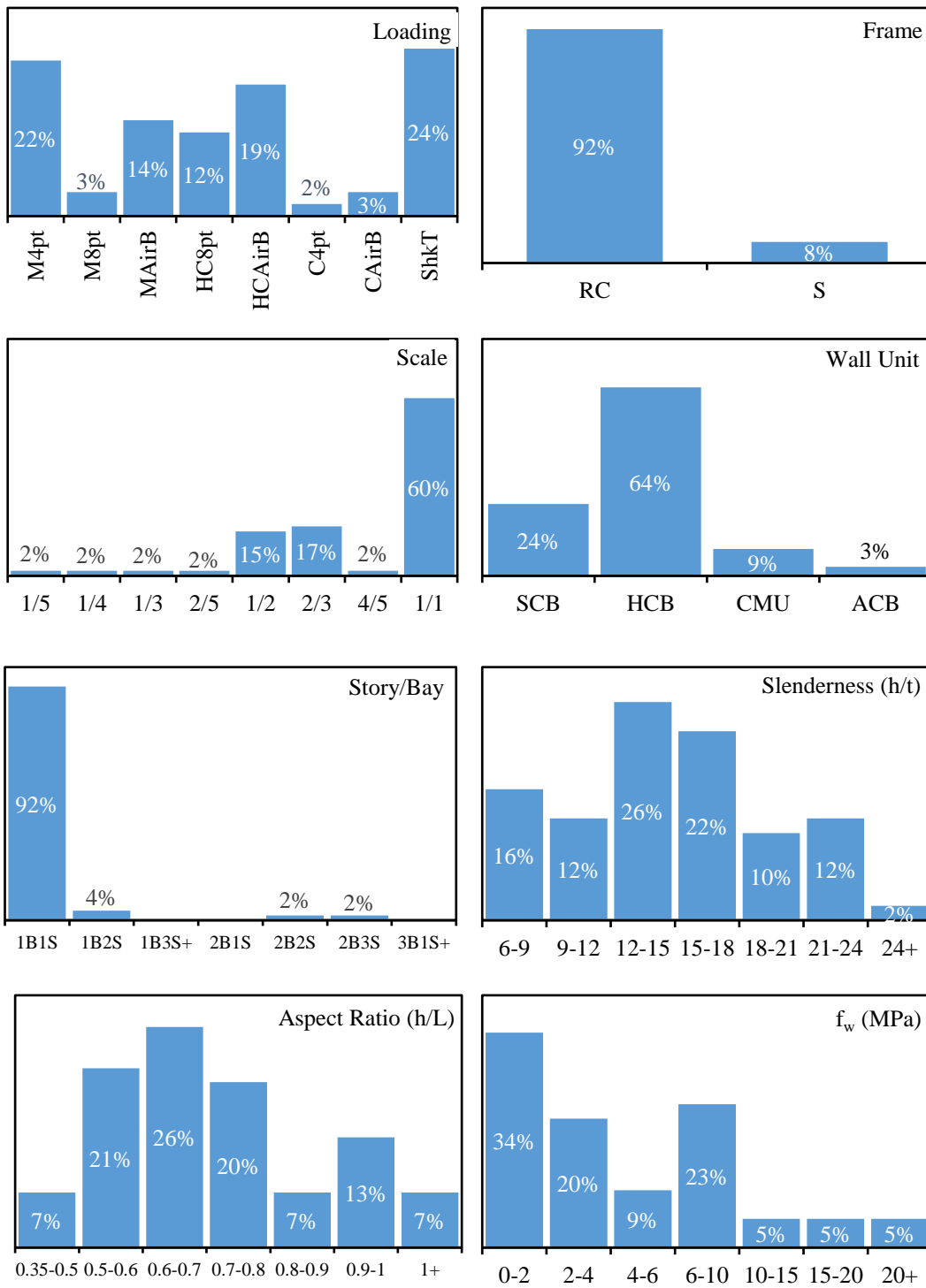


Figure 2.8. Frame specimen properties in the database tested at OOP direction

2.3 Retrofit Techniques for Infill Walls

Improving the seismic performance of interacting infill walls or isolating them from the bounding frames to prevent unfavorable interactions can effectively reduce seismic loss and enhance the resilience of buildings. Numerous studies have been published in the last decades focusing on retrofitting and strengthening infill walls (Furtado et al. 2020b). Various approaches and techniques studied in the literature can be divided into two major groups (Figure 2.9). Non-interacting methods propose isolation joints and/or gaps between the infill wall and the bounding frame aiming at canceling or delaying mobilization of infills so that their unfavorable effects are avoided and frames can be designed without accounting for infill participation. Interacting methods on the other hand promote the involvement of infills in the seismic response. Strengthening infills for a superior response or forcing them towards preferable failure modes are the techniques used to take advantage of infill contribution in terms of strength, stiffness, and increased energy dissipation.

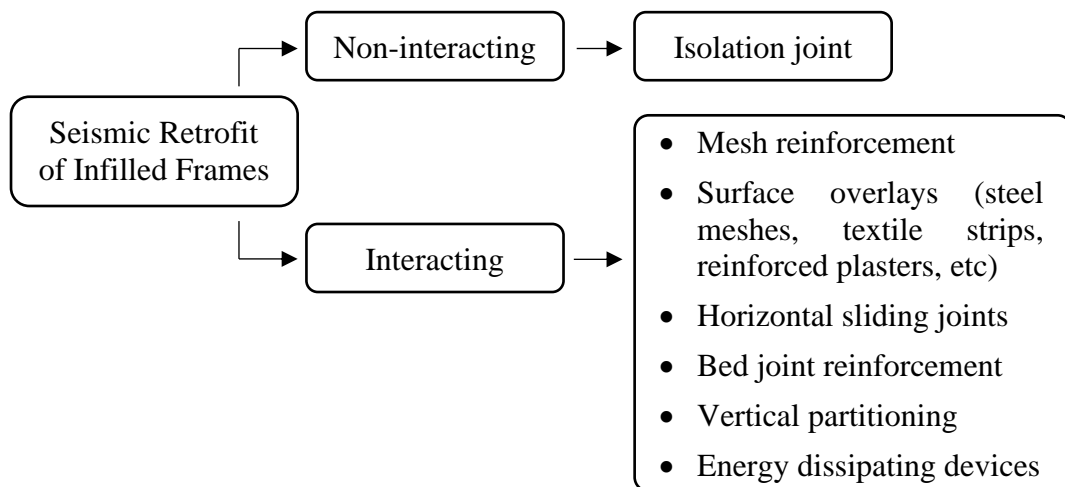


Figure 2.9. Seismic retrofit of infilled frames

Non-interacting techniques rely on disconnecting the infills from columns and the top beam allowing relative displacements in-between without interactions. The main structural challenge in non-interacting retrofit systems is to provide out-of-plane stability of the isolated wall while sustaining weather tightness, fire protection, and

acoustic insulation requirements. Different fill materials, construction practices and connection details are proposed for these purposes (Figure 2.10). Pallares (2016) proposed a seismic isolation brick, whose elastic modulus is much smaller than that of an ordinary masonry brick. By replacing ordinary bricks at the perimeter of the infill panel with the isolation bricks, the interaction between the infill wall and the bounding frame is reduced. Binici (2019) proposed sliding connectors placed inside the aerated concrete blocks attached to assemblers fixed to the inner faces of columns and beams. Marinkovic and Butenweg (2019) proposed a decoupling system with plastic profiles attached to frame members and opposing elastomeric U-profiles that provide flexibility in the IP direction as well as support for OOP loads. Erdem et al. (2021) used U-shaped steel plates attached to aerated concrete blocks and created a gap between the accompanying brick unit within the plate.

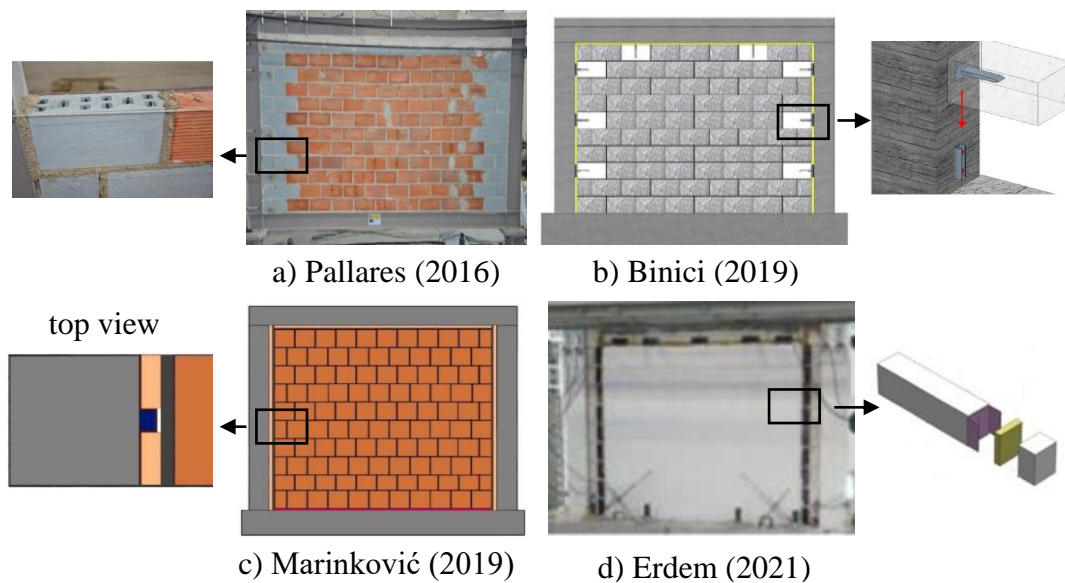


Figure 2.10. Non-interacting retrofit solutions

Mesh reinforcement is the oldest interacting retrofit technique, which involves reinforcement of infills and integration with the bounding frame. This technique simply transforms a “non-structural” infill wall into a designed structural member. Günay (2009) proposed conventional mesh reinforcement via steel bars attached to columns and beams with dowels and covered with poured or shot concrete. Bertero

and Brokken (1983) put forward the idea of strengthening the infill panel with welded wire fabric reinforcement by attaching it firmly on both sides of the infill panel using dowels anchored to the confined regions of the bounding frame (Figure 2.11).

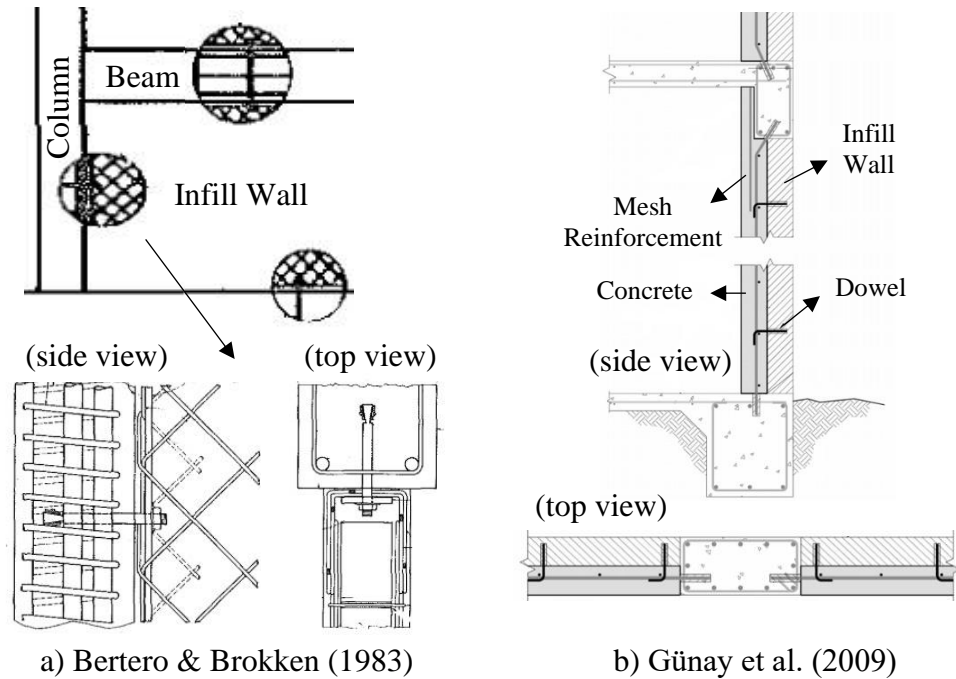


Figure 2.11. Mesh reinforcement of infill walls

Compared to the bare frame, the base shear capacities of unreinforced HCB infilled frame, external wire mesh reinforced frame with a 0.15% reinforcement ratio and external wire mesh reinforced frame with a 0.6% reinforcement ratio were increased by 182%, 274% and 564%, respectively. Considering the change in seismic demand and the increase in base shear capacity, they concluded that infilling moment resisting frames with properly reinforced panels is advantageous in the elastic range in reducing displacement demands and base shear demand/capacity ratios. When large inelastic deformations are concerned, infilled frames with external reinforcement outperform bare frames in developing large inter-story displacement ductility ratios with much lower drift demands.

Horizontal sliding planes created along selected bed joint layers are implemented to divide the infill wall in the vertical direction. Brittle failure modes associated with the formation of a typical diagonal compression strut are prevented, and sliding failure along slip planes is promoted. Forcing the infill wall into sliding failure increases energy dissipation capacity under increasing drift levels and avoids localization of strut forces that result in shear failure of frame members.

Morandi, Milanesi and Magenes (2018) proposed plastic sliding joints laid in the mortar bed joints to partition the masonry walls into four horizontal subpanels. Mısır (2015) used hollow clay bricks with a dry locking mechanism. Preti, Migliorati and Giuriani (2015) laid wooden planks along selected mortar joints (Figure 2.12).

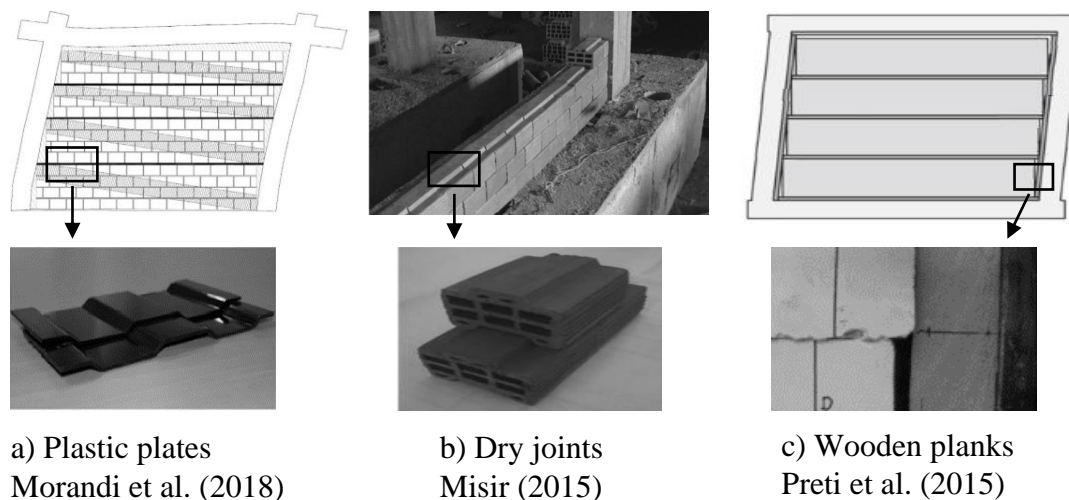


Figure 2.12. Horizontal partition of infill walls with sliding joints

The surface overlay is the most widespread application among interacting retrofit techniques. The overlays can be applied in bands or strips of various orientations or over the full surface of the wall (Figure 2.13). Steel meshes and plates, fiber reinforced polymer (FRP) fabrics, textile reinforced mortars (TRM) and engineered cementitious composites (ECC) are attached to the wall surface by spraying, using adhesive agents and/or anchors. Surface overlays not only improve the seismic behavior against in-plane loads but also reduce the vulnerability of the panel in the out-of-plane direction.

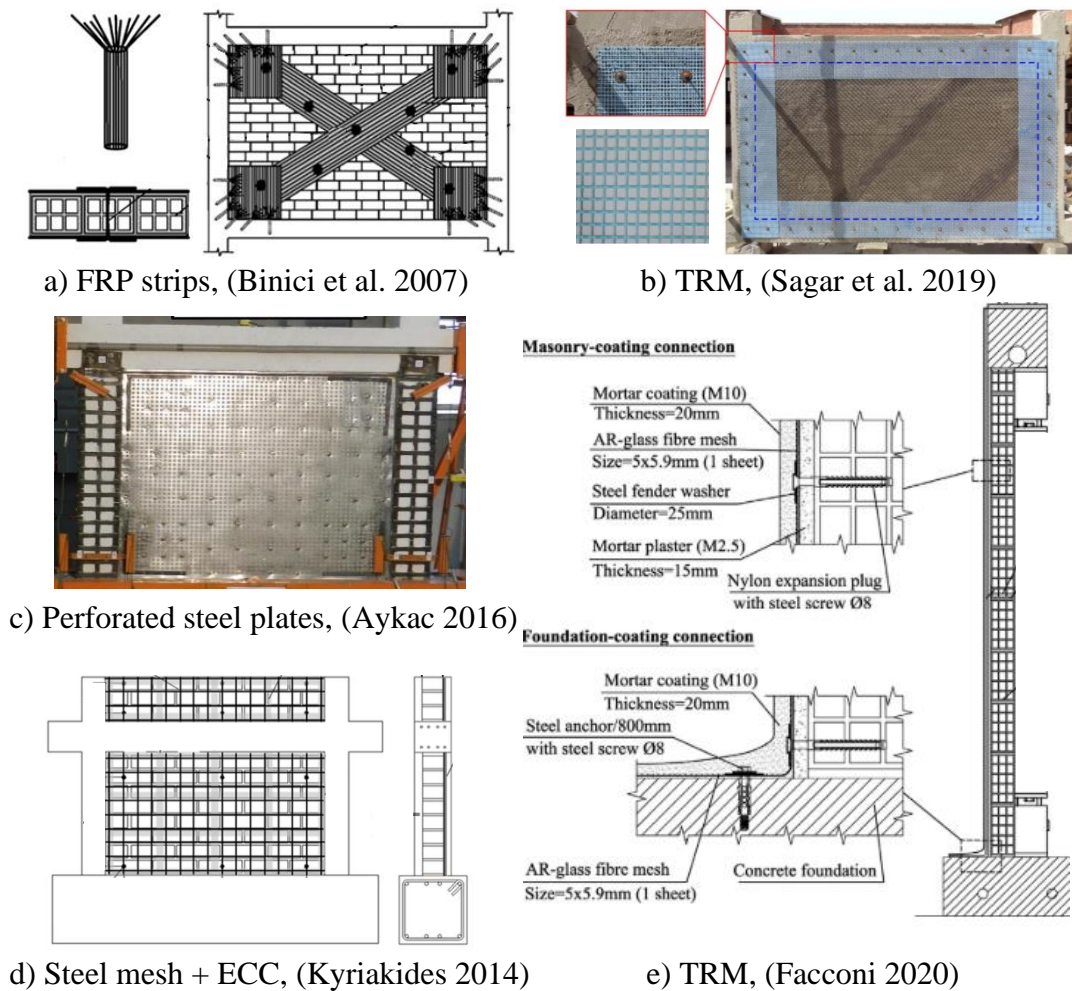


Figure 2.13. Surface overlay of infill walls

Another seismic retrofit technique is to partition infill walls in the vertical direction. The main advantage of vertical splitting of the masonry panel is to increase the aspect ratio of the subpanels, which would prevent the formation of a single compression diagonal and alter the shear dominated deformation mode of the panel to bending, thereby improving its ductility. The lateral stiffness of the wall panel was also decreased, reducing the lateral force demand and damage to the infill wall. Tasligedik and Pampanin (2017) divided the infill wall with channel steels and vertical gaps into several rocking wall pieces, reducing the damage to the wall and the frame. Preti and Bolis (2017) proposes wooden planks equipped with steel connection plates at the ends. Yuen et al. (2018) suggests using polyurethane foam

to fill isolation gaps between the infill subpanels and relying on one-way arching in the vertical direction against earthquake-induced out-of-plane inertial forces. Jiang, Liu and Mao (2015) utilizes internal RC tie columns and horizontal steel tie members to partition the infill and provide out-of-stability (Figure 2.14).

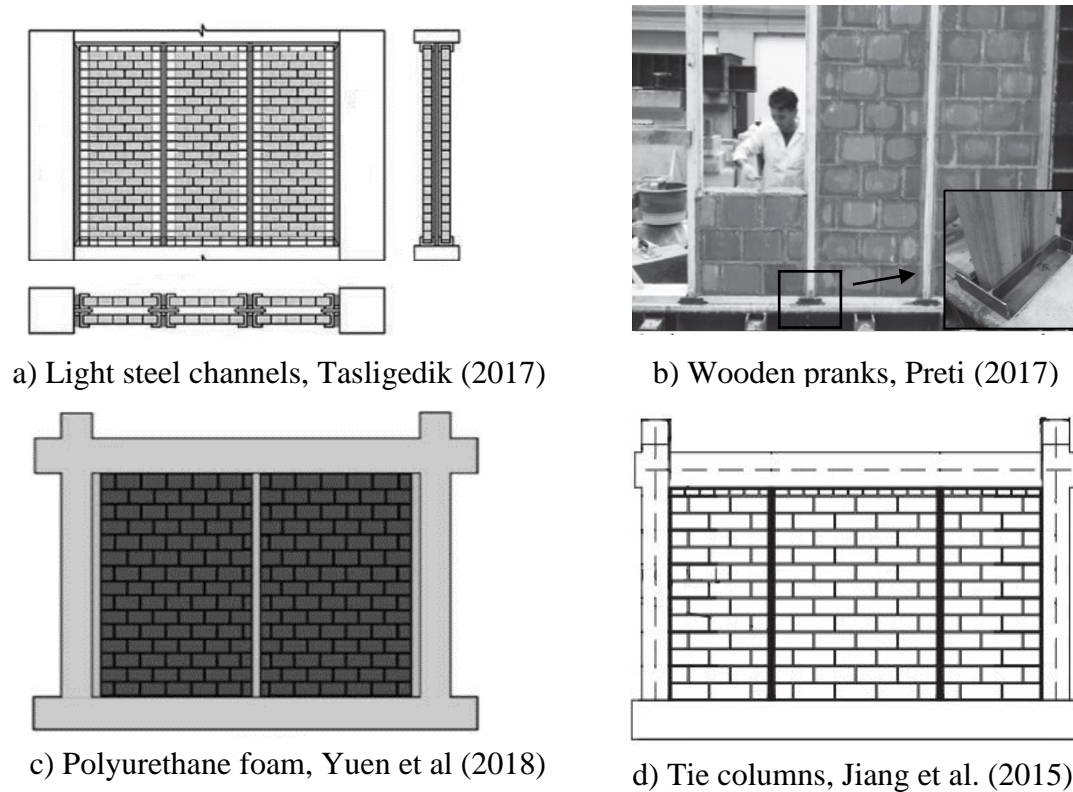


Figure 2.14. Vertical partition of infill walls

Bed joint reinforcement is a common practice for new construction in some countries such as China and Iran. Silva, Vasconcelos and Lourenço (2021) introduced truss-like light reinforcement connected to the frame with angle connectors placed along the bed joints of infill walls with dry vertical joints. Su and Cai (2017) used connection steel rebars as required by the Chinese Seismic Code (GB50011-2010 2010) that are fixed inside the inner faces of columns using high strength adhesive (Figure 2.15).

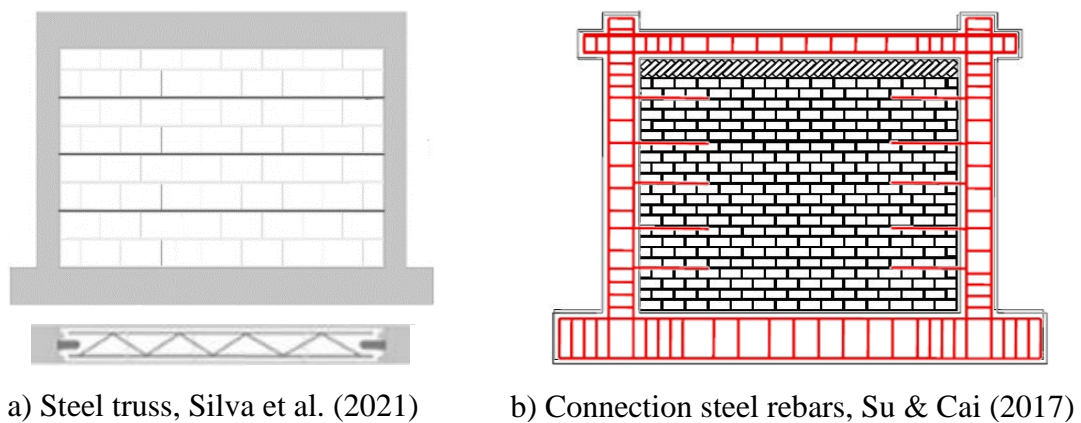


Figure 2.15. Bed joint reinforcement of infill walls

Integration of energy dissipating devices within infill walls or at contact surfaces is another retrofit solution. Lu and Zha (2021) propose a vertical gap and energy dissipating metal connectors to improve the energy dissipation capacity of ordinary infills. The vertical gap in the middle divides the infill panel into two parts. OOP stability is sustained with retainer clips. Aliaari and Memari (2007) proposed a replaceable structural fuse element called seismic infill wall isolator subframe (SIWIS) in between the infill wall and the bounding frame where nonlinear damages are concentrated (Figure 2.16).

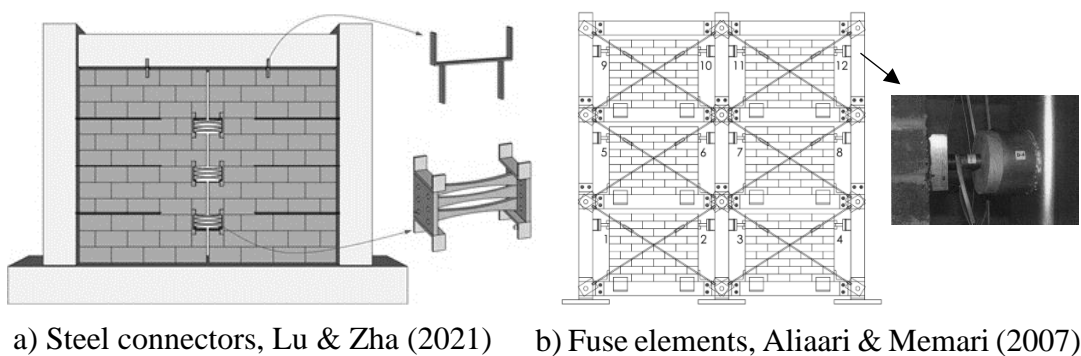


Figure 2.16. Energy dissipating infill systems

2.4 Code Approaches on Design and Assessment of Infill Walls

This chapter reviews seismic code and guideline considerations on the design and evaluation of infill walls under in-plane and out-of-plane seismic actions. Whilst infill walls are not specified as structural members and not typically included in structural design, existing building codes address the influence of the panel on structural performance by introducing design recommendations, exclusive drift limits and simplified formulations (Blasi, De Luca, and Aiello 2018).

Dorji (2020b) examined the approach of eleven national codes to the analysis and design of masonry-infilled frames and concluded that regulations could be classified into two groups. The first approach isolates infill from bounding frame members via gaps and avoids the complexities involved in analyzing infilled frames. However, there is no consensus on the width of the gaps recommended by different codes. The second group takes advantage of the high stiffness and strength of the masonry infill. In this technique, an equivalent-strut modeling strategy is mostly recommended. It is shown that the strut model suggested in each of the codes is different.

Turkish Practice:

The Turkish Building Earthquake Code (2018) is utilized for the design of new construction, assessment of existing buildings, and retrofit design in Türkiye. According to TBEC2018, infill walls do not need to be included in the structural model during the design stage if inter-story drift limits based on the infill wall to bounding frame connection detail are not exceeded. A flexible joint (Figure 2.17) isolating the infill wall from bounding columns and the upper beam is suggested for non-participating infills. In case such flexible joints are present, inter-story drift calculated for RC buildings under an unfactored ($R=1$) earthquake load is limited by $(0.016/\lambda)$. If the wall to frame connection is rigid, story drift is limited with $(0.008/\lambda)$ where λ is the ratio of spectral acceleration at the fundamental period of the building corresponding to design level ($T_R=475$ years) and serviceability level ($T_R=72$ years) earthquakes. λ ratio depends on geographic coordinates, soil class and the

fundamental period of the building and its value is usually between 0.3 and 0.7 (Murat Bikçe and Erdem 2019). If the provided limits are not satisfied, earthquake load calculations should be repeated by increasing the rigidity of the structural system taking infill walls into account. However, neither complete constructive guidelines are provided for the isolation gap and the U-shaped steel plate, nor modeling details are provided for infilled walls unless the wall is strengthened with steel mesh or FRP jacketing.

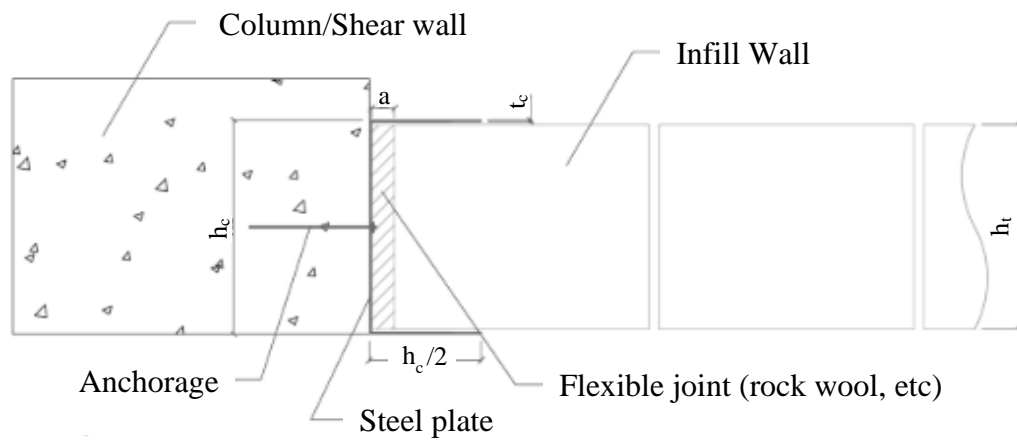


Figure 2.17. A sample detailing for flexible joints, TBEC (2018)

Chinese Practice:

The Chinese Seismic Code (GB50011-2010 2010) requires infill walls to be in full contact with the bounding frame to achieve composite action. Jiang, Liu and Mao (2015) states that in Chinese engineering practice, the interaction between infill walls and the main structure is ignored in seismic analysis and only a period reduction factor is applied for rigidly connected infill walls. Constructional measures were taken by the Chinese seismic code against the unfavorable effects of infill walls on the seismic performance of the main structure. Irrational arrangements were avoided by stating that the plan and vertical layout of infill walls should be uniformly symmetrical and should avoid weak-story and short-column damages. Light wall materials are primarily recommended for wall construction.

Constructional measures recommended in GB50011-2010 for enhancing seismic response are summarized below:

1. Infill walls should be connected to columns at every other 500mm with steel tie bars embedded into concrete and extended into the wall at least 500mm.
2. Horizontal tie beams should be used when the wall height exceeds 4m.
3. Constructional columns should be placed in case the wall length is over 8m or twice the wall height
4. Infill walls between staircases and pedestrian passages should be strengthened with a steel mesh mortar layer.
5. Gable walls at the roof level should be supported with ring beams.

Alternatively, disconnection of the infill wall with the frame is allowed via flexible joints if out-of-plane stability is ensured.

European Practice:

In the design of new buildings according to EC8-Part1 (EN1998-1 2004), the contribution of infills to the strength and stiffness characteristics of the load-bearing structure is neglected. Structural models based on bare frames are used for analysis (Figure 2.18) where infill walls are considered as additional masses and vertical loads only. Damage control of infill walls under service earthquake is exclusively accounted for an inter-story drift limitation (i.e. $\delta_{DLS}=0.5\%$, 0.75% and 1.0% for brittle, ductile and non-interacting non-structural elements, respectively) imposed on the bare frame whereas safety verification in the out-of-plane direction is required under design level earthquake. Cracked stiffness values are recommended for drift calculations based on linear elastic analysis.

Additionally, precautions against possible shear failure of columns under compression strut induced localized forces and irregularity in plan or elevation produced by the infills are addressed in EC 8-Part3 (EN1998-3 2005). However, no definitions are provided on the modeling details and the capacity of infill walls.

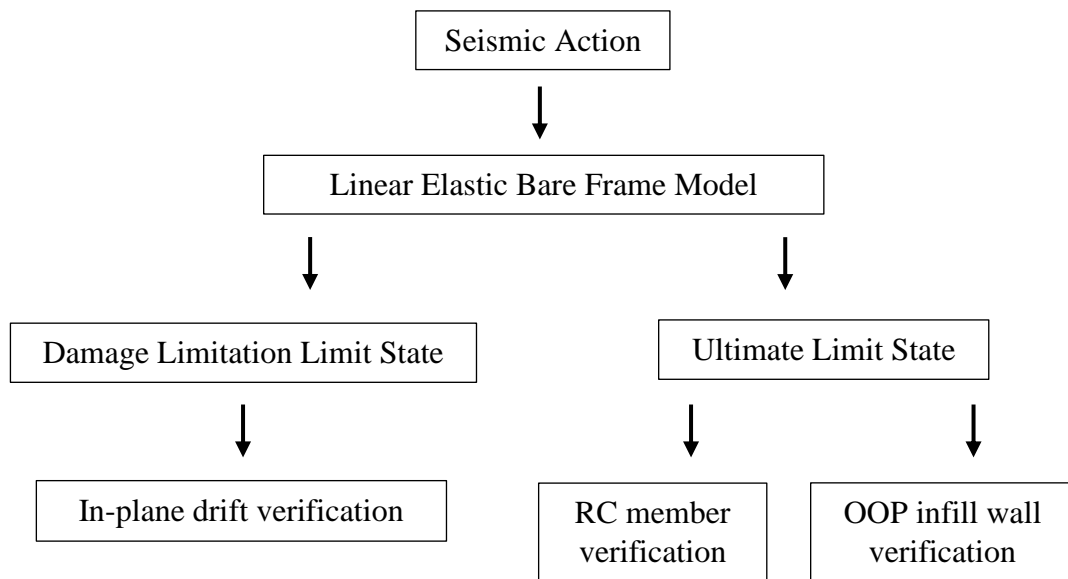


Figure 2.18. Design procedure for infill walls for new construction in the EU

American Practice:

ACI 530 - Building Code Requirements and Specification for Masonry Structures (2013) supplements the legally adopted International Building Code (2018) for new construction and covers the structural design of structural as well as non-structural masonry elements such as infill walls. Appendix B is devoted to the design of masonry infills. ACI 530 differentiates between participating and non-participating infills. Participating infill walls should be designed and detailed in order to actively resist in-plane and out-of-plane seismic forces, whereas non-participating infill is only checked for out-of-plane stability (Figure 2.19). Non-participating infills need to be isolated from the lateral force-resisting system with isolation joints placed at the sides and the top of the bounding frame. Isolation joints need to be filled with materials not able to transfer loads but capable of accommodating inelastic frame displacements of not less than 9.5mm. In order to sustain OOP stability, connectors spaced at most 1.22m apart should be attached to the frame and designed with respect to ASCE 7-16 (2016). ASCE 7-16 defines simple and comprehensive methods for out-of-plane seismic load calculation acting on infill walls. In the design load calculation, dynamic and structural properties of the infill walls such as energy

dissipation capacity (R_p), dynamic amplification with the structure (a_p), and horizontal floor acceleration are taken into account.

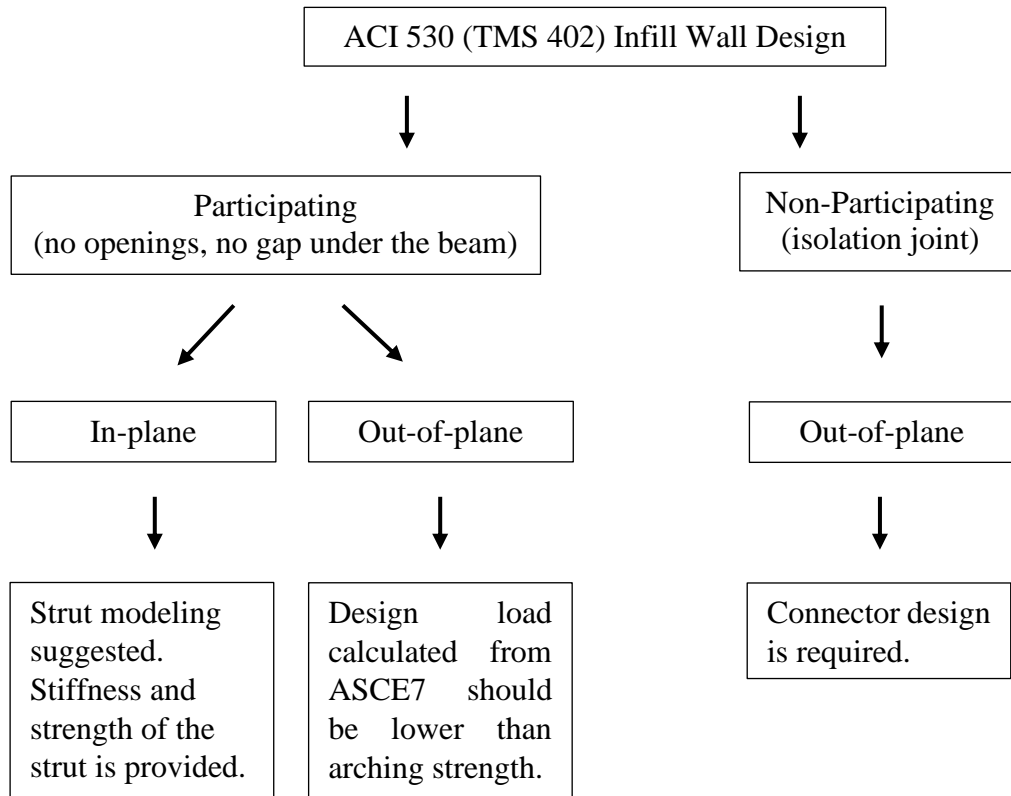


Figure 2.19. Design procedure for infill walls for new construction in the USA

Participating infills are infills without any openings and/or gaps under bounding beams and columns. The maximum ratio of wall height to wall thickness of participating infills is limited to 30. They are considered a part of the lateral force-resisting system. Compression only single equivalent strut model is suggested for participating infills. In-plane design forces in equivalent struts are determined from elastic analysis of braced frames and a simple equation to calculate out-of-plane total seismic design force (F_p) which acts uniformly distributed on the infill wall surface is provided. Additional shear created by an equivalent compression strut is also accounted in the shear design of column and beam ends by increasing design shear and design moment by %10.

For seismic evaluation and retrofit of existing buildings, ASCE41 (2017) classifies the infilled frames based on the relative strength and stiffness of the infill and bounding frame and provides detailed guidelines to model and assess the performance of infill walls in the IP direction. Masonry infill panels are considered primary elements of a seismic-force-resisting system. The use of simplified numerical models with diagonal struts to simulate the effect of the infill is permitted. The procedures for the determination of stiffness, strength, load-deformation characteristics and displacement capacities of infilled frames are provided.

ASCE41 also addresses acceptance criteria for infills exposed to OOP demands. Permissible slenderness ratios for ranges of spectral response accelerations are provided. Finally, a failure envelope based on uncoupled force versus demand ratios in the IP and OOP directions is provided for the consideration of bidirectional loading.

New Zealand Practice:

Similar to American codes, NZSEE (2017) provides options for interacting or non-interacting infills. Chapter 7 of Part C (detailed seismic assessment) is devoted to moment resisting frames with infill walls. Equations for the calculation of OOP demands and capacities are given. In the IP direction, nonlinear finite element analysis accounting for openings, post-yield cracking, and cyclic degradation of masonry is permitted unless validated with experimental data. Alternatively, a generalized strength deformation relationship for infills is given to be used for simple strut models. Calculations of additional shear demands on beams and columns of bounding frames adjacent to solid infills are illustrated.

2.5 Analytical Strut Modeling of Infill Walls

Infilled frames resist analytical modeling. Asteris (2011) states that: “the highly variable nature of the material, the large number of parameters involved, and in particular the presence of openings in infill walls make the modeling of this structural

element very difficult; in most of the cases it is therefore considered a nonstructural one.” Similarly, Shing and Mehrabi (2002) stated that despite more than 60 year-long effort, there are neither well-developed design recommendations nor well-accepted analytical procedures for infilled frames.

In addition to complexities originating from nonlinear RC frame response (i.e. cracking of the concrete, yielding of steel, local bond slip, etc.), nonlinearities arising from cracking and crushing of infill material and loss of contact between the frame and the infill make the modeling of infilled frames challenging. Although refined finite element micro models have been proposed to account for all these nonlinearities, simple approaches are required for large models.

The well-known simplest analytical idealization of infill is diagonal strut modeling. The idea behind the strut model is simple. At a low lateral load level, infill panels and RC frames remain in contact and act as a monolithic system, enhancing the global stiffness of the building. As the load increases, contact between the masonry panel and the surrounding frame is lost due to the separation of the infill from the frame as a result of a lack of tension resistance in between. At this stage, infill frame interaction is restricted to compression corners, which are classically idealized as a frame with an equivalent compression strut (G. Michele Calvi, Bolognini, and Penna 2004).

Strut models present a simple way to simulate the complex response of infilled frames under lateral loads. In this model, a diagonal strut connecting the loaded corner with the opposite diagonal is added to the system, idealizing the resistance of infills. The material and the thickness of the equivalent strut are assumed to be the same as the infill and the main parameter determining the strength and stiffness contribution of the infill remains the width.

Various strut width formulas proposed by different researchers are illustrated in Table 2.1 below.

Table 2.1 Equivalent strut models proposed by various researchers

<i>Author</i>	<i>Strut Width</i>	<i>Remark</i>
Holmes (1961)	$0.333 \times d$	The first model being proposed
Smith & Carter (1969)	From design charts usually $0.1d < w < 0.25d$	The non-dimensional relative stiffness parameter is the main parameter defining strut width: $\lambda = h^4 \sqrt{\frac{E_w t_w \sin 2\theta}{4EI h_w}}$ $E_w, t_w, h_w \rightarrow$ Elastic modulus, thickness and height of infill $EI \rightarrow$ bending stiffness of column $\theta \rightarrow$ angle of diagonal strut to horizontal
Mainstone (1971)	$0.175\lambda^{-0.4} \times d$	This equation was also utilized by FEMA-274 (1997)
Hendry (1981)	$0.5\sqrt{[\alpha_h + \alpha_L]}$	$\alpha_h = \frac{\pi^4}{2} \sqrt{\frac{E_c I_c h_m}{2E_m t \sin 2\theta}}$, $\alpha_L = \pi^4 \sqrt{\frac{E_c I_b L}{2E_m t \sin 2\theta}}$ Also used by CSA S304 (2004)
Liau & Kwan (1983)	$\frac{0.95 \sin 2\theta}{2\sqrt{\lambda}} \times d$	Valid for $25^\circ < \theta < 50^\circ$
Paulay and Priestley (1992)	$0.25 \times d$	Conservative value for practical design
Flanagan and Bennett (2001)	$A = \frac{\pi t_w}{C\lambda \cos \theta}$	Area of strut changes with empirical constant (C) depending on the IP drift

Bending moments and additional shear imposed on member ends are often underestimated in single strut models because the lateral forces are resisted by the compression diagonal. As a result, multiple strut models (Figure 2.20) are proposed for a better estimation of force distribution and better handling of the influence of openings on the response (Asteris et al. 2011).

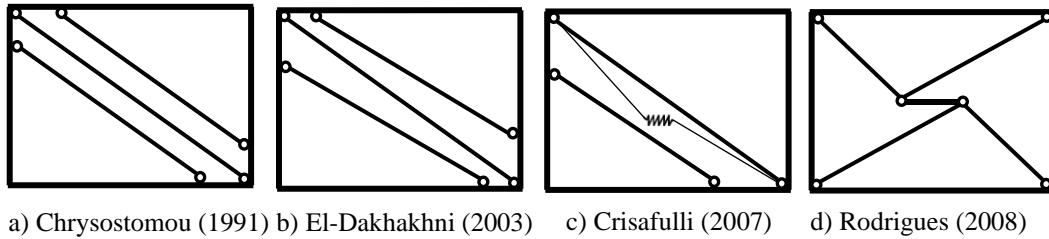


Figure 2.20. Multiple strut models

Infilled frame structures do not exhibit an elastic-perfectly plastic response due to stiffness and strength degradation under cyclic loads. Experiments have shown that the strength and stiffness of infills degrade rapidly under reversed cyclic loadings (Paulay and Priestley 1992). Moreover, opening and closing of cracks on the wall surface and changing of contact length under increasing displacement reversals result in a unique hysteresis shape known as pinching. Thus, different hysteresis models have been proposed for the idealization of the infill response under cyclic loadings (Figure 2.21).

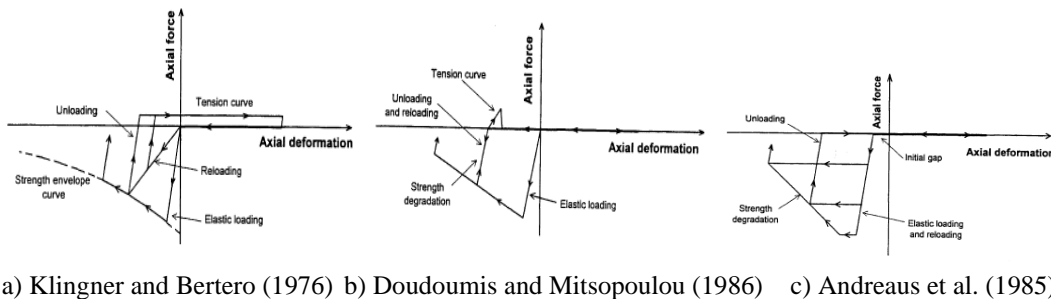
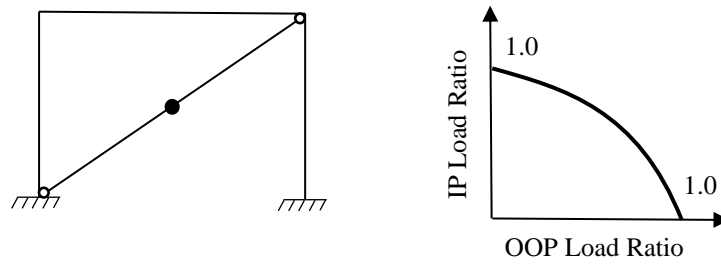


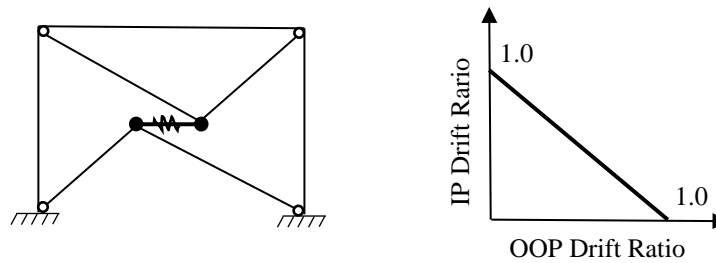
Figure 2.21. Hysteresis models for equivalent strut models

More recently, strut models accounting for coupled loading have been proposed. Mosalam and Gunay (2015) proposed a single strut model with a progressive collapse algorithm via an element removal mechanism where a yield interaction curve between IP and OOP displacement is defined through a convex downward $3/2$ power curve adopted from the strength interaction suggested by Kadysiewski and Mosalam (2009).

On the other hand, Furtado et al. (2016) proposed an equivalent bi-diagonal strut macro model where the failure of the infill, which is adopted by an element removal algorithm, is determined by a linear interaction curve between IP and OOP displacement capacities (Figure 2.22).



a) Mosalam and Günay (2015)



b) Furtado et al. (2016)

Figure 2.22. Infill strut models accounting for IP-OOP interaction

CHAPTER 3

EXPERIMENTAL PROGRAM

A total of 22 half-scaled RC frame tests conducted within the context of the testing campaign are illustrated in Table 1.1. This chapter concerns constructional details and material characterization of the tested infilled frame specimens, test setup, instrumentation and loading protocols.

3.1 RC Frame Specimen

All frame tests were conducted on identical RC frame specimens. The design, scaling and construction details of frame specimens are illustrated below.

3.1.1 Design

The design of the RC frame specimen was carried out as per the Turkish Earthquake Code (2007) considering a 5-story prototype building (Figure 3.1) located in the first seismic zone ($PGA=0.4g$). The building was designed to high ductility requirements of TEC2007 where seismic design rules such as capacity design, strong column-weak beam, ductile detailing of ties and confinement of critical sections were followed. The response reduction factor, R was considered to be 8.0 to match the high ductility level. To decide the seismic weight of the building, dead load (G) plus 30% of the live loads (Q) were considered which resulted in an average axial load ratio of 0.175 (i.e. $N_c/A_c f_c$) on the ground story columns. The contribution of infills to structural response under lateral loads and the contribution of flanges to the beam capacity was ignored as a standard design practice. The grade of concrete used for the building is C25, which corresponds to a 28-day characteristic compressive strength of 25 MPa. The reinforcement bars used are of grade S420, which

corresponds to characteristic yield strength of 420 MPa. Column dimensions, beam dimensions and slab thickness are taken as 40x40cm, 30x40cm and 14cm, respectively.

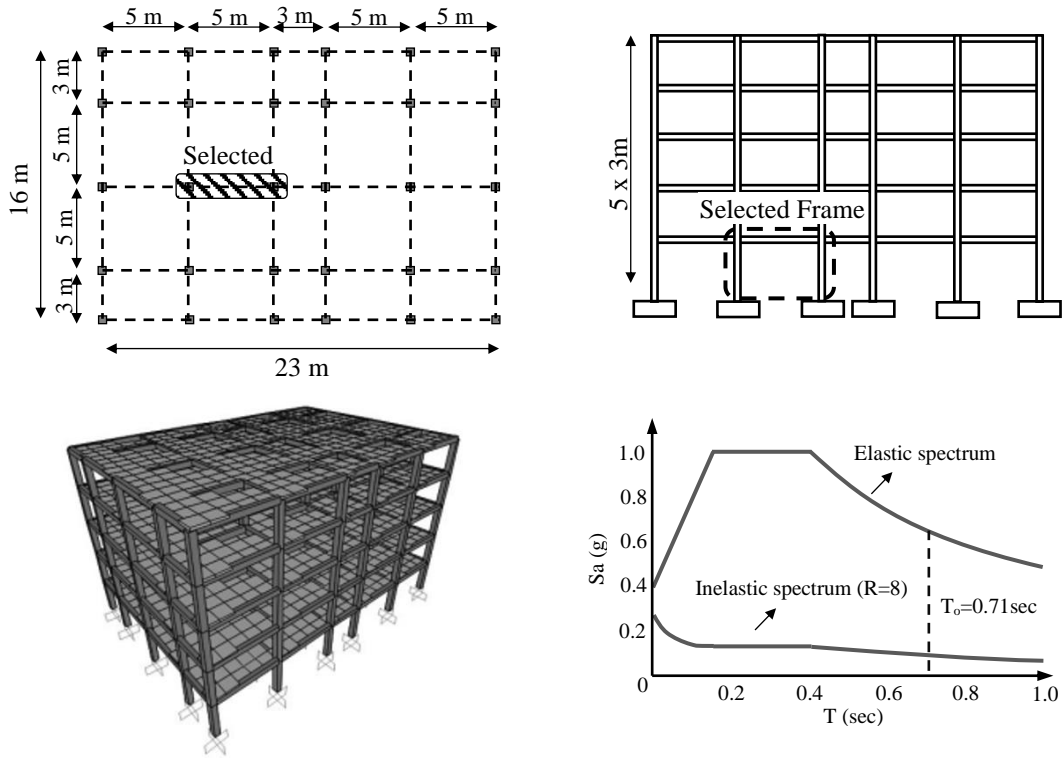


Figure 3.1. Prototype Building

A single frame located at the inner bay of the ground story is selected and scaled to half to represent the frame specimen. The half-scaled test specimen dimensions and reinforcement details are shown in Figure 3.2. The height of the specimen is 1500 mm (1435 mm from the top of the foundation beam to the geometric center of the flanged beam), and the span is 2500 mm. The column sections are 200 mm \times 200 mm, the beam section is 150 mm \times 200 mm, and the foundation beam section is 550 mm \times 400 mm. The top 70 mm of the beam is flanged due to the slab. The slab width is 1000 mm. The thickness of the concrete cover from the end to the bar center is 20 mm for all members. The spacing of the hoops within 300 mm of the beam or column ends is 50 mm, and the spacing of the hoops in the middle of RC members is 100 mm. Deformed bars with 8mm nominal diameter are utilized for longitudinal

reinforcement and plain bars with 6mm nominal diameter are utilized for transverse reinforcement. The gross reinforcement ratio in the columns and the beam is 1.0%. The ratio of tensile reinforcement in the beam is 0.56%.

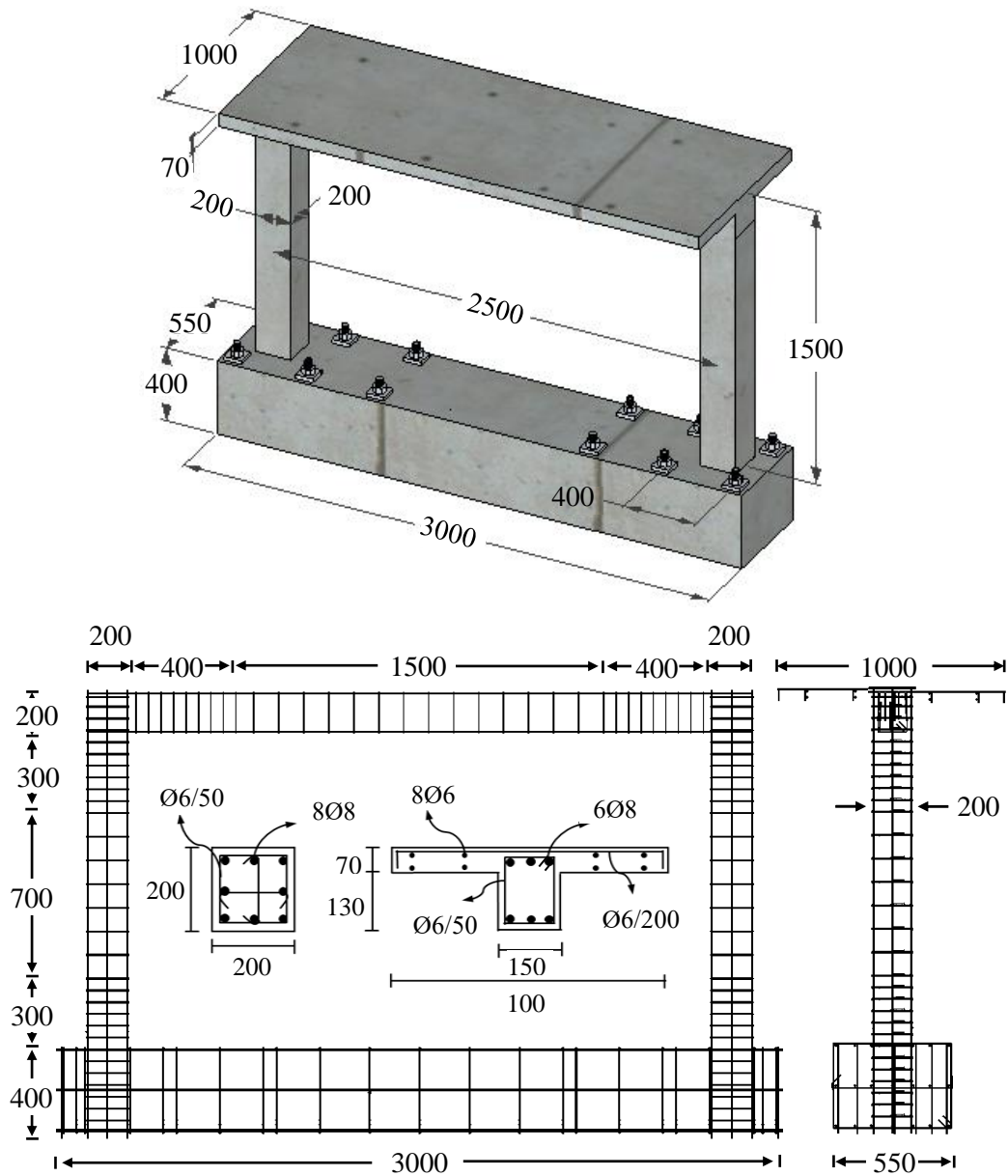


Figure 3.2. The specimen dimension and reinforcement (All units in mm)

To better represent actual loading conditions of the selected subframe, weight blocks were placed on top of a flanged beam representing a distributed slab loading of 10.25kN/m. Vertical axial loads applied concentrically on top of both columns were

arranged considering the compressive strength of each test specimen such that the resulting axial load ratio of columns (i.e. N_c/f_cA_c) was equated to 0.175 corresponding to the axial load ratio of the ground story columns of the 5 story prototype structure. The applied compressive load increased the cracking moment as well as the moment capacity of the columns and prevented the columns from developing tension under lateral excitations.

In order to calculate the moment capacities of the column and beam sections of the scaled specimens, XTRACT (Chadwell and Imbsen 2004) section analysis software was utilized. The influence of the flange as well as confinement of transverse reinforcement on the section capacity is accounted in section modeling. Material definitions of concrete and reinforcing steel were made according to TBEC2018 considering material test results (Figure 3.3).

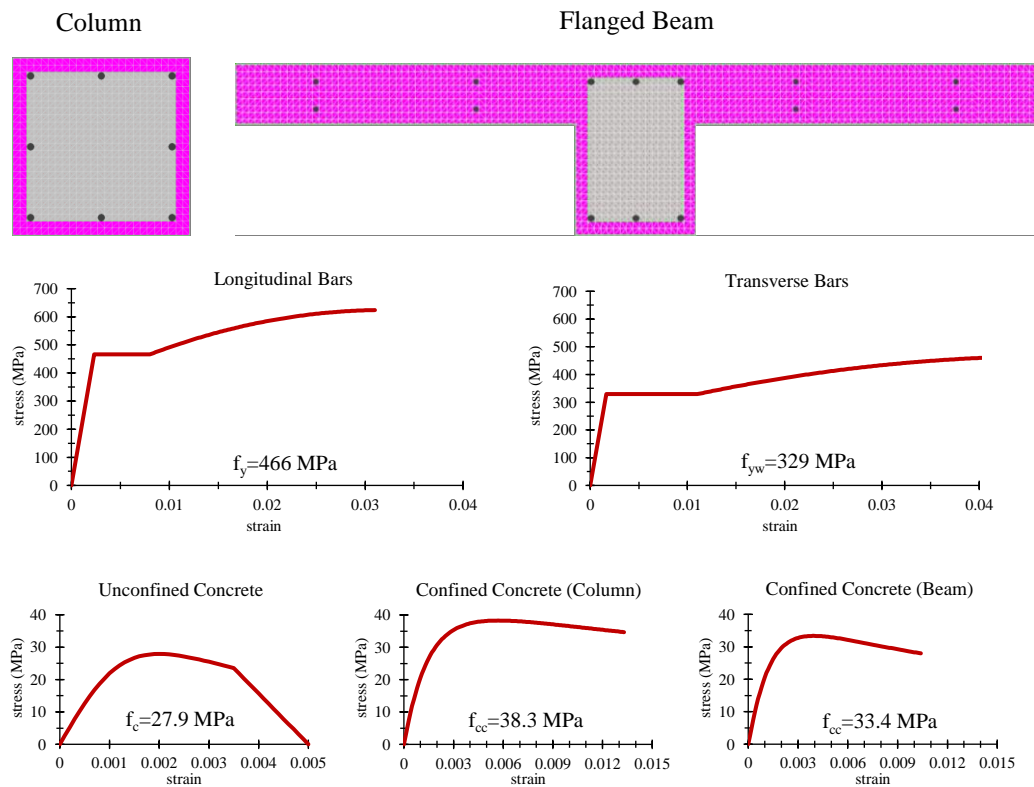


Figure 3.3. Member sections and materials for bare frame specimen

Moment curvature and interaction diagram for columns and the flanged beam are illustrated in Figure 3.4. Although strong column-weak beam principles of TEC2007 ensuring a minimum 20% increased capacity for the column was followed, when flanged section dimensions and additional reinforcement of the slab were accounted for, beam capacity was calculated close to the column capacity. The axial compressive load corresponding to $0.175f_cA_c$ is taken as 193 kN in the moment-curvature analysis of columns. The ultimate moment capacities of the columns and the beam were calculated as 28.2 kN.m and 19.5 kN.m (-27.2 kN.m), respectively.

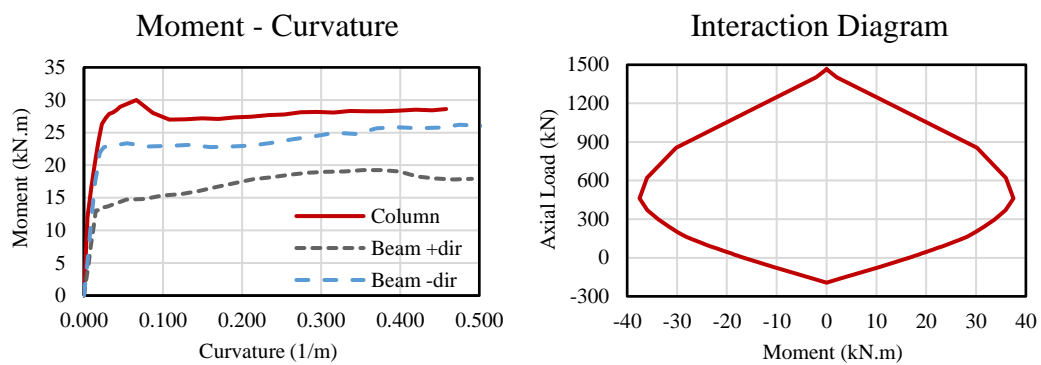


Figure 3.4. Column and beam section capacities of bare frame specimen

3.1.2 Scaling

Due to the limitation of available facilities, a scaling factor of two was adopted for frame specimens. Section and frame dimensions were scaled by half. Same axial load ratio (i.e axial load divided by the compressive strength of concrete) of the prototype structure was sustained by arranging the vertical load on the columns of the scaled test specimen. Longitudinal and shear reinforcement ratios of the scaled RC members were arranged to be the same as the prototype counterparts. Material properties were sustained as the same. The maximum aggregate size was selected 11.2 mm in order to consider the scale effects in the fracture process zone (Saouma et al. 1991). The scaling for the frame specimen followed the similitude requirements for static inelastic modeling of reinforced concrete structures (Harris and Sabnis 1999) as presented in Table 3.1.

The drawbacks of scaling for the laboratory tests of reinforced concrete specimens are identified by Brokken and Bertero (1981) as such: “Many parameters are greatly influenced by model scale. For example, aggregate interlock plays an important role in the behavior of cracked regions, having a potentially large effect on energy dissipation characteristics. Also, the bond properties of reinforcement vary with the bar size. Furthermore, the effects of fabrication errors increase as the scale is decreased. Hence geometric scaling introduces modeling errors, some of which cannot be avoided. Thus, the sub assemblages should be modeled to the largest scale which can be accommodated, ideally full size.” On the other hand, Lu et al. (1999) stated that half scale was adequate to predict the load-deformation response of full-scale companion provided that the member sizes and material properties were detailed to be compatible with the similitude law. As a matter of fact, as illustrated in Figure 2.7, among 154 in-plane only tests which are also listed in Appendix A, only 23% are conducted in full scale.

Table 3.1 Summary of scale factors for RC models (Harris and Sabnis, 1999)

	<i>Quantity</i>	<i>Dimension</i>	<i>Scale Factor</i>
Material-Related Property	Concrete stress	FL^{-2}	1
	Concrete strain	-	1
	Modulus of concrete	FL^{-2}	1
	Poisson's ratio	-	1
	Specific weight	FL^{-3}	$1/S_L$
	Steel stress	FL^{-2}	1
	Steel strain	-	1
	Modulus of steel	FL^{-2}	1
	Bond stress	FL^{-2}	1
Geometry	Linear dimension	L	S_L
	Displacement	L	S_L
	Angular displacement	-	1
	Area of reinforcement	L^2	S_L^2
Loading	Concentrated load	F	S_L^2
	Line load	FL^{-1}	S_L
	Pressure	FL^{-2}	1
	Moment	FL	S_L^3

3.1.3 Construction

Reusable 4 mm thick modular steel formworks allowing vertical casting were used to construct frame specimens in desired geometry (Figure 3.5). Formwork parts were laser cut and machine bent from steel plates. Connection details allow the attachment of parts to each other using bolts and nuts for easy fabrication.

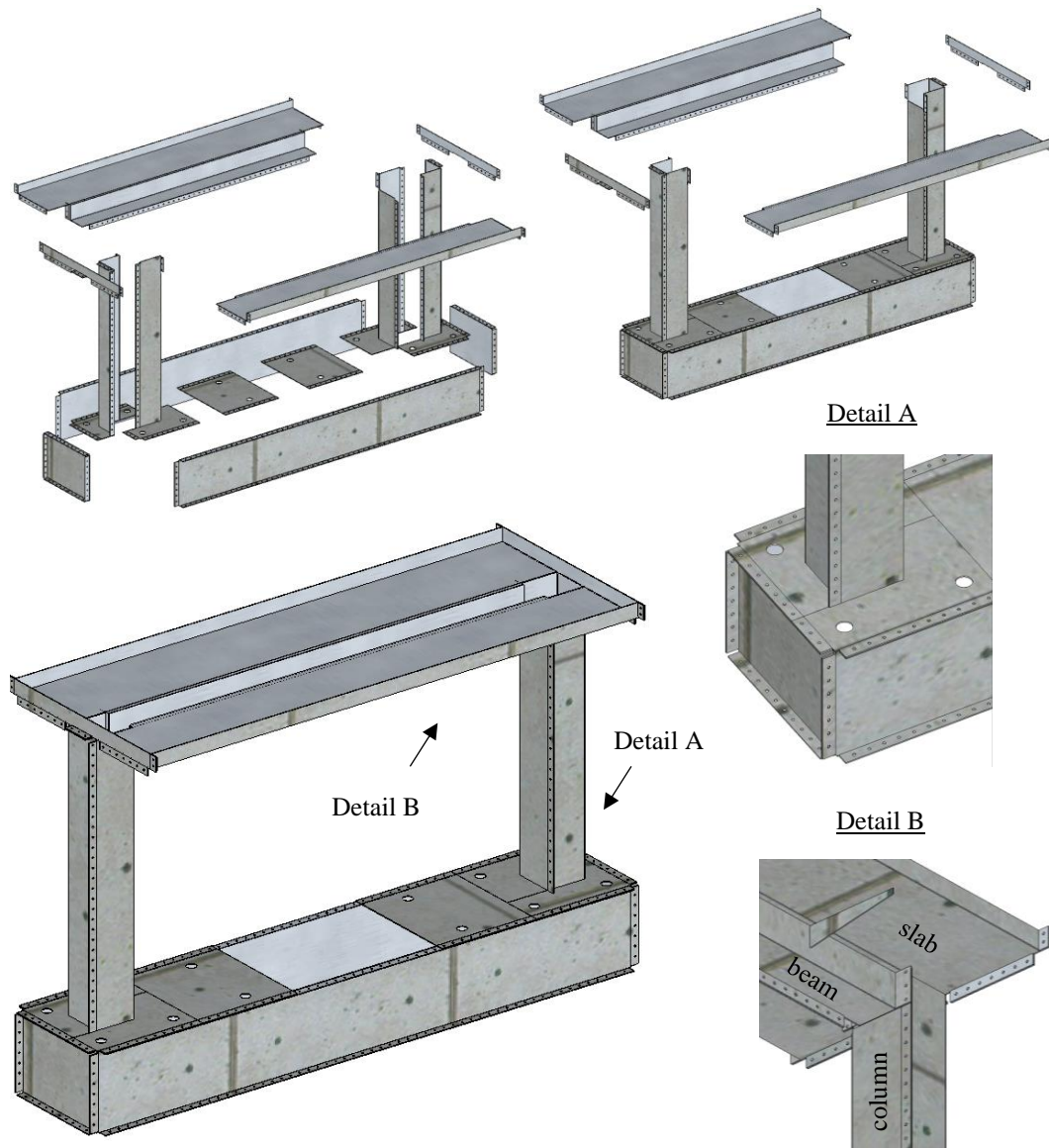


Figure 3.5. Details of modular formwork designed to cast frame specimens

Specimens were cast in a two-phased pouring operation. Initially, the reinforcement cage for the foundation beam and columns was built. All transverse bars were bent into 135 hooks to simulate code-compliant detailing. Strain gauges were attached to desired locations on the longitudinal bars. 12 steel tubes through which anchor bars used to fix frame specimen to the transfer slab will penetrate were carefully placed in their appropriate locations and secured to the reinforcement by welding (Figure 3.6.a). The prepared reinforcement cage was placed inside the foundation beam formwork. In the first phase, foundation concrete was cast (Figure 3.6.b). Remaining reinforcements were placed (Figure 3.6.c), formworks for the columns, beam and slab were assembled and the remaining members were cast monolithically in the second phase (Figure 3.6.d). During casting the second phase and while the concrete is wet, column longitudinal bars were welded to 200 x 200 x 10 mm³ steel plates in order to prevent bar slip and create a metallic surface for the attachment of vertical hydraulic jacks placed above the columns (Figure 3.6.e). The surface of the slab was finished (Figure 3.6.f) and the specimen was cured.

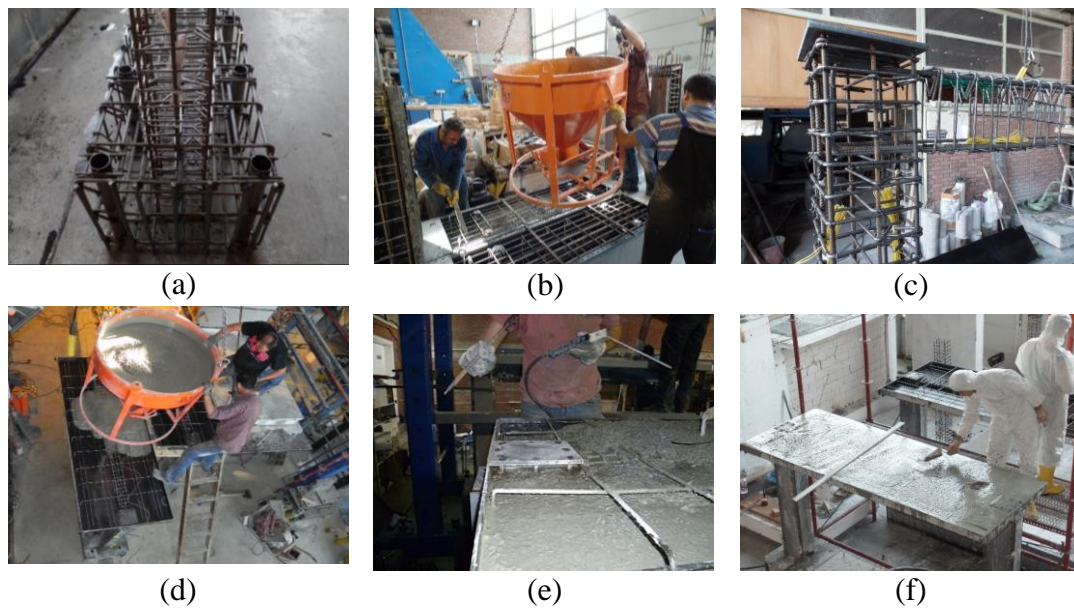


Figure 3.6. Construction stages of frame specimens

Self-compacting ready mixed C25 grade concrete (i.e. targeted characteristic compressive strength of 25 MPa) from a local distributor is used in both phases. The

aggregate size of the concrete was below 11.2 mm and the water to cement ratio was around 0.65. Concrete mixers pour concrete into a concrete bucket and a crane was used to transfer concrete. Poured concrete was vibrated using both internal and external formwork vibrators. Cylinder samples were taken and labeled to evaluate the compressive strength, split tensile strength and modulus of elasticity of the concrete (Figure 3.7).

The placement of frame specimens over the transfer slab is illustrated in Figure 3.8. Eye nuts attached to threaded anchor rods embedded inside the foundation beam were used to transfer frame specimens with the crane.



Figure 3.7. Concrete casting and sampling

Before placing the specimen on the transfer slab, a creamy plaster of paris paste was laid on the surface. Nuts of anchor rods are tightened, checking the alignment of columns in the vertical direction and the beam in the horizontal direction using a water gauge. Weight blocks representing dead plus 30 percent of the live load were placed on the slab. In order to sustain distributed loading conditions and not to prevent bending of the flanged beam under increased lateral deformations, instead of a continuous steel beam, weight blocks of 500 x 500 mm² bearing area were utilized and roller supports were placed between the slab and the weight blocks (Figure 3.8).



Figure 3.8. Placement of frame specimens on the transfer slab

3.2 Masonry Infill Walls

Two experienced masons constructed all the masonry walls. Master Nihat constructed infills with clay masonry units and master Murat constructed infills with aerated concrete blocks. All masonry walls were laid in a running bond pattern without openings. In order to simulate actual construction practice, infill walls were constructed after weight blocks simulating distributed slab loading were placed on top of frame specimens. This way, possible contact forces between the upper beam and the wall due to beam deflection are eliminated.

Aerated concrete blocks were cut to a half scale using a bandsaw. Due to difficulties in the production or manufacture of clay brick units with high void ratios in desired dimensions, available clay bricks closest to the dimensions of a scaled brick unit were ordered. Although the length and width of standard full-size bricks are equal, ordered bricks have twice the length compared to their width which ended in a

reduction of the total number of required bed joints to half and vertical stacking of brick units.

All clay brick units were soaked into the water before being laid. A general-purpose mortar with a 6/1/1 volumetric ratio of sand/cement/lime was utilized for mortar joints and plastering of clay bricks. A ready-mix joint mortar is utilized for aerated concrete blocks. Horizontal (vertical) mortar joint dimensions were roughly 10 (6) mm and plaster thickness were 10 mm on each side of the infill walls. Constructed infill walls were secured tightly inside the RC frame specimen by filling the remaining gaps on the two sides of the infill and under the beam with mortar except for the isolated frame specimens.

After testing of bare control specimen (BF), a total of 9 infill configurations constructed with different materials and retrofit techniques were tested. The first six infilled frame specimens were constructed with hollow clay bricks (HCB) and aerated concrete blocks were used for the last three. The first infilled test specimen (CB) was built with HCB and general-purpose cement mortar. The second specimen (CBP) was constructed in the same way as the first except 1 cm thick plaster was applied on both sides of the wall. The third specimen (CBMR) was reinforced with light steel meshes on both sides. The fourth (TieC) and fifth specimens (TieS) were constructed without plaster and strengthened with horizontal steel ties, the former using continuous ties mounted to steel profiles anchored to the column inner faces at both sides and the latter using staggered configuration attached at one side only. A special HCB with a dry locking mechanism in the bed joints was used for the construction of the sixth specimen (LB). The seventh specimen (AB) was built with aerated concrete blocks without plaster and a 2cm gap under the beam. The eighth specimen (ABI) was constructed similarly to the seventh but with a 1cm gap at contact surfaces with columns and the upper beam. Gaps were filled with flexible polyurethane foam. The ninth specimen (ABRP) was built with a fiber mesh reinforced mortar applied to both sides of the wall.

3.2.1 HCB Infill (CB)

CB frame specimen represents typical infill wall construction practice in Turkiye. A single leaf masonry wall was constructed inside the RC frame specimen using hollow clay bricks (HCB) of $185 \times 95 \times 100 \text{ mm}^3$ (length x width x thickness) size and a 65% void ratio. The compressive strength of the HCB was 10 MPa (3 MPa) when loaded parallel (perpendicular) to openings.

Because of the high void ratio, bricks were laid with their openings parallel to the horizontal direction which is in line with the usual practice. Due to the lack of scaling in brick units' length and the necessity of aligning openings in the horizontal direction, scaled brick units were stacked vertically which is different from the general horizontal block laying style (Figure 3.9). General purpose mortar was utilized for the mortar joints. All the gaps left between the wall frame interface were filled with mortar.



Figure 3.9. Construction of HCB infilled frame

3.2.2 HCB Infill with Plaster (CBP)

The very same construction practice is followed for the CBP frame specimen except for the application of 1cm thick plaster on both sides of the wall and filling the 2 cm gap under the top beam with polyurethane foam (Figure 3.10).



Figure 3.10. Construction of HCB infilled frame with plaster

3.2.3 HCB Infill with Steel Mesh Reinforcement (CBMRP)

CBMR frame specimen adopts exterior reinforcing of infill walls for strengthening unreinforced clay brick masonry infills. Light mesh reinforcement placed at both sides of the infill was connected with tie wires passing through holes drilled at various locations on the panel (Figure 3.11). Light steel meshes of 25 mm nominal pitch and 2 mm wire diameter attached to both sides of the masonry wall ($\rho_t=0.2\%$, total reinforcement ratio in plan) were connected using 1 mm tie wires at 12 wires per meter square density. Tie wires connecting meshes on both sides of the wall were tightened with nippers to ensure shear transfer between the masonry wall and added steel meshes. A 10 mm thick plaster was applied over steel meshes to prevent corrosion.

Added exterior mesh reinforcement was not attached to the bounding frame. The bilateral connection is achieved by tie wires passing through drilled holes. Composite action of the wall with steel meshes enhanced infill wall performance under IP and OOP loading. Construction steps that are compatible with Figure 3.11 are illustrated below:

- a. Holes were drilled on mortar joints.
- b. Mesh reinforcement available in 1.2m width rolls is cut to the required length.
- c. Mesh reinforcement is leaned against the wall on both sides.
- d. Tie wires passing through the drilled holes are used to fasten mesh reinforcement on both sides of the wall to each other.
- e. Regular purpose plaster is applied over the steel mesh.



Figure 3.11. Construction sequence of CBMR specimen

3.2.4 HCB Infill with Continuous Horizontal Steel Ties (TieC)

In order to integrate infill walls with the bounding frames and achieve a continuous load path between the two, a structural connection is needed. Polat Gülkan (2015) proposed a tie system where flat slotted steel plates laid along bed joints are locked to closed U-shaped steel profiles which are anchored to columns. The connection between the steel profile and the plate is simply satisfied by inserting and rotating which enables free movement of the plate in the vertical direction whereas horizontal movement is restricted so steel plates act like horizontal reinforcement. The connection only works in the horizontal direction and enables free movement in the vertical direction, which allows flexibility during the construction of the wall. The main goal of the proposed system is to develop a feasible, effective and affordable technology that will permit structural designers to design infill walls in RC frames that will (1) ensure a good degree of composite action between the infill walls and the parent reinforced concrete frame through mechanical coupling, and (2) ensure that in-plane and out-of-plane capacity of walls are explicitly taken into account during design. Figure 3.12 shows the conceptual illustration of the proposed tie system.

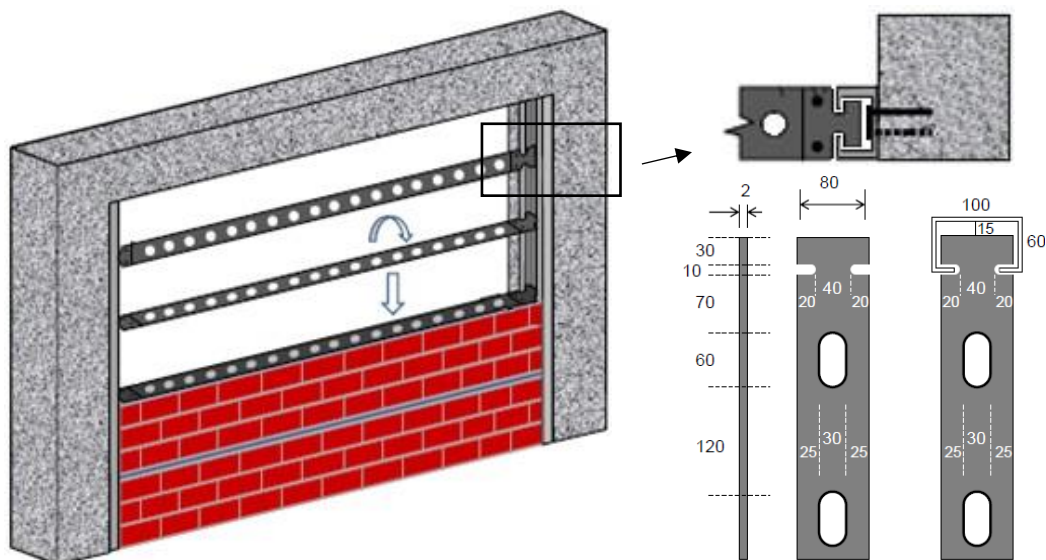


Figure 3.12. Horizontal steel ties spanning full length between the columns

TieC frame specimen composed of horizontal slotted steel ties, placed at bed joints in every 3 courses of masonry unit and connected at both ends to the closed U-shaped profiles attached to columns. Construction steps of TieC compatible with Figure 3.13 are illustrated below:

- a. Drill 5 holes on the inner faces of columns for screw anchors.
- b. Anchor closed U-shape steel profiles to columns at both sides.
- c. Lay the first layers of the wall and fit a flat plate as illustrated in Figure 3.12.
- d. Place flat plates at every other bed joint.

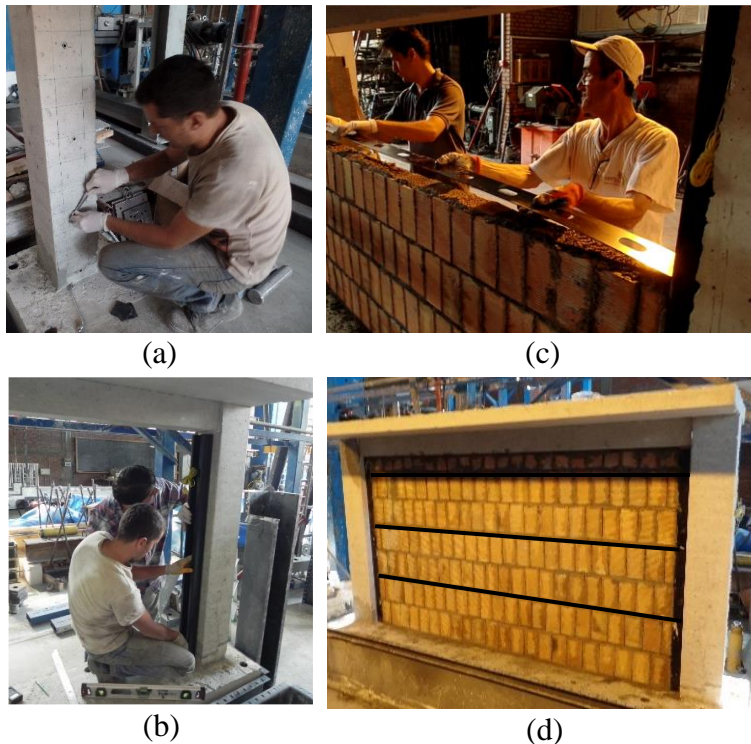


Figure 3.13. Continuous horizontal steel tie (TieC) application

3.2.5 HCB Infill with Staggered Horizontal Steel Ties (TieS)

Another possible arrangement of the mentioned tie system simplifying integration to the frame is TieS which involves staggering the horizontal ties in elevation and

attaching only one end to closed U profiles (Figure 3.14). Although a continuous connection between the columns is not satisfied, the proposed system is still capable of creating slip planes that would favor a sliding wall failure and prevent falling out of the masonry under out-of-plane accelerations that would enhance OOP response.

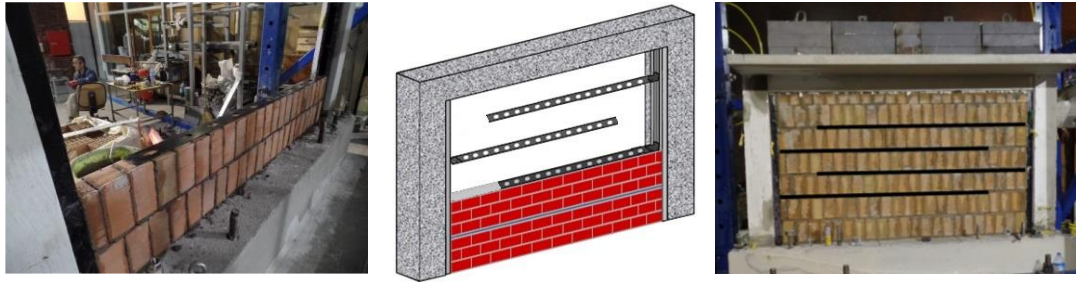


Figure 3.14. Staggered horizontal steel tie (TieS) application

3.2.6 LB Infill with Plaster (LBP)

Locking bricks (LB) are hollow clay bricks, also known as isolation bricks on the local market, with a dry shear key locking mechanism. They are normally laid their holes perpendicular to the ground leaving head joints free of mortar. Our suggestion is to rotate locking bricks 90 degrees so that they are locked in bed joints. This way, dry horizontal slip layers were formed without jeopardizing the arching mechanism against OOP forces. Construction steps compatible with Figure 3.15 is given below:

- a. The first layer of locking bricks is laid (starting bricks).
- b. General-purpose mortar is applied to head joints.
- c. Bed joints are left dry thanks to the interlocking mechanism.
- d. The gap under the top beam is filled with mortar.
- e. 1 cm thick plaster made of general-purpose mortar is applied on both faces.
- f. The surface of the plaster is washed with lime for better tracking of cracks.

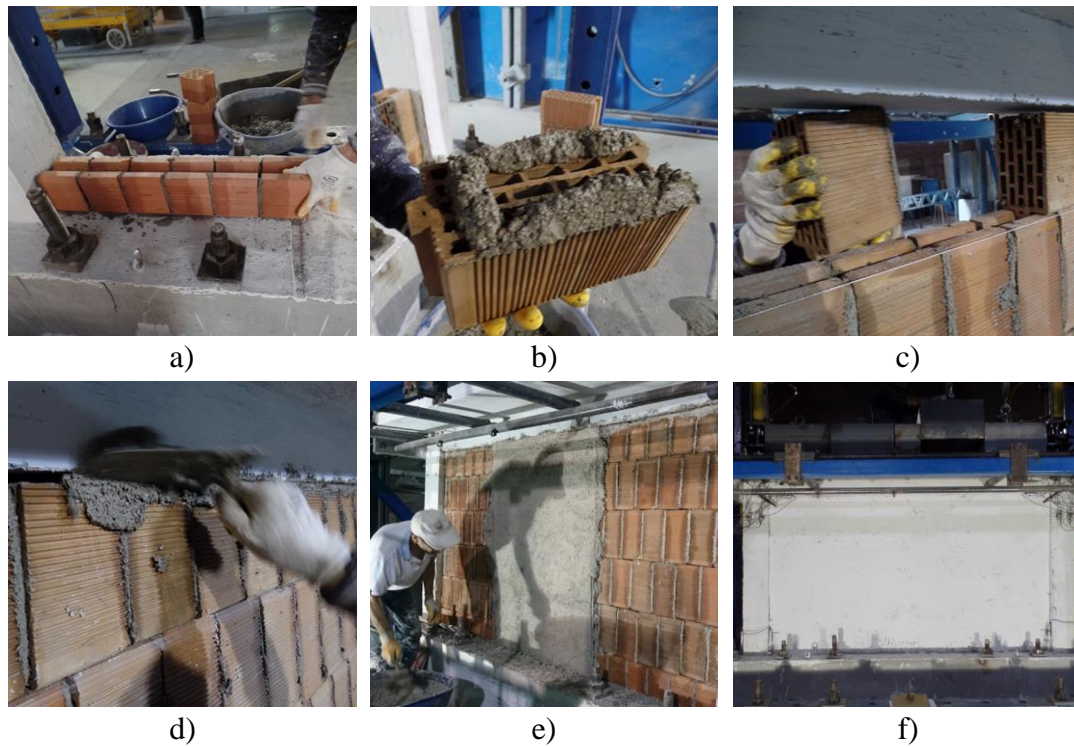


Figure 3.15. Construction sequence of LBP specimen

3.2.7 ACB Infill (AB)

AB frame specimen was constructed with aerated concrete block (ACB) units of 350 kg/m^3 dry density and $300 \times 125 \times 100 \text{ mm}^3$ (length x width x thickness) size. At 3rd and 6th layers of ACB, a perforated L-shaped steel profile was mounted to enhance wall to frame interaction and a 2 cm thick gap is left under the top beam to protect the infill wall from service level induced deflections of the beam in line with the usual construction practice in Türkiye (Figure 3.16). Before constructing the wall, a 2 cm thick layer of general purpose mortar was used to level the bottom surface and fill gaps at the sides of the wall with the columns. 2 cm gap under the upper beam was filled with flexible polyethylene foam. A ready-mixed, 2 mm thick interface mortar having 8.4 MPa compressive strength was applied to the head and bed joints.

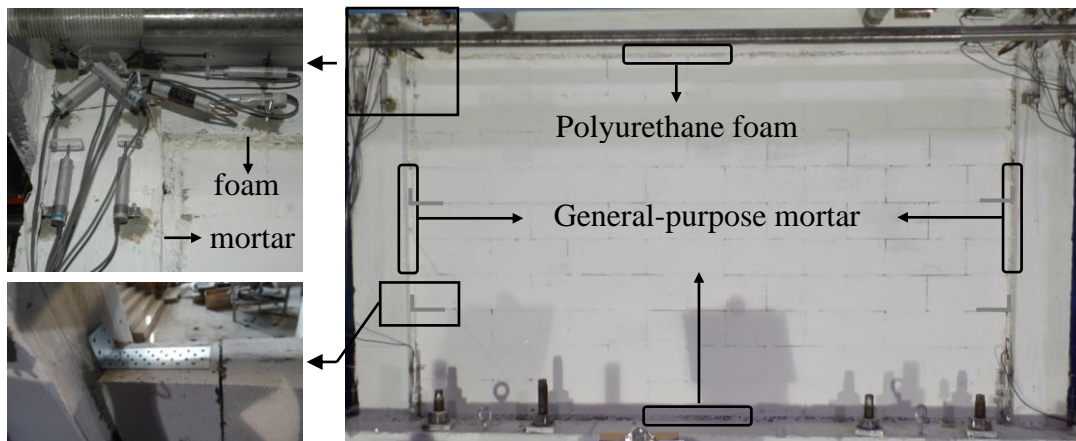


Figure 3.16. Construction details for AB specimen

3.2.8 ACB Infill with Isolation Joint (ABI)

The ABI frame specimen was constructed using materials similar to the AB frame specimen mentioned above. This time, a 2 cm thick gap was left between the contact surfaces of the infill wall with the columns and the upper beam and no additional L-shaped steel profiles were mounted promoting integration. All the gaps were filled with flexible polyethylene foam. Construction steps compatible with Figure 3.17 are illustrated below:

- a. The upper surfaces of ACB units are roughened for better joint mortar adhesion.
- b. Ready-mix ACB adhesive was applied to the head and bed joints.
- c. Wall is constructed by leaving a 10 mm diameter plain bar next to columns in order to create an isolation gap of desired thickness.
- d. Bars were removed and the gap next to columns was filled with polyurethane foam.
- e. The gap under the beam is similarly filled with polyurethane foam.
- f. No plaster or paint is applied to the wall surfaces.

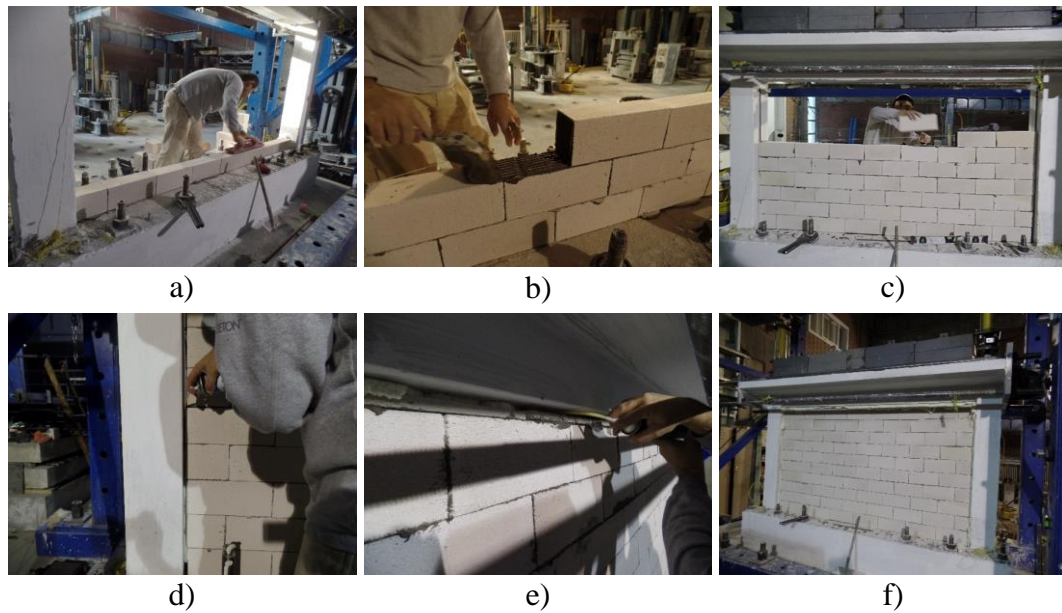


Figure 3.17. Construction stages for ABI specimen

3.2.9 ACB Infill with Fiber Mesh Reinforced Plaster (ABRP)

The ABRP frame specimen was constructed similar to the AB frame specimen mentioned above. Use of general purpose mortar over the foundation beam and at contact surfaces with columns, use of steel L profiles at 3rd and 6th course of ACB and a 2 cm gap under the upper beam were repeated in wall construction. Following the construction of the AAC infill wall, a 5 mm thick first layer of plaster having 1.0 MPa compressive strength was applied to the wall. Then, the fiber mesh grid having 4 mm nominal pitch and 160gr/m² density was placed on still fresh plaster. The second layer of 5 mm thick plaster was applied on top of the fiber mesh. The meshes were neither attached to the bounding frame nor the masonry panel via connectors, nails, or anchors.

The construction stages of the ABRP frame specimen compatible with Figure 3.18 is summarized below:

- a. General purpose leveling mortar application on top of the foundation beam

- b. Application of an L-shaped steel profile
- c. Application of polyurethane foam to fill the gap under the upper beam
- d. Application of the first layer of plaster
- e. Placement of fiber net
- f. Application of the second layer of plaster

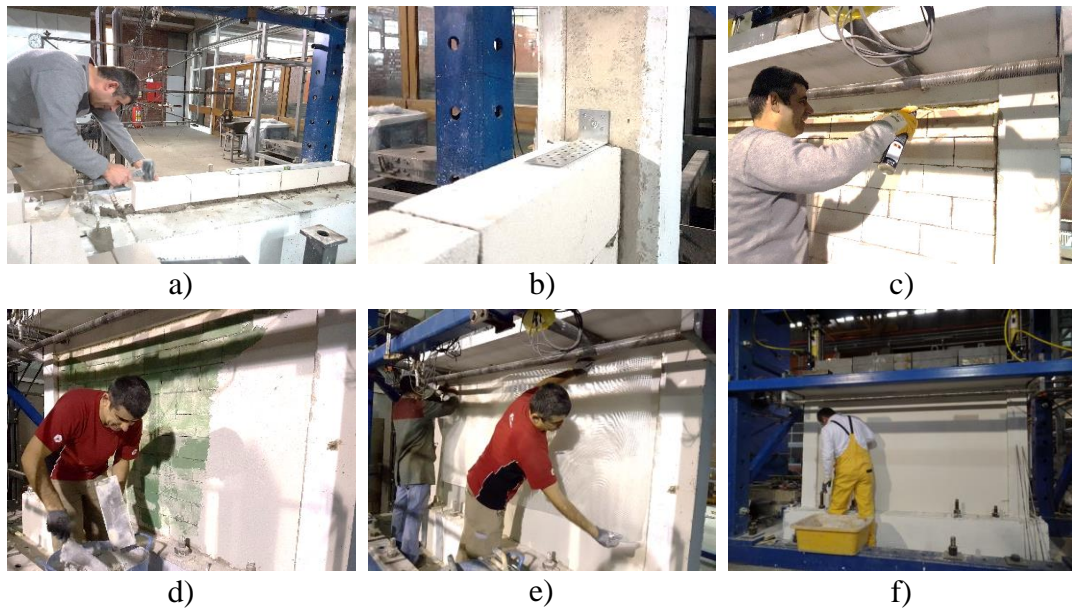


Figure 3.18. Construction sequence of ABRP specimen

3.3 Experimental Study

A testing setup capable of exerting 3 directional loading (i.e. vertical gravity loads and horizontal bidirectional earthquake loads) on the frame specimens was designed and constructed in METU Uğur Ersoy Structural Mechanics Laboratory. The gravity loads were simulated by steel weight blocks placed over the beam and manually controlled hydraulic jacks placed on top of columns. Earthquake induced out-of-plane (OOP) loading was applied by subjecting infill walls to a monotonically increasing pressure using an airbag. In-plane (IP) seismic demands were simulated by incremental reverse cyclic displacement excursions applied using a servo

controlled hydraulic jack. The structural response was recorded carefully during tests including the development of damage on frame members and infills, the yielding of reinforcement, hysteretic behavior of the frame, etc.

3.3.1 Test Setup

A test setup was built in METU Uğur Ersoy Structural Mechanics Lab to observe and measure structural response parameters of infilled frame specimens under simulated gravity and seismic loads. Several assemblies were constructed in order to fix the frame specimens tightly onto the strong floor, support and arrange the positions of horizontal and vertical actuators, and mount instruments for measurement.

3.3.1.1 In-plane Tests:

The overview of the in-plane testing setup is illustrated in Figure 3.19 below.

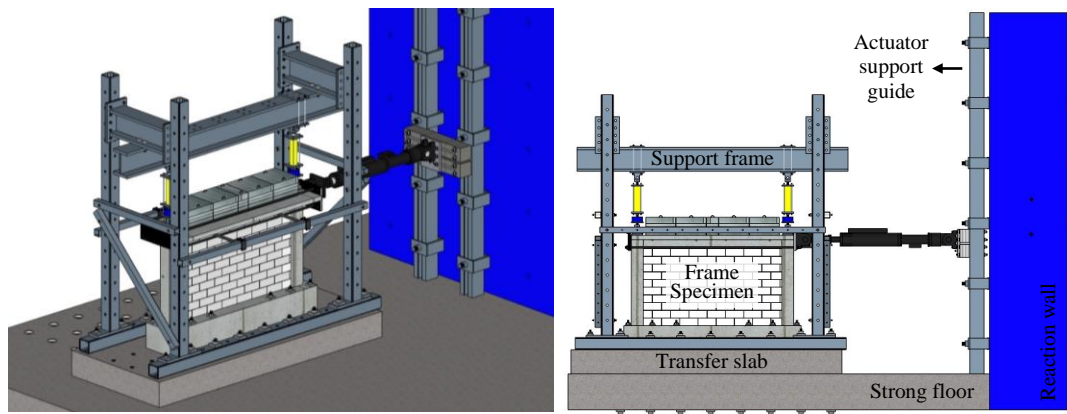


Figure 3.19. In-plane testing setup

Loading Mechanism

IP only tests involve placement of weights blocks over the upper beam simulating uniformly distributed slab loading, application of uniaxial compressive loading on top of columns simulating gravity loading from upper stories and implementation of

reversed displacement cycles imitating IP seismic loading. Loading devices, namely weight blocks and hydraulic jacks in vertical and horizontal directions are illustrated in Figure 3.20 below.

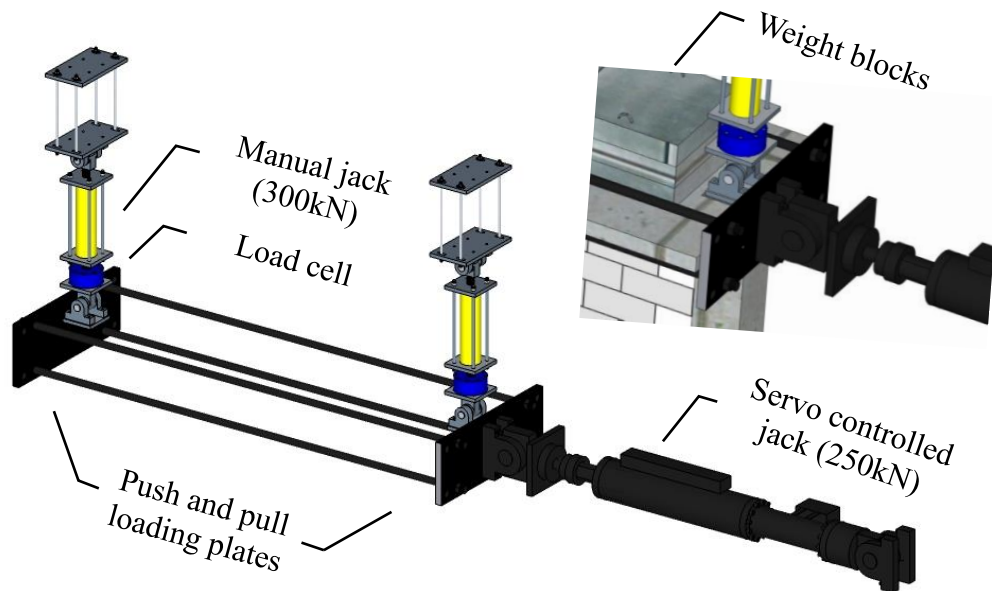


Figure 3.20. The vertical and horizontal loading assembly

Steel weight blocks having 500 mm x 500 mm bearing area were placed over the flanged beam (Figure 3.8) to idealize slab loading equal to 10.25 kN/m. Rollers were placed under the weight blocks in order not to restrict bending of the beam under lateral load. Two 300 kN capacity manually controlled, two-way hydraulic jacks were installed vertically on top of columns to idealize gravity loads. A rigid steel frame fixed to the strong floor was used to accommodate the vertical jacks. Uniaxial loading was ensured by pin-ends and measured by Cas LS-30 model loadcells. Before imposing lateral loading, the axial load ratio (i.e. $N/A_c f_{ck}$) of columns was arranged to 0.175 depending on the measured concrete compressive strength of the tested frame and maintained by small adjustments during testing.

The lateral load was transferred to the frame by two 40 mm thick steel loading plates placed at the ends of the flanged upper beam. One end of the 250 kN capacity servo-controlled hydraulic jack imposing IP displacement cycles was attached to the

pushing plate with a hinged connection, and the other end was connected to the actuator support guide attached to the reaction wall. Four 45mm diameter steel bars were used to connect loading plates in order to transmit pulling force. No prestressing is applied to the connection bars.

Transfer slab

The spacing of 50 mm diameter holes located on the 600 mm thick strong floor of the lab is 500 mm in both directions. For an effective fixation of the frame specimens to the rigid floor, a transfer slab is constructed between the strong floor and the frame specimen. Before casting the concrete of the transfer slab, steel tubes and hexagonal steel rods with internal threads were placed at desired locations and secured by welding to the reinforcement cage (Figure 3.21). After hardening of concrete, the transfer slab was transferred and permanently fixed to the strong floor with 16 post-tensioned 45 mm diameter anchor rods passing through the steel tubes placed inside the transfer slab and the existing holes on the strong floor. Similarly, the foundation beam of each frame specimen was fixed to the transfer slab using 12 threaded anchor rods of 35 mm diameter. The bottom ends of the anchor rods were screwed to the internal threads left on the surface of the transfer slab and nuts were attached to the upper ends. Later, nuts were tightened for post-tensioning of the anchor rods against sliding and rocking of the frame specimen under IP and OOP loading.

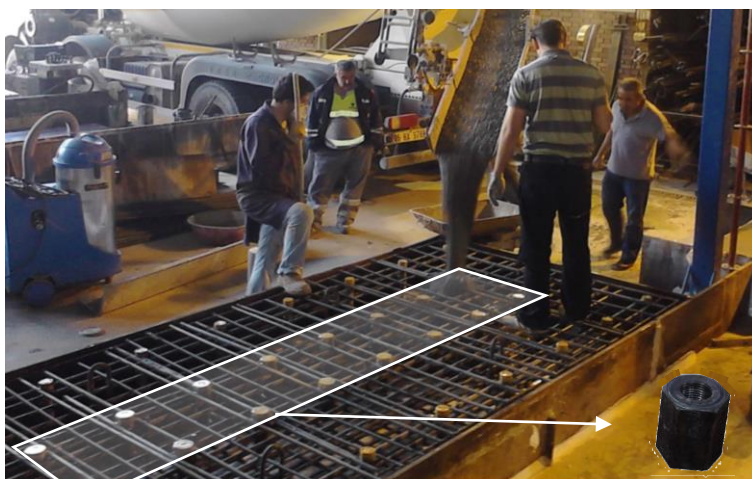


Figure 3.21. Construction of transfer slab

3.3.1.2 Out-of-plane Tests:

An overview of the testing assembly and instrumentation setup is illustrated in Figure 3.22. Similar to IP tests, prior to OOP loading, the frame specimen was loaded in the vertical direction using weight blocks and manually controlled hydraulic jacks placed on top of columns. 8 post-tensioned anchor rods were used to fix the foundation beam to the transfer slab preventing the frame specimen from tilting under out-of-plane (OOP) loads. In order to support the frame specimen in the OOP direction, 4 ball transfer bearings placed on one side of the upper beam were used. A loading assembly based on the application of airbag induced constant pressure in the OOP direction was constructed. The OOP displacement profile of the infill was captured by 15 linear variable displacement transducers (LVDT) attached to the LVDT support cage. Piano wires were used to connect LVDTs to the 6mm diameter anchor bolts embedded into the wall with epoxy.



Figure 3.22. Out-of-plane testing setup

Loading Mechanism

Due to bidirectional nature of earthquakes, inertial forces created on the wall surface due to earthquake induced accelerations in the out-of-plane direction were idealized as uniformly distributed loading. An airbag attached mechanism is used for the application of uniform pressure on the wall surface. The airbag was mounted on a stiffened backing wooden frame resting on a linear guide which was approached to

the infill wall by means of a load cell attached and a pin-ended hydraulic jack. The linear guides ensure friction-free translational motion of the assembly. A 5 kN counterweight was placed over the ball transfer units sitting on the linear guides to ensure stability against tilting (Figure 3.23).

The attached 100 kN capacity load cell is used to measure the total force applied in the OOP direction. After approaching to the frame specimen with the hydraulic jack, the airbag pushes the infill wall in the OOP direction to the desired pressure by pumping air into the airbag. A pressure transmitter was utilized to determine the pressure inside the airbag. The pressure inside the airbag is increased manually throughout the tests until the failure.

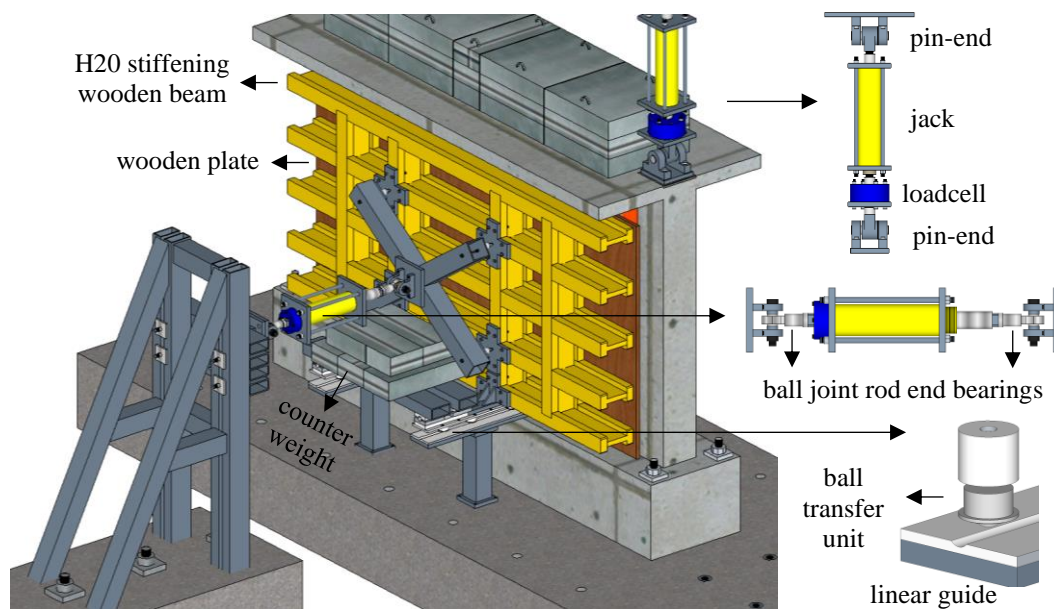


Figure 3.23. Out-of-plane loading assembly details

3.3.1.3 Bidirectional Tests:

A unique loading strategy for the simultaneous application of bidirectional earthquake loads was implemented for the investigation of OOP strength reduction under increasing IP demands. After the OOP capacity of the infill wall was

determined, 1/3 and 2/3 of the capacity were applied with an airbag, kept constant and increasing IP displacement reversals were applied up to failure. IP and OOP testing setups were combined with minor modifications for this purpose. In order to eliminate friction forces, a 2 mm thick teflon sheet (coefficient of friction=0.10) was nailed to the infill wall at four corners before implementing pressure with the airbag.

A scaled 3-D drawing of the experimental setup for bidirectional tests created using Sketch-up (2016) is illustrated in Figure 3.24 below.

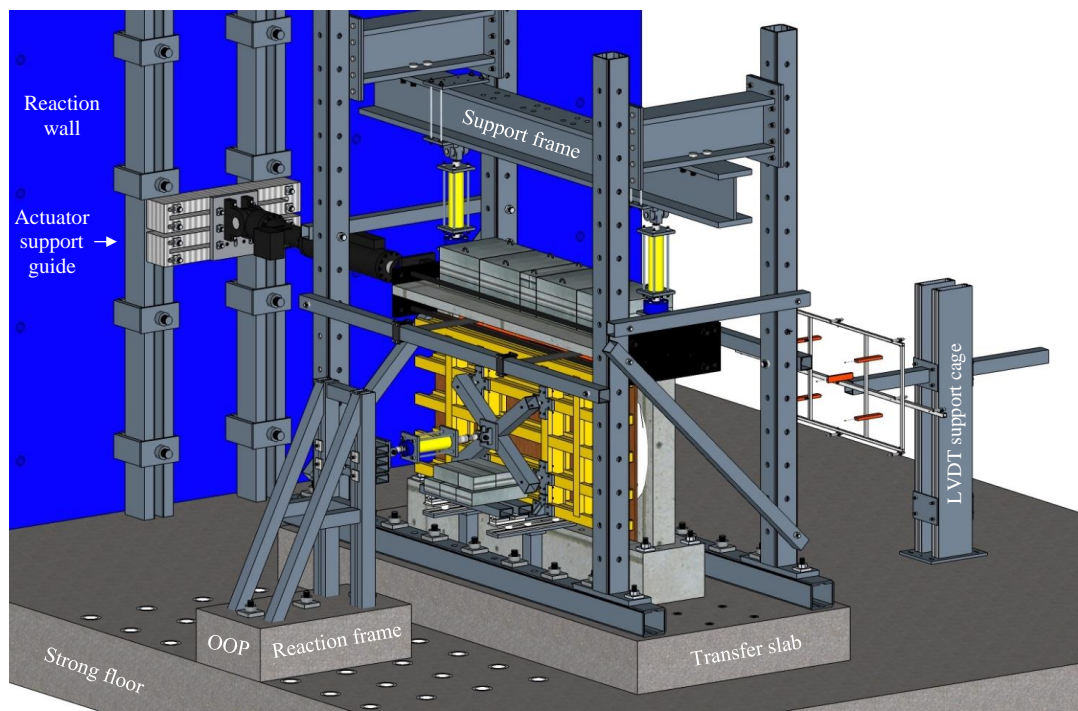


Figure 3.24. Experimental setup for multi directional tests

3.3.2 Instrumentation

The IP response of the frame specimen and the OOP response of infill walls were monitored through 63 channels of transducer output (Table 3.2). IP load, deformation and strain measurements were taken at locations shown in Figure 3.25.a. OOP load and deformations measurement locations are illustrated in Figure 3.25.b.

Loads implemented by actuators were tracked by 4 loadcells. Additionally, for OOP tests, a pressure transmitter was utilized to measure the pressure inside the airbag. 12 strain gages attached to longitudinal reinforcements at the ends of columns and beams were utilized to identify the yielding of frame members. 15 linear variable displacement transducers (LVDT)'s were used for OOP deformation monitoring. In order to better capture the elastic stiffness of the infill wall in the early stages of OOP loading, an additional and more sensitive LVDT with 10 mm stroke capacity is temporarily placed on a stick to record the center deflection of the wall. It is removed during testing when the center deflection approaches stroke capacity. Finally, 30 LVDTs were employed to measure lateral displacement, end rotation of frame members, sliding and uplifting of foundation beam, shear distortion of beam-column joints and the infill wall (Figure 3.25).

All of the measurement instruments were connected to the Vishay Scanner 5100B model data acquisition system accommodating up to 20 channels of inputs. 4 scanners were chained together to create an 80-channel system. Strain Smart software was utilized for calibration of transducers and recording experimental data. 2 recordings were taken at each second throughout testing.

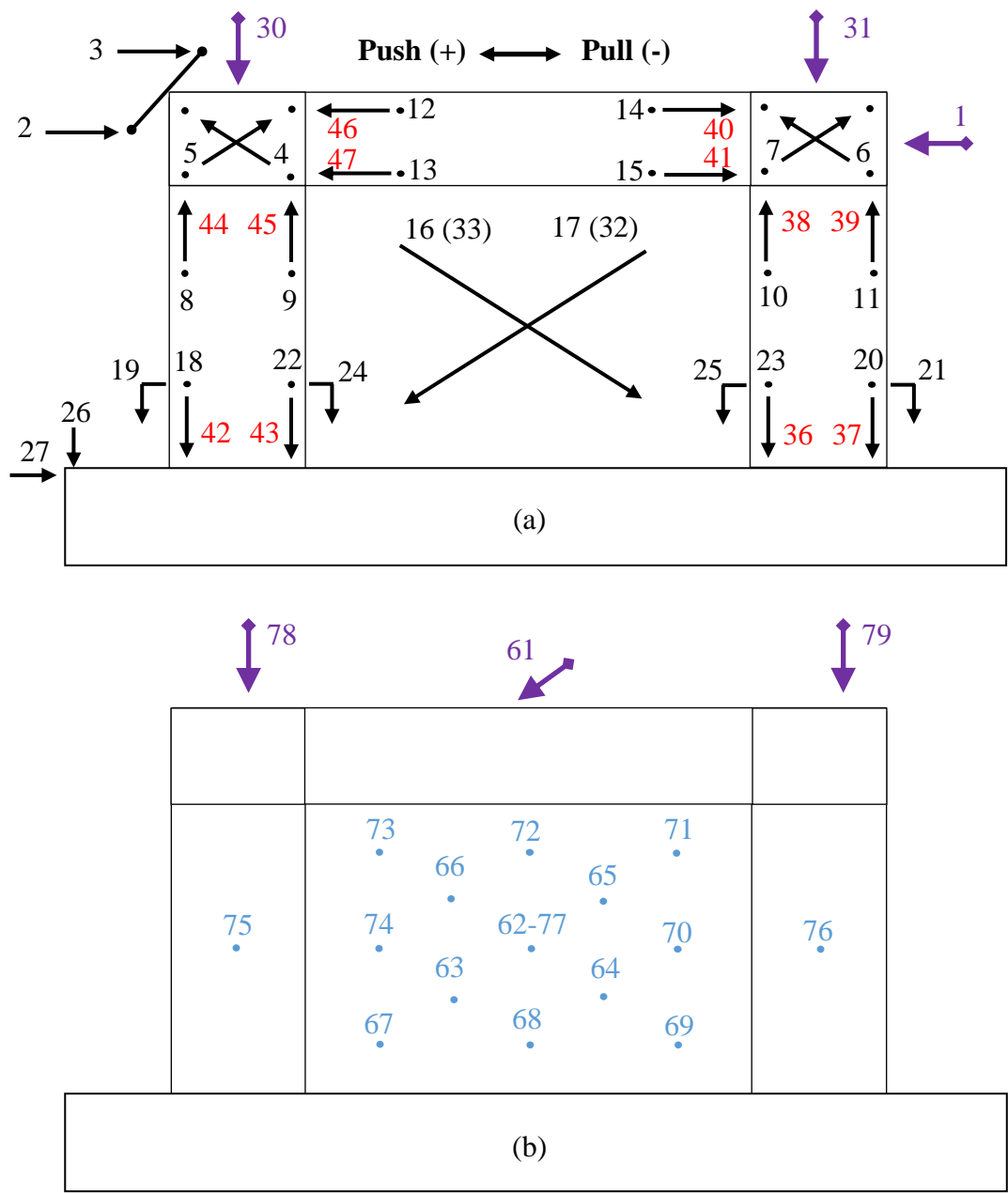
One end of the utilized pancake loadcells was rigidly attached to actuators with threaded transfer bolts produced from hexagonal or circular solid steel rods using a lathe. The other end of the loadcell is also rigidly attached to a laser-cut separating plate using bolts and nuts. Uniaxial response of the combined actuator-loadcell assembly is ensured by attaching hinges at both ends.

Support and arrangement of 15 LVDTs used to monitor the OOP movement of the wall were achieved by designing a steel cage that is fixed to a strong floor via anchor bolts. LVDT's with larger stroke capacity were closer to the center of the wall. Since OOP loading was monotonically increased until the collapse, a 1.5m distance is provided between the wall and the cage to prevent damage to LVDT's during the collapse. Piano wires were used to connect LVDTs to the threaded rods embedded into the wall with epoxy and rubber bands were used to tighten wires.

Table 3.2 Instrumentation of frame specimen tests

<i>Ch.</i>	<i>Test</i>	<i>Dir.</i>	<i>Device</i>	<i>Exp.</i>	<i>Ch.</i>	<i>Test</i>	<i>Dir.</i>	<i>Device</i>	<i>Exp.</i>
1	IP	↔	Loadcell	50t	41	IP	—	StrainGauge	10mm
2	IP	→	LVDT	200mm	42	IP		StrainGauge	10mm
3	IP	→	LVDT	200mm	43	IP		StrainGauge	10mm
4	IP	↘	LVDT	20mm	44	IP		StrainGauge	10mm
5	IP	↗	LVDT	20mm	45	IP		StrainGauge	10mm
6	IP	↘	LVDT	20mm	46	IP	—	StrainGauge	10mm
7	IP	↗	LVDT	20mm	47	IP	—	StrainGauge	10mm
8	IP	↑	LVDT	30mm	48				
9	IP	↑	LVDT	30mm	49				
10	IP	↑	LVDT	30mm	50				
11	IP	↑	LVDT	30mm	51				
12	IP	←	LVDT	30mm	52				
13	IP	←	LVDT	30mm	53				
14	IP	→	LVDT	30mm	54				
15	IP	→	LVDT	30mm	55				
16	IP	↘	LVDT	50mm	56				
17	IP	↗	LVDT	50mm	57				
18	IP	↓	LVDT	30mm	58				
19	IP	↓	LVDT	30mm	59				
20	IP	↓	LVDT	30mm	60(1)*	OOP		PressureT.	1bar
21	IP	↓	LVDT	30mm	61(2)	OOP	←	Loadcell	10t
22	IP	↓	LVDT	30mm	62(3)	OOP	→	LVDT	200mm
23	IP	↓	LVDT	30mm	63(4)	OOP	→	LVDT	100mm
24	IP	↓	LVDT	30mm	64(5)	OOP	→	LVDT	100mm
25	IP	↓	LVDT	30mm	65(6)	OOP	→	LVDT	100mm
26	IP	↓	LVDT	20mm	66(7)	OOP	→	LVDT	100mm
27	IP	→	LVDT	20mm	67(8)	OOP	→	LVDT	50mm
28	IP	↓	LVDT	20mm	68(9)	OOP	→	LVDT	50mm
29	IP	→	LVDT	20mm	69(10)	OOP	→	LVDT	50mm
30(19)	IP	↕	Loadcell	30t	70(11)	OOP	→	LVDT	50mm
31(20)	IP	↕	Loadcell	30t	71(12)	OOP	→	LVDT	50mm
32	IP	↘	LVDT	50mm	72(13)	OOP	→	LVDT	50mm
33	IP	↗	LVDT	50mm	73(14)	OOP	→	LVDT	50mm
34	IP				74(15)	OOP	→	LVDT	50mm
35	IP				75(16)	OOP	→	LVDT	30mm
36	IP		StrainGauge	10mm	76(17)	OOP	→	LVDT	30mm
37	IP		StrainGauge	10mm	77(18)	OOP	→	LVDT	10mm
38	IP		StrainGauge	10mm					
39	IP		StrainGauge	10mm					
40	IP	—	StrainGauge	10mm					

*Channel number in parenthesis is valid for OOP only tests.



36 - 47 Strain gage ↔ Load cell
 62 - 77 LVDT (OOP) 2 - 33 LVDT (IP)

Figure 3.25. Instrumentation labelling a) In-plane, b) Out-of-plane

12 strain gages were attached to the longitudinal bars at member ends (3-4 cm from the face of joints) of each frame specimen tested under IP only loading (Table 1.1). Kyowa Type KFG-10mm-120Ohm strain gages were attached to the machined,

sanded and cleaned surface of the bars with Kyowa CC-33A gage cement such that the longitudinal direction of the gage is in good alignment with the longitudinal direction of the reinforcement. Kyowa AK22 coating clay agent has been applied around the strain gauge attached reinforcement against wet and vibrations during casting and placement of concrete. After installation, strain gages were checked with an ohmmeter. The strain gauge attachment steps are illustrated in Figure 3.26.

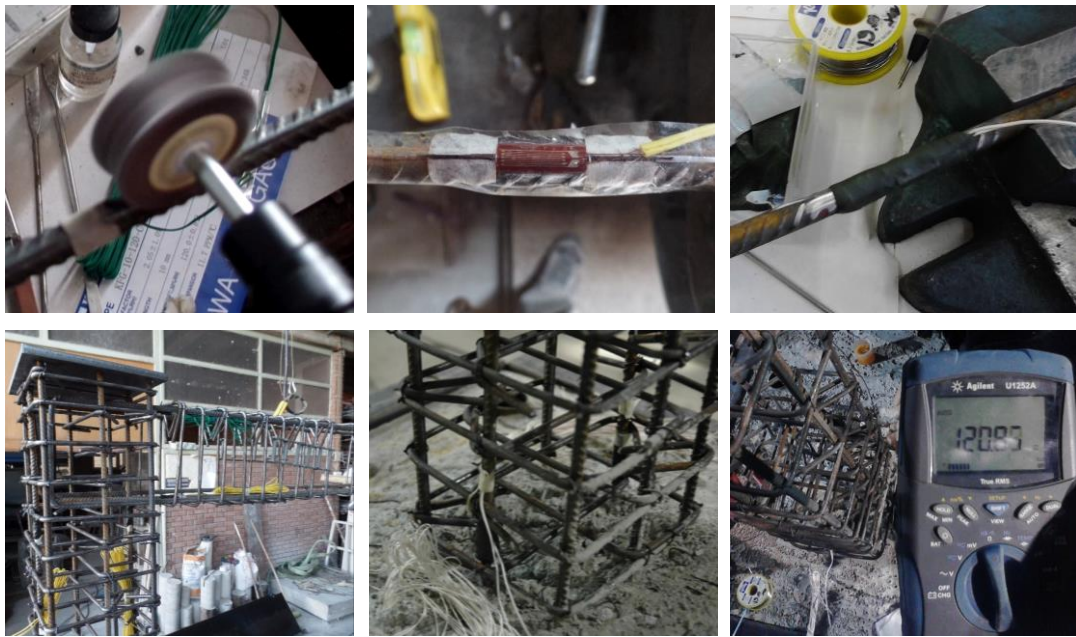


Figure 3.26. Strain gauge attachment to longitudinal bars

Kyowa DTH-A LVDTs with 10 mm, 20 mm, 30 mm and 50 mm stroke capacities were utilized for displacement measurement at various locations of the frame specimen. For specimens tested under IP demands, column end deformations within the potential plastic hinge were measured by using LVDTs attached to 6mm diameter threaded rods embedded into the frame specimen with epoxy (Figure 3.27). The transducers to measure column and beam end curvatures were placed with a gauge length equal to the member depth following the proposal of Bayrak (1998).

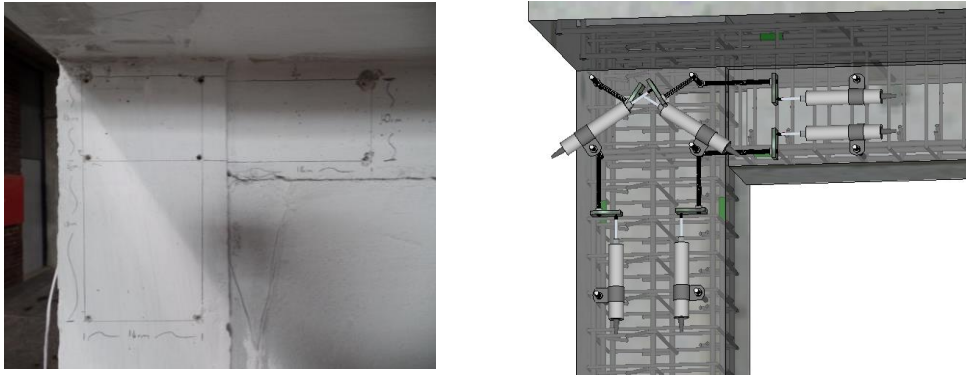


Figure 3.27. LVDT attachment to frame specimen

3.3.3 Loading Protocol

Three different protocols were utilized for in-plane, out-of-plane and bidirectional loading cases. In all cases, the same vertical loading approach simulating the axial load levels of the prototype structure was utilized before applying lateral displacement excursions or OOP loads, or bidirectional loading. Weight blocks corresponding to 10.25 kN/m distributed loading were placed on top of the flanged upper beam and columns were loaded to an axial load ratio of 17.5% (i.e. $N/A_c f_c$) using manually controlled hydraulic jacks installed on their top.

3.3.3.1 In-plane Tests

The loading protocol for the IP only tests were composed of vertical actions plus quasi-static incremental displacement cycles. A 250 kN capacity servo-controlled actuator moving in displacement control was utilized. The loading history features two displacement cycles at designed target drift levels of 0.35%, 0.5%, 1.0%, 1.5%, 2.0%, 2.5%, 3.0%, 3.5% and 4.0% (Figure 3.28). Lateral displacements were calculated by averaging Ch2 and Ch3 (Figure 3.25.a) placed at two corners of the slab and at the same elevation as the centroid of the flanged beam which is 1435 mm from the top of foundation beam. At every second cycle of the target drifts, the test is paused, infill damage is photographed and cracks on frame members were painted.

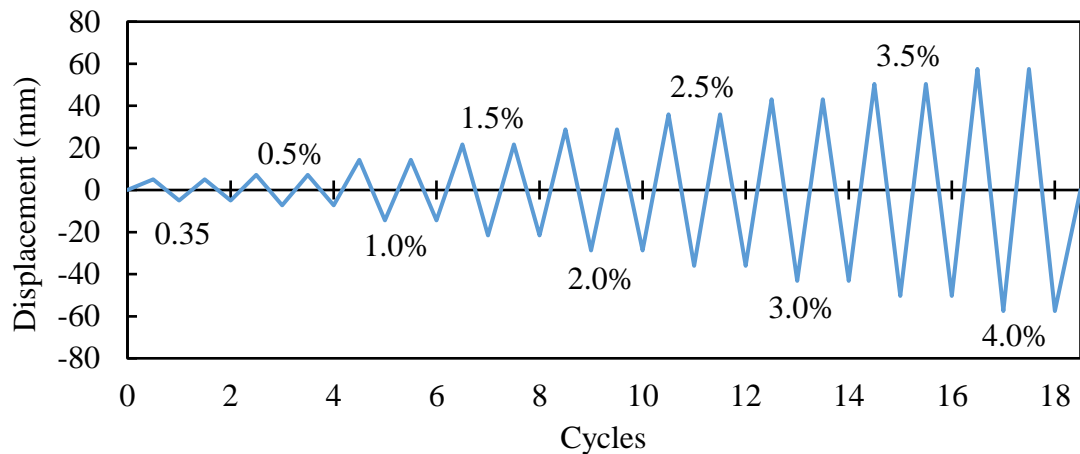


Figure 3.28. In-plane loading protocol

Weight blocks were lifted and loads on vertical actuators were released before activating the data acquisition system and put back on the specimen after activation to capture beam end rotations and rebar strains due to gravity loading. The vertical load was controlled manually during the tests and corrected by pausing the experiment at zero loads of the hysteresis curve.

3.3.3.2 Out-of-plane Tests

The OOP only tests were conducted after application of gravity loads on columns and the beam through implementation of out-of-plane pressures. The pressure of the airbag was increased monotonically until the failure of the wall.

3.3.3.3 Bidirectional Tests

After determining the OOP capacity of the infill wall from the previous test, the bidirectional tests were conducted under the effect of constant OOP pressure (equal to 33% or 66% of the OOP capacity), the vertical actions and quasi-static incremental displacement cycles until failure of the infill wall.

CHAPTER 4

MATERIAL CHARACTERIZATION

A complete investigation of the strength and deformation characteristics of all materials involved in infilled RC frame specimen construction including materials utilized for retrofit measures was carried out. Concrete and mortar specimens sampled during casting and construction of the frames and infill walls were tested prior to the corresponding frame test. Longitudinal and transverse bars, fiber and steel mesh reinforcement and brick units were also tested for characterization. Additionally, masonry prisms constructed with hollow clay brick (HCB) and aerated concrete block (ACB) units were tested under uniaxial compression, diagonal tension, sliding, and bending actions to identify load-displacement characteristics.

A wide scatter of test results is expected for masonry specimens due to insufficiently controlled laboratory environmental conditions, manufacturing and testing procedures and workmanship. Thus, a sufficient number of repetitions is required to provide a satisfactory statistical characterization of mechanical properties (Calvi et al., 1996). Accordingly, three samples were constructed for each prism test and the test results were averaged to determine mechanical properties.

Material and masonry prism tests were conducted at METU Materials Lab and METU Uğur Ersoy Structural Mechanics Lab following well recognized material testing specifications. Force-controlled hydraulic press and U-test testing machine, servo-controlled MTS testing machine and screw jack attached electric motor controlled testing setups were employed for force and displacement-based testing. Innovative test setups were designed and constructed for 4-point bending and sliding shear testing of masonry prisms.

4.1 Material Tests

Material test results for concrete, reinforcing steel, brick units, mortar, fiber and steel meshes, tie wires and horizontal steel ties are illustrated in this section.

4.1.1 Concrete

C25 grade super liquid ready mixed concrete with a targeted 28-day characteristic compressive strength of 25 MPa (i.e. $f_{ck}=25$ MPa) was ordered from the same concrete plant for all frame specimens. The aggregate size of the concrete was below 11.2 mm and the water-cement ratio was 0.65.

For each batch of concrete, standard 150 mm diameter cylindrical concrete samples were taken. Concrete samples were sulfur-graphite capped and tested for compressive strength (ASTM C39-21) on 7th, 14th and 28th days to monitor strength gain. At least 3 samples were tested for compressive strength and split tension strength (ASTM C496-17) on the day of the frame experiment (Figure 4.1). Depending on the compressive strength, the axial load ratio of columns was arranged to 0.175 using vertical jacks over columns.



Figure 4.1. Concrete sampling and testing

Compressive strength (f_c), split tension strength (f_{st}), test date and age of concrete at the test day for concrete specimens are illustrated for each frame specimen in Table 4.1 below.

Table 4.1 Concrete specimen test results

Frame	BF							CB						
Cast/Test Date	16-04-2014 / 17-07-14							16-04-2014 / 09-05-14						
Specimen	N1	N2	N3	N4	N5	mean	st.dev	N1	N2	N3	N4	N5	mean	st.dev
f _c (MPa)	25.7	26.4	28.7	30.6		27.9	2.3	25.5	19.4	22.0	21.9	22.9	23.3	2.2
f _{st} (MPa)	2.5	2.9	2.9			2.8	0.3	2.4	2.8	2.9			2.7	0.3
Age of Concrete	91 Days							23 Days						

Frame	CBP							CBMR						
Cast/Test Date	22-01-2015 / 29-05-15							01-08-2014 / 29-08-14						
Specimen	N1	N2	N3	N4	N5	mean	st.dev	N1	N2	N3	N4	N5	mean	st.dev
f _c (MPa)	27.0	27.7	23.9	25.9	27.3	26.4	1.5	33.8	32.6	35.3	33.6	32.8	33.6	1.1
f _{st} (MPa)								2.0	2.8	2.1	2.67		2.4	0.4
Age of Concrete	127 Days							28 Days						

Frame	TieC							TieS						
Cast/Test Date	01-08-2014 / 10-09-14							10-10-2014 / 29-12-14						
Specimen	N1	N2	N3	N4	N5	mean	st.dev	N1	N2	N3	N4	N5	mean	st.dev
f _c (MPa)	35.6	33.1	36.2	33.8	34.3	34.6	1.3	32.3	31.6	32.8	34.6	34.9	33.3	1.5
f _{st} (MPa)	2.9	2.5	2.7	2.9		2.8	0.2	3.2	2.9	2.5	2.95		2.9	0.3
Age of Concrete	40 Days							80 Days						

Frame	LBP							AB						
Cast/Test Date	12-03-2015 / 25-12-15							22-01-2015 / 18-02-15						
Specimen	N1	N2	N3	N4	N5	mean	st.dev	N1	N2	N3	N4	N5	mean	st.dev
f _c (MPa)	28.7	29.0	27.1			28.2	1.0	25.5	24.5	24.6			24.9	0.5
f _{st} (MPa)	2.2	2.0				2.1	0.1	2.2	2.0				2.1	0.1
Age of Concrete	288 Days							27 Days						

Frame	ABI							ABRP						
Cast/Test Date	10-10-2014 / 28-11-14							12-03-2015 / 31-03-15						
Specimen	N1	N2	N3	N4	N5	mean	st.dev	N1	N2	N3	N4	N5	mean	st.dev
f _c (MPa)	32.5	31.8	32.8			32.3	0.5	18.8	18.8	19.1			18.9	0.2
f _{st} (MPa)	3.2	2.9	3.0	2.9		3.0	0.1	1.7	2.0	1.6			1.7	0.2
Age of Concrete	49 Days							19 Days						

4.1.2 Reinforcing Steel Bars

Two different types of steel bars were used for reinforcing RC frame specimens. Longitudinal reinforcements were S420 grade (i.e. $f_{yk}=420$ MPa), 8 mm diameter deformed bars whereas transverse reinforcements were cold drawn 6 mm diameter plain bars produced specifically for the half scaled frame specimens due to unavailability of deformed bars in 6 mm diameter. The first two frame specimen experiments (i.e. BF and CB) were conducted with existing reinforcements in the lab which are labeled as T1 to T6 in Table 4.2. A new batch of reinforcement was ordered for the remaining tests which are labeled as NN2 to N14 in Table 4.2.

Uniaxial tensile testing was carried out for all reinforcement specimens in accordance with ASTM A370 (2021) standard using MTS 647 Testing Machine (Figure 4.2). All of the rebar samples were cut to 250 mm in length. Deformed bars were weighted for the determination of nominal diameter and three deformed bar samples were rounded on the lathe in order to attach strain gauges. Displacement readings were recorded with a 50 mm capacity Epsilon brand extensometer. Additionally, 5 mm long high strain capacity and 10 mm long standard capacity Kyowa brand strain gages were attached to plain and machined bars for a more accurate determination of young's modulus.



Figure 4.2. Uniaxial tensile testing of reinforcing bars

The stress-strain curves of the reinforcing bars (i.e. N2 to N14) tested under displacement-based uniaxial loading are illustrated in Figure 4.3.

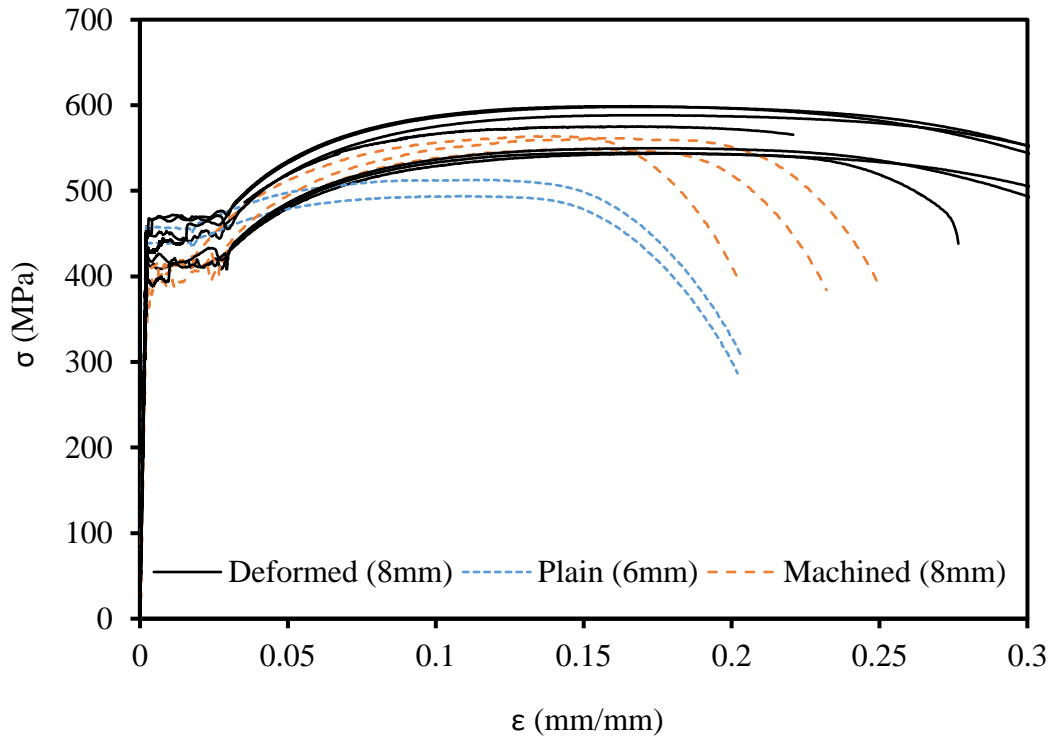


Figure 4.3. Stress-strain graph for reinforcing bars

The nominal diameter of a deformed bar is equivalent to the diameter of a plain bar having the same weight per length as the deformed bar. The average nominal diameter of 8 mm deformed bars was calculated as 8.38 mm. The measured mechanical properties of the reinforcing bars are summarized considering nominal diameters and 8mm diameter for deformed bars in Table 4.2.

For deformed bars, the yield stress (f_y) and maximum stress (f_u) values are provided based on the nominal diameters and assuming an 8mm diameter which is used in section analysis of frame specimens where the diameter of longitudinal bars was taken as 8mm. Modulus of elasticity is calculated from linear curve fitting on the measured data prior to yielding. Strain gauge measurements which provide more reliable data were relied upon where available.

Table 4.2 Mechanical properties of reinforcing bars

<i>Specimen</i>	<i>ID</i>	f_y (MPa)	f_u (MPa)	f_y^* (MPa)	f_u^* (MPa)	E (GPa)	ϵ_{Fu} (mm/mm)	δ_u (mm/mm)		
Plain Bars (6mm) for BF and CB frame specimens	T1	326	465					0.390		
	T2	330	468					0.407		
	T3	330	465					0.377		
Average		329	466					0.391		
Plain Bars (6mm)	N4	457	513			207	0.119	0.204		
	N6	439	494			199	0.108	0.202		
Average		448	504			203	0.114	0.203		
Deformed Bars (8mm)	Machined	N7	413	562	453	617	200	0.160	0.251	
		N8	403	549	442	602	199	0.150	0.232	
		N9	400	564	439	619	190	0.140	0.204	
	Deformed	N2	449	575	493	631	197	0.164	0.221	
		N3	416	544	457	597	183	0.182	0.277	
		N10	450	598	494	656	200	0.167	0.387	
		N11	411	544	451	597	196	0.162	0.368	
		N12	424	550	465	604	185	0.177	0.335	
		N13	449	599	493	657	214	0.166	0.362	
		N14	429	588	471	645	191	0.008	0.388	
		Deformed Bars (8mm) for BF and CB frame specimens	T4	427	543	468	595			0.300
			T5	445	569	488	625			0.325
			T6	445	578	488	625			0.320
		Average		428	566	466	621	195	0.148	0.305

* Based on 8mm diameter for deformed bars

4.1.3 Brick Units

Aerated concrete blocks (ACB), hollow clay bricks (HCB) and isolation bricks with dry locking key mechanism (LB) were utilized in the construction of infill walls. Wall sections on a vertical cut and masonry unit dimensions are illustrated in Figure 4.4. All brick units were half-scaled representatives of full-scaled originals except lacking scaling in the vertical direction of HCB and LB units. Clay bricks were laid with their holes parallel to the horizontal direction resulting in vertical stacking whereas ACB units were laid by horizontal stacking.

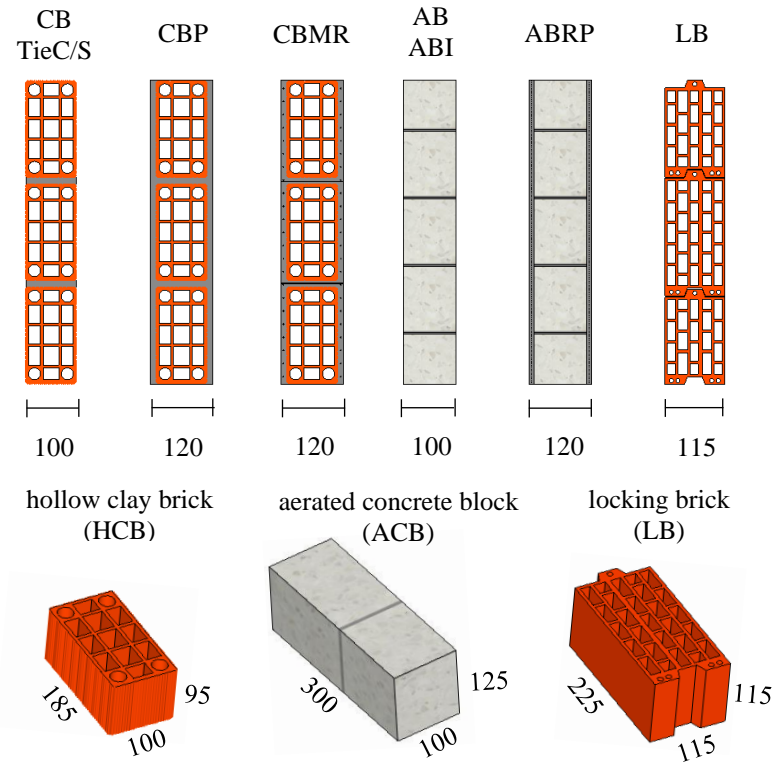


Figure 4.4. Tested infill walls and utilized brick units

Half-scaled G2/350 type ACB units which are $300 \times 125 \times 100 \text{ mm}^3$ (length x height x thickness) in size and 350 kg/m^3 in dry density were ordered from AKG company. The product catalog (AKG Gazbeton 2017) specifies the characteristic compressive strength and density of the units as 2.2 MPa and 450 kg/m^3 . Binici (2019) conducted uniaxial compression tests on eight 100 mm cubes and measured the mean compressive strength as 2.45 MPa. HCB units ordered from the Artuğ clay brick factory located in the city of İskenderun were $190 \times 95 \times 100 \text{ mm}^3$ in size. The average void ratio and unit weight of the HCB units were measured as 65% and 1120 gr respectively. All the voids of the HCB were filled with loose fine sand and the volume of the sand is measured with a beaker for void ratio measurement. The mean compressive strength of the HCB units was measured as 10 MPa when loaded parallel to the holes and 3.5 MPa when loaded perpendicular to the holes (Figure 4.5). The unit weight and void ratio of clay locking bricks which are $225 \times 115 \times 115 \text{ mm}^3$ in size were measured as 2300 gr and 53%, respectively.





Tested Specimens				
Wall unit	HCB	HCB	HCB	ACB
Loading dir.	horizontal	vertical	transverse	vertical
Ave. strength	$f_{b,h}=9.7$ MPa	$f_{b,v}=3.7$ MPa	$f_{b,t}=3.4$ MPa	$f_{b,v}=2.5$ MPa

Figure 4.5. Compressive strength of the masonry units

4.1.4 Mortar

General purpose mortar with a volumetric sand/cement/lime ratio of 6/1/1, compliant with ASTM Type N, was used as joint mortar and plaster for walls constructed with clay bricks. The cement and lime meet the requirements of TS EN 197-1 CEM IV/B(P) 32.5N and TS EN 459-1 CL 70-S standards, respectively. The maximum particle diameter of the sand was limited to 3mm. Dry components conforming to mentioned mix ratio was placed inside a wheelbarrow and stirred with a shovel (Figure 4.6). Water was gradually added to the dry mixture until desired consistency is achieved and samples were taken from each batch for material characterization.



Figure 4.6. Production and sampling of mortar

The water content of each batch is arranged according to flow diameter measurements. The mortar sample is placed on a flow table and dropped 25 times within 15 seconds as defined in ASTM C1437 (2013) (Figure 4.7). A flow diameter between 205 and 215 mm is achieved for all samples.



Figure 4.7. Flow tests conducted for mortar consistency

For walls constructed with ACB, ready-made interface mortar and plaster were used by adding a specified amount of water and stirring with a drill until the desired workability was ensured. The mean compressive strength of the interface mortar and the plaster was measured as 8.40 MPa and 1.11 MPa by Binici (2019).

50 mm cube, $40 \times 40 \times 160 \text{ mm}^3$ prisms and 100mm cylindrical mortar samples were taken, cured in the lab and tested in accordance with ASTM C109 (2013), ASTM C348 (2014), ASTM C349 (2014) and ASTM C469 (2014) standards (Figure 4.8 and Table 4.3). Although mortar samples had the same mixture ratios and consistency, due to the age of mortar at test day and inherent variation in mechanical properties of ingredients, there is a dispersion in mechanical properties of mortar among different frame specimens.



Figure 4.8. Tests on mortar specimens

Table 4.3 Mortar test results

Frame	CB									
Test Date	11-09-14									
Specimen	N1	N2	N3	N4	N5	N6	N7	N8	mean	st.dev
$f_{mc,cylinder}(MPa)$	6.77	6.55	8.22	6.22					6.94	0.88
Age of Mortar	129									

Frame	CBP									
Test Date	18-05-15									
Specimen	N1	N2	N3	N4	N5	N6	N7	N8	mean	st.dev
$f_{mc,prism}(MPa)$	2.19	1.81	2.97	2.61	2.26	1.73	1.99	2.49	2.26	0.42
$f_{mt,prism}(MPa)$	0.86	0.74	1.03	0.86	0.81	0.61	0.67	0.93	0.81	0.14
Age of Mortar	91									

Frame	CBMR									
Test Date	30-08-14									
Specimen	N1	N2	N3	N4	N5	N6	N7	N8	mean	st.dev
$f_{mc,cylinder}(MPa)$	3.33	3.22	3.22						3.26	0.06
Age of Mortar	16									

Frame	TieC									
Test Date	11-09-14									
Specimen	N1	N2	N3	N4	N5	N6	N7	N8	mean	st.dev
$f_{mc,cylinder}(MPa)$	2.11	3.22	1.78						2.37	0.76
Age of Mortar	23									

Frame	TieS									
Test Date	31-12-14									
Specimen	N1	N2	N3	N4	N5	N6	N7	N8	mean	st.dev
$f_{mc,cube}(MPa)$	3.13	2.95	2.94						3.01	0.10
Age of Mortar	28									

Frame	LBP									
Test Date	25-12-15									
Specimen	N1	N2	N3	N4	N5	N6	N7	N8	mean	st.dev
$f_{mc,cube}(MPa)$	5.42	5.68	5.48	5.57	6.01				5.63	0.23
$f_{mc,prism}(MPa)$	6.04	5.83	6.10	5.96	5.29	5.64			5.81	0.30
$f_{mt,prism}(MPa)$	1.38	1.15	1.27	1.38	1.17	1.38			1.29	0.11
Age of Mortar	18									

4.1.5 Mesh Reinforcement

Fiber and steel mesh reinforcements utilized for surface overlay oriented retrofit of aerated concrete block (ACB) and hollow clay brick (HCB) walls were tested under uniaxial tension (Figure 4.9).



Figure 4.9. Testing of mesh reinforcement a) Fiber (Todorovic 2019), b) Steel

The fiber mesh employed for the ACB laid walls was Styrol Butadien Copolymer (SBC) with a unit weight of 160 gr/m^2 and grid size of 4 mm in both directions. Each filament had a width and thickness of 1.2 mm and 0.5 mm. Todorovic (2019) conducted uniaxial tensile tests on three specimens under displacement controlled loading protocol. The uniaxial tensile strength of the mesh obtained from the average of three uniaxial tensile strength tests was 20 N/mm which corresponds to an average ultimate strength of 117 MPa based on the net area of filaments. The results also revealed that the mesh was characterized by limited ductility (i.e. $\delta u/\delta y \approx 1.5$). On the other hand, steel mesh reinforcement utilized for HCB laid walls has 2mm diameter wires with 25mm pitch in both directions. Four test specimens were prepared by cutting a line of wire from the mesh. The uniaxial tensile strength of the mesh obtained from the average of three uniaxial tensile strength tests was 70 N/mm which corresponds to an average ultimate strength of 550 MPa based on the net area

of steel wires. Test results for one line of 2 mm wire within steel mesh reinforcement are illustrated in Figure 4.10 below.

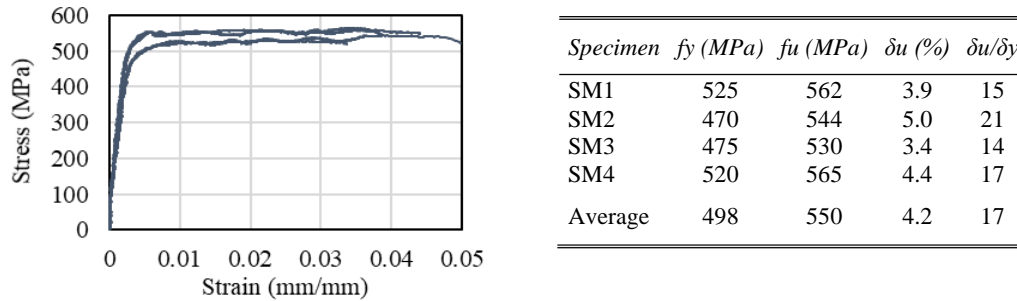


Figure 4.10. Steel mesh reinforcement test results

4.1.6 Tie Wire

General purpose tie wires with 1.3mm diameter were used for attaching reinforcing bars as well as mesh reinforcements placed at both sides of the CBMR frame specimen. Uniaxial test results for four tie wire specimens are provided in Table 4.4 below. Results indicate that an average 1.3 mm diameter tie wire yields around 30 kg and ruptures around 50 kg.

Table 4.4 Mechanical properties of tie wire

<i>Specimen</i>	<i>f_y (MPa)</i>	<i>f_u (MPa)</i>	<i>δu (%)</i>	<i>δu/δy</i>
TW1	185	340	30	325
TW2	207	355	26	251
TW3	222	370	-	-
TW4	222	355	29	262
Average	209	355	28	268

4.1.7 Horizontal Steel Ties

Uniaxial tension testing for horizontal steel ties and steel channels utilized for HCB Infill with Continuous Horizontal Steel Ties (TieC) and HCB Infill with Staggered Horizontal Steel Ties (TieS) frame specimens were conducted by the producer (Ereğli Demir ve Çelik Fabrikaları A.Ş.) according to DIN EN 10025-2-2004. Measured mechanical properties are illustrated in Table 4.5 below.

Table 4.5 Mechanical properties of steel tie and channel

	<i>Tie</i>	<i>Channel</i>
Standard	S235JR	S355J2C+N
f_y (MPa)	340	458
f_u (MPa)	429	573
δu (%)	34	30

4.1.8 Summary of Material Tests

The measured average strengths of materials involved in the construction of frame specimens are illustrated in Table 4.6. Concrete for all frame specimens was ordered from the same producer with the same mix design. Since the frame is scaled to half, a super liquid and self-compacting concrete were selected to minimize possible difficulties in placement. So, the slump test was not possible for consistency checks of purchased batches. Depending on the ambient temperature, time of transport and inability of the concrete plant to sustain the same mix-design for low volumes of concrete (due to half scaling, casting in two phases and availability of only two formworks, usually 2 m³ of concrete was ordered instead of the full capacity of the concrete mixer), water-cement ratio of the ordered batches fluctuated resulting in scattered compressive strengths. However, concrete samples were tested prior to frame tests and the axial ratio of columns was arranged accordingly to minimize the influence of scattered concrete strength on the moment capacity of columns. Steel tension tests were conducted on two different batches first of which was used in BF

and CB frame specimens. Mortar for all clay brick laid walls were produced by applying the same volumetric ratios and checking the consistency of each batch. Mortar was sampled during the construction of infill walls and masonry prism specimens which took place on the same day. However, there is an inevitable lag between the execution of frame and prism tests. Mortar specimens were tested together with the prisms and the measured mortar strength was not representative of the mortar strength of the tested infill wall. Besides, a standard sampling and testing procedure was implemented only after the 3rd frame experiment. Mortar samples of the first three frame tests, namely CB, CBMR and TieC, were 75 mm diameter cylindrical specimens whereas others were cubic and prismatic samples defined in previously mentioned ASTM specifications for mortar characterization.

In order to overcome non-standardized sampling and time-based strengthening issues, a separate batch of mortar was produced and a vast range of prismatic, cubic and cylindrical samples was taken. Samples were tested at different times to idealize strength gain with time and different samples were tested together to identify size effect. As a result, a fourth-order linear polynomial equation was derived for age correction where strength after 28th day is assumed constant (Figure 4.11).

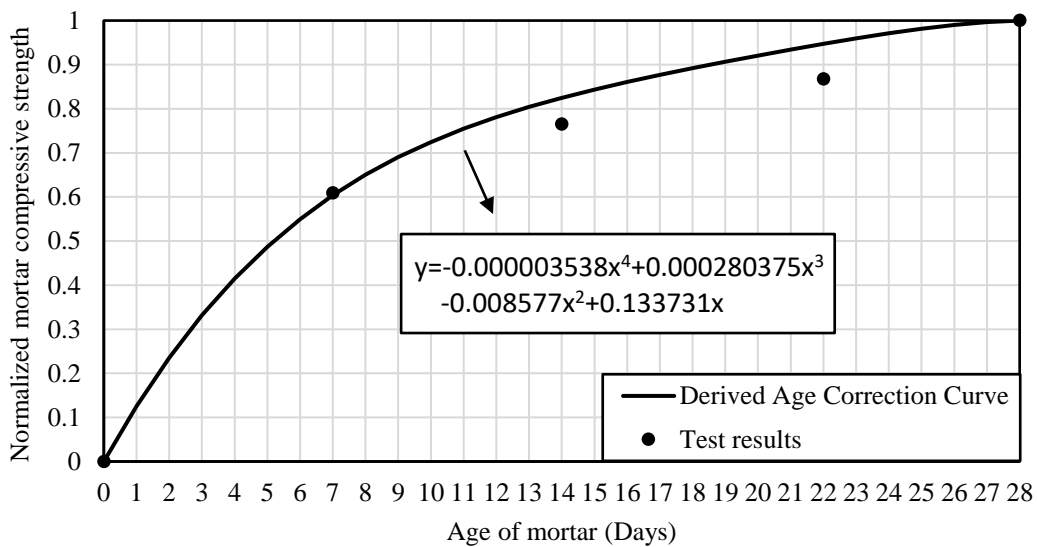


Figure 4.11. Time based mortar compressive strength correction curve

Additionally, a conversion coefficient of 1.15 was identified to be multiplied with cylindrical specimen strength in order to convert it to prism strength. The age and size corrections were applied to predict the prism mortar compressive strengths of infill walls on the frame test day (Table 4.6).

Table 4.6 Average material strengths at frame test day

Frame	Concrete		Steel ^a				Mortar ^b	Brick	
	f_c (MPa)	f_{st} (MPa)	Deformed (8mm)		Plain (6mm)		f_m (MPa)	Unit Type	f_b (MPa)
			f_y (MPa)	f_u (MPa)	f_y (MPa)	f_u (MPa)			
BF	27.9	2.8	482	618	328	466	-	-	-
CB	22.3	2.7					466	623	448
CBP	26.4	-	2.3						
CBMR	33.6	2.4	3.7						
TieC	34.6	2.8	2.6						
TieS	33.3	2.9	3.0						
LBP	28.2	2.1	6.2	LB	-				
AB	24.9	2.1	8.4	ACB	2.5				
ABI	32.3	3.0							
ABRP	18.9	1.7							

a. Based on 8 mm diameter of the deformed bars instead of the nominal diameter

b. Age and size corrections were made to determine material strength on frame test day

4.2 Masonry Prism Tests

Masonry prism specimens were constructed right after the finalization of infill wall construction by the same mason and using the same materials whose geometrical and mechanical properties have been presented in the previous section. The samples were cured under the same conditions as the infill walls. Masonry prism tests under uniaxial compression (ASTM C1314, 2014), diagonal compression (ASTM E519, 2010), sliding shear (EN 1052-3, 2002) and bending (ASTM E518, 2015) have been conducted. Additionally, the influence of plaster and bilateral steel mesh reinforcement on the axial and shear capacity of prisms was investigated.

All tests were conducted using a 200 kN capacity test setup based in METU Uğur Ersoy Laboratory which is capable of displacement controlled loading (Figure 4.12). The bottom loading plate of the setup is resting on an electric motor controlled screw jack. A CAS LS-20t brand loadcell was attached in between the screw jack and the bottom loading plate to measure exerted loads. The rigid upper beam of the setup is fastened to four threaded rods with nuts which allow vertical arrangement of the top beam by loosening the nuts moving the rigid beam in the vertical direction with the crane and tightening the nuts. An additional manually controlled two-way hydraulic jack might be attached to the upper beam for fine adjustment of the gap between the test specimen and the upper loading plate.

All the transducers were connected to Vishay 5100B data acquisition system. Displacements were monitored on both sides of the specimens using 10mm capacity Kyowa DTH-A LVDTs attached via threaded anchor rods embedded with epoxy. LVDT readings on both sides of the were averaged to minimize possible bending deformations. After LVDTs were secured against falling damage with loosely connected tie wires, displacement-based loading is exerted with a screw jack until the failure of the prism specimens.

Displacement measurements from attached LVDTs were divided with the gage lengths and converted into average axial strains. The corresponding stresses were determined based on the gross area of the tested prism. No correction factors were applied to the test results presented in this section. In order to calculate young's modulus and/or shear modulus, a secant line between 5% and 50% of ultimate strength was drawn for the relevant stress-strain curve.



a) Diagonal tension b) Uniaxial compression c) 4-point bending

Figure 4.12. Setup for masonry prism tests

4.2.1 Uniaxial Compression Test

Uniaxial compression tests were conducted for three different orientations of HCB and in the vertical direction of ACB units considering its horizontal stacking (Figure 4.13). Three HCB masonry prisms were sampled after the construction of CB, CBP, CBMR, TieC and TieS frame specimens. Tests on three ACB prisms were conducted by Lana Todorovic (2019) and Beyazıt Bestami Aydın (2022).



Figure 4.13. Uniaxial compression testing of masonry prisms

In order to ensure uniaxial loading, specimens were carefully capped with high strength cement lime mixture paste. After carefully placing and centering the specimen on the bottom loading plate, the upper loading plate was placed, its alignment was checked and a ball joint is placed to ensure uniaxial loading (Figure 4.14.a-b). LVDTs were placed and their orientations were checked on both sides of the specimen (Figure 4.14.c).

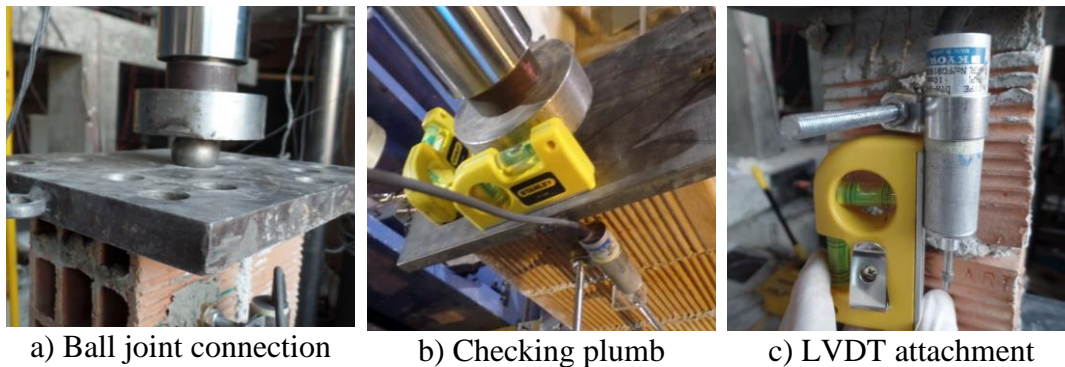
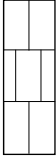



Figure 4.14. Masonry prism uniaxial test setup details

Results for performed uniaxial tests of masonry prisms without plaster are documented in Table 4.7. The ACB prism tests were conducted by Todorovic (2019). The average compressive strength of all HCB prism tests was 1.30 MPa for the vertical direction (i.e. perpendicular to openings) and 1.65 MPa for the horizontal direction (i.e. parallel to openings which is the strong direction of bricks), respectively. Likewise, the average of prism compression tests on ACB prisms is 0.97 MPa.

Table 4.7 Uniaxial compression test results for masonry prisms w/o plaster

<i>Date of Test</i>	<i>Wall Unit</i>	<i>Loading Direction</i>	<i>Mortar Strength (MPa)</i>	<i>Compressive Strength (MPa)</i>	<i>Young's Modulus (MPa)</i>	<i>Ultimate Strain (x1000)</i>	
11.09.2014	HCB	↓	6.94	1.39	3109	0.81	
19.04.2015	HCB		2.26	1.04 (0.25)	1967 (267)	0.87 (0.17)	
09.09.2014	HCB		3.26	1.48 (0.25)	3247 (208)	0.70 (0.08)	
12.09.2014	HCB		2.37	1.19 (0.10)	2361 (62)	0.74 (0.09)	
20.01.2015	HCB		↑	3.01	1.41 (0.02)	3084 (541)	0.68 (0.13)
Average:			3.57	1.30 (0.16)	2754 (500)	0.76 (0.07)	
15.04.2015	HCB	↓	2.26	1.77 (0.26)	1993 (162)	5.28 (2.27)	
24.09.2014	HCB		3.26	1.97 (0.07)	2306 (135)	5.00 (0.75)	
24.09.2014	HCB		2.37	1.71 (0.19)	1391 (82)	5.37 (0.50)	
23.01.2015	HCB		↑	3.01	1.14 (0.13)	3360 (688)	6.13 (3.89)
Average:			2.73	1.65 (0.31)	2178 (759)	5.44 (0.42)	
ACB		Average:	8.63	0.97 (0.04)			

*Numbers in parenthesis stand for standard deviation

** Tests on ACB prisms were conducted by Todorovic (2019)

Stress-strain curves for HCB masonry prisms are illustrated in Figure 4.15. The ultimate strain capacity of HCB prisms is 7 times larger when loaded parallel to openings (horizontal direction of the wall) compared to loading perpendicular to openings. The modulus of elasticity of the tested HCB masonry prisms was 2075 (1465) times their compressive strength when loaded in the vertical (horizontal) direction of the wall.

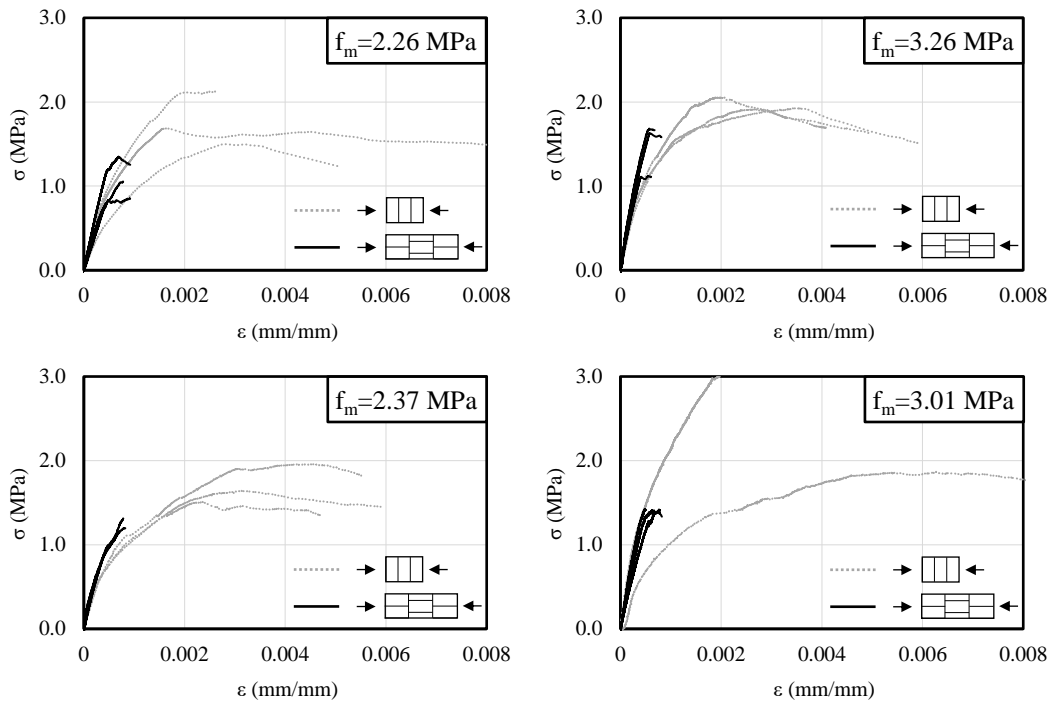


Figure 4.15. Stress-strain curves of HCB prisms under uniaxial compression

4.2.2 Diagonal Tension Test

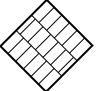
The shear strength capacity of infill walls which is also equivalent to diagonal tensile strength is usually determined by applying compressive force along the diagonal of a square prism specimen. Accordingly, square masonry prism specimens of 700 x 700 mm² dimensions were constructed for diagonal tension tests. Two LVDTs in horizontal and vertical directions are attached at 50 cm apart on both sides of the specimens to measure contraction and elongation along diagonals. LVDT readings recorded on both sides of the specimens were averaged to minimize possible bending deformations. Half scaled replica of shear toes defined in ASTM E519 was produced and placed at the loaded ends of the prisms (Figure 4.16). The ball joint placed over the upper shear toe ensures uniaxial loading. Load and displacement measurements were converted to shear stress and shear strain values according to formulas proposed in ASTM E519.



Figure 4.16. Diagonal compression test

Results of performed diagonal tension tests of masonry prisms without plaster are illustrated in Table 4.8 and Figure 4.17. The average shear strength and shear modulus values calculated for all HCB prism tests were 0.22 MPa and 853 MPa, respectively.

Table 4.8 Diagonal tension test results for masonry prisms w/o plaster

<i>Date of Test</i>	<i>Wall Unit</i>	<i>Loading Direction</i>	<i>Mortar Strength (MPa)</i>	<i>Shear Strength (MPa)</i>	<i>Shear Modulus (MPa)</i>	<i>Ultimate Strain (x1000)</i>
22.09.2014	HCB		6.94	0.27	889 (3)	2.75 (0.13)
24.04.2015	HCB	↓	2.26	0.15 (0.02)	772 (227)	1.13 (0.30)
16.09.2014	HCB		3.26	0.34 (0.02)	964 (188)	
19.09.2014	HCB	↑	2.37	0.11 (0.02)	625 (144)	0.52 (0.48)
19.01.2015	HCB		3.01	0.22 (0.02)	1013 (116)	0.93 (0.89)
Average:			3.57	0.22 (0.08)	853 (136)	1.33 (0.85)

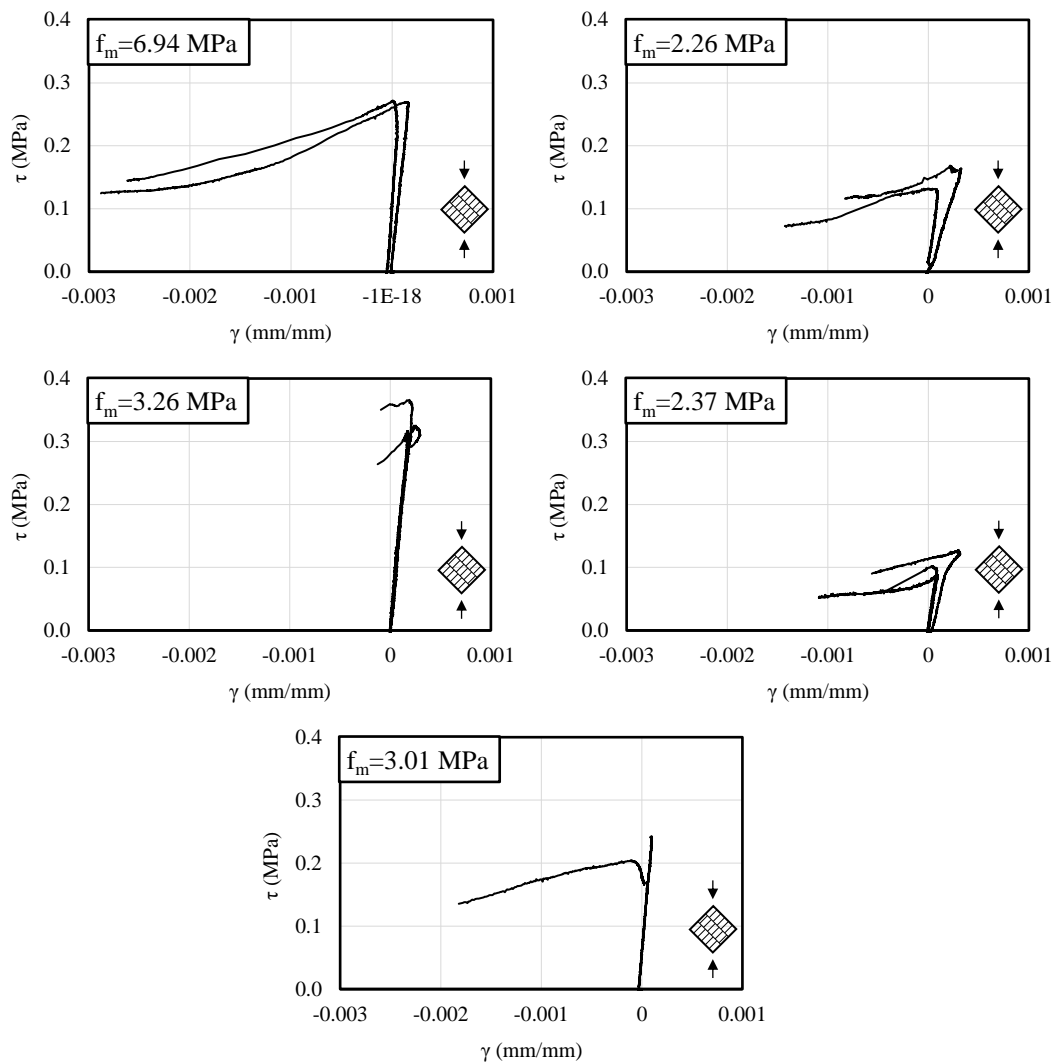


Figure 4.17. Stress-strain curves of HCB prisms under diagonal tension tests

4.2.3 Sliding Shear Test

The mortar joints create planes of weakness and potential sources for crack initiation and propagation. Cracking of along bed joints is a typical infill failure mode observed after earthquakes. Slip induced debonding between the mortar joint masonry unit interface and/or cracking of mortar joints due to slip along the interface under shear loading lead to significant stiffness degradation and material damping. In order to determine the sliding capacity of mortar joints split shear tests were conducted.

Tests were conducted according to EN 1052-3. An original test setup was designed for the application and monitoring of confining pressure on the failure surfaces of prisms. Rubber glued loading plates placed on both sides of the specimen apply confining pressure to failure surfaces by tightening the nuts of the threaded rods. For sensitive measurement of the loads transferred to both ends, CAS SBS-500L brand S type load cells with 500kg capacity were also attached to the same threaded rods on the front and back sides of the specimen. In order to ensure uniaxial loading which is very critical in sliding shear tests, ball joints were used in the vertical as well as the horizontal directions (Figure 4.18). As confining pressure is constantly monitored during testing, in case of more than a 10% drop of confining pressure during the experiment, fine adjustment is made by tightening the nuts.



Figure 4.18. Sliding shear test of masonry prisms

Once desired confining pressure is applied and it is sustained until failure of the joints, shear strength at various normal stress levels was determined leading to identify the Mohr-Coulomb surface at the interface between brick and mortar joints (Figure 4.19). After 7 successful tests at various lateral confining pressure levels, cohesion is determined as 0.161 MPa and friction angle is calculated as 60 degrees.

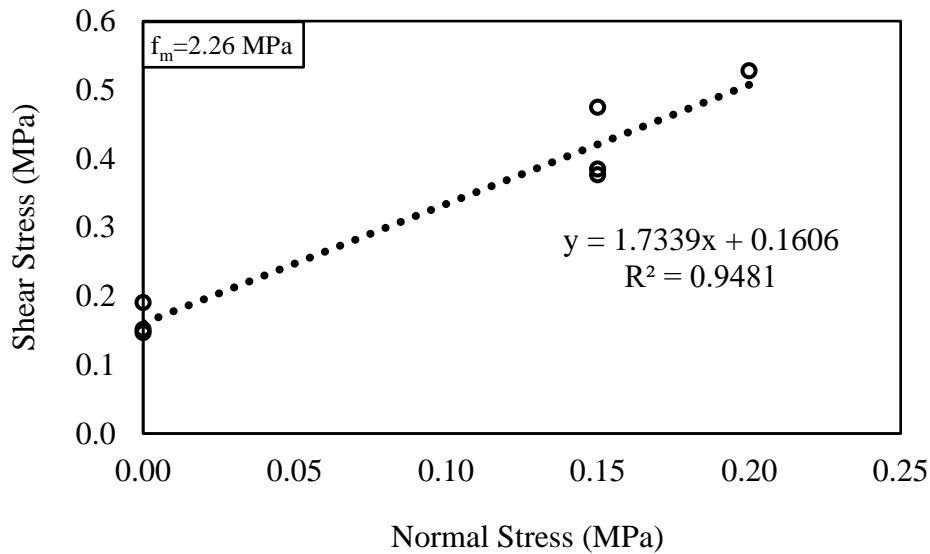


Figure 4.19. Mohr-Coulomb failure surface after sliding tests

4.2.4 Bending Test

The flexural bond strength of masonry beam prisms was calculated in accordance with ASTM E518. A four-point bending test setup was constructed (Figure 4.20). All four points of contact with the masonry prism were roller cylinders with ball joints at the ends which eliminate frictional forces. CAS SBS-500L brand S type load cells with 500kg capacity were utilized for sensitive measurement of loading. Specimens were forced to fail in the direction orthogonal to the mortar bed joints simulating out-of-plane loads and forcing the infill wall arching in the vertical direction. HCB beam prisms consisted of 4 courses of bricks laid using general purpose mortar ($f_m=4.07 \text{ MPa}$), whereas ACB prisms tested by Todorovic (2019) consisted of 7 blocks glued together with ACB mortar ($f_m=8.63 \text{ MPa}$).

The test campaign included 11 specimens. Six specimens were ACB beam prisms of 300mm width and 100mm thickness three of which had reinforced plaster overlay ($t=10 \text{ mm}$ on each face) and the remaining three were tested without plaster. The remaining five specimens were HCB beam prisms three of which had bilateral steel

mesh reinforcement and plaster the other two had plaster only (t=10 mm on both faces) and the last one was without plaster.

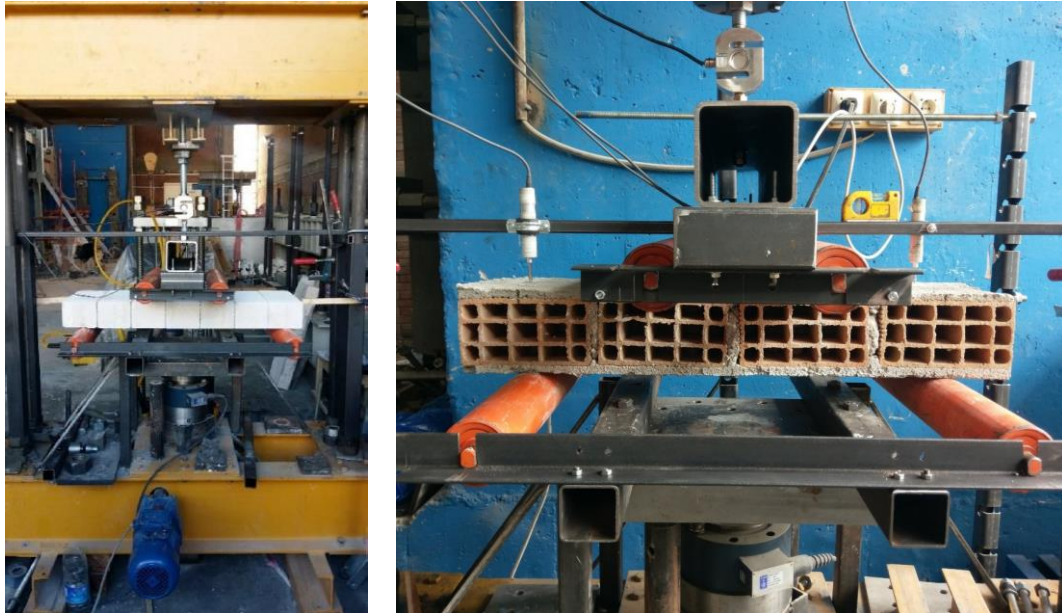
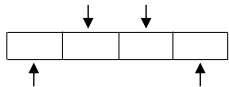


Figure 4.20. Bending tests of masonry beam specimens

Test results are illustrated in Table 4.9. Mesh reinforcement for HCB and ACB masonry beam prisms increased the bending capacity 4 and 5 times, respectively.

Table 4.9 Bending test results for masonry beam prisms

<i>Wall Unit</i>	<i>Plaster</i>	<i>Loading Direction</i>	<i>Mortar Strength (MPa)</i>	<i>Modulus of Rupture (MPa)</i>
HCB	No		4.07	0.23
HCB	Yes		4.07	0.30 (0.04)
HCB	Yes (steel mesh)		4.07	0.94 (0.11)
ACB	No		8.63	0.19 (0.02)
ACB	Mesh (fiber mesh)		8.63	0.96 (0.15)

4.2.5 Influence of Plaster and Mesh Reinforcement

The influence of plaster and bilateral mesh reinforcement was investigated through additional prism tests. All tested specimens have the same mortar ($f_m=2.26$ MPa) and were constructed by the same mason with the same HCB units. Uniaxial compression, diagonal tension and bending tests were conducted as clarified in previous sections. It is observed that the presence of plaster and mesh reinforcement changes the failure mechanism (Figure 4.21) and improves load and displacement capacity. Test results are shown in Table 4.10.

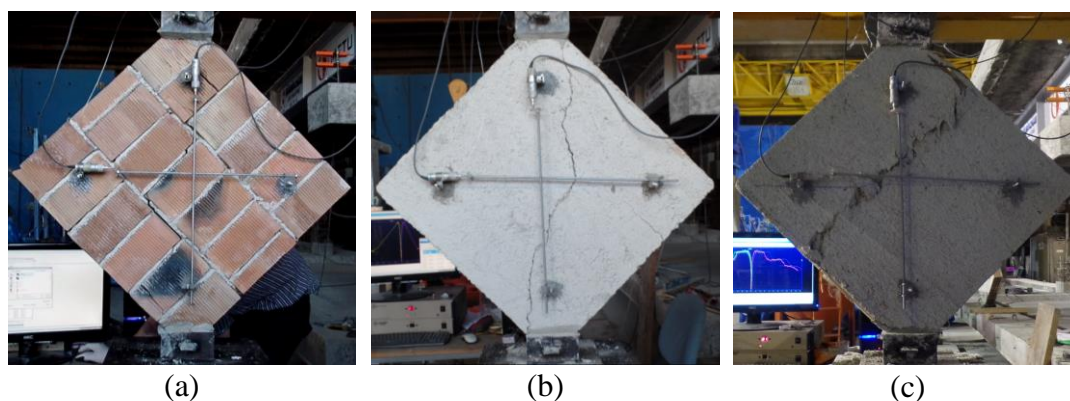


Figure 4.21. Failed diagonal tension specimens a) CB, b) CBP, c) CBMR

Bilateral mesh reinforcement increased the shear and bending capacity of masonry prisms, whereas the presence of plaster only increased shear capacity. The least affected parameter by the presence of plaster and mesh reinforcement is the uniaxial compressive strength and modulus of elasticity.

Table 4.10 Comparison of CB, CBP and CBMR prism specimens

<i>ID</i>	$f_{w,v}$ (MPa)	$E_{w,v}$ (MPa)	$f_{w,h}$ (MPa)	$E_{w,h}$ (MPa)	τ_w (MPa)	G_w (MPa)	$f_{w,t}$ (MPa)
CB	1.09	2266	1.77	1655	0.12	657	0.23
CBP	1.04	1967	2.59	1993	0.33	1411	0.30
CBMR	1.00	-	2.92	1695	0.33	1106	0.94

CHAPTER 5

EXPERIMENTAL RESULTS

Review of experimental observations, assumptions in post-processing of the raw data and presentation of post-processed experimental data recorded during testing will be illustrated in this chapter.

5.1 Assumptions and Corrections in Processing Raw Data

Assumptions and corrections on experimental data measured during the testing of the frame specimens were illustrated in this section.

5.1.1 Correction for Lateral Component of Vertical Jacks

The base shear of the tested frame specimens was measured using a loadcell attached to the horizontal jack used to push and pull the frame in the lateral direction. Under increasing lateral displacement cycles, the bottom ends of vertical jacks sway with the frame, whereas their top end attached to the rigid support frame stays still resulting in deviation from the initial vertical orientation. Post-processing of the raw experimental data begins with a correction for the measured base shear of the tested specimen, considering the lateral component of the vertical jacks due to increasing lateral displacement cycles.

The lateral component of the force recorded on the vertically oriented hydraulic jacks placed on top of columns was calculated at each recorded step depending on the corresponding measured lateral displacement of the frame and the axial load on the vertical jacks using the equation below:

$$V_{\text{cor}} = V_{\text{raw}} + \frac{(F_{v1} + F_{v2})}{\sqrt{(L_v^2 + \delta^2)}} \times \delta$$

Where the symbols used in the equation is illustrated in the Figure 5.1 below:

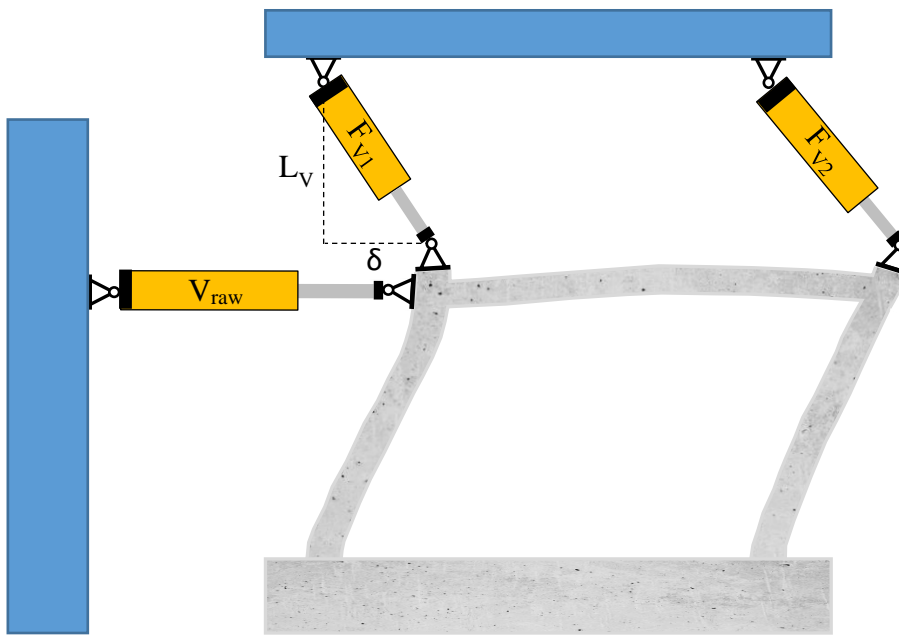


Figure 5.1. Base shear correction due to vertical jacks

An additional correction was made in case the initial orientation of vertical jacks were off plumb, which can be identified by the generation of lateral force upon application of vertical load before application of lateral displacements.

Measured and corrected hysteresis responses of tested frames are illustrated in Figure 5.2 below.

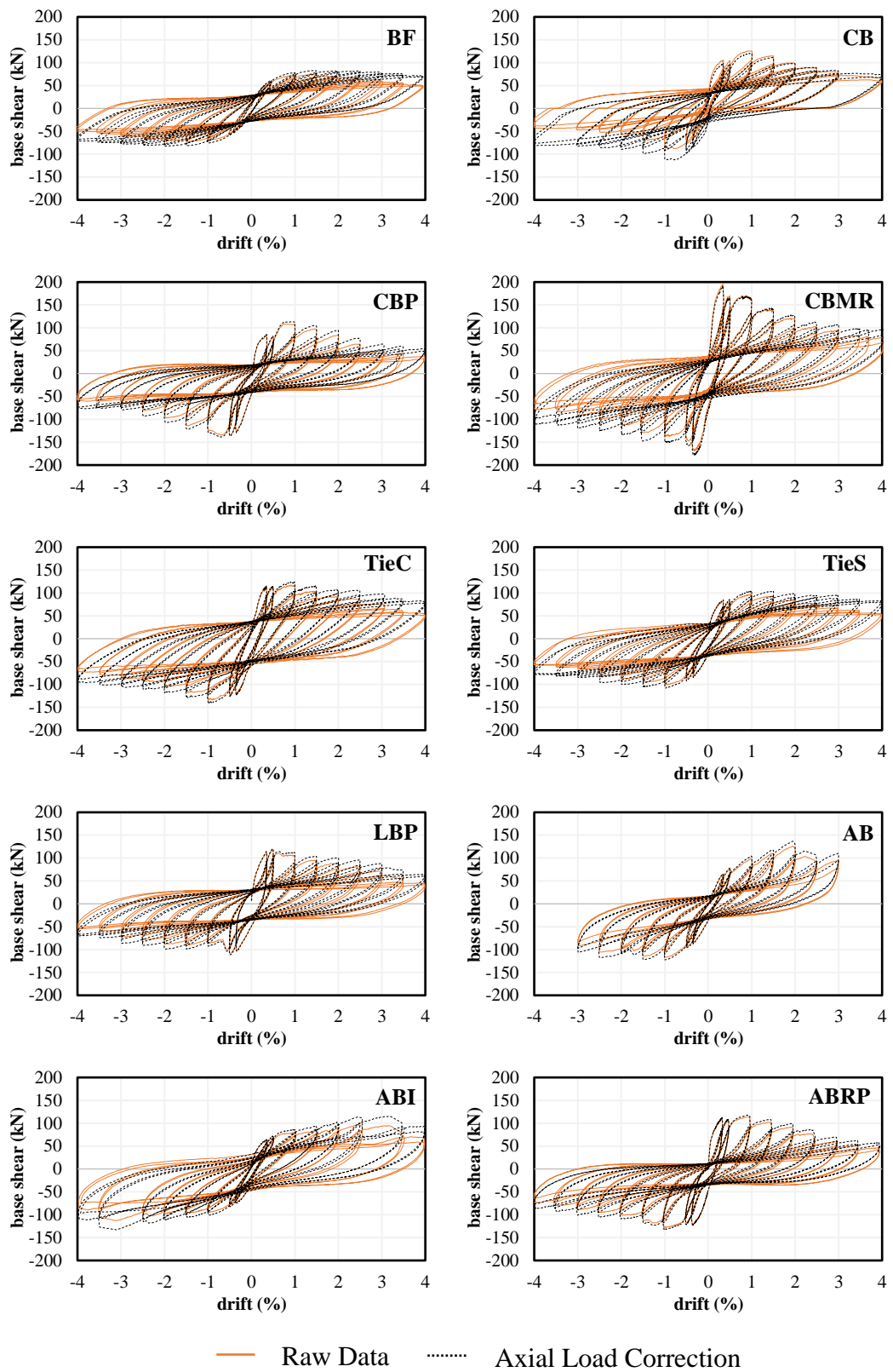


Figure 5.2. Axial load correction on hysteresis responses of tested specimens

5.1.2 Curve Fitting for Hysteresis Loops

A similar method employed by various researchers to identify the infill wall (IW) response was followed by subtracting the bare frame (BF) response from infilled frame (IF) response (Alwashali et al. 2018; Blasi, De Luca, and Aiello 2018; De Risi et al. 2018; Gaudio et al. 2019; Hak, Morandi, and Magenes 2013; Lin et al. 2016; B. A. Mehrabi et al. 1996; Morandi, Hak, and Magenes 2018a; Turgay et al. 2014). A direct subtraction of IF experimental data from BF experimental data is impossible since recorded lateral displacements of BF and IF tests were not coincident. In order to derive a continuous hysteresis loop of IW, the subtraction was made by idealizing each experimental cycle with four separate 6th-order polynomial equations fitted to predetermined regions of each displacement cycle (Figure 5.3). In case of a sudden drop in load due to the initiation of major damage on the wall, the number of separate equations was increased to sustain a good match between the experimental and the fitted data.

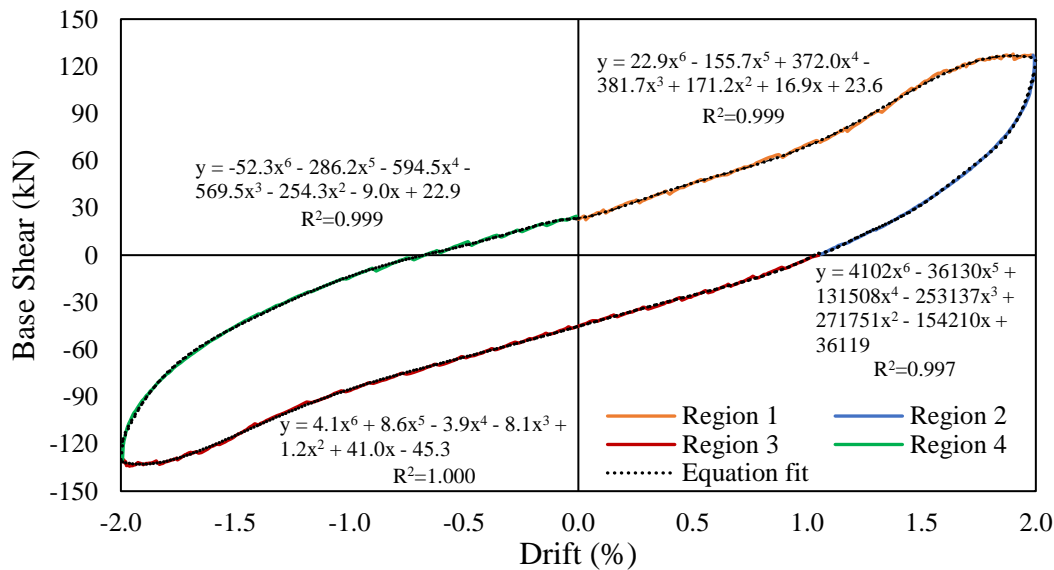


Figure 5.3. Equation fit for displacement cycle of CBMR specimen at 2% drift

Equation fit for the measured and axial load correction applied hysteretic responses of tested frames are illustrated in Figure 5.4 below.

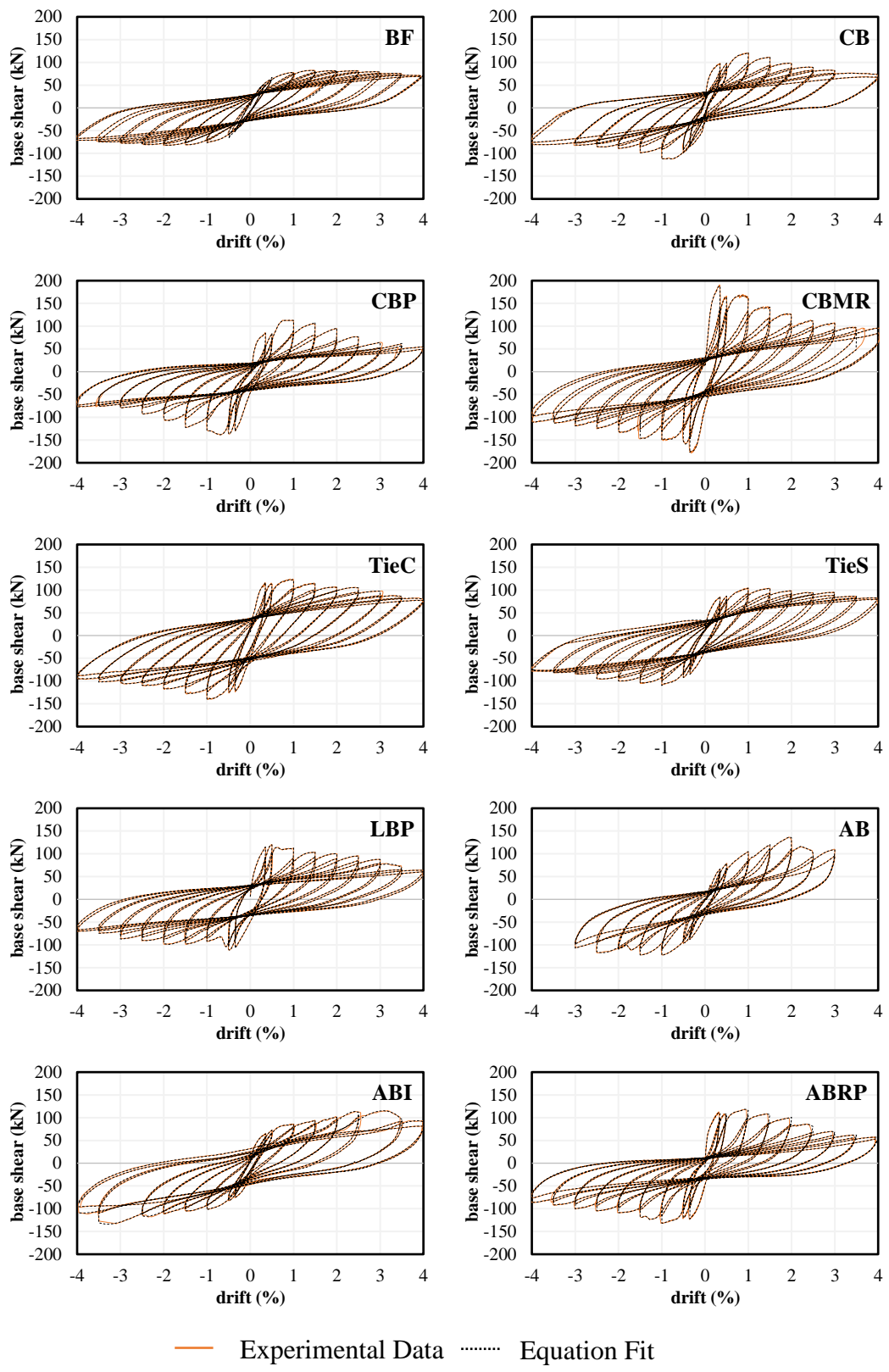


Figure 5.4. Equation fits to experimental hysteresis data

5.1.3 Calculation of Member End Rotations and Curvatures

Lateral drift (i.e. IDR) is calculated by averaging LVDT measurements taken at both ends of the flange corresponding to the geometric center of the flanged beam, which is 1443 mm from the face of the foundation. LVDT measurements taken at a distance equal to the effective depth of beam and column sections (i.e. 180mm) from the face of beam-column joints or the foundation were used to determine member end rotations. The bottom end of the columns was equipped with 4 LVDTs, allowing for the averaging of the end rotation measured on both sides, whereas column tops and beam ends were equipped with 2 LVDTs attached on one side (Figure 5.5).

End rotation is calculated using the equation provided below:

$$\theta_{\text{end}} = \frac{(\Delta_{\text{end},1} - \Delta_{\text{end},2})}{d_{\text{LVDT}}}$$

Where $\Delta_{\text{end},1}$ and $\Delta_{\text{end},2}$ are LVDT measurements attached to opposite sides of member ends and d_{LVDT} is the distance between centers of the LVDT's.

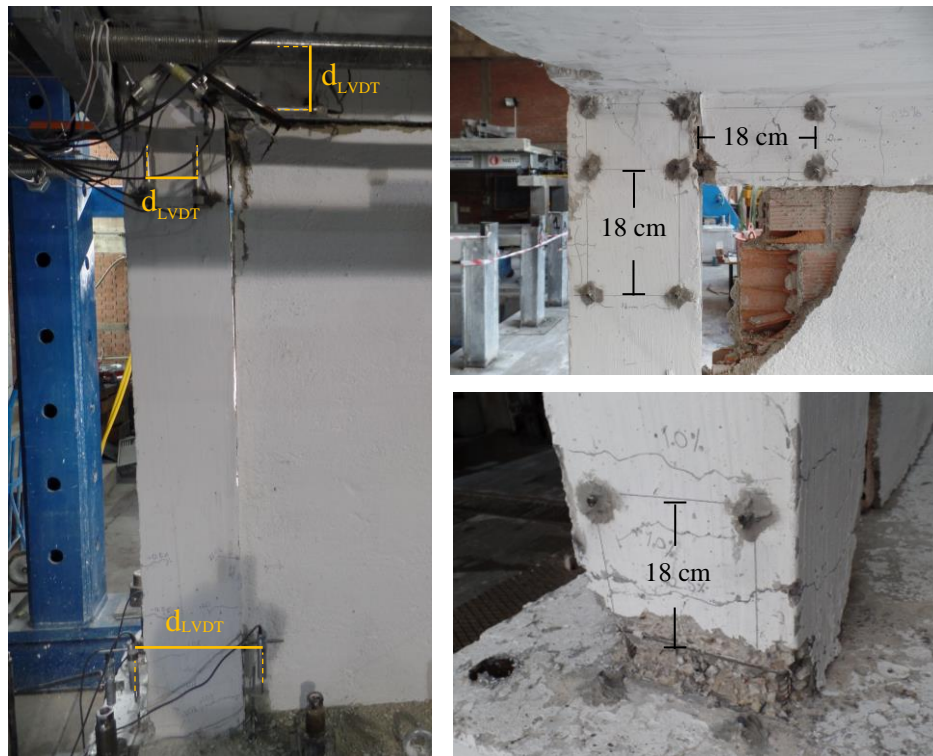


Figure 5.5. LVDT attachment locations

The yielding of a member can be calculated by identifying yield rotation, a jump in strain gage measurements attached to longitudinal bars at member ends, or from yield curvature calculated from the equation given below:

$$\varphi_{\text{end}} = \frac{(\epsilon_{\text{end},1} - \epsilon_{\text{end},2})}{d_{\text{bars}}}$$

Where $\epsilon_{\text{end},1}$ and $\epsilon_{\text{end},2}$ are strain measurements and d_{bars} is the distance between the longitudinal bars (i.e. 160 mm) to which the strain gages were attached.

5.2 In-plane Cyclic Loading Test Results

RC frame specimens tested under increasing in-plane displacement reversals are illustrated in Table 5.1 below.

Table 5.1. RC frame specimens tested at IP direction

<i>Test No</i>	<i>Wall Unit</i>	<i>Plaster</i>	<i>Retrofit</i>	<i>Abbreviation</i>
1	Bare	-	-	BF
2	HCB	No	No	CB
3	HCB	Yes	No	CBP
4	HCB	Yes	Steel mesh overlay	CBMR
5	HCB	No	Infill-tie (cont.)	TieC
6	HCB	No	Infill-tie (staggered)	TieS
7	LB	Yes	Dry slip joints	LB
8	ACB	No	No	AB
9	ACB	No	Isolation joint	ABI
10	ACB	Yes	Fiber mesh overlay	ABRP

Key: HCB – Horizontal Clay Brick, LB – Locking Brick, ACB – Aerated Concrete Block

The following sections will illustrate a detailed description of structural and infill wall damage sequences for the tested specimens at target lateral drift levels. Additionally, graphical and tabular presentation of post-processed experimental data will be provided for a better understanding of structural response.

5.2.1 Bare Frame (BF)

The bare frame specimen was tested before infilled frame tests in order to identify the influence of different wall systems on the seismic response. BF is a half-scaled, one-story, one-bay inner ground frame of a five-story prototype building designed according to the high ductility design requirements of Turkish Earthquake Code (2007).

Backbone curves corresponding to the first and second cycles and the identification of yield force and maximum base shear is illustrated in Figure 5.6. Yielding of the frame corresponds to the first strain jump in frame members.

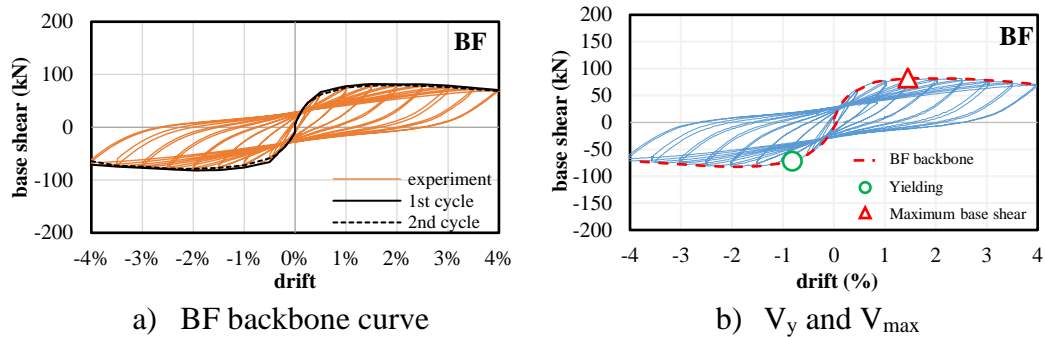


Figure 5.6. Load-displacement response of BF specimen

The propagation of damage for BF is illustrated in Figure 5.7. The initial flexural cracking was observed at the bottom plastic hinge zones of two frame columns and the beam end close to the reaction wall after the load reversal corresponding to a 0.5% drift level. When the story drift reached 1.0%, existing cracks on the column surface further developed, approaching the columns' geometric center at the bottom end. Several new cracks opened at the top end of the columns, and new flexural cracks were observed at the beam ends. The peak lateral strength reached 82.2 kN in the positive direction at 1.41% drift and -82.2 kN in the negative direction at -1.91%. In the subsequent displacement cycles, the structure maintained a load resistance greater than 80% of the peak load until the termination of the test at 4% drift. Flexural cracks at beam ends presented an extensional trend to the upper RC slab at 1.5% drift. When the story drift reached 2.0%, hairline diagonal shear cracks were spotted at beam-column joints, flexural cracks closest to the column lower end widened to 1.25 mm, and the crushing of cover concrete was initiated. Buckling of the first longitudinal reinforcement took place at 2.5% drift. When the story drift reached 3.0%, cover concrete spalled at column tops, crushing extended at column bottoms and buckling of additional longitudinal bars at column bottoms took place. When the drift ratio of the frame reached 3.5%, the cover concrete at the column lower ends was crushed entirely, resulting in severe buckling of several longitudinal bars.

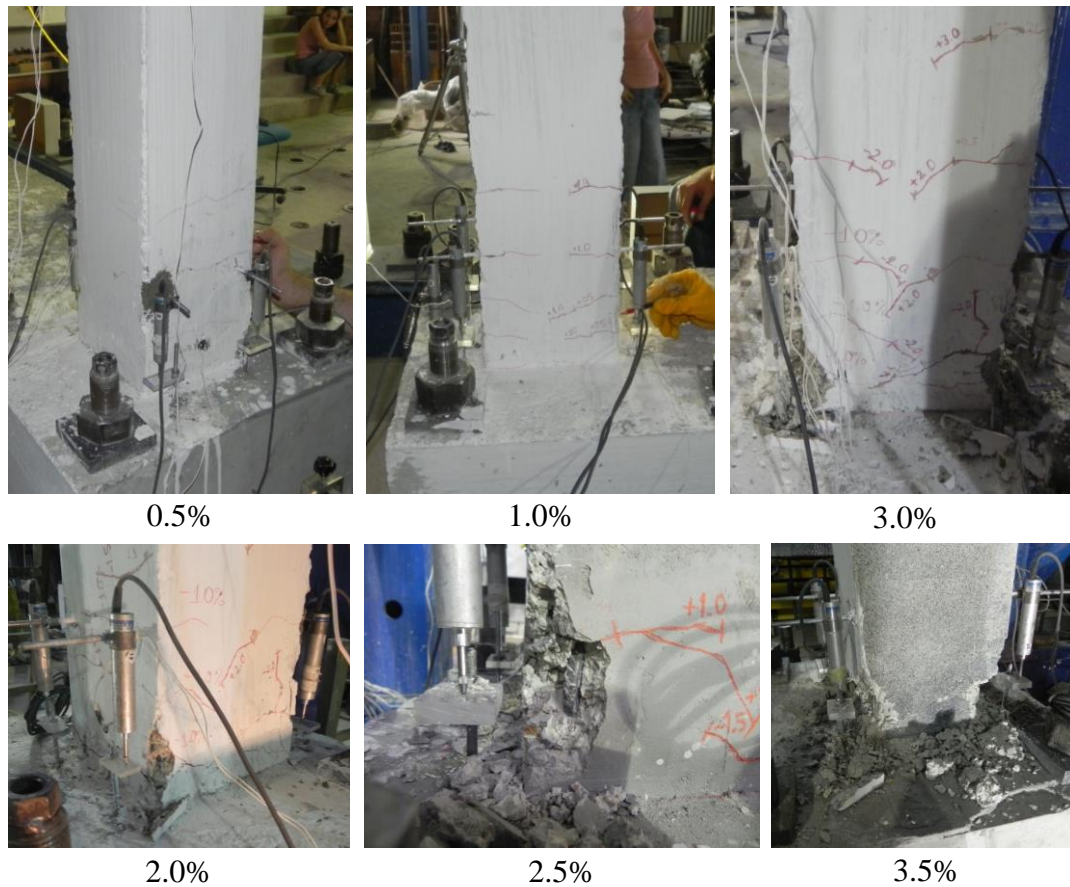


Figure 5.7. Propagation of column damage for BF

5.2.2 HCB Infilled Frame Specimen (CB)

An infill wall constructed with hollow clay bricks (HCB) of a 65% void ratio was tightly secured inside the bare frame filling the interface between the wall and the frame with mortar. No plaster was applied over the infill wall. Utilized brick units are typical for Turkish construction practice. Due to the difficulty of producing half-scaled hollow brick units, readily available bricks that were scaled only in the thickness and the horizontal direction but not in the vertical direction of the wall were used. Lack of scaling in the vertical direction resulted in vertical stacking of the units which influenced the failure mechanism and the capacity. The compressive strength of the mortar on the test day is approximated as 3.3 MPa (Table 4.6).

Backbone curves corresponding to the first and second cycles of infilled frame (IF) and infill wall (IW), distribution of base shear among the wall and the bounding frame, energy dissipation of the wall and the frame at target drifts are illustrated in Figure 5.8. Yielding of the frame corresponds to the first strain jump in frame members.

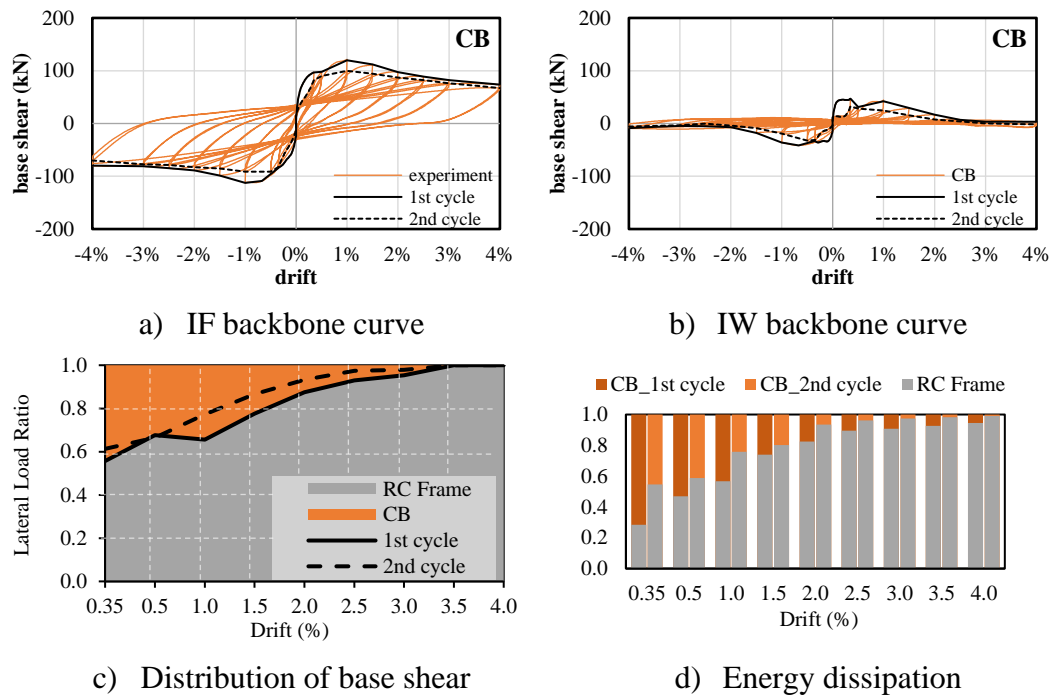


Figure 5.8. Load-displacement response of CB specimen

a) Wall Damage

Due to the absence of plaster and whitewashing of the brick units, identifying the cracking on the wall was difficult (Figure 5.9). Photos taken every 6 seconds from a fixed position in front of the wall were investigated to capture wall movements. No visible cracking on the wall drew attention at 0.35% drift. Separation of the wall from the upper beam was noticed at 0.5% drift.

Up to 0.5% drift, lateral displacement demand was accommodated by rotation of brick units due to vertical arrangement, which is not the case for the horizontal arrangement, as illustrated by Suzuki et al. (2017). The vertical arrangement makes

the infill wall more accommodating for lateral displacement by disturbing the formation of compression diagonal through the rocking of brick units.

When the story drift reached 1.0%, the bricks below the upper beam gradually peeled off due to the vertical pressure exerted on them by the upper beam. A horizontal sliding plane formed between the second and the third brick units from the bottom. The peak lateral strength reached 121.6 kN (-112.7 kN) at 1.00% (-1.00%) drift in the positive (negative) direction. A diagonal compression strut was triggered when the story drift reached 1.5%. Upper brick units were crushed and spalled, leading to an opening under the upper beam. When the story drift reached 2.0%, the upper layer of bricks was completely crushed and considerably spalled. A combination of sliding and diagonal cracking was observed. The area of opening increased leaving the infill wall extremely vulnerable to OOP failure since the arching action in the vertical direction is completely lost due to the crushing and spalling of bricks under the beam.

At story drift levels of 2.5% and 3.0%, the upper layer of brick completely spalled. Sliding and rocking action took place together, possibly with decreasing width of the compression strut due to a decrease in contact length. At 4% drift, the sliding plane formed over the second layer of brick units dominated the response.

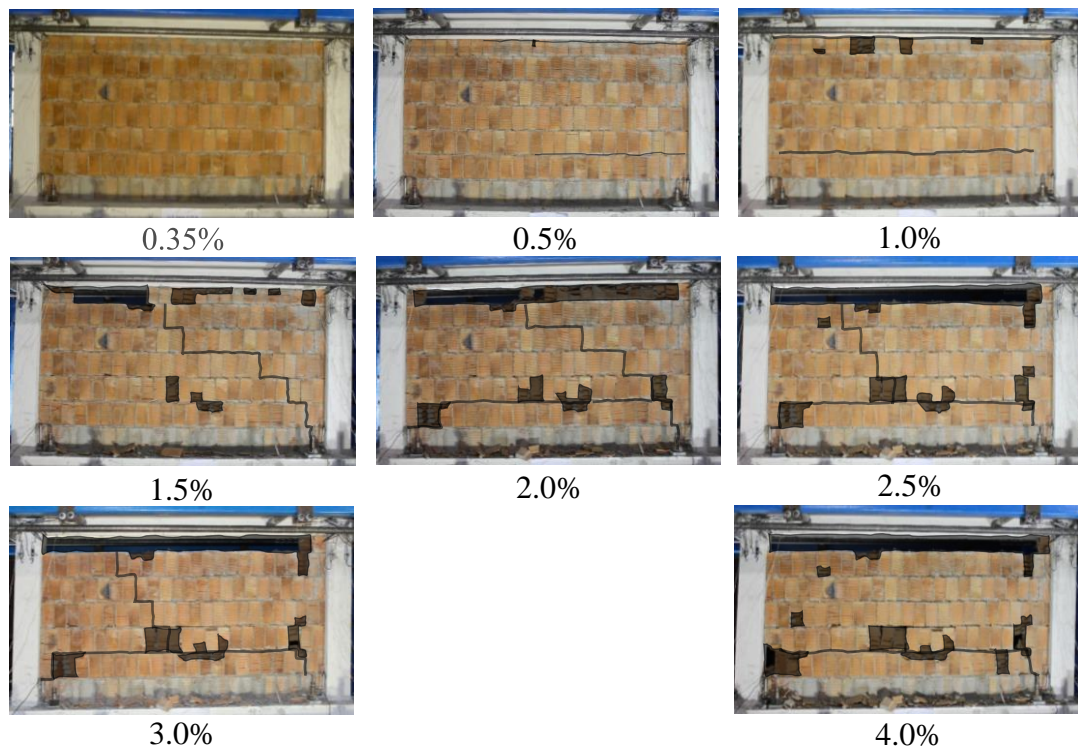


Figure 5.9. Sequence of damage propagation for CB

b) Frame Damage

As for damage to frame members, flexural cracking of the beams and the columns were initiated at 0.35% and 0.5% drift levels, respectively. Flexural cracks at column lower ends propagated through the geometric center and spread to the mid-height of the column at 1.0% and 1.5% drifts. New flexural cracks extending through the slab were formed at beam ends and column tops, and the first hairline shear crack was formed at the beam-column joint at 2.0% drift. The width of the flexural beam crack closest to the face of the column approached 1.5mm. Crushing of column lower end initiated at 2.5% drift followed by the buckling of first reinforcement at 3.0% drift. When the story drift reached 4.0 %, the crushing of concrete and buckling of reinforcements spread to both sides of the column at the lower ends (Figure 5.10).

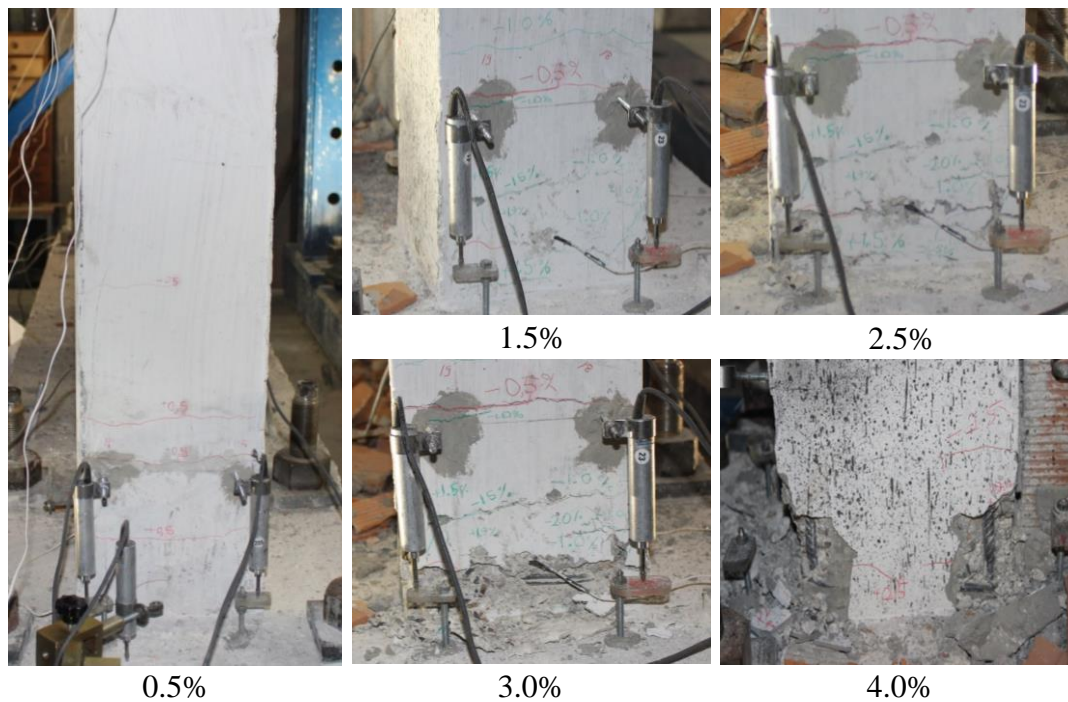


Figure 5.10. Propagation of damage for CB frame

5.2.3 HCB Infilled Frame Specimen with Plaster (CBP)

In order to investigate the influence of plaster on the structural response, 10 mm thick plaster made of general purpose mortar (see page 96) was applied on both faces of the infill wall. The same hollow brick units and joint mortar utilized for CB specimen were used in the construction of the CBP. The plaster was whitewashed with lime in order to differentiate the cracking on the wall surface. The compressive strength of the mortar is estimated as 3.7 MPa on the test day.

Backbone curves corresponding to the first and second cycles of the infilled frame (IF) and infill wall (IW), distribution of base shear among the wall and the bounding frame, and energy dissipation of the wall and the frame at target drifts are illustrated in Figure 5.11. Yielding of the frame corresponds to the first strain jump in frame members.

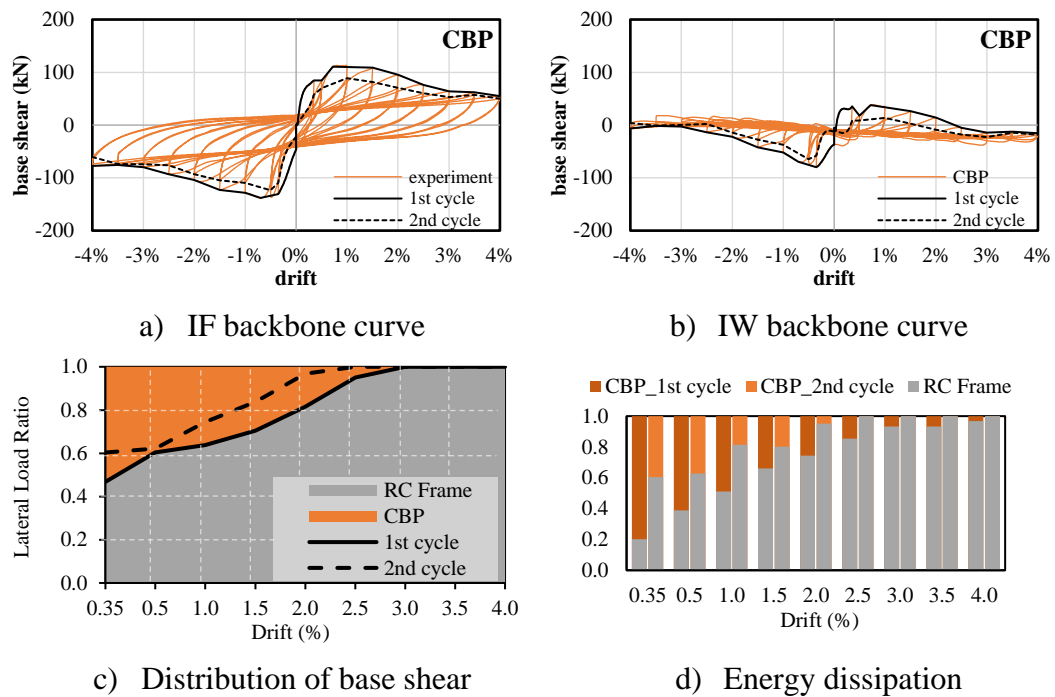


Figure 5.11. Load-displacement response of CBP specimen

a) Wall Damage

The damage to the CBP was characterized by diagonal cracking followed by crushing damages at four corner zones (Figure 5.12). Detachment of masonry panel from bounding frame along upper beam and column interfaces were identified at 0.35% drift. Interface cracking becomes distinctive, and plaster crushing was initiated at upper corners at 0.5% drift. When the drift reached 1.0%, an apparent sliding and shear coupled crack emerged in the push direction and a major diagonal crack close to the upper beam-leeward column corner emerged in the pull direction. The peak lateral strength reached 112.8 kN in the positive direction at 0.98% drift and -138.2 kN in the negative direction at -0.70% drift. Spalling of plaster and crushing of brick units were observed at the upper corners of the wall at 1.5% and 2.0% drift levels, respectively.

When the drift reached 2.5%, spalling of some brick units and corner crushing at all corners were confirmed. Diagonal compression strut formation was interrupted after the falling of crushed brick units at the corners. Contact length between the panel

and the bounding frame is reduced, resulting in reduction of panel contribution to lateral resistance.

Compared to the clay brick infilled frame without plaster, the wall response was changed due to plaster restricting the rotation motion of individual brick units. With the further increase of displacement reversals, more brick units fall off, and the ultimate damage was reached by extensive corner crushing.

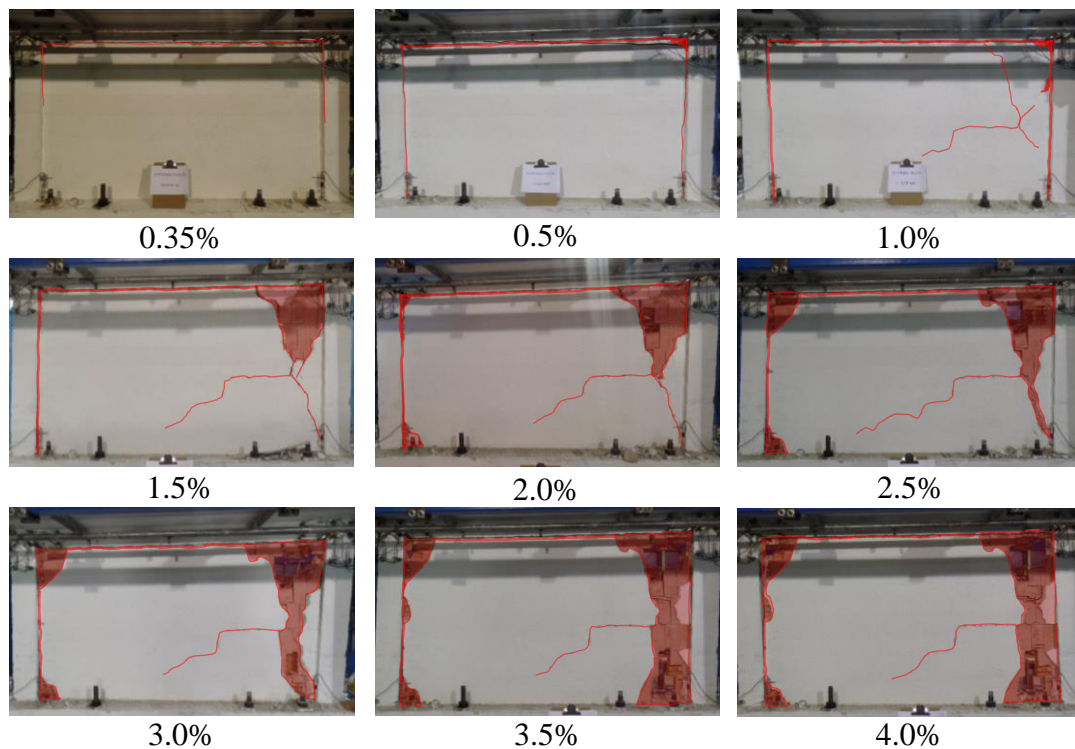


Figure 5.12. Sequence of damage propagation for CBP

b) Frame Damage

Damage to RC frame members under increasing displacement reversals was illustrated in Figure 5.13. Initial flexural cracks emerged at beam ends around 0.35% drift. Flexural and hairline shear cracking emerged at column lower ends and beam ends at 0.5% drift, respectively. When the drift reached 2.0%, the flexural cracks at beam ends and tension faces of column lower ends spread to the slab and the column mid-height, respectively. With the increase of drift, several new cracks were

confirmed at beam ends and column lower ends. Crushing of cover concrete at column lower ends took place at 3.0% drift. As the amplitude of displacement cycles increased, spalling of cover concrete accompanied by the buckling of the longitudinal reinforcement at the column lower ends was identified at 3.5% and 4.0% drift levels, respectively. At the ultimate damage state, initiation of concrete crushing at beam ends was detected.

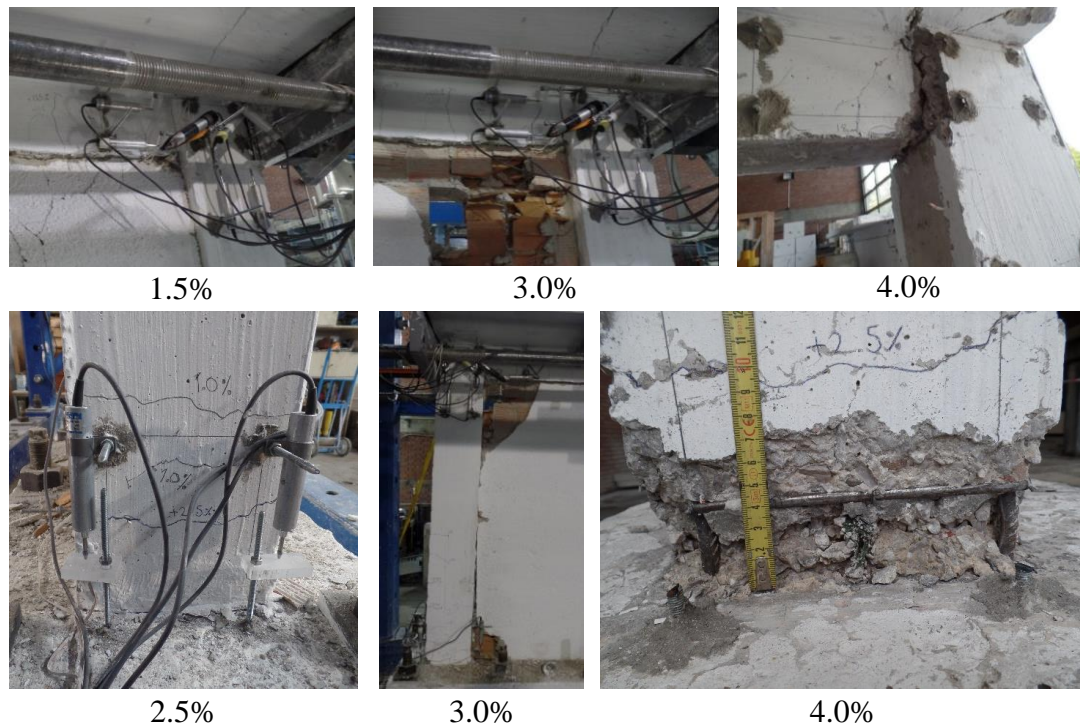


Figure 5.13. Propagation of damage for CBP frame

5.2.4 HCB Infilled Frame with Steel Mesh Reinforcement (CBMR)

Light steel wire meshes of 2 mm diameter and 25 mm pitch were used to strengthen the HCB infilled frame specimen. Steel meshes placed at both sides of the wall was connected bilaterally with tie wires passing through the holes drilled on the wall surface. A final layer of 10mm thick plaster made of ordinary cement mortar was applied on both sides. The estimated compressive strength of the plaster mortar at

the frame test day was 3.7 MPa (Table 4.6) and the tensile strength of the steel mesh was 70 N/mm.

Backbone curves corresponding to first and second cycles of infilled frame (IF) and infill wall (IW), distribution of base shear among the wall and the bounding frame, and energy dissipation of the wall and the frame at target drifts are illustrated in Figure 5.14. Yielding of the frame corresponds to first strain jump in frame members.

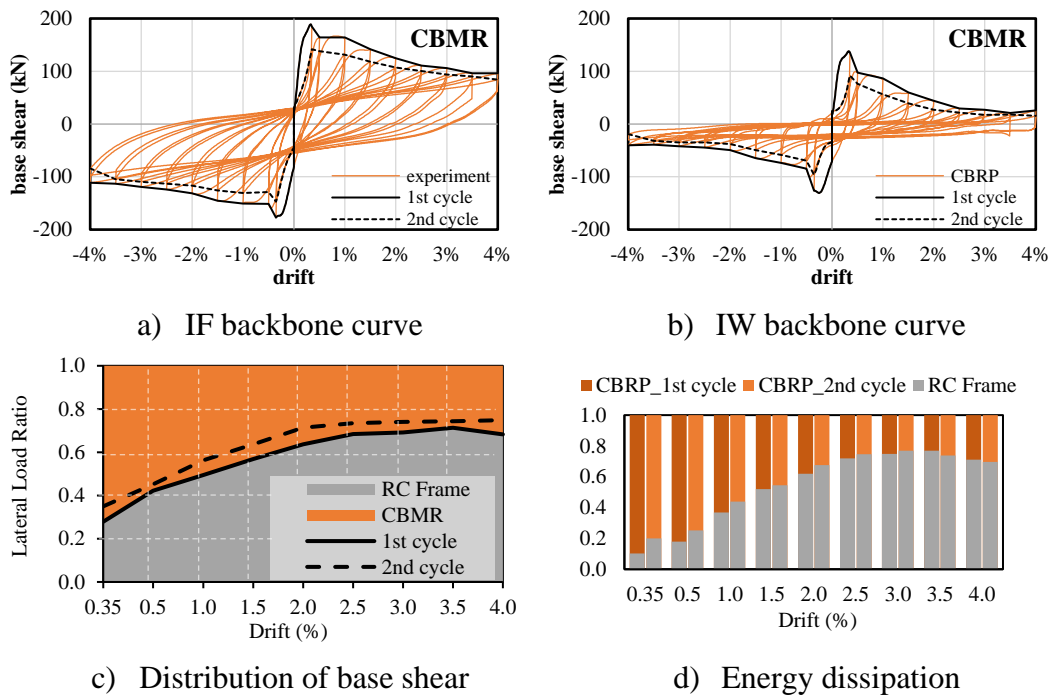


Figure 5.14. Load-displacement response of CBMR specimen

a) Wall Damage

The CBMR damage under for increasing levels of lateral drift was illustrated in Figure 5.15. Due to increased capacity and stiffness of the infill wall by bilateral mesh reinforcement application, the peak lateral strength was reached at 0.35% drift at which sliding under the upper beam and disintegration of infill panel from columns close to upper corners were noticed. The peak lateral strength in the positive and negative directions was measured as 188.7 kN at 0.33% drift and -177.5 kN at -0.35% drift, respectively. Corner crushing initiated at 0.5% drift manifesting itself by peeling off the plaster and local buckling of the mesh reinforcement in restricted

areas close to the ends of the upper beam. The gap formed between the infill and the upper corner at the leeward column side was large enough to see through. When the drift reached 1.0%, corner crushing at the upper corners become more prominent. Crushing of brick units was inspected at corners at 1.5% drift. Under increasing displacement reversals, no additional wall damage was noticed. Infill panel response was governed by sliding under the upper beam, reduction of the contact length due to increasing disintegration of the infill panel from the bounding frame and limited corner crushing at upper corners. No diagonal or horizontal cracking of the plaster covering bilaterally attached steel mesh reinforcement was noticed.

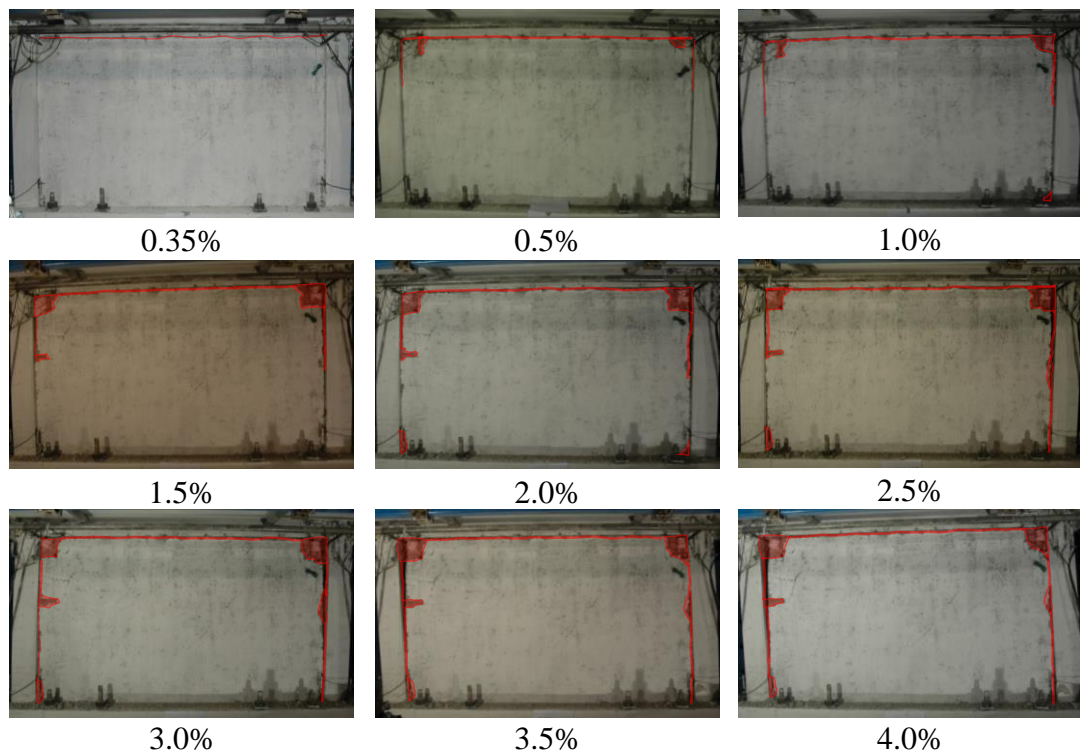


Figure 5.15. Sequence of damage propagation for CBMR

b) Frame Damage

Damage to frame members was summarized in Figure 5.16. Hairline shear cracking at beam ends and flexural cracking at column bottoms were confirmed at 0.35% drift. The flexural cracks at column lower ends spread along the entire height of columns at 0.5% drift. In addition to widening shear cracks, distinctive flexural cracks

extending through the slab were noticed at beam ends at 1.0% drift. Additionally, several new flexural cracks were confirmed at the plastic hinge region of column lower ends. When the drift level reaches 1.5%, flexural cracks appeared at column upper ends and additional shear and flexural cracks opened at beam ends and column lower ends. Initiation of flexural cracking at column upper ends was another observation. When the drift level reaches 2.0%, several new flexural cracks appeared within the plastic hinge region of column lower ends. Crushing of cover concrete at beam ends and initiation of additional flexural cracks at column upper ends were confirmed at 2.5% drift. Cover concrete crushing of column lower ends was observed at 3.5% drift. When the drift level reaches 4.0%, buckling of longitudinal reinforcement at column lower ends and beam ends was observed.

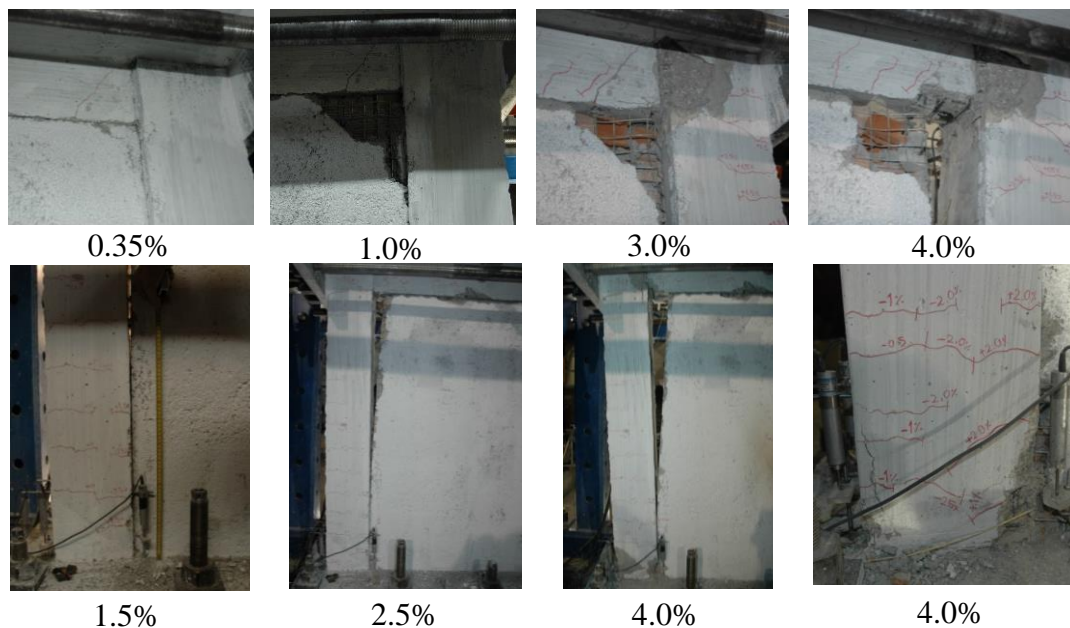


Figure 5.16. Propagation of damage for CBMR frame

5.2.5 HCB Infilled Frame with Continuous Steel Ties (TieC)

Three layers of horizontal steel ties (i.e., perforated plates) placed along every other bed joint were locked mutually into closed steel channels anchored to the inner faces of columns for the TieC frame specimen. No plaster was applied and the wall was

whitewashed for better identification of cracks. The estimated compressive strength of the mortar at the frame test day was 2.6 MPa (Table 4.6).

Backbone curves corresponding to first and second cycles of infilled frame (IF) and infill wall (IW), distribution of base shear among the wall and the bounding frame, and energy dissipation of the wall and the frame at target drifts are illustrated in Figure 5.17. Yielding of the frame corresponds to first strain jump in frame members.

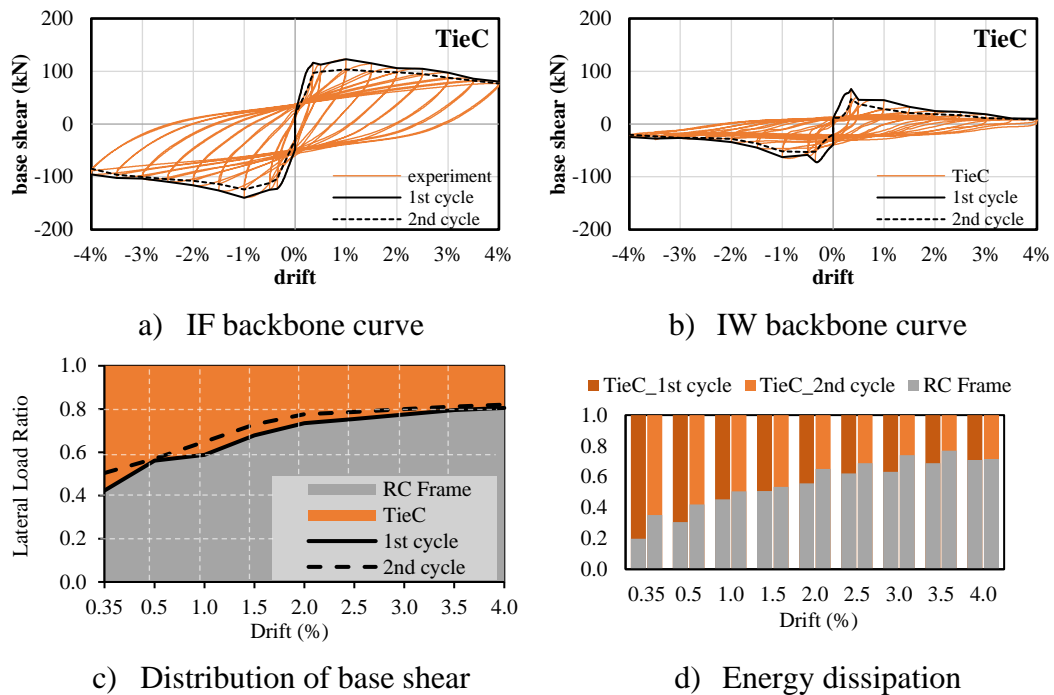


Figure 5.17. Load-displacement response of TieC specimen

a) Wall Damage

The infill panel response of TieC was governed by successive sliding along ties without diagonal cracking or corner crushing damages (Figure 5.18). The first sliding plane was formed at the top tie level at 0.35% drift. The second sliding plane was activated at 1.0% drift along with the bottom tie level. The peak lateral strength was reached at 122.7 kN (-139.5kN) lateral force and 0.96% (-1.00%) lateral drift in the positive (negative) direction. Outer layers of individual bricks started to peel off at 1.5% drift located below the activated slip planes. Brick units started falling off and one can see through the wall at 2.5% drift. The third sliding plane was activated at

3.5% drift along with the middle tie level. Ultimate damage was reached at a 4.0% drift level by the formation of successive slip planes at horizontal steel tie levels, peeling off the outer layers of brick units and falling of bricks, especially under the upper beam.

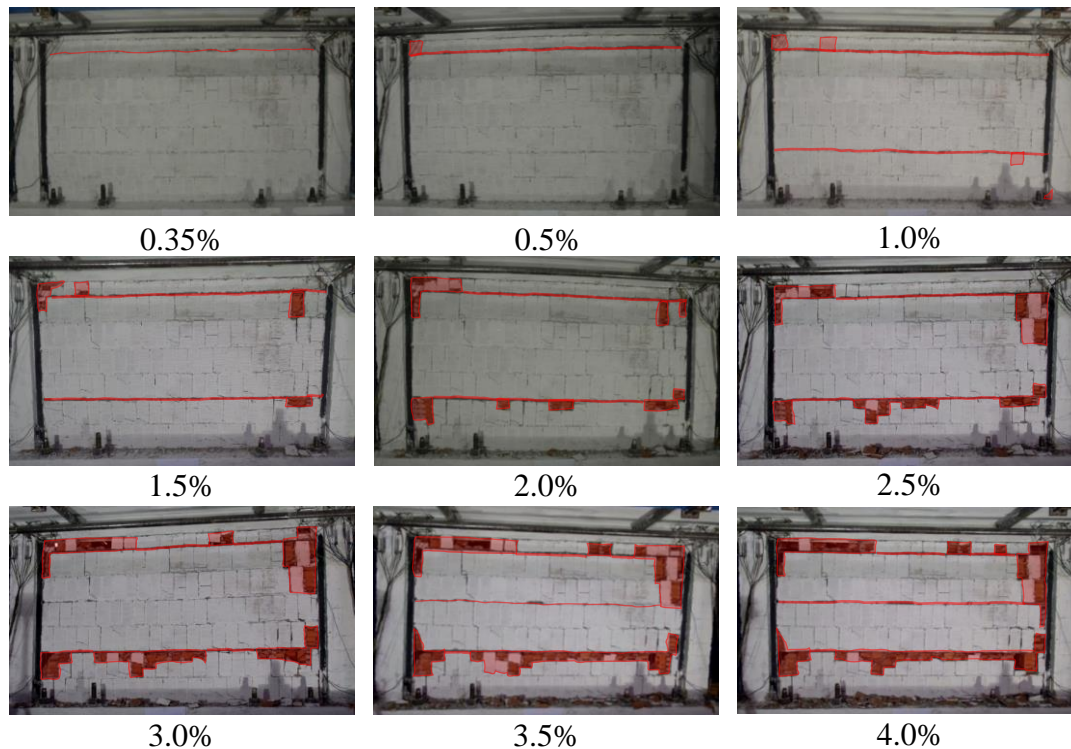


Figure 5.18. Sequence of damage propagation for TieC

b) Frame Damage

The evolution of damage at beam ends and column lower ends were shown in Figure 5.19. First flexural cracks emerged at beam ends and column upper ends at 0.35% drift. Flexural cracking at column lower ends started at 0.5% drift and spread through the mid-height of the columns at 1.0% drift. Beam flexural cracks extended through the slab and diagonal hairline shear cracks were confirmed at beam-column joints at 1.5% drift. Several new flexural cracks were confirmed at plastic hinge regions of columns at 2.0% drift. Flexural cracks at column upper ends appeared and cover concrete crushing initiated at column lower ends at 2.5% drift. Concrete crushing at beam ends and cover concrete spalling at column lower ends leading to the exposure

of longitudinal and transverse steel bars were confirmed at 3.0% drift. When the drift reached 3.5%, crushing and spalling of concrete at column lower ends developed further. At the ultimate drift cycle of 4.0%, exposed longitudinal bars started buckling at column lower ends. Severe damage in terms of crushing and spalling of concrete cover and exposure of reinforcement at beam ends and bar buckling at column lower ends were observed at the ultimate drift of 4.0%.

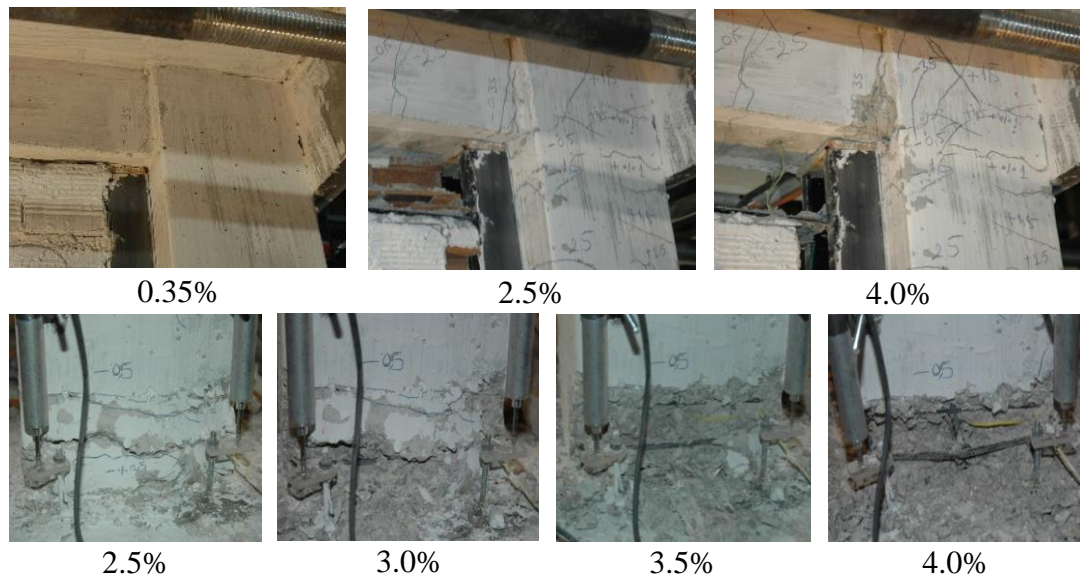


Figure 5.19. Propagation of damage for TieC frame

5.2.6 HCB Infilled Frame with Staggered Steel Ties (TieS)

Four layers of perforated plates attached to steel channels at one end and free at the other were used for TieS frame specimen. The plates were placed along every other bed joint in staggered orientation. No plaster was applied and the wall was whitewashed for better identification of cracks. The estimated compressive strength of the mortar at the frame test day was 3.0 MPa (Table 4.6).

Backbone curves corresponding to first and second cycles of infilled frame (IF) and infill wall (IW), distribution of base shear among the wall and the bounding frame,

and energy dissipation of the wall and the frame at target drifts are illustrated in Figure 5.20. Yielding of the frame corresponds to first strain jump in frame members.

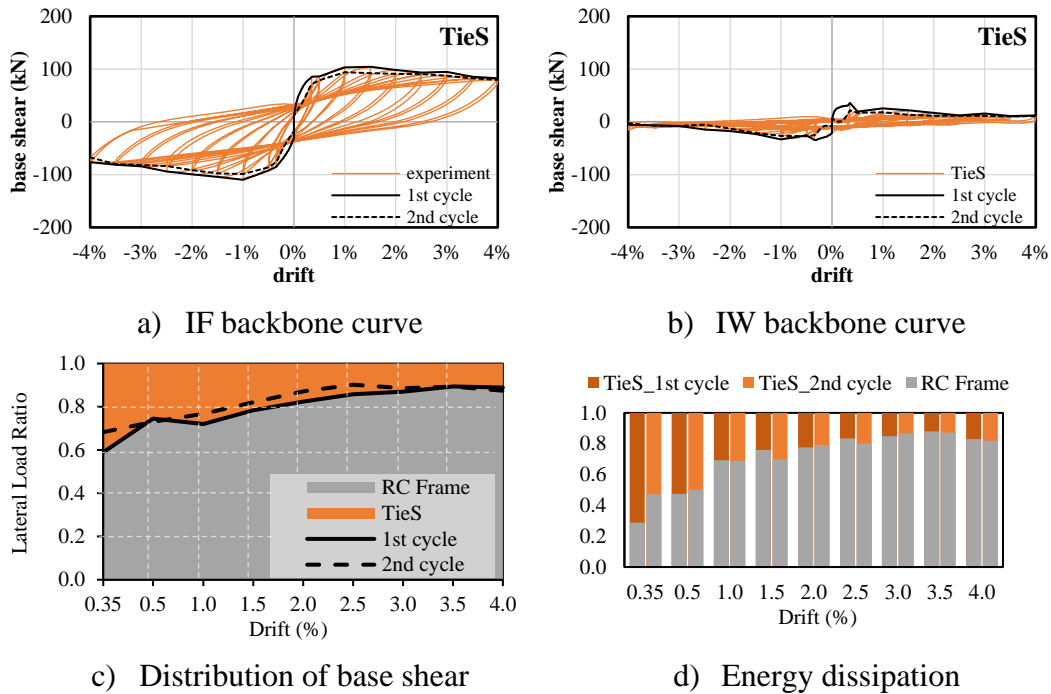


Figure 5.20. Load-displacement response of TieS specimen

a) Wall Damage

The cyclic response of the TieS frame specimen was dictated by successive slip planes created at tie levels (Figure 5.21). The first horizontal sliding crack was observed at 0.35% along the bottom plate. As the amplitude of displacement cycles increased, additional slip planes created along other ties. The peak lateral strength was reached at 104.1 kN (-109.7 kN) lateral force and 1.50 % (-1.00%) lateral drift in the positive (negative) direction. Some brick units gradually started to peel off at 2.0% drift and some others fall off when the drift reaches 4.0% drift.

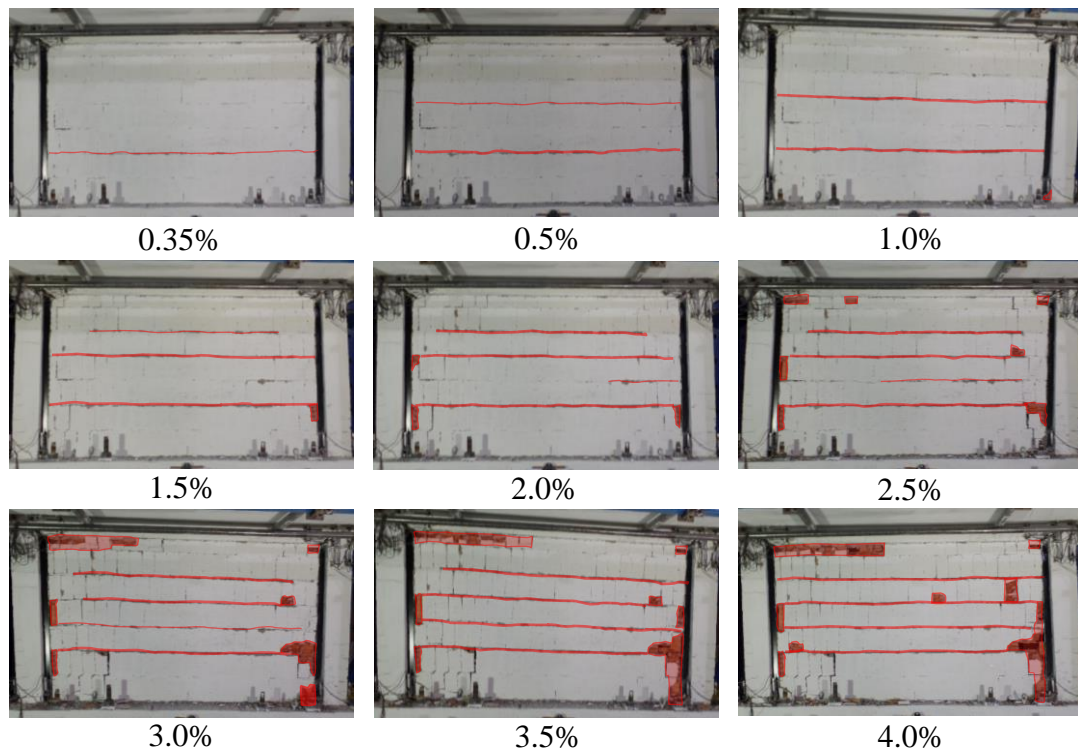


Figure 5.21. Sequence of damage propagation for TieS

b) Frame Damage

The development of column and beam damages on frame members were illustrated in Figure 5.22. Flexural hairline crack initiated at column lower ends and beam ends at 0.35% drift were followed by propagation of flexural cracks to the mid-height of the columns at 0.5% drift. When the drift reached 1.0%, several new flexural cracks appeared at the plastic hinge region of column lower ends and beam ends. The flexural cracks on the tension side of the column lower ends propagated through the geometric center of the column section. Horizontal cracks at column upper ends appeared and beam flexural cracks propagated into the slab at 1.5% drift. Cover concrete started to crush at column lower ends at 2.0% drift. Diagonal shear cracks initiated at beam-column joints and cover concrete at beam ends started to crush at 2.5% drift. When the drift reached 3.0%, the cover concrete at column lower ends started to spall, making some reinforcing rebars expose. The first longitudinal bar buckling was observed at 3.5% drift at leeward column. Column lower ends were

severely damaged by the crushing of cover concrete in both directions and buckling of several longitudinal bars at 4.0% drift.

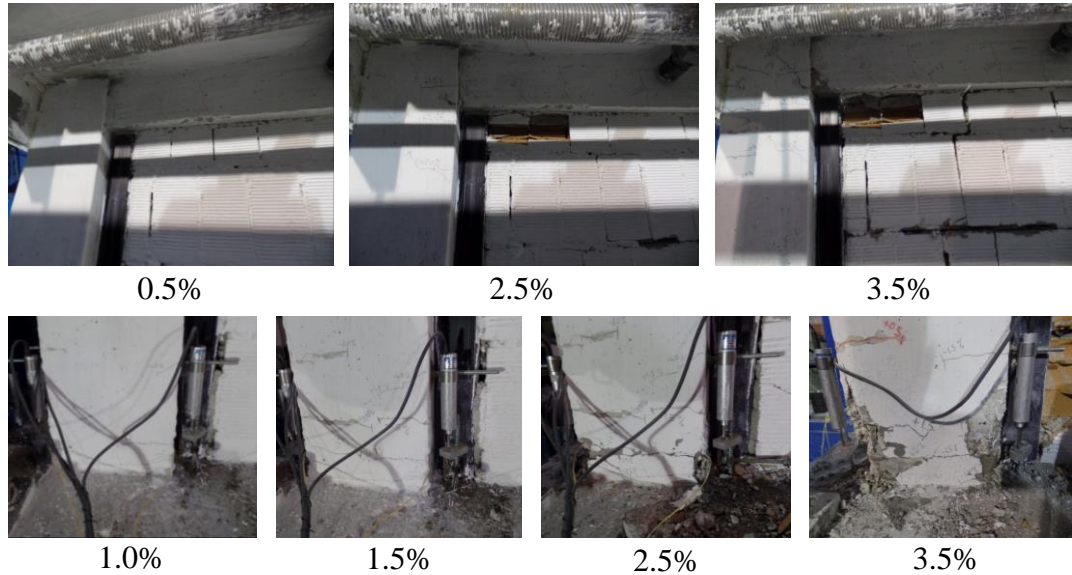


Figure 5.22. Propagation of damage for TieS frame

5.2.7 LB Infilled Frame with Plaster (LBP)

The infill panel was constructed with a special type of HCB where a dry locking mechanism is present in bed joints. 10 mm thick ordinary plaster was applied on both faces of the wall. The estimated compressive strength of the mortar was 6.2 MPa (Table 4.6).

Backbone curves corresponding to first and second cycles of infilled frame (IF) and infill wall (IW), distribution of base shear among the wall and the bounding frame, and energy dissipation of the wall and the frame at target drifts are illustrated in Figure 5.23. Yielding of the frame corresponds to first strain jump in frame members.

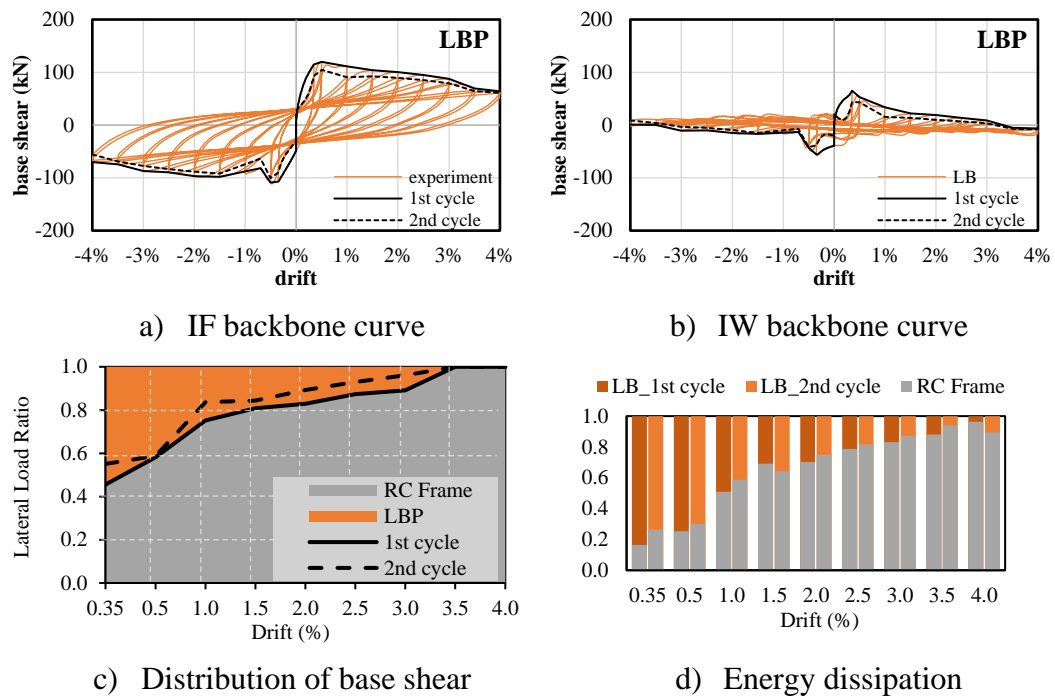


Figure 5.23. Load-displacement response of LBP specimen

a) Wall Damage

Damage propagation of LBP is illustrated in Figure 5.24. An obvious sliding crack at the frame-wall interface under the upper beam was observed at 0.35% drift. First horizontal sliding cracks emerged from the inner column face and extended to the wall mid-length at 0.5% drift. The peak lateral strength was reached at 119.7 kN (-111.4 kN) in the positive (negative) direction at 0.50% (-0.47%). Emerged horizontal cracks widened and extended, merging at the center and dividing the wall horizontally into two pieces at 1.0% drift. Mortar begins to spall and bending cracks emerged at the bottom of columns and spread towards the middle of the column at the same drift level. When the drift reached 1.5%, the upper part of the horizontally divided wall starts to slide over the bottom part. When the drift reached 2.0%, corresponding to 28.8 mm lateral displacement, some bricks were crushed and the outer layers of some others started to peel off. Sliding between the upper and the bottom pieces of the wall was measured as 25 mm by drawing a vertical line passing through the major horizontal crack at the undeformed position of the wall (i.e., at

zero drift). Spalling of mortar and crushing of brick units extended at 2.5% drift. When the drift reaches 3.0%, corresponding to 43.2 mm lateral displacement, sliding between the upper and the bottom pieces of the wall was measured as 40 mm. Some bricks were crushed and fall off, forming openings in the wall. Another major horizontal crack emerged when the drift reached 3.5%, dividing the wall into three pieces. Crushing and spalling of brick increased and the wall is damaged very seriously, jeopardizing its integrity. When the drift reached 4.0%, sliding over two horizontal sliding layers was distinguished. Crushing, spalling and holes on the wall increased.

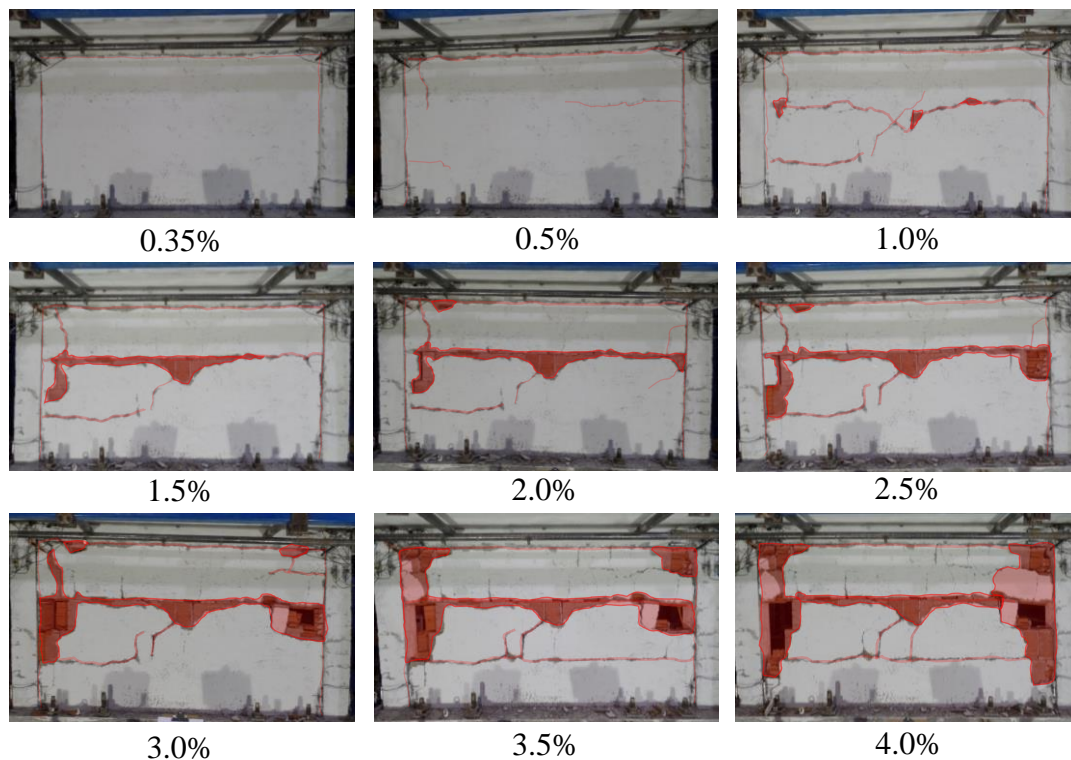


Figure 5.24. Sequence of damage propagation for LBP

b) Frame Damage

Small bending cracks appear at the bottom of the columns and shear/flexural cracks initiated at the beam ends at 0.35% and 0.5% drift levels. Flexural cracks on column lower ends spread through the mid-height, the first hairline shear crack observed at the beam-column joint and bending cracks on the beam ends extended to the slab at

1.0% drift. When the drift reached 1.5%, several new flexural cracks emerged within the plastic hinge region of column lower ends and the existing cracks widened and extended towards the geometric center of the column. The crack pattern on RC members remained unchanged from this drift level on, with the width of the existing cracks kept widening under the increasing displacement reversals. When the drift reached 2.0%, the bending crack width at the beam end widened to 1.5 mm. When the drift reached 3.5%, spalling of the concrete cover was observed at column bases and some longitudinal and transverse bars were exposed (Figure 5.25). When the drift reached 4.0%, buckling of longitudinal reinforcement took place at the bottom of the column. Spalling of the concrete cover was observed at column lower ends and some longitudinal and transverse bars were exposed.

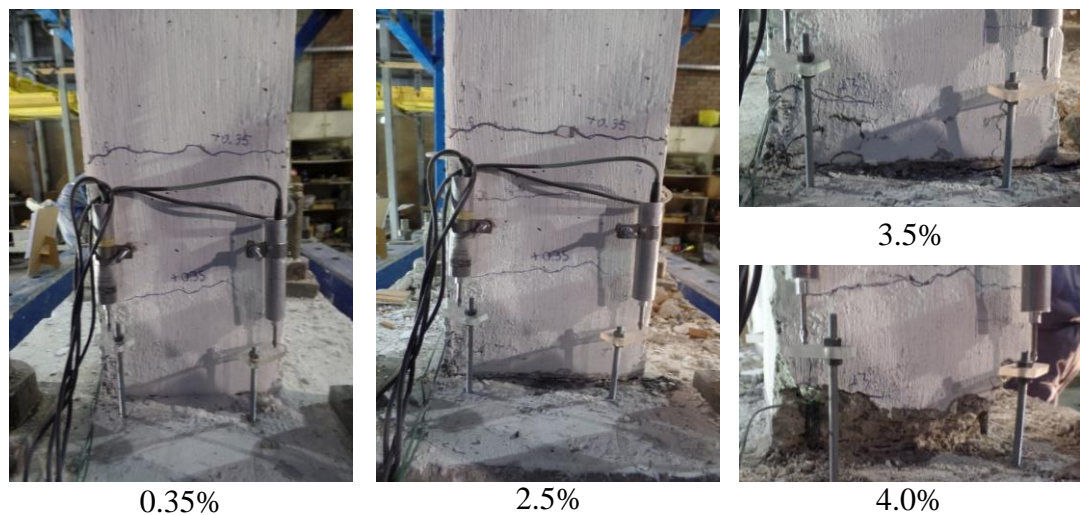


Figure 5.25. Propagation of column damage for LBP

5.2.8 ACB Infilled Frame (AB)

Half-scaled aerated concrete blocks of 350 kg/m^3 dry density and 2.5 MPa compressive strength were utilized to construct the infill panel. 20 mm isolation gap (40 mm for unscaled frame) was left between the upper beam and the wall. Flexible polyurethane foam was sprayed to fill the gap. The surface of the aerated concrete blocks was whitewashed with lime to identify wall damage better. Unlike other

frame specimens, in-plane testing of this specimen was stopped at 3.0% drift to test the damaged specimen in an out-of-plane direction. Weight blocks were removed, and a vibration generator was attached to the slab (Figure 5.26). Five one-way accelerometers were utilized to measure floor and wall accelerations. Dynamic loading of the frame under harmonic force generated by the vibration generator was conducted under varying frequencies. Unfortunately, due to the 20 mm gap under the upper beam and cracking of the interface between the columns and the infill panel, imposed harmonic forces on the slab could not be transferred to the infill panel.



Figure 5.26. OOP testing of damaged AB frame with vibration generator

Backbone curves corresponding to first and second cycles of infilled frame (IF) and infill wall (IW), distribution of base shear among the wall and the bounding frame, and energy dissipation of the wall and the frame at target drifts are illustrated in Figure 5.27. Yielding of the frame corresponds to first strain jump in frame members.

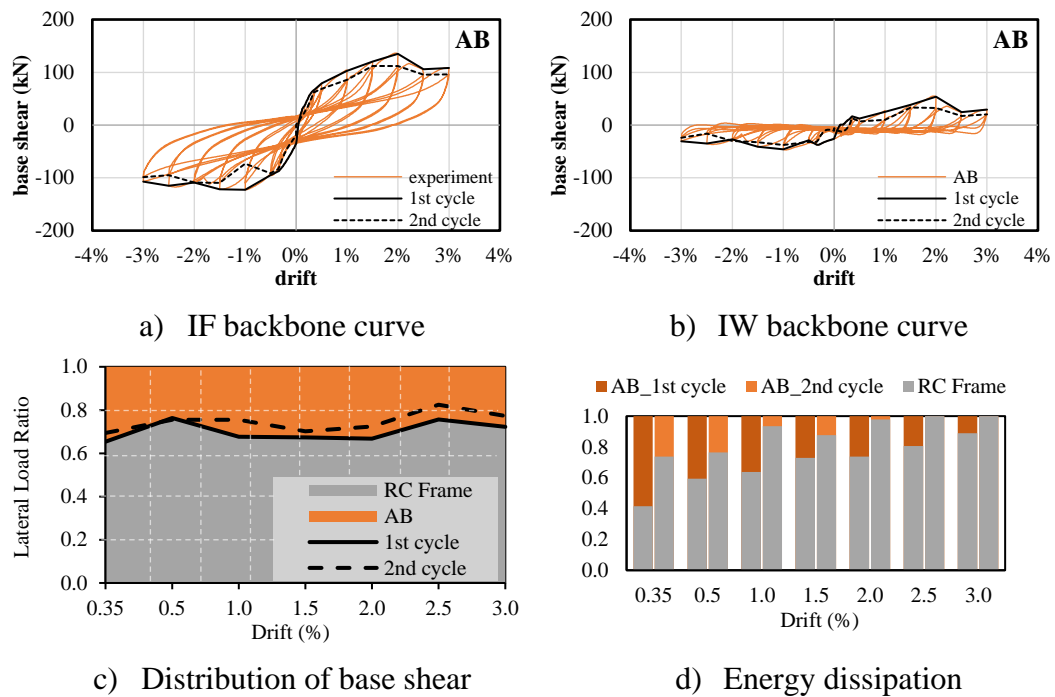


Figure 5.27. Load-displacement response of AB specimen

a) Wall Damage

Infill panels constructed with aerated concrete blocks behave extremely brittle due to the fragile nature of blocks and thin and strong mortar layers not allowing any relative motion between blocks such as sliding or rotation. Diagonal cracking dominated the infill wall response for the tested specimen. Several diagonal cracks emerged and widened with increasing drift in both directions of loading (Figure 5.28). Despite the 20 mm thick flexible joint under the upper beam, cracking of the wall initiated very early at 0.13% drift. The same cracking pattern was preserved with increasing crack widths until 1.0% drift. The positive and negative peak lateral strength was measured as 136.7 kN at 1.95% drift and -123.2 kN at -0.98% drift, respectively. When the drift reaches 1.5%, a major diagonal crack splitting the wall into two pieces emerged in the pull direction. A second major diagonal crack was initiated parallel to the first one at 2.0% drift in the pull direction. Response in the push direction was governed by a corner diagonal crack close to the bottom left corner up to 2.0% drift. This crack separated the right-bottom corner units from the

wall, which indicates the rocking behavior of the panel. A second major crack initiated close to the upper left corner at 2.5% drift.

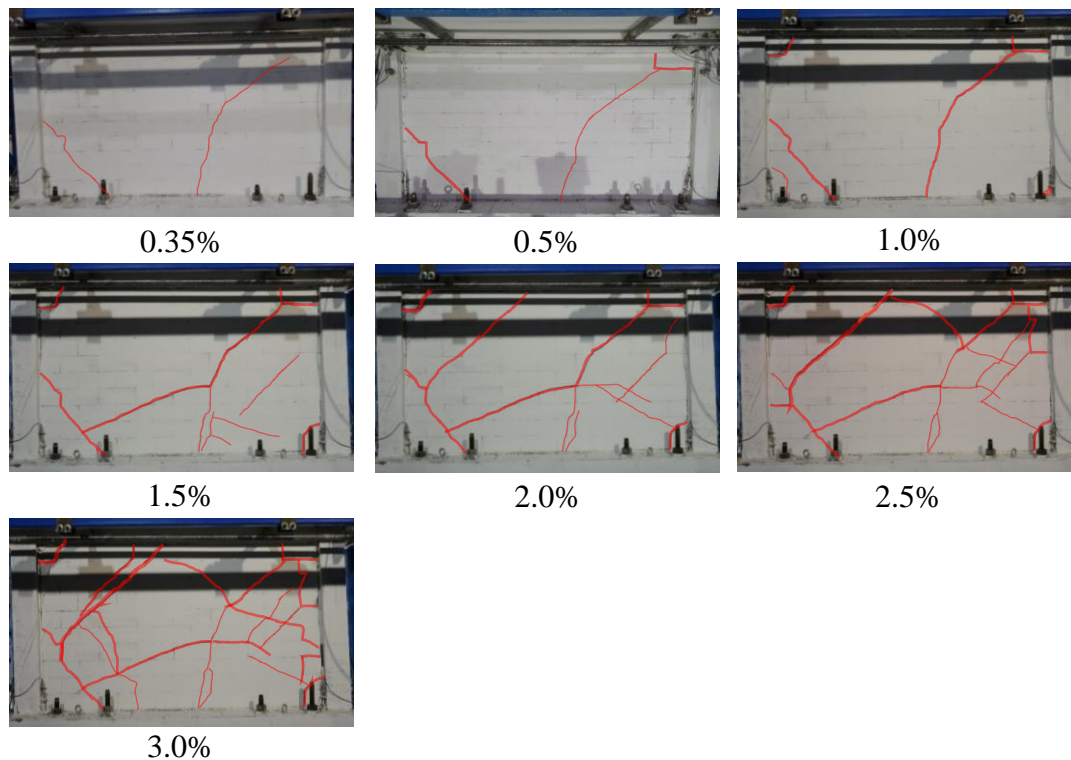


Figure 5.28. Sequence of damage propagation for AB

b) Frame Damage

Beam and column end damages of the infilled frame specimen are illustrated at different drift levels in Figure 5.29. Hairline flexural cracks emerged at 0.35% and 0.5% drift levels at beam ends and column bottoms become easily detectable with the naked eye at 1.0% drift. Flexural cracks at beam ends propagated into the slab and new flexural cracks opened at column tops at 1.5% drift. When the drift level reached 2.0%, several new flexural cracks emerged within the plastic hinge region of the column bottoms. Concrete crushing initiating at column bottoms at 2.5% drift ends up spalling cover concrete at 3.0% drift. As the test was terminated at this drift level, no buckling of reinforcement was observed.

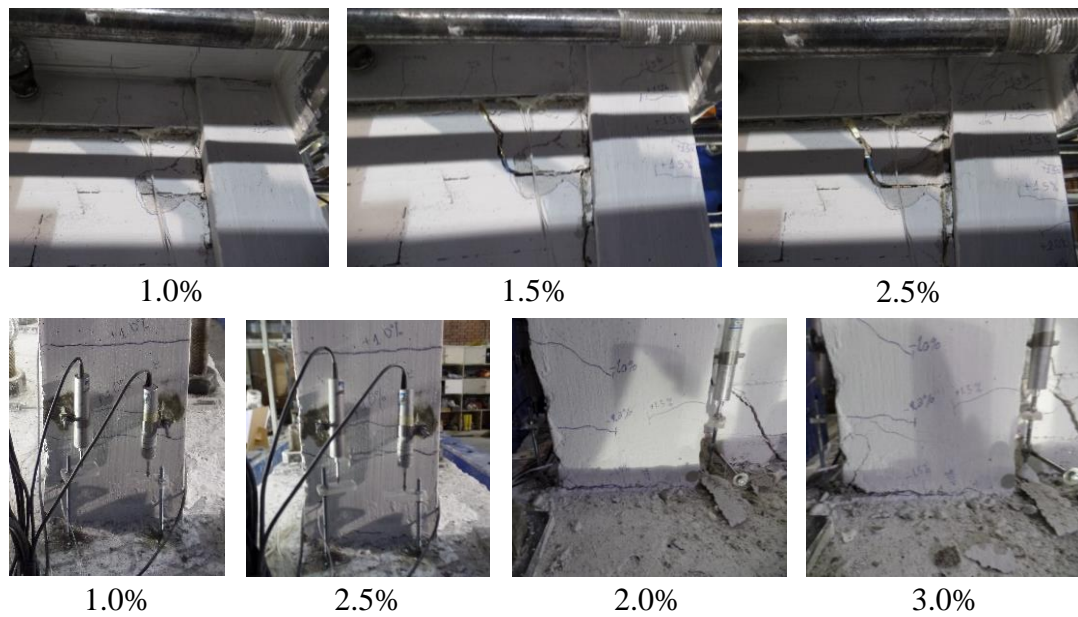


Figure 5.29. Propagation of damage for AB frame

5.2.9 ACB Infilled Frame with Isolation Joint (ABI)

Half-scaled aerated concrete blocks were utilized in the construction of the infill panel. 20mm isolation gap (40 mm for unscaled frame) was left between the columns, upper beam and the infill panel. Flexible polyurethane foam was sprayed to fill the gap. The surface of the AAC blocks was whitewashed with lime to identify wall damage better.

Backbone curves corresponding to first and second cycles of infilled frame (IF) and infill wall (IW), distribution of base shear among the wall and the bounding frame, and energy dissipation of the wall and the frame at target drifts are illustrated in Figure 5.30. Yielding of the frame corresponds to first strain jump in frame members.

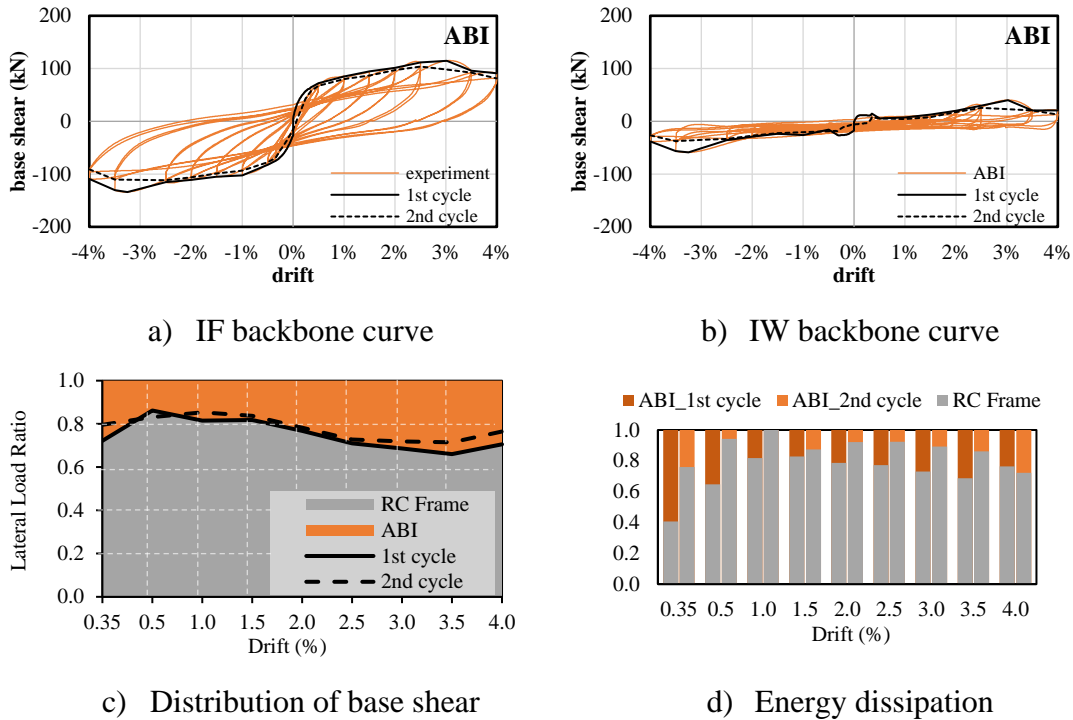


Figure 5.30. Load-displacement response of ABI specimen

a) Wall Damage

The crack pattern and damage evolution for the wall and the RC frame were illustrated in Figure 5.31 and Figure 5.32, respectively. Although the wall panel was isolated from the frame, cracking started unexpectedly as early as 0.35% drift, corresponding to 5 mm lateral displacement. Diagonal cracks passing through the blocks and the bed joints emerged perpendicular to compression diagonal close to the corners of the wall. The same crack pattern was observed with increasing crack widths until 2.5% drift (36 mm lateral displacement), where a major diagonal shear crack appeared in the pull direction. The lateral load continued to increase until 3.07% (-3.29%) drift, corresponding to a peak resistance of 115.1 kN (-133.9 kN).

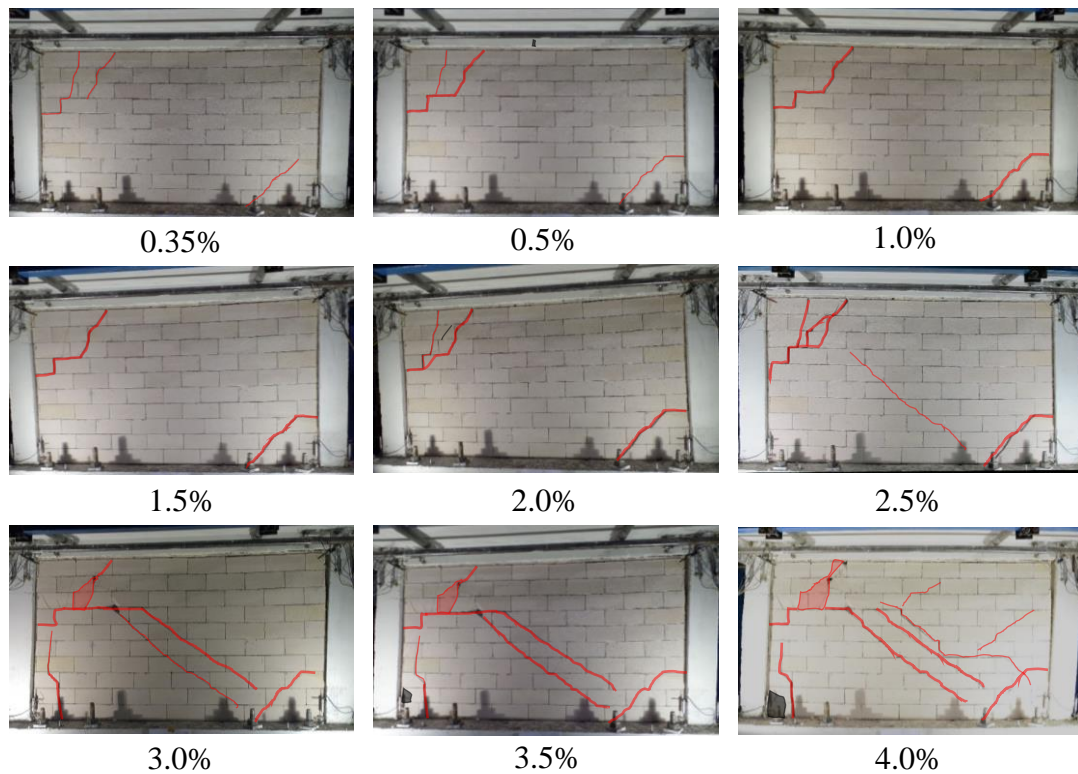


Figure 5.31. Sequence of damage propagation for ABI

Ultimate wall damage was achieved by attaining two new diagonal shear cracks parallel to the initial major diagonal crack and crushing at corner zones of the infill. A high level of pinching was observed as the opening and closing of the cracks were delayed due to the presence of the gap. Sliding of the wall panel on top of the RC foundation was observed until the closing of the isolation gaps, followed by the activation of the wall panel.

b) Frame Damage

The initial flexural cracks were confirmed at the RC frame's column bases and beam ends around 0.35% drift. New flexural cracks appear, and the original cracks gradually widen at 0.5% drift. Flexural cracks at column bases penetrated from the outer edge to the geometric center, the flexural cracks at beam ends extended towards the slab and hairline shear cracks emerged at beam-column joints at 1.0% drift. When the drift reaches 1.5%, flexural cracks at beam ends and column bases reached 1.0

mm in width and several flexural cracks emerged at the top of columns. Crushing of cover concrete at column bases initiated at 2.5% drift. Spalling of concrete and exposure of the bars took place at column ends at 3.0% and 3.5% drift levels. Spalling of concrete at beam ends was observed. No buckling took place in any of the RC member reinforcements. Severe damage in terms of crushing and spalling of concrete cover and exposure of reinforcement was confirmed at beam ends and column bottoms at the ultimate drift of 4.0%.

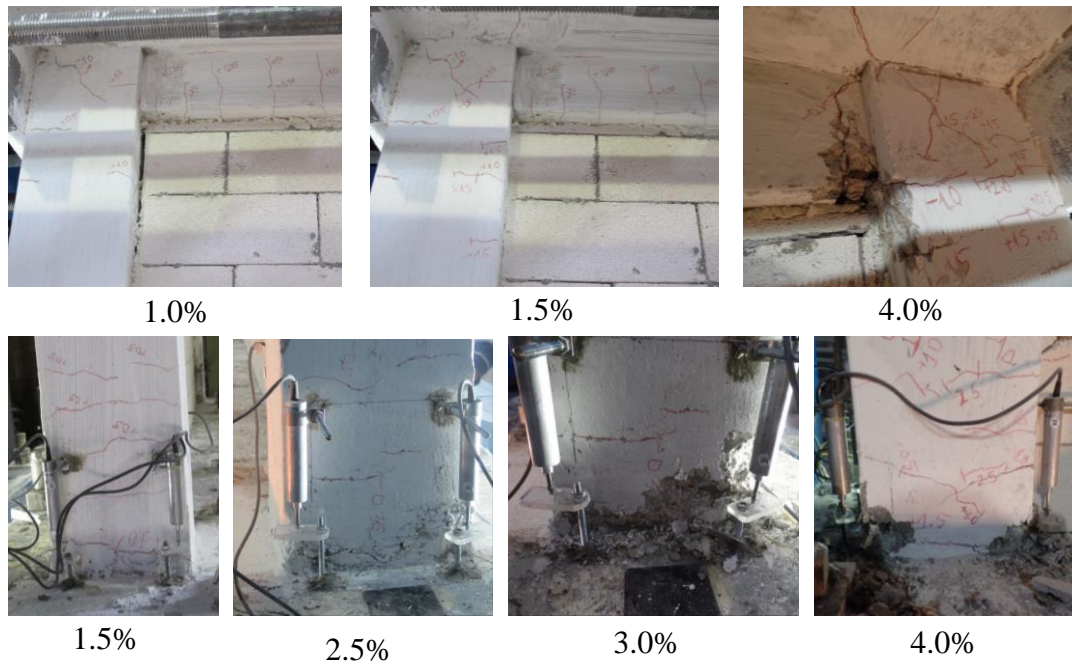


Figure 5.32. Propagation of damage for ABI frame

5.2.10 ACB Infilled Frame with Fiber Mesh Reinforced Plaster (ABRP)

A fiberglass reinforced plaster was applied over the infill panel constructed with aerated concrete blocks. The compressive strength of the plaster was 1.0 MPa and the tensile strength of the fiber mesh was 20 N/mm. A 20 mm gap was left under the beam to represent typical construction practice in Türkiye for AAC utilized infill panels. Backbone curves corresponding to first and second cycles of infilled frame (IF) and infill wall (IW), distribution of base shear among the wall and the bounding

frame, and energy dissipation of the wall and the frame at target drifts are illustrated in Figure 5.33.

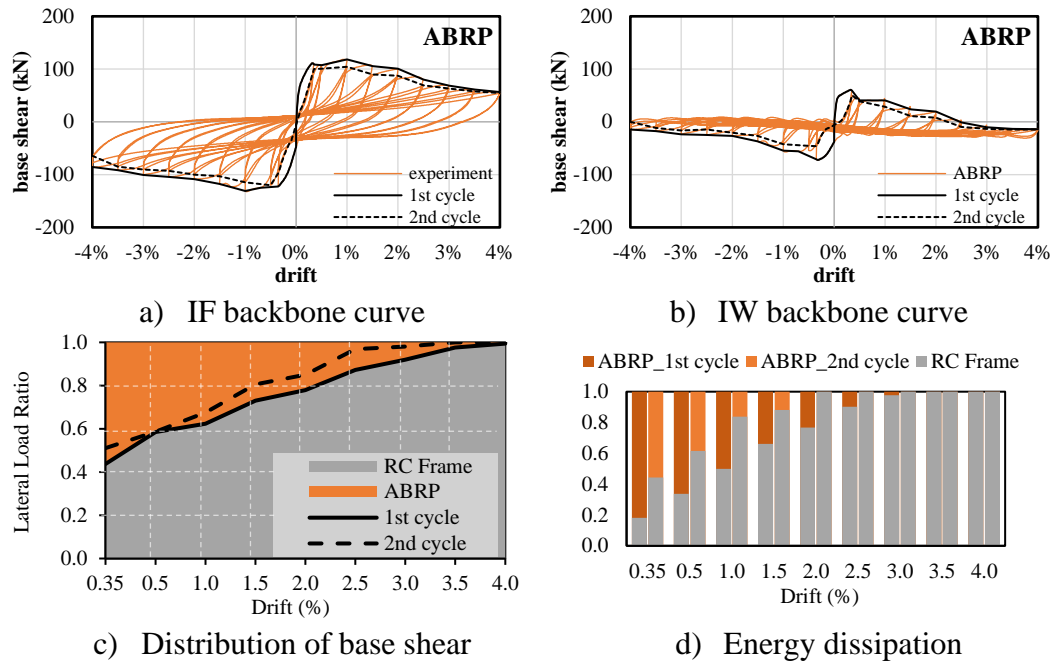


Figure 5.33. Load-displacement response of ABRP specimen

a) Wall Damage

Fiberglass mesh reinforcement of the plaster suppressed the cracking of the infill panel until the termination of the displacement reversals at 4% drift (Figure 5.34). Wall response was characterized by successive disintegration from the bounding frame, sliding under the beam and corner crushing at increased lateral displacements. The only noticeable wall damage was the sliding crack under the upper beam up to 1.0% drift, after which initiation and development of corner crushing were confirmed. The peak lateral strength reached 118.5 kN in the positive direction at 0.94% drift and -132.2 kN in the negative direction at -0.97% drift.

Spalling of the plaster was first confirmed at 1.5% drift followed by crushing of the aerated brick units at the upper corners at 2.0% drift. Corner crushing spread to all corners and become more visible after 3.0% drift. Despite the crushing corners, the unity of the infill panel was preserved until the end of displacement excursions.

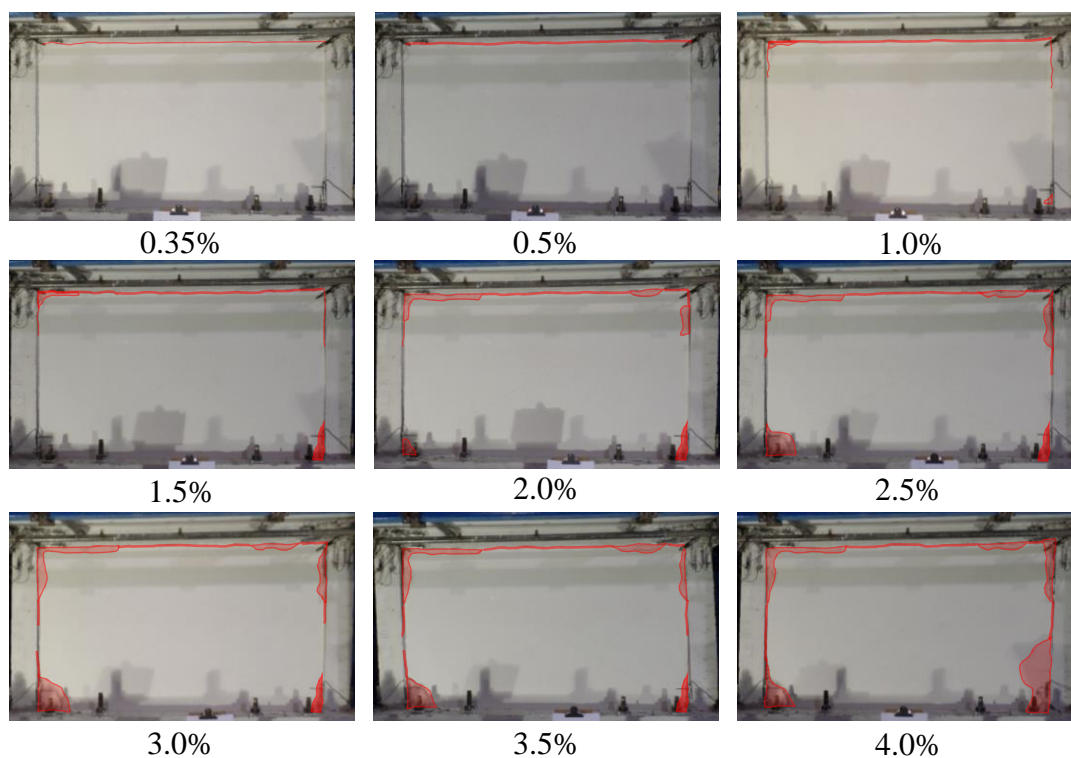


Figure 5.34. Sequence of damage propagation for ABRP

b) Frame Damage

The evolution of damage on frame members was illustrated in Figure 5.35. Flexural cracking at column bottoms and flexural/shear cracking at beam ends were observed at 0.35% drift. Hairline flexural cracks at column bases spread through full column height at 0.5% drift. Additional flexural cracks confirmed at beam ends and disintegration of the infill panel from the bounding frame at corners become visible at this level. When the drift reaches 1.0%, the beam flexural crack closest to the joints become extensive and several new cracks appeared close to the mid-length of the beam. New flexural cracks were confirmed at column tops. First hairline shear cracks were confirmed at beam-column joints. At 1.5% and 2.0% drifts, beam flexural cracks propagated into the slab. When the drift reaches 2.5%, concrete crushing begins at beam ends and shear cracks widen at beam-column joints. Crushing of column base concrete started at 3.0% drift followed by spalling cover concrete and buckling of longitudinal reinforcement at 3.5% drift. Cover concrete crushed, spalled

and several bars at column bases buckled at 4.0% drift. Severe damage to beam ends and column bottoms was observed at the ultimate damage state.

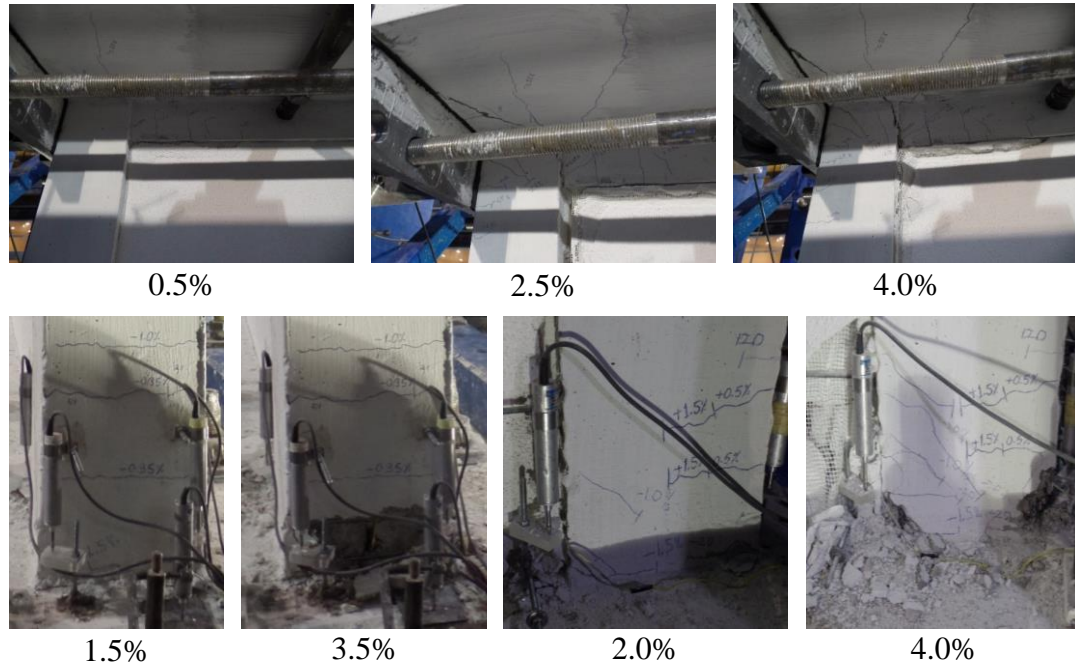


Figure 5.35. Propagation of damage for ABRP frame

5.2.11 Summary of IP Damage Propagation

The ultimate damage states of the infilled frame specimens are illustrated in Figure 5.37. A summary of structural and infill wall damages experienced by tested frame specimens is shown below:

The bare frame (BF) experienced a typical ductile flexural frame response with localized damages at member ends through plastic hinges. The column and beam ends were yielding around 0.7% and 1.3% drift levels. Maximum capacity reached at 82.2 kN (-82.2 kN), corresponding to 1.4% (-1.9%) drift. Crushing of column bottoms initiated at 2.0% drift, followed by the buckling of longitudinal bars at 2.5%.

Clay brick infilled frame (CB) experienced a sliding dominated panel response accompanied by rotation of brick units due to vertical orientation. The vertical

arrangement of brick units made the infill wall more accommodating for the lateral displacement by disturbing the formation of compression diagonal through the rotation of brick units. Suzuki (2017) compared the seismic response of ¼ scaled infilled frames with brick units' vertical and horizontal orientation. They concluded that vertically stacked walls did not show a diagonal strut unlike horizontal stacking due to the rocking of each independent brick unit, as illustrated in Figure 5.36. The contribution of the horizontally stacked wall to lateral strength was 25% higher than the vertically stacked wall. As a result, the vertically stacked infill wall's seismic performance was lower than that of the horizontally stacked wall. The maximum capacity of the tested frame specimen was reached at 121.6 kN (-112.7 kN), corresponding to 1.0% (-1.0%) drift. After reaching the peak strength, brick units at the top layer started to crush and spall progressively, leading to a vulnerable situation for OOP failure at 2.0% drift. Increasing drift cycles end up with a complete loss of the top layer of bricks and the infill contribution diminished.

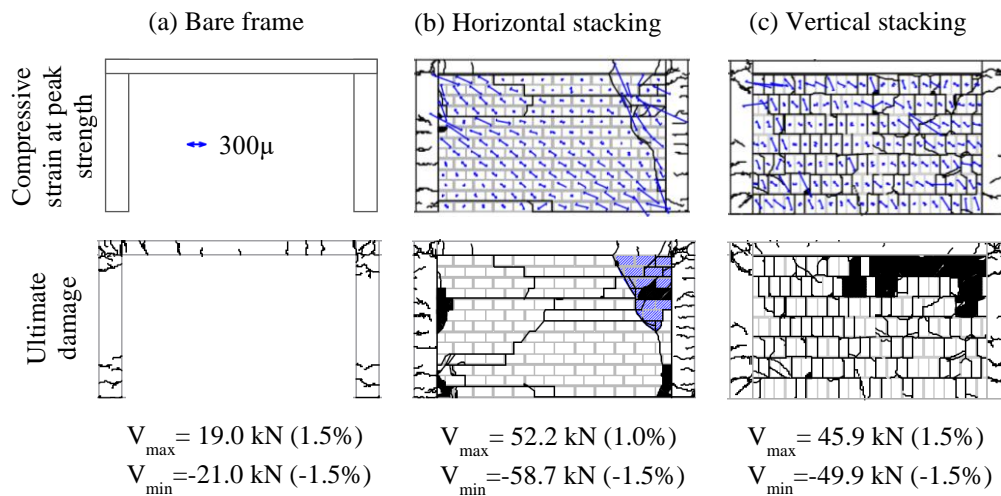


Figure 5.36. Influence of brick stacking direction (Suzuki et al. 2017)

Clay brick infilled frame with plaster (CBP) showed a completely different panel failure mechanism compared to the abovementioned specimen due to the inclusion of the plaster restricting individual rotation of brick units. The damage progression of the brick infilled panel with plaster was characterized by diagonal cracking

followed by crushing damages at four corner zones. Maximum capacity was reached at 112.8 kN (-138.2 kN), corresponding to 0.98% (-0.7%) drift. Spalling off the plaster initiated at 1.5% drift close to the upper corners progressed into crushing and falling of the brick units starting from 2.0% drift. After losing the wall area at corners, the major diagonal strut was interrupted and infill contribution decayed rapidly.

Clay brick infilled frame with bilateral mesh reinforcement (CBMR) showed a superior seismic response by preventing early cracking of the wall under early drifts corresponding to moderate earthquake and preserving integrity and contribution of the wall under increased drifts corresponding to design level earthquake. Due to the increased capacity and stiffness of the clay brick panel, the peak lateral strength was reached at 188.7 kN (-177.5 kN), corresponding to 0.33% (-0.35%) drift. The base shear capacity of the bare frame was increased by 130% compared to a 68% increase in the absence of mesh reinforcement. After reaching peak strength, a rapid degradation started, yet no diagonal cracking or horizontal sliding of the wall was visually observed under increasing load reversals. The dominant wall response was the detachment of the wall from the frame with local corner crushing damage. The strengthened infill wall stayed intact until the end of the loading protocol corresponding to 4% lateral drift. Although diagonal shear cracks were initiated at beam ends at early drifts, failure of the beam was flexure-dominated (i.e., bar buckling). The column and beam ends yielded around 0.85% and 1.6% drift levels. Crushing started at 2.5% drift, leading to buckling of longitudinal bars at column bottoms and the beam ending at 4.0% drift. Damage on beam ends was more severe than the previously mentioned frame specimens.

Aerated concrete block infilled frame (ACB) behaved extremely brittle due to the fragile nature of blocks and thin and strong mortar layers not allowing any relative motion between blocks. Diagonal cracking dominated the infill wall response for the tested specimen. Several diagonal cracks emerged and widened with increasing drift in both directions of loading. Despite the 20 mm thick flexible joint under the upper beam, cracking of the wall was initiated very early at 0.13% drift. Maximum capacity

was reached at 136.7 kN (-123.2 kN), corresponding to 1.95% (-0.98%) drift. Different cracking patterns, such as rocking and diagonal cracking, observed in the push and pull directions led to different capacities attained at different drift levels in opposite directions.

Aerated concrete block infilled frame with isolation gap (ABI) cracked unexpectedly early at 0.35% drift corresponding to 5 mm lateral displacement. Emerged diagonal cracks close to the corners separated the corner units from the wall, indicating the rocking behavior of the isolated panel. Closing of the gaps and activation of the diagonal strut started at 1.5% drift, corresponding to 21.6mm lateral displacement, followed by a major diagonal shear crack that appeared in the pull direction at 2.5% drift. Maximum capacity was reached at 115.1 kN (-133.9 kN), corresponding to 3.07% (-3.29%) drift. The formation of two parallel distinctive diagonal cracks characterized the ultimate damage pattern. A high level of pinching was observed as the opening and closing of the cracks were delayed due to isolation gaps. Sliding of the wall panel on top of the RC foundation was observed until the closing of the isolation gaps, followed by the activation of the wall panel. Late activation of the diagonal strut prevented the progression of frame damage such that no bar buckling occurred, unlike all other tested frame specimens.

Aerated concrete block infilled frame with fiberglass mesh reinforced plaster (ABRP) performed very well in suppressing the visual damage on the infill panel, whose response was characterized by successive disintegration from the bounding frame, sliding under the beam and localized corner crushing at increased lateral displacements. Maximum capacity was reached at 118.5 kN (-132.2 kN), corresponding to 0.94% (-0.97%) drift. Corner crushing spread to all four corners intercepting the diagonal strut action at 3.0% drift. Despite the crushing corners, the unity of the infill panel was preserved until 4.0% drift. As for confining frame, hairline shear cracks confirmed at beam-column joints and beam ends at early drifts did not dictate the response. Plastic hinges were formed at member ends. Most severe damage was experienced at column bottoms, at which crushing started around 3.0%

drift followed by complete crushing of cover concrete and buckling of several bars at 4.0% drift.

Locking clay brick infilled frame with plaster (LBP) experienced an apparent sliding dominant panel failure due to the dry-locking mechanism presented in the bed joints. Horizontal cracking on bed joints emerged from the column inner faces at 0.5% drift, where the peak lateral strength was attained in push (119.7 kN) and pull (-111.4 kN) directions. Emerged horizontal cracks progressed into slip planes leading to the decaying of the lateral capacity. Deformation of the wall concentrated on the slip plane created on the fourth bed-joint layer from the bottom at 1.5% drift. The second slip plane was formed along with the second bed-joint layer from the bottom at 3.5% drift. The ultimate damage pattern was reached by localized crushing of brick units between the formed slip planes. As for the bounding RC frame, severe plastic hinging of column bottoms with spalling of concrete cover (at 3.5% drift) and buckling of several longitudinal bars (at 4.0% drift) were documented.

Clay brick infilled frame with continuous horizontal steel tie (TieC) response was governed by successive sliding along with continuous ties without diagonal cracking or corner crushing damages. The formation of distinctive slip planes at the upper, lower and middle tie levels occurred at 0.35%, 1.0% and 3.5% drift levels, respectively. Maximum capacity was reached at 122.7kN (-139.5kN), corresponding to 0.96% (-1.0%) drift. Outer layers of individual bricks started peeling off at 1.5% drift and improved by falling brick units at 2.5%. Ultimate damage was reached at 4.0% drift by the formation of successive slip planes at horizontal steel tie levels, peeling off the outer layers of brick units and falling of brick units, especially under the upper beam. Frame damage was concentrated at member ends in terms of plastic hinges. Spalling of cover concrete at beam ends and buckling of several bars at column bottoms were observed at ultimate drift.

Clay brick infilled frame with stepped horizontal steel tie (TieS) behaved similarly to the abovementioned specimen. Slip planes were created along with 1st, 3rd, 4th and 2nd ties from the bottom of the wall at 0.35%, 0.5%, 2.0% and 3.0% drift levels,

respectively. As lateral drift demand was accommodated by four slip planes, wall damage in terms of spalling and crushing was decreased. Maximum capacity was reached at 104.1kN (-109.7kN), corresponding to 1.5% (-1.0%) drift. The bricks gradually started to peel off and some brick units fall off, forming holes on the infill panel at 2.0% and 4.0% drift. Bounding frame damage was similar to the abovementioned specimen (i.e., plastic hinges at member ends, severe damage in terms of bar buckling at column bottoms).

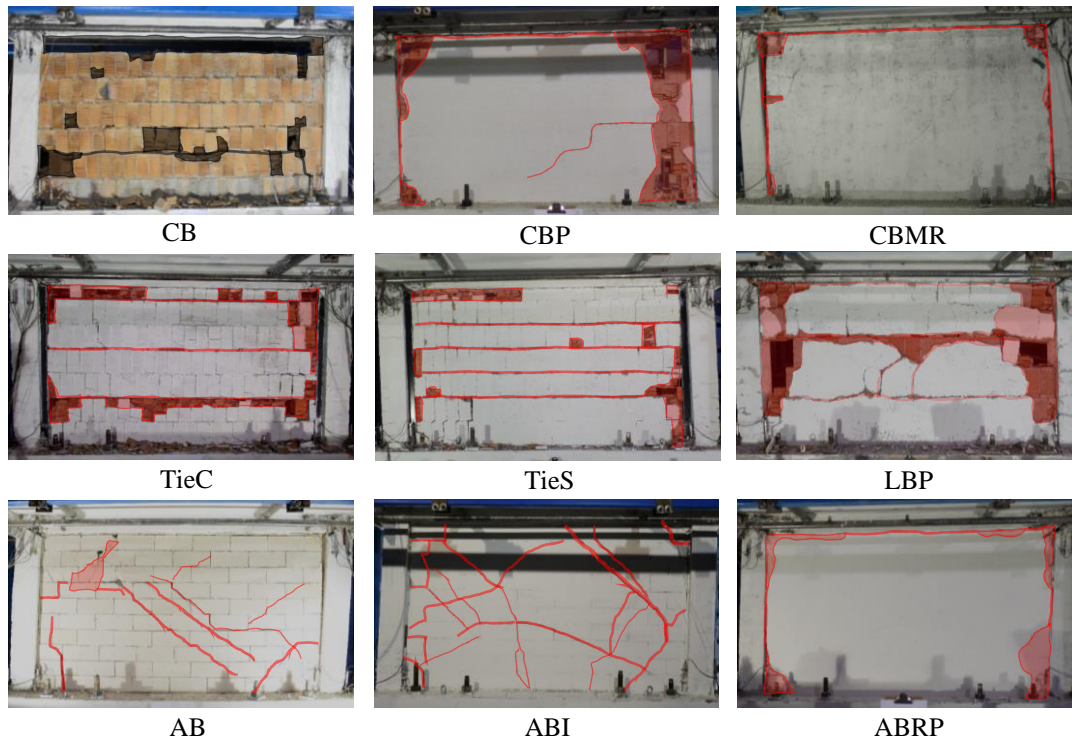


Figure 5.37. Ultimate IW damages under IP loading

5.2.12 Summary of Measured Response

The hysteresis response of the tested frames and extracted hysteresis response of infill walls are illustrated in Figure 5.38 and Figure 5.39, respectively. Infill wall response was identified by subtracting the hysteretic response of bare frame from infilled frames.

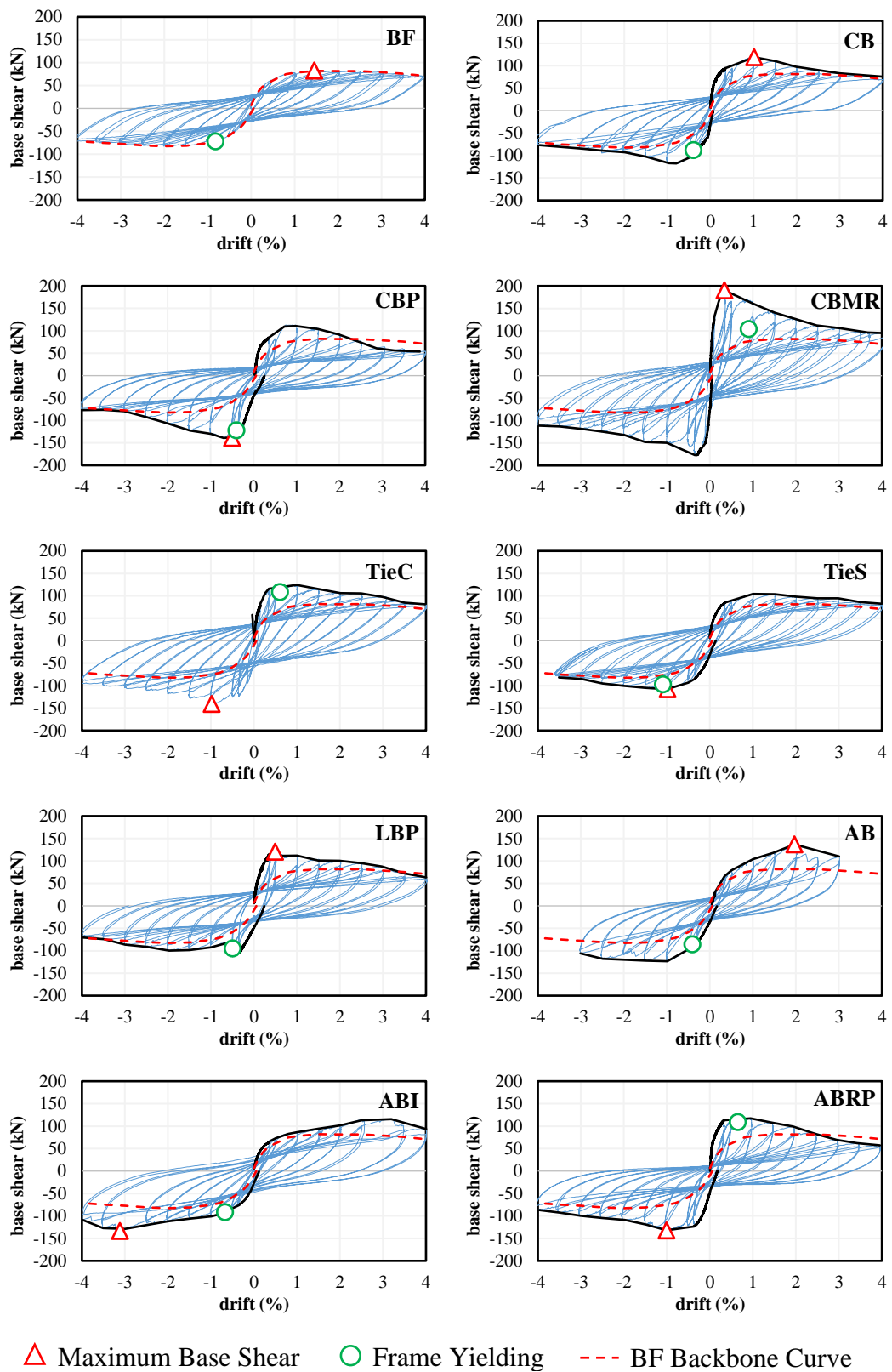


Figure 5.38. Hysteretic response of tested RC frame specimens

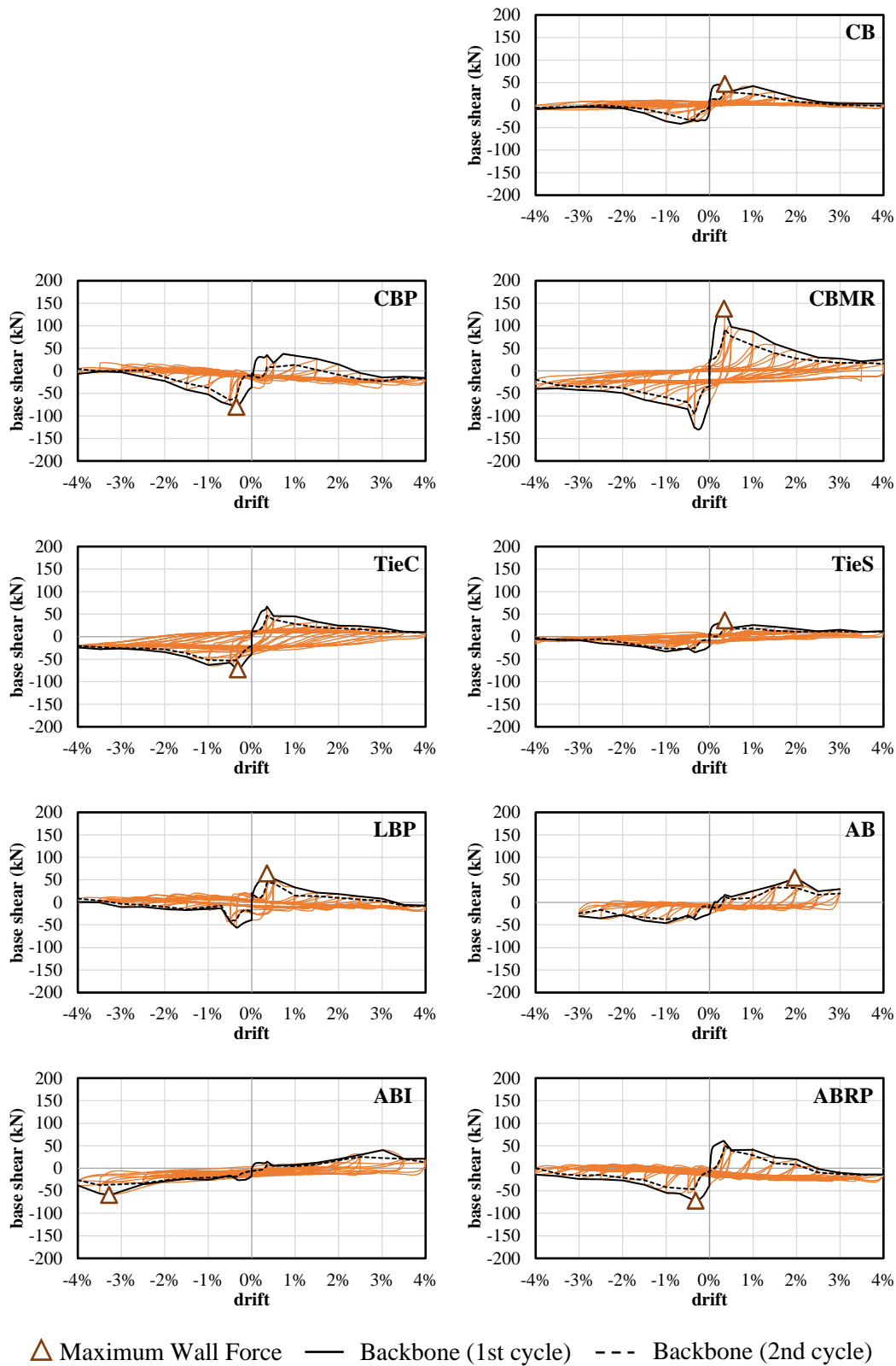


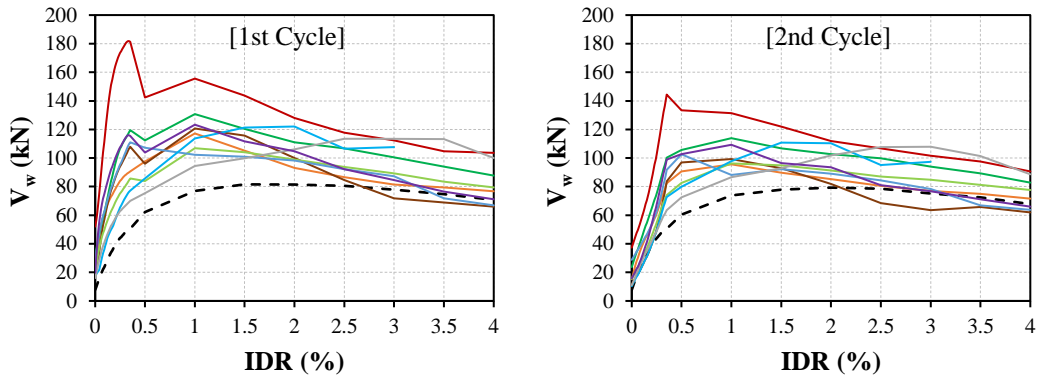
Figure 5.39. Extracted hysteretic response of infill walls

The bare frame's maximum capacity (BF) reached 1.4% lateral drift and a 20% reduction of base shear capacity was observed at the ultimate drift of 4.0%. Excluding the specimen with the isolated infill wall (ABI), all infilled frames reached their capacities under 1.0% lateral drift. The strength deterioration of the infilled frames after reaching their capacities was more rapid than the BF. Hysteretic responses of all infilled frames exhibited apparent pinching behavior. Infill walls increased the base shear capacity of the BF 1.64 times on average. The minimum increase is observed for TieS (1.3 times) and the maximum increase is observed for CBMR (2.3 times).

The BF hysteresis loop is narrower than the infilled frames and encloses smaller cyclic loop areas, indicating a lesser energy dissipation. CBMR, ABRP, and TieC walls with thicker hysteresis loops exhibit superior hysteretic behavior in dissipating energy, particularly as drift levels increase. The high amount of pinching observed for all infilled frames at significant drifts can be explained by the opening and closing of gaps at interfaces, the presence of friction between masonry infill and the enclosing structural frame, the opening and closing of cracks on the wall surface, and bar slip at the column bases.

Measured displacement envelopes for the tested infilled frames and extracted infill walls derived by averaging the absolute values at target displacements corresponding to push and pull directions are presented in Figure 5.40 for the first and second loading cycles. It is observed that infill wall strength deteriorates rapidly after reaching peak strength, and its contribution is almost completely lost after 2.5% drift with the exception of the isolated frame (ABI), in which effective infill contribution began after 1.5% drift and reached its maximum at 3.5% drift. All other infills attained their peak strengths at about 0.4% drift followed by a sudden strength drop resulting in 50% reduction in their contributions around 1.6% drift.

Infilled Frame Response



Infill Wall Response

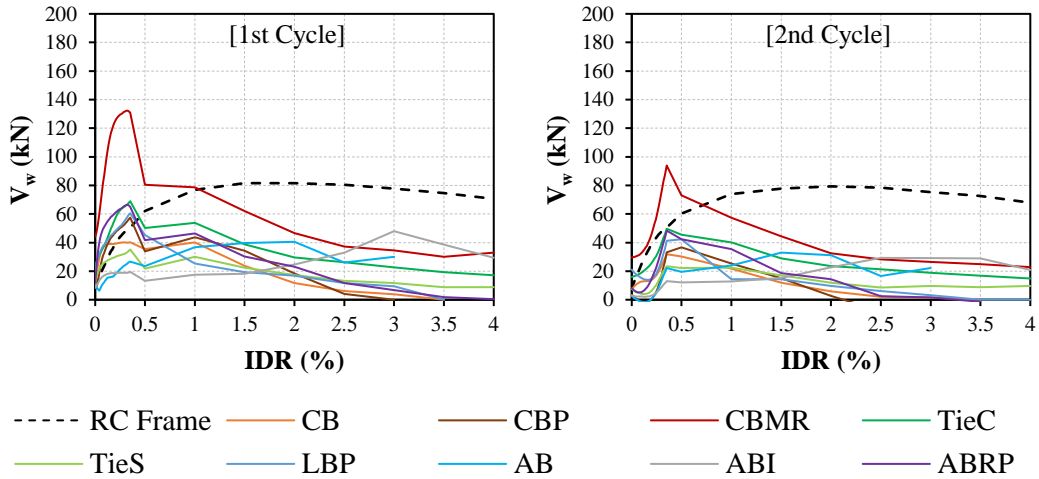


Figure 5.40. Averaged backbone curves

Load displacement response parameters such as initial stiffness (K_i), secant stiffness (K_{sec}), maximum base shear (V_{max}), base shear at yielding of the first frame member (V_y) for the tested infilled frames are summarized in Table 5.2 and extracted response parameters of infill walls are outlined in Table 5.3.

Deviation from the initial lateral stiffness of the infilled frames corresponded to the attainment of 40% of the maximum IF capacity (V_{max}). Consequently, the initial stiffness of the infilled frames (K_i) was determined using 10% and 40% of V_{max} in the first displacement cycle's push direction. Deviation from the initial lateral stiffness implicates deviation from the composite behavior of the infill wall and the

boundary frame manifested by cracking due to sliding under the upper beam and disintegrating the infill wall from the bounding frame. The attainment of the infill wall's maximum capacity ($V_{w,max}$) was accompanied by apparent visual damage. For the tested specimens, drift levels corresponding to the yielding of the first RC member (δV_y) were higher than the attainment of wall capacities ($\delta V_{w,max}$), indicating that infill walls are more sensitive to damage than the structural components, thereby they may undergo apparent damage before the yielding of the reinforcement in RC members.

Table 5.2. Load displacement response parameters under IP loading

<i>Frame ID</i>	K_i^1 (kN/mm)	K_{sec}^2 (kN/mm)	V_y^3 (kN)	δV_y^3 (%)	V_{max} (kN)	δV_{max} (%)
BF	12.9	4.0	63.7	0.67	82.2	1.41
CB	57.3	8.4	88.1	0.39	121.6	1.00
CBP	46.2	13.7	121.8	0.40	138.2	0.70
CBMR	62.6	39.6	169.7	0.85	188.7	0.33
TieC	30.2	8.9	108.8	0.54	139.5	1.00
TieS	34.5	4.8	97.0	0.60	92.5	1.00
LBP	45.5	16.6	95.0	0.49	119.7	0.50
AB	15.7	4.8	87.6	0.44	136.4	1.96
ABI	17.4	2.6	91.5	0.67	133.9	3.29
ABRP	86.7	8.7	109.5	0.65	132.2	0.97

¹ Initial stiffness calculated between 0.1-0.4 V_{max} at positive dir. (i.e. $K_i = [V_{0.4V_{max}} - V_{0.1V_{max}}] / [\delta_{0.4V_{max}} - \delta_{0.1V_{max}}]$).

² Secant stiffness (K_{sec}) calculated at maximum base shear (i.e. $K_{sec} = V_{max} / \delta V_{max}$) at positive direction.

³ Corresponds to the yielding of the first RC member determined from strain gauge readings.

The drift level at which the infilled frames (V_{max}) and the infill walls ($V_{w,max}$) reach maximum capacity are often different. For CBMR, LBP and ABI, the maximum capacity of the infilled frames was determined by the attainment of the peak strength of the infill wall. Whereas for other infilled frames, mutual influence of the infill wall and the RC frame was observed, such that peak lateral strength was reached at a displacement between the maximum capacity of the infill wall ($\delta V_{w,max}$) and the

BF (δV_{\max_BF}). Principal parameters impacting the drift associated with the achievement of the IF lateral capacity are the relative strength and stiffness of the wall and the boundary frame, as well as the failure mode of the wall.

Table 5.3. Extracted load-displacement response parameters of infill walls

Wall ID	First cycle		Second cycle			
	$V_{w,max}$ (kN)	$\delta_{Vw,max}$ (%)	$V_{w,max}$ (kN)	$\delta_{Vw,max}$ (%)	$\delta_{0.5Vw,max}$ (%)	$\delta_{0.2Vw,max}$ (%)
CB	47.1	0.35	32.5	0.35	1.45	2.15
CBP	79.8	0.35	64.8	0.50	1.26	2.04
CBMR	138.1	0.33	95.8	0.35	1.56	NA
TieC	72.3	0.32	53.0	0.50	2.41	NA
TieS	36.1	0.35	27.2	0.50	1.94	3.68
LBP	65.1	0.35	43.6	0.35	0.88	2.19
AB	55.1	1.96	37.7	1.00	2.41	-
ABI	59.0	3.28	37.3	3.50	NA	NA
ABRP	72.2	0.32	50.5	0.35	1.80	3.60

The degradation of lateral stiffness of the tested frame specimens was provided against imposed drifts in Figure 5.41. The stiffness degradation at target displacements was calculated considering averaged secant stiffnesses for the push and pull directions of the envelope curve. IF specimens exhibited an initial lateral stiffness five times that of the BF on average. However, the initial lateral stiffness reduced 3.5 times upon attainment of wall capacities around 0.4% drift. The lateral stiffness of infilled frames converged to BF around 2.5% drift level except for ABI and CBMR specimens.

The energy dissipation characteristics of the tested frame specimens were provided against imposed drifts in Figure 5.42. Overall, TieC and CBRP infill specimens performed the best and all infilled frames dissipated more energy and responded

stiffer than the BF as expected, except isolated specimen (ABI), which acts similarly to the BF until considerable interaction was gained around 1.5% drift.

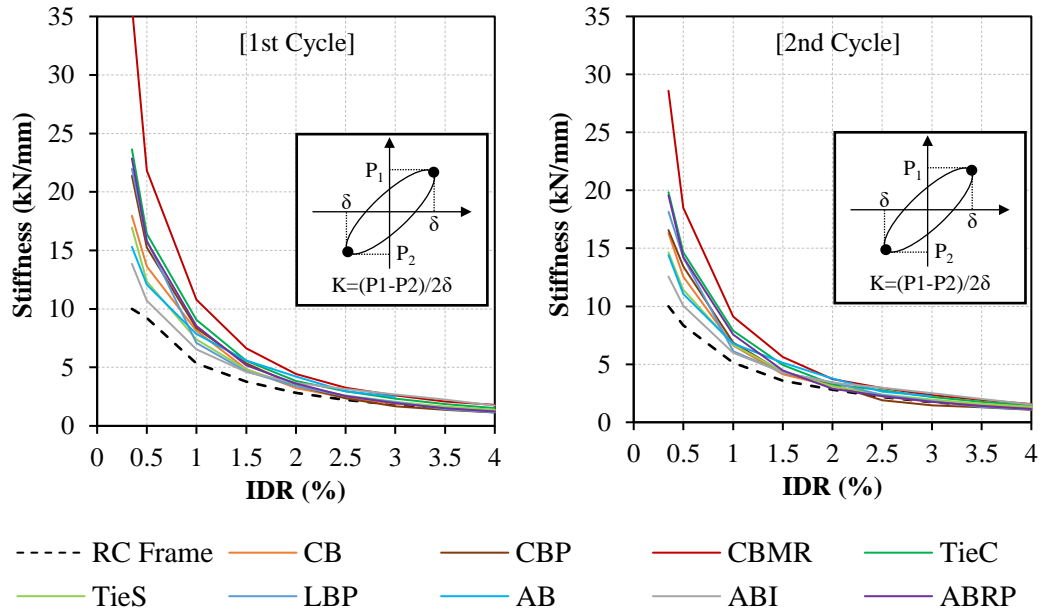


Figure 5.41. Stiffness degradation of tested infilled frames

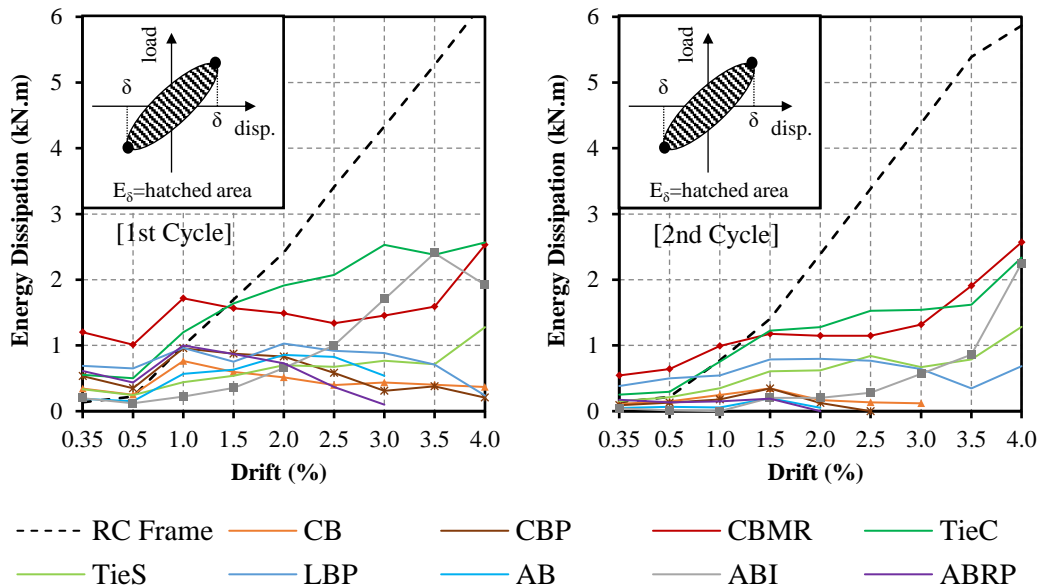


Figure 5.42. Energy dissipation of infill walls

The relative contribution of the infill wall and bounding RC frame to the lateral load resistance considering the first loading cycle at each target displacement, is demonstrated in Figure 5.43. In order to reveal the in-cycle deviation, the second loading cycles are also presented in the figure with dashed lines. Such visualization of measured experimental data allows a better perception of the load distribution among the infill wall and the bounding frame, whose maximum capacities were reached at different drift levels. Although tested infill walls were made of light materials, the walls resisted half the lateral load imposed on the IF specimens at 0.35% drift. Reduction and total dissipation of infill wall contribution to the lateral resistance around 2.5% lateral drift are observed excluding ABI, CBMR and Tie systems.

Similar comparisons were made between the energy dissipation capacities of the infill walls and the bounding RC frame for the initial and second loading cycles at each target displacement (Figure 5.44). The energy dissipation at a particular target drift was computed for the first and second displacement cycles. The region encompassed by a closed hysteresis loop indicates the dissipated energy during the cycle. For cycles with low amplitude, the infill walls dissipated more energy than the RC frame. Due to the plastic hinging of frame members and the quick deterioration of the infill wall, the RC frame dissipates the majority of the energy as drift increases. Due to the possible smoothing of crack surfaces, repeated cycles at the same drift level resulted in smaller hysteretic loops for the infill walls. Consequently, far less energy was dissipated during the second cycle of target displacements, particularly below 1.0% drift. Due to the dominance of sliding in its reaction, LBP and tie systems exhibited limited in-cycle degradation of dissipated energy. Similarly, the inclusion of mesh reinforcement increased the ductility of the masonry wall, limiting the in-cycle reduction in energy dissipation.

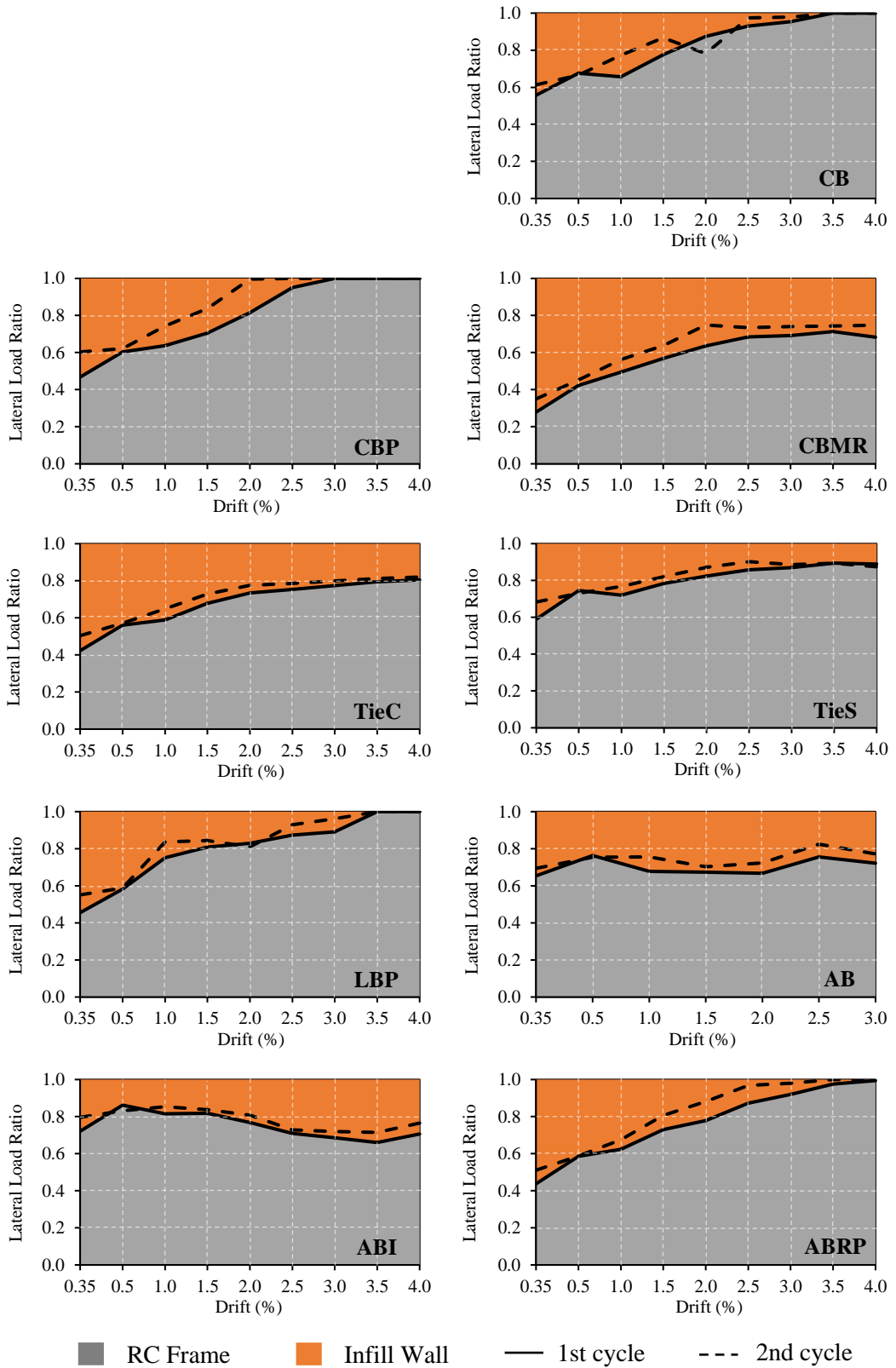


Figure 5.43. Distribution of lateral force among IW and bounding frame

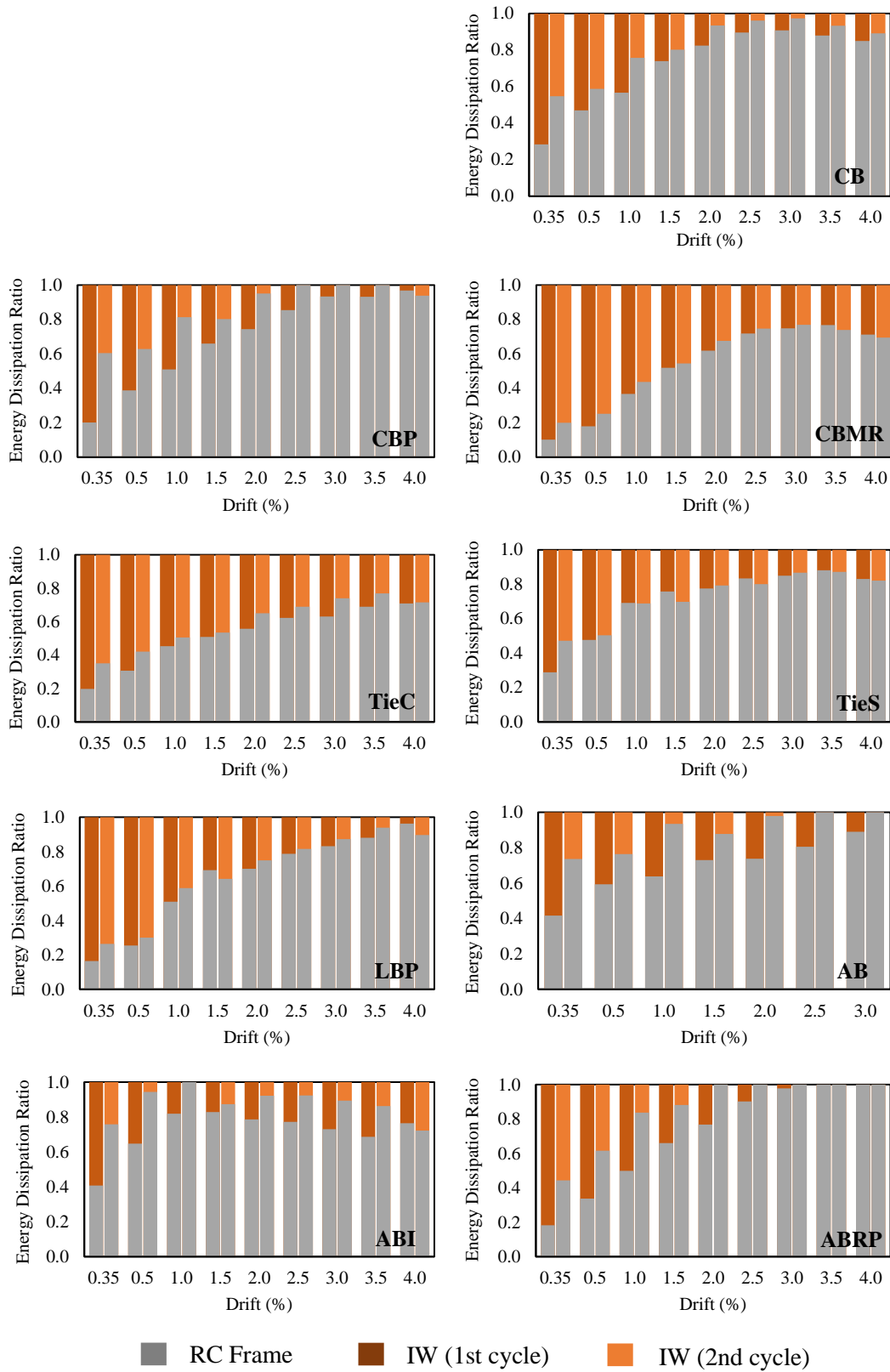


Figure 5.44. Distribution of energy dissipation among IW and bounding frame

5.3 Out-of-Plane Monolithic Loading Test Results

The wall surface was subjected to out-of-plane seismic forces via an airbag-induced, uniformly distributed loading. Transfer joints were used to restrain lateral movement of the upper beam aimed at preventing OOP bending of the RC test frame, which was secured to the ground with prestressed bolts. Before building the wall, the columns were loaded up to 17.5% of compressive capacity in the vertical direction and steel weight blocks were laid on the slab idealizing live and dead slab loads. Figure 5.45 illustrates the OOP testing environment, while Chapter 3.3.1.2 details of the testing assembly.



Figure 5.45. Front and back views of OOP test setup

Loading was imposed by a controlled increase of the air pressure inside the airbag until the failure of the wall. OOP displacements were measured with 13 LVDTs attached at different locations on the wall's surface. OOP force was measured using a 10-ton capacity load cell mounted between the reaction frame and the wooden OOP loading assembly resting on a linear guide (Figure 5.46). In order to avoid damage during a collapse, the LVDTs were fixed to a platform placed 1.5 m away from the specimen and connected to the rods planted at the specified points with epoxy using piano wires.

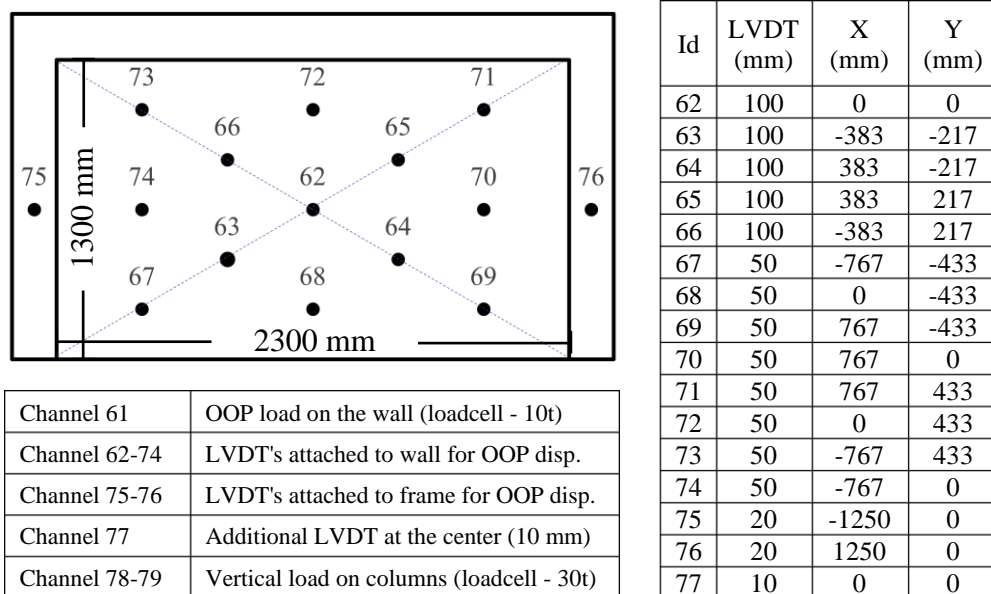


Figure 5.46. OOP Instrumentation

The infill walls tested under increasing OOP pressure are illustrated in Table 5.4 below. The weight of the walls was determined by measuring wall debris after the finalization of the tests. The compressive strength of the mortar (f_{mc}) is the average of the mortar prism tests conducted at the frame test date.

Table 5.4. OOP monolithic tests

<i>Tested Wall</i>	<i>Wall Unit</i>	<i>Plaster</i>	<i>Wall Weight (kg)</i>	<i>f_{mc} (MPa)</i>	<i>Retrofit</i>	<i>Test Date</i>
CB	HCB	No	297	5.61	No	05-05-2016
CBP	HCB	Yes	445	3.44	No	29-04-2016
CBMR	HCB	Yes	465	5.78	Steel mesh overlay	24-05-2016
TieC	HCB	No	280	6.93	Horizontal steel plate	25-07-2016
LBP	LB	Yes	484	5.58*	Dry bed joints	16-05-2016
ABRP	ACB	Yes	200	8.40	Fiber mesh overlay	12-01-2017

*Mortar was only used at head joints for the LBP specimen.

5.3.1 Damage Propagation

The ultimate damages of specimens tested under OOP loading are illustrated in Figure 5.47 below.

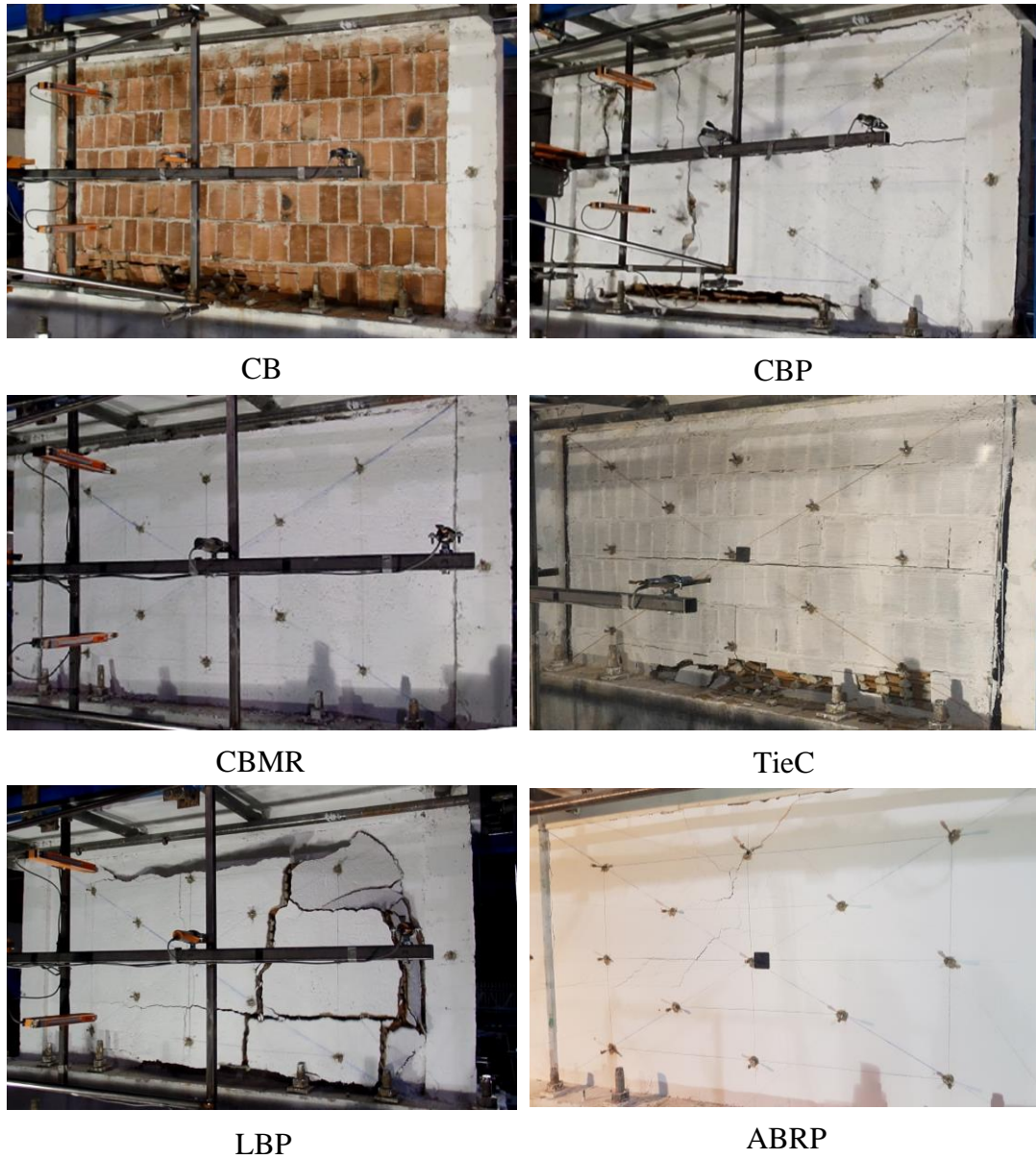


Figure 5.47. Ultimate infill damages under OOP loading

The ultimate damage patterns of tested specimens are illustrated in Figure 5.48. In CB, CBP, and TieC specimens, a significant central horizontal crack appeared at a

displacement of 2 mm OOP, or 0.15 percent OOP drift. Bricks in the bottom row of the CB and TieC specimens were crushed, forming a three-joint arch mechanism. In the CBP specimen, the bottom row crushing was accompanied by a vertical crack. Although LBP prevented the crushing of brick units, the development of vertical cracks after two significant horizontal fractures led to a sudden failure. Specimens with surface overlays, namely CBMR and ABRP, reached the collapse state through arching in the horizontal direction without sudden collapse but with gradual degradation under increasing displacement demands.

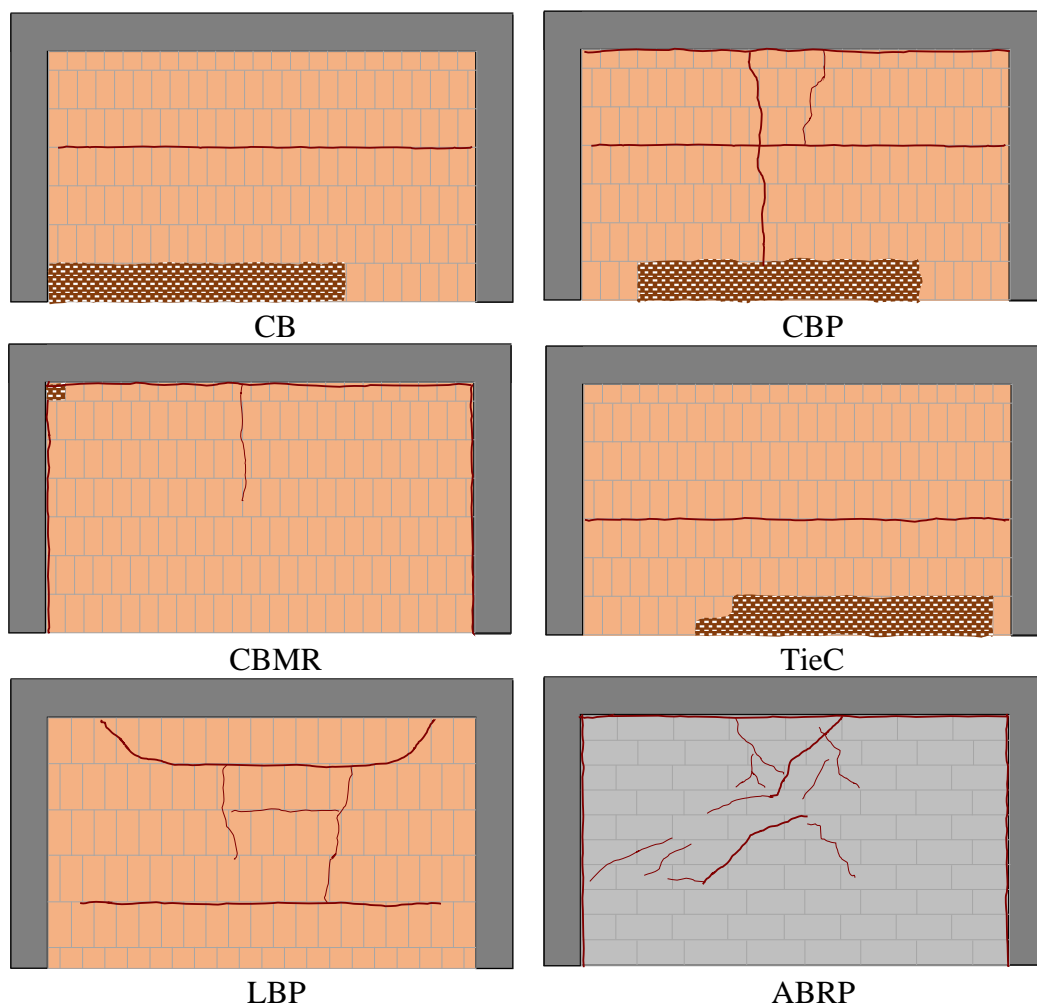


Figure 5.48. Ultimate damage patterns of infills under OOP loading

These observations are confirmed by the displacement contours shown in Figure 5.49 for the onset of cracking and failure stages.

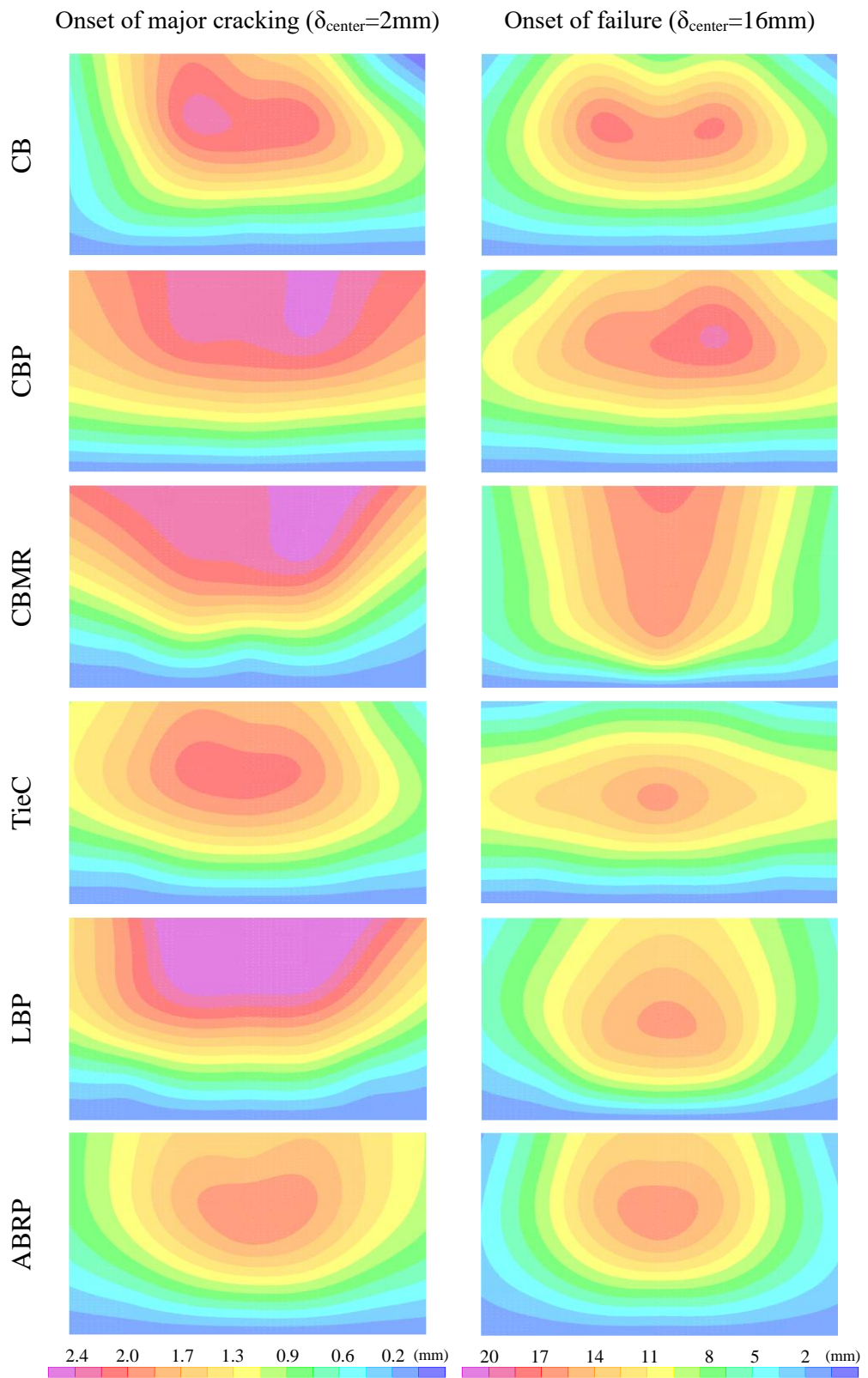


Figure 5.49. OOP displacement profile of infills

The top line of the infill wall tends to deflect freely because there is no contact between the infill and the upper beam for the CB, CBP, CBMR, and LBP specimens, according to the observed displacement pattern at 2 mm central displacement, which corresponds to the onset of major crack formation. However, the sides and the bottom are supported (Figure 5.49). While the observed displacement for the CB, CBP, LBP, and ABRP specimens resembled a two-way mechanism at the time of failure, the TieC and CBMR specimens showed signs of a one-way mechanism in the horizontal and vertical directions, respectively. The contact between the infill and the upper beam was understood to be maintained for the CB, CBP, and LBP specimens despite increased displacements after the infills cracked.

5.3.2 Load-Displacement Response

The measured total load versus central deflection is shown in Figure 5.50. The out-of-plane loads were measured with a 10-ton capacity load cell pin connected to the wooden assembly supporting the airbag. The displacement was measured at the central node and the drift was calculated by dividing the central displacement by the height of the wall.

The load - displacement parameters of the tested specimens are shown in Table 5.5. In this table, d_y and d_u represent the cracking and collapse displacements at the wall center, f_y and f_u represent the wall cracking and collapse strengths, respectively. Initial stiffness (K_i) was calculated between two points corresponding to 5% and 50% of the wall capacity (f_u).

CB and TieC specimens were constructed without plaster. Thus, their initial stiffnesses were smaller than the others. However, yield displacement and ultimate displacement of all the specimens were close to each other. By comparing the capacities of CB and CBP specimens, it can be concluded that plaster (10 mm on each face) increased the OOP capacity by 43%.

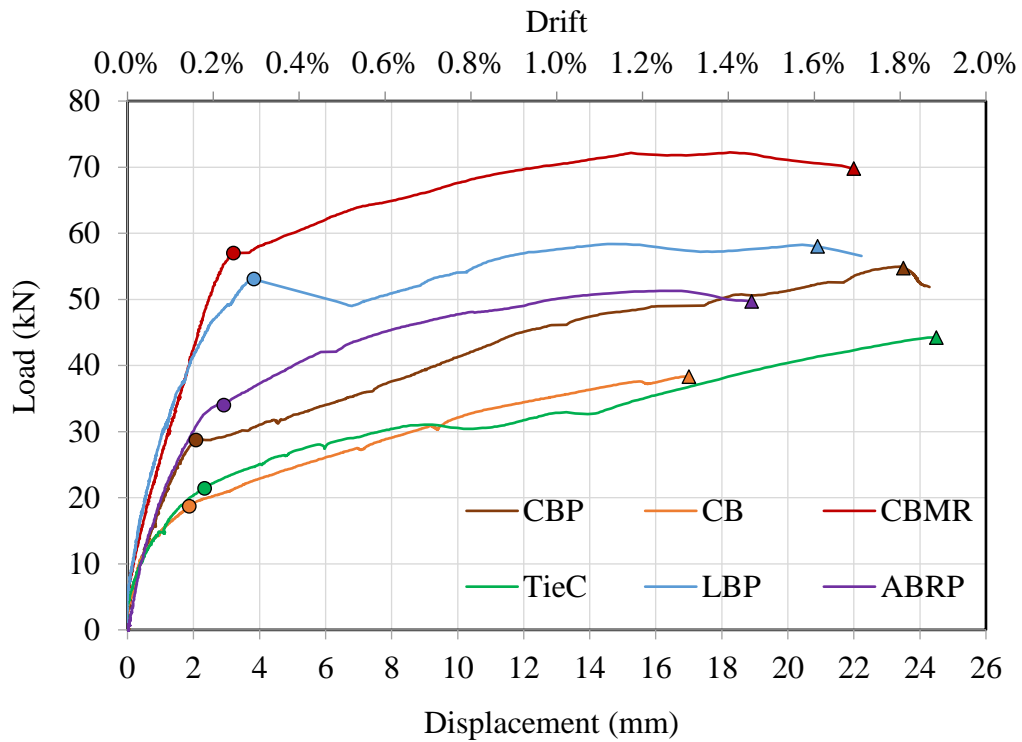


Figure 5.50. Load displacement curves in OOP direction

Table 5.5. Load displacement response parameters for OOP loading

Wall Specimen	K_i (kN/mm)	d_y (mm)	d_u (mm)	f_y (kN)	f_u (kN)	d_u/d_y	f_u/f_y	$f_u/f_{u,cb}$
CB	8.75	1.87	17.0	18.7	38.3	9.09	2.05	1.00
CBP	13.6	2.07	23.5	28.7	54.7	11.4	1.91	1.43
CBMR	19.9	3.21	22.0	57.0	69.8	6.85	1.22	1.82
TieC	7.86	2.34	24.5	21.4	44.2	10.5	2.07	1.15
LBP	25.1	3.83	20.9	53.1	58.0	5.46	1.09	1.51
ABRP	16.8	2.92	18.9	34.0	49.7	6.47	1.46	1.30
Ave	15.3	2.71	21.1	35.5	52.5	8.28	1.63	1.44
St.dev	6.06	0.68	2.58	14.7	10.1	2.17	0.39	0.23

5.3.3 OOP Response Summary

The first reaction of the tested systems to the OOP loading was forming an arching mechanism in horizontal and vertical directions. The linear trend in load-displacement response is disturbed by the appearance of a visible crack along bed joints at mid-height for all tested systems. The rate of increase of load slowed down in response to rapidly increasing displacement demands after the first crack. Following this phase, differences were observed in the failure mechanisms of tested systems.

CBMR and ABRP specimens released the load under increasing displacements rather than sudden collapse upon reaching displacement capacity. Tested infill walls failed at a rate of 1.4% to 1.8% of the wall's height. Ultimate displacements were 8 times larger than the cracking displacements. Maximum load capacities are 1.63 times larger than cracking loads on average.

The infilled specimens CB, CBP, and LBP suddenly collapsed following the brick crushing at the lower course, forming a three-pinned arch mechanism in the short direction (Figure 5.47).

Although the TieC specimen experienced a similar three-pinned arc mechanism, taking advantage of the horizontal steel plates, more ductile behavior was observed with increased displacement and load capacities.

CBMR and ABRP specimens did not collapse but deteriorated under increasing displacements where rigid wall blocks separated by yield lines were easily identified.

Additional OOP monolithic tests conducted by Selin Aktaş (2023) using the same test setup with perforated masonry walls with window and door openings are recommended to identify openings' influence on the OOP response.

5.4 Simultaneous Bidirectional Loading Test Results

In order for infill walls to contribute IP resistance of bounding frames, lateral drift levels should be limited and OOP stability should also be preserved. Due to the biaxial nature of seismic loads and IP drift reversals, walls are exposed to OOP forces treating stability. For the IP response, the behavior is driven by lateral story drift, which is a displacement quantity. Yet, in the OOP direction, behavior is driven instead by inertial forces dependent on floor level acceleration in building frames (Gülkan et al. 2015).

In order to investigate the influence of prior IP damage on the OOP capacity of the infilled frames, six specimens which are shown in Table 5.6, were tested under constant OOP and cyclic IP loading. Applied forces in the IP and OOP directions were measured using load cells on all specimens. LVDTs were positioned at the centroid of the slab to measure IP story displacements and at 15 different locations on the wall surface to measure OOP wall displacements. Measurements were recorded until the out-of-plane collapse of the wall or a sudden degradation of the wall capacity of more than 20 %.

The identical IP displacement history applied to IP-only tests was utilized in IP direction and the out-of-plane pressure was maintained at a constant $1/3$ or $2/3$ of the infill wall's OOP capacity which were determined in the OOP-only tests.

Details of the test setup, loading protocol and instrumentation were illustrated in Chapter 3.3.1.3.



Figure 5.51. Test setup for combined IP and OOP loading of infilled frames

Table 5.6. Biaxial infilled frame tests

<i>Specimen</i>	<i>OOP Load Ratio*</i>	<i>Wall Unit</i>	<i>Plaster</i>	<i>Wall Weight (kg)</i>	<i>f_{mc} (MPa)</i>	<i>Retrofit</i>	<i>Test Date</i>
CBP_0.33	0.33	HCB	Yes	445	5.65	No	08-06-2016
CBP_0.66	0.66	HCB	Yes	445	5.82	No	20-06-2016
CBMR_0.33	0.33	HCB	Yes	465	4.37	Steel mesh overlay	16-10-2019
TieC_0.33	0.33	HCB	No	280	3.75	Horizontal steel plate	08-12-2016
LBP_0.33	0.33	LB	Yes	484	5.47	Dry bed joints	01-07-2017
ABRP_0.33	0.33	ACB	Yes	200	8.40	Fiber mesh overlay	03-02-2017

- Ratio of constant OOP load to OOP capacity

5.4.1 Damage Propagation

The ultimate damages of specimens tested under combined loading are illustrated in Figure 5.52 below. Inter story drift ratio (IDR) where the collapse takes place is also identified in the same figure for all tested specimens.

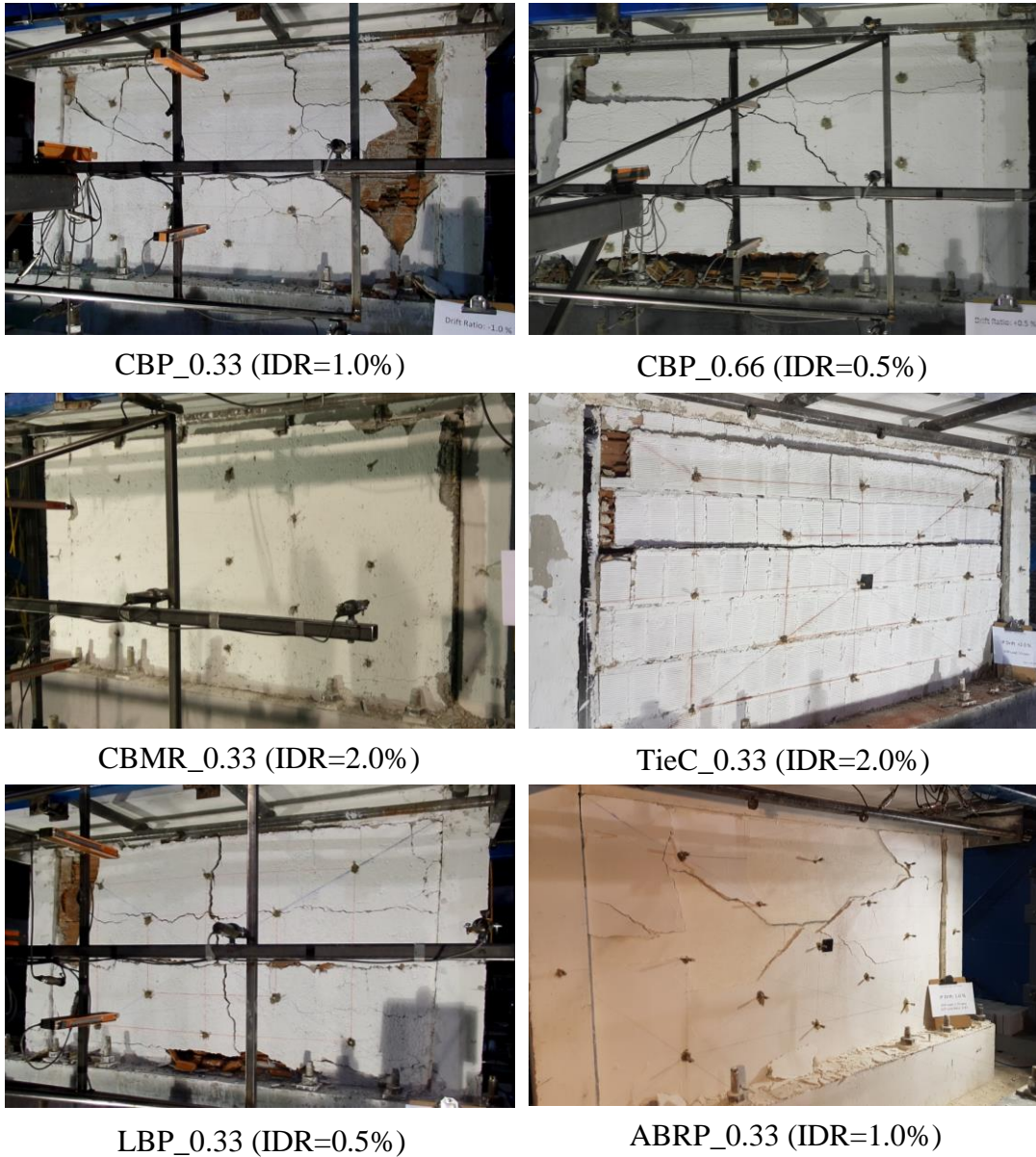


Figure 5.52. Ultimate infill damages under combined loading

CBB_0.66 and LBP_0.33 specimens reached their ultimate capacities through crushing bricks at the bottom layer similar to OOP only loading and CBP_0.33 experienced failure following crushing bricks in the upper side of the compression diagonal. Failure of all mentioned specimens was sudden. Infill walls improved with horizontal steel plates and surface overlays experienced a strength degradation instead of total collapse. CBMR_0.33 specimen experienced a sliding failure. The infill wall was displaced in the OOP direction as a rigid body. TieC and ABRP underwent excessive bulging, yet the integrity of the infills was preserved. Cracking and crushing damage on the walls before failure is shown in Figure 5.53.

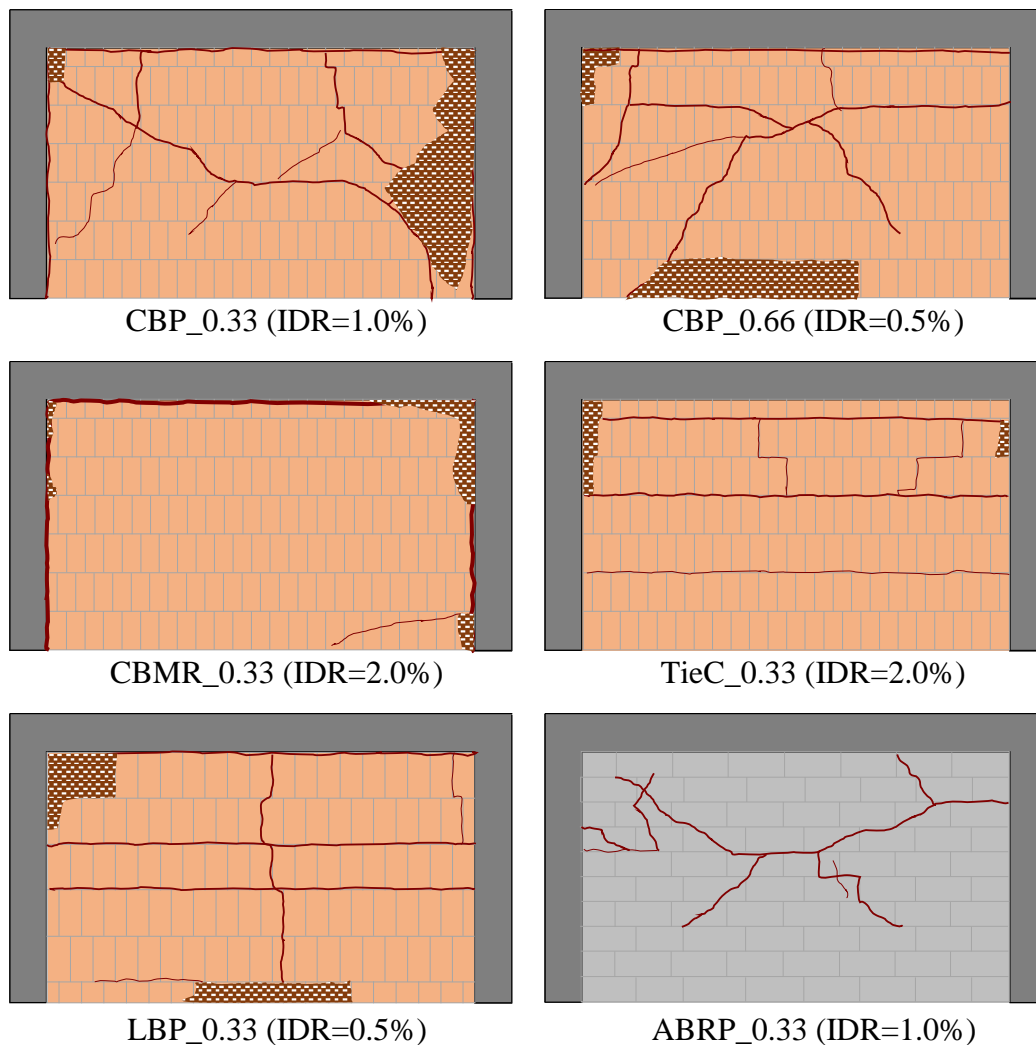


Figure 5.53. Ultimate damage patterns of infills under combined loading

The OOP displacement pattern of the tested walls corresponding to the push direction of the first cycles at 0.35%, 0.50% and 1.00% target drifts are illustrated in Figure 5.54 below. Rotation of the wall from the base is observed for CBMR in the cycles following 0.35%. TieC and LBP specimens were dominated by arching in the short direction, whereas CBP specimens experienced arching in the long direction and loss of contact with the upper beam.

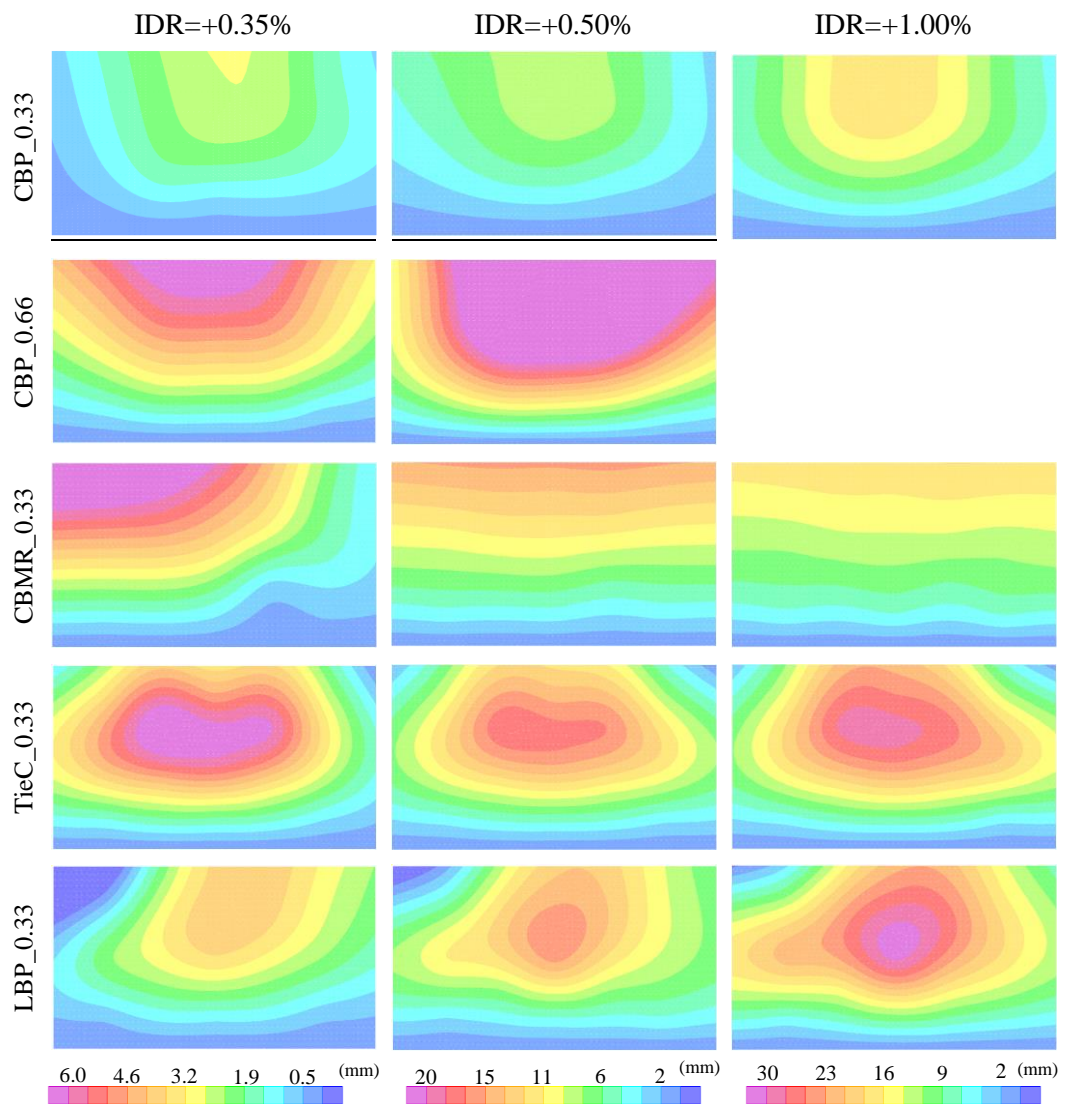


Figure 5.54. OOP displacement profile under combined loading

5.4.2 Load Displacement Response

The influence of IP damage on the OOP displacements is investigated by drawing OOP displacements against increasing IP drifts at target IP drifts (Figure 5.55). OOP central displacement increase as a result of IP damage. As each IP displacement cycle is repeated twice at predefined targets, OOP displacements also increase within a cycle. The IP drift levels given in Figure 5.55 correspond to the push and pull directions of first and second cycles at target IP drifts. It can be inferred from the figure that CBMR and TieC systems were able to increase the displacement capacity of the wall and resulted in failures at more prominent IP and OOP drifts.

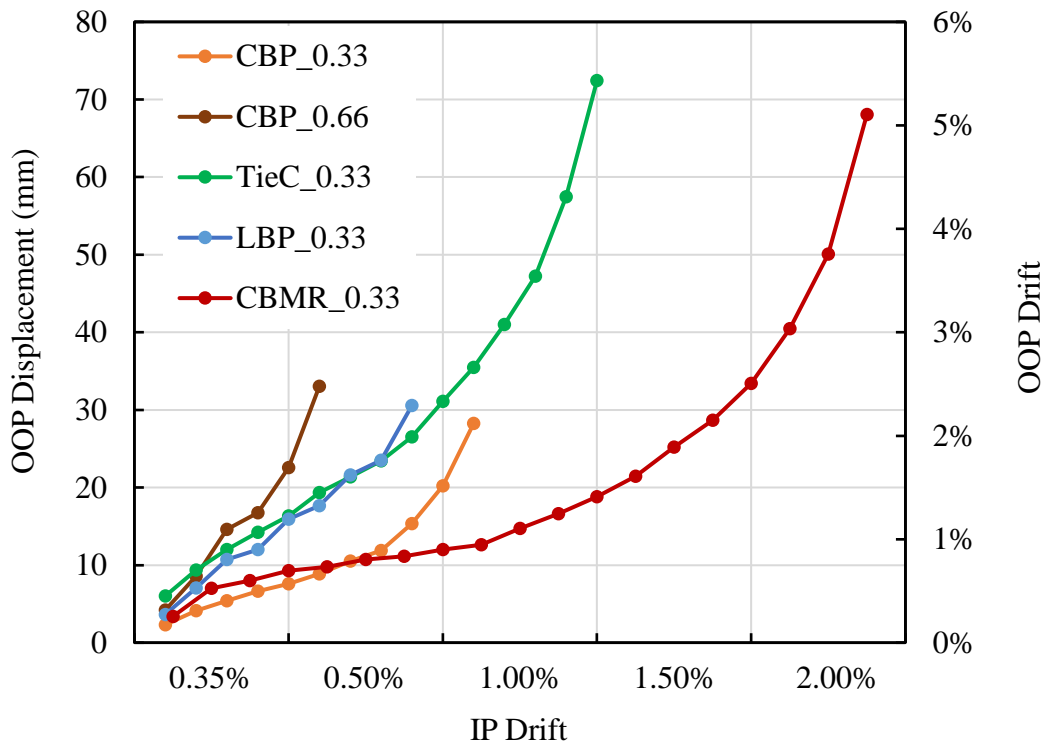


Figure 5.55. OOP central displacement under increasing IP drift

5.4.3 Failure Envelope

The obtained interaction diagram derived from IP only, OOP only and combined testing of the specimens is shown in Figure 5.56. In-plane capacity is represented by IDR in the horizontal axis and the vertical axis represents OOP load capacity ratio (i.e., the ratio of the out-of-plane load applied during the test to the out-of-plane load capacity of the infill determined from the out-of-plane only test). IP capacity of the walls in the absence of OOP forces relied upon the near collapse damage state of walls from IP-only test results and performance criteria set of infill walls (Figure 6.2). It can be inferred from the figure that OOP loading has a negative impact on the IP drift capacity and that the interaction depends on the selected infill system.

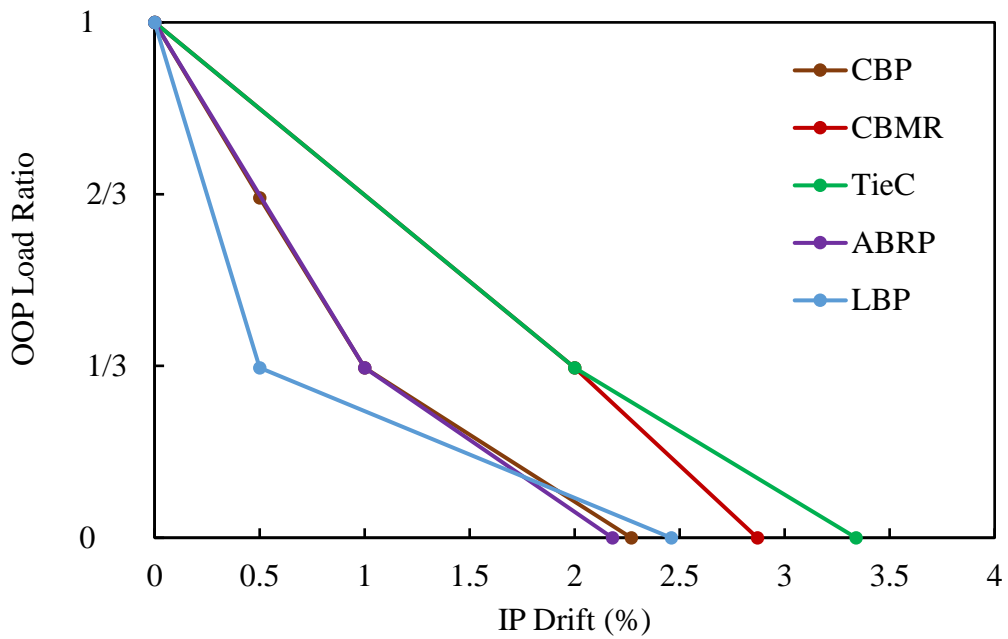


Figure 5.56. IP and OOP interaction diagram

CHAPTER 6

PERFORMANCE ASSESSMENT

6.1 Introduction to Performance Assessment of Infill Walls

Numerous researchers noted the significance of infill walls on the seismic performance of framed RC buildings. Calvi and Bolognini (2001) stated that for damage or serviceability limit states, the effects of infills are often so strong that the ductility of the structural systems and even the seismic force for which the bare frame was designed to have little impact on the final performance. The influence of infills frequently determines the buildings' damage limitation or serviceability limit state. The possibility of immediate use or a short-term repair largely depends on the damage sustained by each infill panel. Sucuoglu (2013) highlighted infill wall performance from the viewpoint of the residents, claiming that following a moderate earthquake, even though the structural system was undamaged, occupants left the building due to infill damage. The failure of the seismic codes to define performance for infill walls, particularly for moderate-level earthquakes, is because of the difference between the structural engineer's performance aim and the performance perception of the occupants. In this respect, unless infill contribution is taken into account, present seismic design and evaluation philosophies based purely on RC member ductility principles may be insufficient to forecast the real projected damage. It is crucial to include infill wall damage in the formulation of the global limit state because failing to consider infill walls can result in substantial risks to human life and building occupancy (Tiziana Rossetto 2004).

This chapter aims to summarize the previous studies on the performance assessment of infill walls, and propose a new methodology to examine the IP seismic performance for infill wall systems constructed with different materials and easy-to-apply retrofit techniques introduced in Chapter 3.2.

6.2 Previous Studies on the Seismic Performance of Infill Walls

Evaluation of a building's performance necessitates establishing performance goals and quantifying the acceptable level of damage. Damage limit states (DLSs) designate the severity of damage to structural and non-structural elements and the viability of repair measures. The DLSs should be correlated with structural response parameters such as displacements, rotations, and accelerations. In seismic codes, strain or rotation limits for steel and RC structural members were defined for each performance level after extensive research. However, damage quantification for masonry infill walls is more difficult due to multiple parameters that complicate their response. Key challenges include the heterogeneous and brittle nature of masonry walls, the variability of its components and quality of construction, the interaction with the surrounding frame, and the interaction between IP and OOP damages (Gu and Lu 2005).

Multiple attempts have been made to define DLSs for infill walls. The commentary section of ASCE41 (2017) provides simple definitions of acceptable IP damage for infill walls corresponding to different performance levels. The immediate occupancy (IO), life safety (LS), and collapse prevention (CP) performance levels were associated with significant visual cracking, substantial cracking, and damage, indicating a high likelihood of local or total OOP wall collapse.

Some researchers define different damage states (DS) through a broad description of the extent and severity of infill damage; others additionally relate such damage levels to the peak load of the infill or the attainment of specified strength reduction ratios (De Risi et al. 2018). However, there is no scientific consensus on the definition of DS for masonry infills, and not every researcher has correlated their proposed DS with seismic code-defined performance levels. A summary of various DS definitions for different performance levels is presented in Table 6.1 based on a comprehensive literature survey.

Table 6.1. Definition of infill wall damage for different performance levels

Author	DS	DS1 (Slight-Negligible)	DS2 (Light)	DS3 (Moderate)	DS4 (Severe)
	PL	Operational	Immediate Occupancy (Damage Limitation)	Life Safety (Significant Damage)	Near Collapse (Collapse Prevention)
Baggio et al. (2007)		Cracks up to 2 mm due to separation, slight diagonal cracking with widths <1mm	Separation cracks (width>2 mm). Diagonal cracks of a few mm. Visible crushing at panel corners and localized expulsion.		Damages heavier than the previous ones, including collapse.
Chiozzi & Miranda (2017)		Hairline cracks up to 2mm wide, concentrated in mortar joints, plaster or along the interfaces. Very light repair needed.	Beginning of significant diagonal cracks >2mm wide, possible but very limited sliding btw joints and localized crushing of units. Heavier repair.		Wide diagonal cracks (> 4mm) with significant sliding and widespread crushing/spalling. Repair not feasible, reconstruction advised.
Gaudio et al. (2019)		Detachment between the panel and the RC frame. Light diagonal cracking with widths <1mm.	Cracking extended to 25-35% of the panel area. Failure of corner brick units at 10% of the panel area.	Crushing and spalling of brick units at 30% of the panel area.	IP or OOP collapse of the panel.
Cardone & Perrone (2015)		Separation of the infill from top beam and mid-height columns, light diagonal cracking (width<1 mm)	Extensive diagonal cracking (<2mm) at 25-30% of panel area, possible failure of brick units at 10% of panel area.	Brick spalling at 30% of panel, corner crushing, spalling of large plaster, sliding in the mortar joints. Repair not feasible.	In-plane or out-of-plane collapse.
Morandi et al. (2018b), Sassun et al. (2016)		Slight cracking concentrated along top beam and the column upper height. A cosmetic damage without the need for repair.	Repairable damage due to diagonal cracking or sliding. Very limited crushing and spalling of a few units at upper corners.	Severe and widespread damage, not threatening lives. Renewal of the panel highly be required. Spalling and crushing of limited bricks.	A large amount of masonry panel area is crushed/spalled
Colangelo (2013)		Onset of cracking in the bricks, the first noticeable stiffness reduction.	Moderate cracks before attaining the maximum strength of the infilled frame.	Extensive cracks with tensile splitting and falling of the outer layer of a few bricks. Repairable.	So many broken bricks repair unreasonable, reconstruction needed.
Rossetto & Elnashai (2003)		Cracking at wall-frame interfaces or opening corners. Diagonal cracking of panel. Limited crushing of bricks at upper corners.	Increased crushing of bricks at upper corners. Start of structural damage. Diagonal shear cracking of RC members at exterior frames.	Extensive panel cracking, falling bricks, OOP bulging. Partial infill failure, heavier damage in frame members.	Near total infill failure. RC member failure in shear.
Gu & Lu (2005)		-	Minor cracks and falling of small pieces of plaster. Only local repair work is needed.	Significant cracking and flaking but without stability loss. Repairable.	Wall panel loses its integrity leading to collapse.
Calvi & Bolognini (2001)		No panel damage. Fully operational.	Light panel damage. Operational.	Severe panel damage not threatening lives. Repairable.	Very heavy panel damage. Life danger.
Lu & Zha (2021)		The infill wall is slightly separated from the frame, there are hairline cracks with a width of less than 1.5 mm.	Diagonal and stepped cracks are formed, width<3.0 mm. Limited sliding of the bricks in the mortar joints, and local crushing of corner bricks.	Existing cracks propagate with widths >3.0 mm. Obvious sliding of bricks in the mortar joints, progressed crushing and spalling of bricks	The infill wall is slightly separated from the frame, and there are hairline cracks with a width of less than 1.5 mm.

Calvi and Bolognini (2001) related the infill wall DLSs to specific points on the axial stress-strain curve of the compression diagonal. No damage, light damage, and severe damage were associated with the infill wall reaching its maximum capacity, a 50% decrease in capacity, and a complete loss of capacity, respectively (Figure 6.1a).

Gaudio et al. (2019) visually quantified infill damage and proposed four DS based on the physical infill damage severity. He determined visually inspected DS's on the force- displacement envelope of infill walls derived from the difference between the IF and the bounding RC frame by analyzing 105 experimental tests presented in the literature. According to the data gathered, the drift values for slight damage (DS1), light damage (DS2), severe damage (DS3), and collapse (DS4) were approximately 0.25, 0.80, 2.50, and 4.10 times the drift at the in-plane capacity of the solid infill walls (Figure 6.1b).

De Risi et al. (2018) analyzed 60 collected tests to characterize infill wall response and identify four DLS's primarily based on the ratio of cracked and crushed area to the total wall area of the infill wall, as proposed by Cardone and Perrone (2015). In the absence of reliable experimental data to identify drift ratios corresponding to defined DS's, they employ strength reduction ratios depicted on the generalized strength-deformation relationship for infill walls (Figure 6.1c).

Gu and Lu (2005) differentiated three performance levels, namely functional, damage control, and collapse, for damage quantification of infill walls corresponding to peak strength reduction ratios of 0%, 30%, and 70%, respectively, based on an extensive survey conducted to evaluate the IP lateral displacement capacities.

6.3 A Methodology for Performance Assessment of Infill Walls

DLSs for the weak infill wall systems utilized in the ductile test frame in this study is determined based on the specified points located on the normalized lateral load-displacement envelopes. Four points (A, B, C, and D) on the extracted load-

displacement curve of infill walls differentiate the DS's for operational, immediate occupancy, life safety, and near collapse performance limit states (Figure 6.1d).

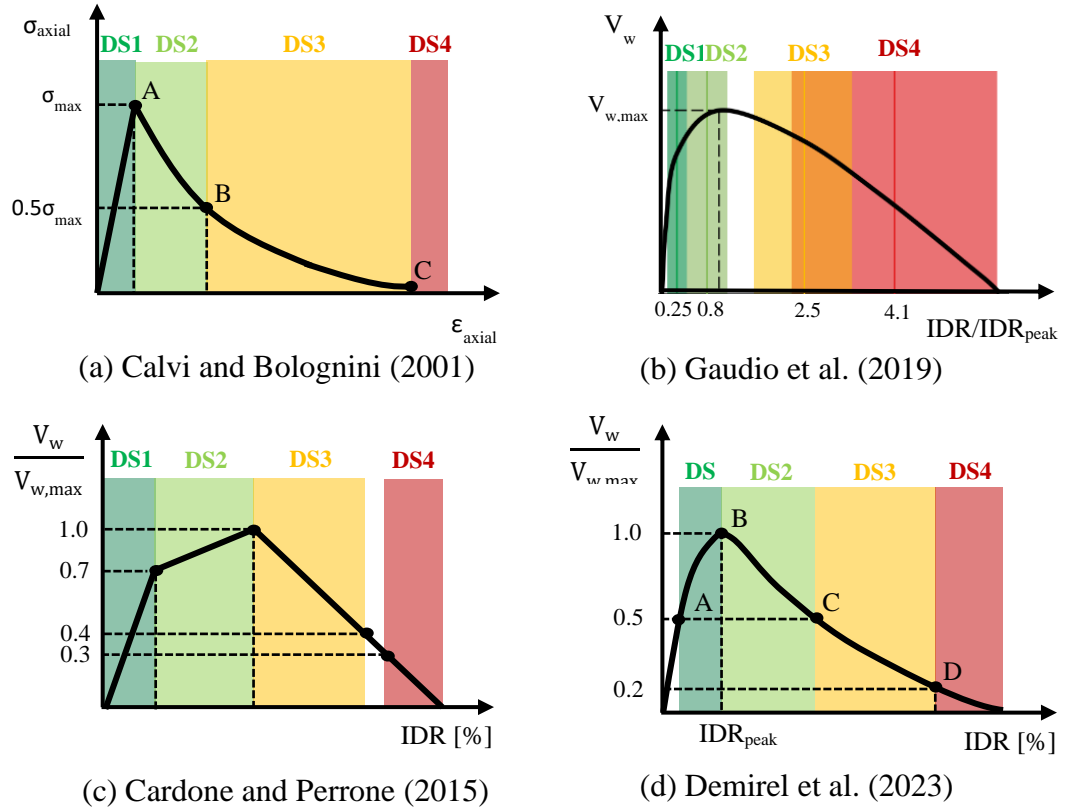


Figure 6.1. Definition of damage states for infill walls

The suggested DLSs, corresponding damages observed during tests and appropriate repair procedures are illustrated below:

Point A (DLS1) relates to operational (OP) PL, where continuous operation and services should not be disturbed following an earthquake. The first decrease in lateral stiffness in the force displacement response of tested infilled frames identifies this PL. According to the results of frame specimen testing, cracking strength was reached at approximately 0.08% drift, which roughly corresponds to 50% of peak wall strength ($0.5V_{w,max}$). Previous research (Dolšek and Fajfar 2008; Alwashali et al. 2018; De Risi et al. 2018) suggests a cracking to peak strength ratio of between 0.6 and 0.8 for infill walls; however, a lower ratio is observed, possibly due to the use of weak infill walls. Since the initial drift cycle of the applied loading protocol

begins at 0.35%, it was not possible to create a detailed damage description for the OP DS. Analysis of video recordings revealed hairline cracking under upper beam infill wall interface.

Due to the different stiffness characteristics of the infill walls and the surrounding frames, it is inevitable that the plaster will crack at the interface between the wall and the frame. Interface cracking can be considered light damage that can be repaired cosmetically with minimal effort and expense. At this damage limit state, a decrease in the structure's lateral load carrying capacity is not anticipated.

Point B (DLS2) is related to the attainment of maximum infill wall capacity ($V_{w,max}$) and is associated with IO PL. On the average, point B corresponded to 0.40% drift (Table 7.3) for the tested infill walls, with the exception of ABI where the infill is isolated. Observed damage manifested as complete interface cracking along the wall's perimeter, the initiation of horizontal or diagonal hairline cracks revealing the dominant wall damage mechanism, localized spalling of plaster and peeling off of the outer layer of individual bricks under the beam and close to the upper corners. Since no deterioration has yet occurred, infill damage is minimal and infill capacity is maintained despite a reduction in stiffness.

Local plastering of the cracks and spalled areas is deemed to be an appropriate minimal repair measure. In spite of the fact that infill damage is repairable, as the compression diagonal reaches its ultimate capacity, deficient frames may experience shear failures at beam-column joints and/or member ends, which may initiate a decline in global structural capacity. The global system's lateral rigidity is reduced as a result of the cracking of the infills altering the dynamic response due to period change.





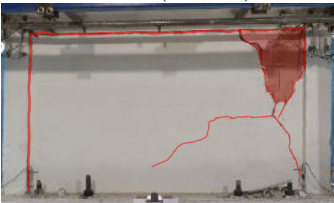
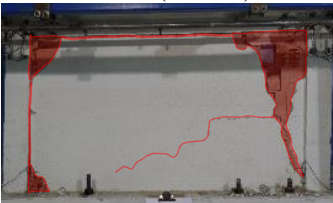


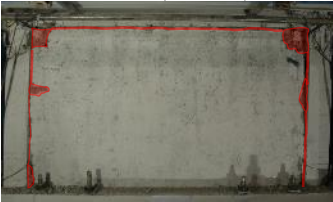
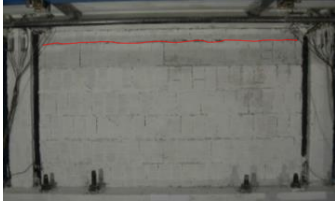



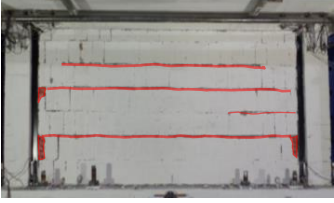




Point C (DLS3) separates LS and CP performance levels and corresponds to a 50% reduction in infill wall capacity ($0.5V_{w,max}$). Except for isolated infill (ABI), tested specimens reached point C around 1.5% drift (Table 7.3). At this point, the damage mechanism of the infill walls was clearly identified. This limit state is characterized by corner crushing, spread and enlargement of cracks, spalling of the plaster to a

greater extent, crushing of wall units, and localized wall area loss. Reduced infill wall capacity indicates permanent damage.

Restoration of the initial capacity and rigidity necessitates extensive repair measures, including removal of the plaster, demolition of the loosened wall area, local reconstruction or grout injection for the demolished region, and application of new plaster and paint. Although the infill wall retains 50% of its capacity, the OOP stability of the wall is compromised by the increased in-plane damage, which could lead to weak story formation during the earthquake excitation, as stated by Dolsek and Fajfar (2001) based on the damage observations after the 1999 Kocaeli ($M_w=7.4$) earthquake. This performance level may indicate the onset of significant building damage.

Point D (DLS4) marks upper limit for CP performance level, identified by 80% reduction in the infill wall capacity (i.e., $0.2V_{w,max}$). This limit relates to the integrity loss of the infill wall. Tested specimens reached this level at about 2.5 % drift on the average (Table 7.3). Almost all of the infill wall's contribution to lateral load resistance was lost, indicating severe damage. During tests, crushing and subsequent falling of brick units as well as extensive cracking were observed. Significant loss of infill contribution indicates the failure of the strut mechanism, so the lateral displacement demands imposed by the enclosing frame must be satisfied by rigid body motion within the wall body, such as sliding over horizontal/diagonal cracks or rocking motion.

A repair may not be possible due to the smoothed sliding joints, widened cracks, and spalled large wall areas. It is advised that the wall be demolished and then rebuilt. Almost the entirety of the contribution of the infill wall to lateral stiffness, strength, and energy dissipation is lost. The structural period increased, and the RC frame is solely responsible for the global structural response. Depending on the number of infill walls, the building could experience a significant reduction in lateral strength and deformation capacity.

	DS2 ($V_{w,max}$) (Immediate Occupancy)	DS3 ($0.5V_{w,max}$) (Life Safety)	DS4 ($0.2V_{w,max}$) (Near Collapse)
CB	 0.35% (-0.67%)	 1.73% (-1.42%)	 2.38% (-1.94%)
CBP	 0.72% (-0.35%)	 1.81% (-1.55%)	 2.18% (-2.36%)
CBMR	 0.33% (-0.26%)	 1.33% (-1.46%)	 2.87% (NA)
TieC	 0.35% (-0.32%)	 1.46% (-1.92%)	 3.34% (NA)
TieS	 0.35% (-0.33%)	 1.89% (-2.07%)	 NA (-3.48)
LBP	 0.35% (-0.33%)	 1.04% (-0.60%)	 2.55% (-2.37%)

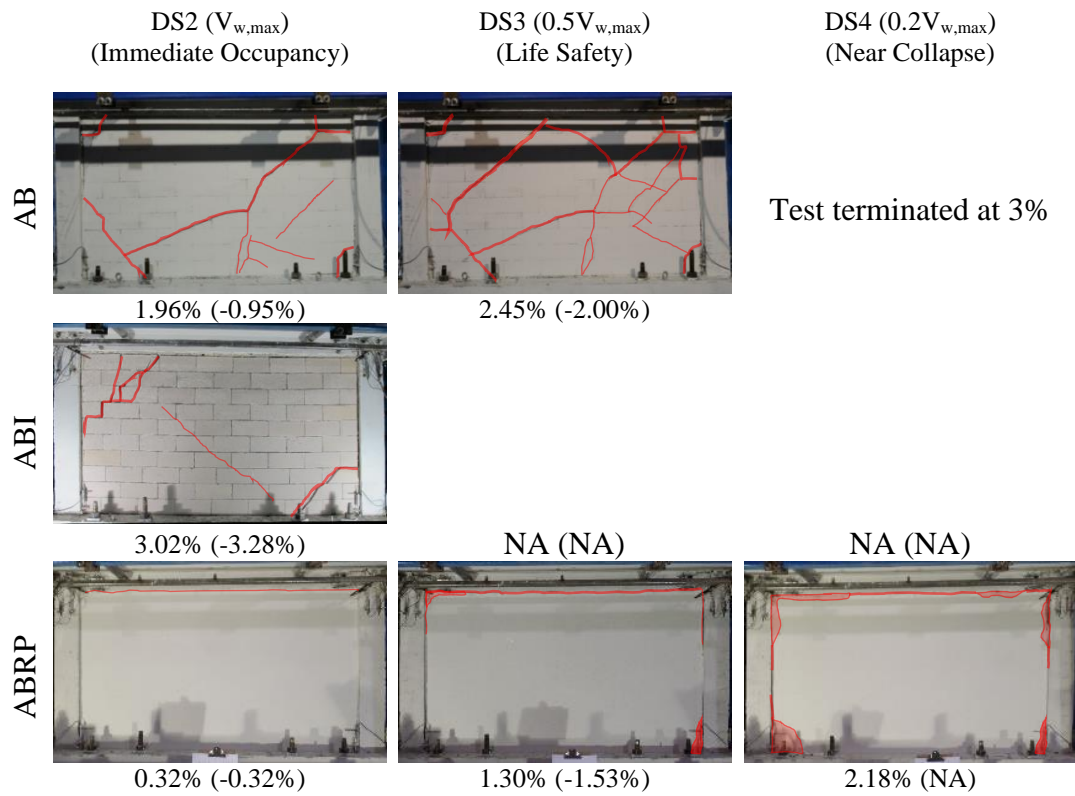


Figure 6.2. Infill wall damages for proposed DLS's: push (+), pull (-)

Location of proposed DLS's on the backbone of second cycle for tested infilled frames are illustrated in Figure 6.3. Comparison of the proposed limits with similar studies in the literature is given in Table 6.2 below.

Table 6.2. Mean IDR associated with damage states for solid infill walls

Damage State	Gaudio et al. (2019)	Sassun et al. (2016)	Cardone Perrone (2015)	Colangelo (2013)	Lu Zha (2021)	Shah et al. (2021)	De Risi et al. (2018)	Demirel (2023)
DS1 (Light)	0.08	0.18	0.15	0.03	0.20	-	0.08	0.08
DS2 (Moderate)	0.33	0.46	0.40	0.35	0.50	0.38	0.34	0.40
DS3 (Heavy)	0.97	1.05	1.00	0.85	1.00	1.82	0.87	1.50
DS4 (Collapse)	1.72	1.88	1.75	1.62	2.00	2.37	1.61	2.50

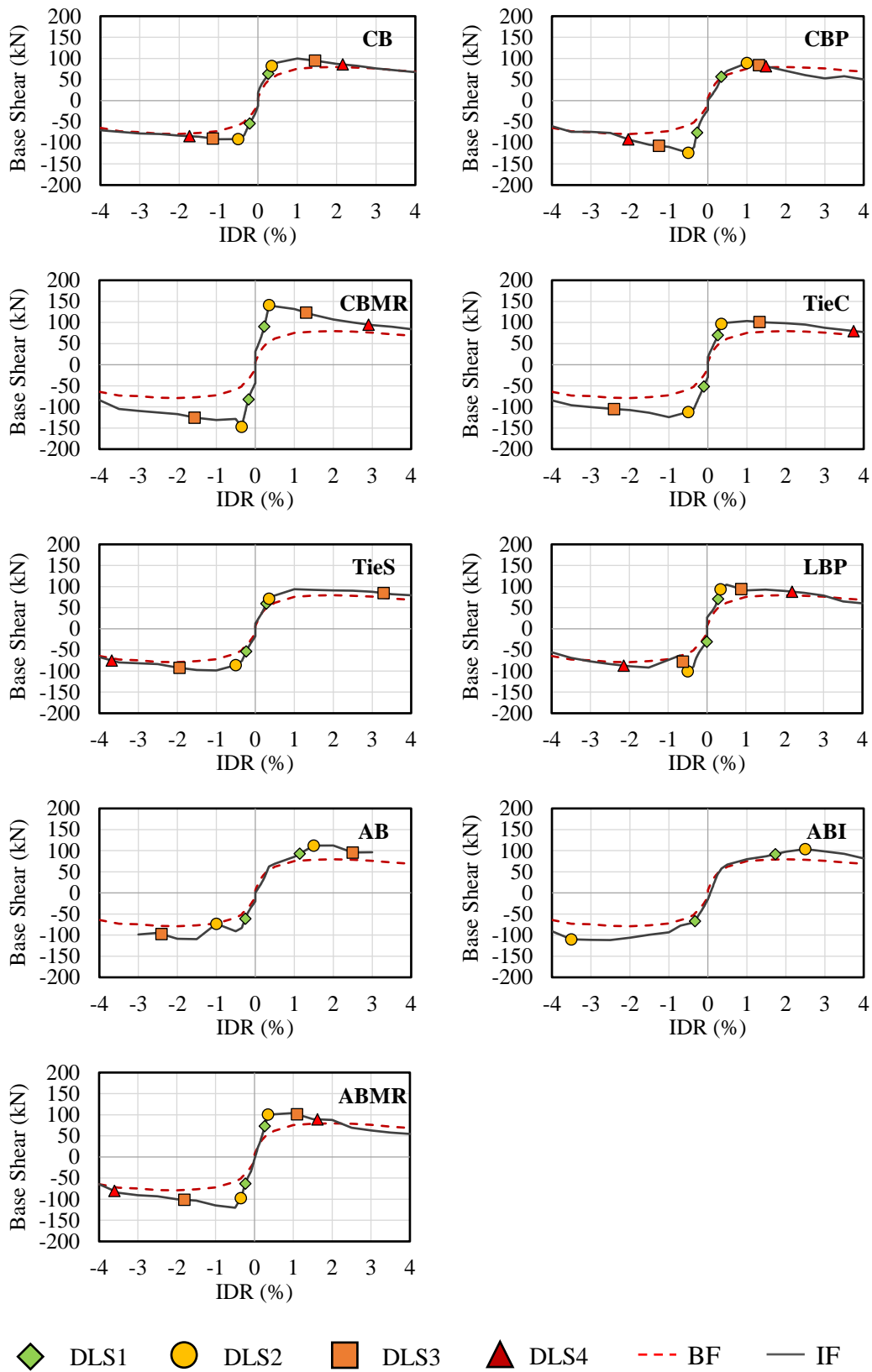


Figure 6.3. Proposed DLS's on infilled frame backbone (2nd cycle)

CHAPTER 7

CONCLUSION

Half-scaled RC frame specimens infilled with various wall units and improved infill systems were tested under IP, OOP and combined loading. Methods for improving seismic performance of infilled frames such as isolation of the infill from the bounding frame, application of mesh overlays on the wall surface, and creation of horizontal slip planes were investigated. High ductility design requirements were followed in RC frame design. Additional shear reinforcement was provided at beam and column ends to ensure flexure dominated response without shear failure. Column dimensions were 200 mm x 200 mm with a reinforcement ratio of 1.0% and axial load ratio was arranged to 0.175% before implementing lateral load reversals. Beam dimensions were 150 mm x 200 mm and the reinforcement ratio was 1.0%. The aspect ratio of the infill walls (i.e., length divided by height) was 0.56. Light infill units such as ACB and HCB were utilized.

IP loading was simulated with repeated increasing displacement reversals at target displacements imposed by servo-controlled piston and OOP loading was simulated with an airbag pushed against the wall monolithically. Displacements, strains and forces were tracked by various measurement devices attached to member ends and the surface of the wall during testing.

The development of RC frame and infill wall damage in response to increasing displacement reversals was reported. In order to extract the experimental hysteretic responses of the infill walls, the bare frame response was subtracted from the infilled frame response using polynomial equations fit to corresponding hysteresis curves. Under increasing drifts and displacement cycles, the relative contribution of the bare frame and the infill wall to lateral resistance and energy dissipation was identified.

Specific consideration was given to the definition of appropriate damage states for infill walls that meet the general performance requirements stipulated by international standards.

Structural Damage under IP Loading:

The test results indicated that the bare frame and boundary frames of the infilled frame specimens experienced plastic hinging of member ends as expected. No shear failure of frame members or rupture of reinforcement was observed in any tests. Flexural cracks emerged at column bottoms and hairline cracks initiated at beam ends in all tested frame specimens within the first cycle of displacement reversals corresponding to 0.35% lateral drift. Flexural cracking was observed in a restricted member end region for the bare frame. Yet, boundary frames of the infilled specimens experienced flexural cracking spreading up to the mid-height of the columns. Yielding of frame members initiated within second and third displacement cycles corresponding to 0.5% and 1.0% drifts. On average, beam ends of the tested infilled frames experienced early yielding at 0.62% drift, followed by column bottoms at 0.86% drift.

Structural damage at increasing drifts was concentrated on column bottoms where cover concrete crushing, spalling of crushed concrete, exposure of reinforcement and buckling of longitudinal bars were observed in all tested frame specimens except no bar buckling was experienced in infilled frame specimen with isolation gap. Concrete crushing of column bottoms was initiated at 2.5% drift leading to bar buckling around 3.5% to 4.0% drift levels (Table 7.1).

Drift levels corresponding to severe damage on RC frame members were between 2.0% to 4.0% drifts and were similar for all tested frames. Experiencing similar structural damages for drift levels larger than 2.0% can be explained by loss of infill contribution and the lateral resistance provided solely by the bounding frame after 2.0% lateral drift.

Table 7.1 Lateral drift at first bar yielding of the frame member

<i>RC Member</i>	<i>BF</i>	<i>CB</i>	<i>CBP</i>	<i>CBMR</i>	<i>TieC</i>	<i>TieS</i>	<i>LBP</i>	<i>AB</i>	<i>ABI</i>	<i>ABRP</i>
Column 1 bottom	0.82	0.39	0.67	1.21	0.85	1.09	0.78	0.71	0.76	0.67
Column 2 bottom	0.67	0.80	0.64	0.85	1.63	1.34	0.94	NA	0.67	0.65
Column 1 top	1.41	1.92	3.12	NY	NY	1.77	2.40	2.44	NY	NY
Column 2 top	0.86	1.90	3.67	NY	NY	NY	2.43	NA	2.36	1.49
Beam 1 right	1.16	0.76	0.66	NY	0.60	1.20	0.40	0.45	1.11	0.44
Beam 1 left	1.34	0.39	0.40	1.56	1.12	0.66	0.48	NA	0.67	1.28

Key: NY - Not Yielded, NA - Not Available

Infill Wall Damage under IP Loading:

The maximum capacity of the bare frame was reached around 1.5% drift and a limited reduction in base shear capacity was observed under increasing displacement cycles afterward (i.e., 20% capacity drop at the ultimate drift, 4.0%). Excluding the specimen with an isolated infill panel, all infilled frames reached their capacities under 1.0% lateral drift and the strength reduction of the infilled frames after reaching their capacities was much faster than the bare frame. Reduction of lateral stiffness and strength of infilled frames after reaching the peak strength can be associated with damages to infill panels such as diagonal cracking, sliding, crushing and spalling of units, especially near corners and under the upper beam. Hysteretic responses of all infilled frames showed apparent pinching behavior independent of the failure type of the infill panel. Infill panels increased the base shear capacity of the bare frame 1.6 times on average. A minimum increase is observed for clay brick infill with stepped horizontal steel ties (1.3 times) and the maximum increase is documented for clay brick infill with bilateral steel mesh reinforcement (2.3 times).

All the IF specimens experienced early cracking (i.e., below 0.35% drift) at beam-wall interfaces due to differences in the stiffnesses of the bounding frame and the infill wall. Debonding of the infill wall from the bounding frame manifested itself by opening gaps close to upper leeward corners visually inspectable from 0.5% drift. Due to the stiffer character of masonry walls, the maximum capacity of the walls reached around 0.35% to 0.5% drifts, accompanied by the initiation of horizontal or diagonal cracks revealing the dominant damaging mechanism of the wall. Horizontal ties and locking bricks ensured sliding failure of the wall, whereas surface overlays such as bilateral mesh reinforcement and textile reinforced mortars resulted in corner crushing failure of the wall. Diagonal cracking and sliding were observed in all the remaining infill systems.

Although tested infill walls were light, their presence dominated the lateral response in terms of added lateral stiffness and strength until reaching the maximum capacity of the walls. The bare frame reached its maximum load capacity at 1.4% (-1.9%) drift, whereas the infilled frame specimens reached their capacities around 1.0% (-0.8%) drift on average. The only exception was the isolated frame at which peak resistance was attained at 3.1% (-3.3%) drift (Table 7.2). The contribution of the infill wall to the lateral stiffness and capacity starts decaying rapidly upon reaching the peak strength of the wall as the wall damage progresses in terms of initiation of new cracks, widening of existing cracks, spalling of plaster, spalling of outer layers of brick units and crushing/falling of wall units. The contribution of the infill wall to the lateral resistance diminishes at around 2.5% drift, after which the infill wall becomes vulnerable to out-of-plane failure due to excessive in-plane damage unless proper improvement measures such as surface overlays and horizontal steel plates are implemented.

The inclusion of fiberglass or steel mesh reinforcement overlays was highly beneficial in suppressing visual damage to the infill panel and preserving the unity of the panel under increasing displacement reversals. Despite the superior performance of these panels, their contribution to lateral capacity decayed rapidly due to the crushing damages observed at corners and the reduction of the contact

length resulting in reduced strut widths. Using horizontal steel ties or locking bricks enforced sliding dominant panel behavior under in-plane loading cycles through horizontal slip planes. Despite unexpected early cracking, infilled frame with isolation joints performed well under large drifts. Retarded contribution of the infill wall initiated at 2.0% drift to lateral resistance avoided the rapid decay of stiffness and capacity of the infilled frame and postponed the severe damage to structural members.

Table 7.2 IDR (%) for the major frame and wall damages for IP tests

		<i>BF</i>	<i>CB</i>	<i>CBP</i>	<i>CBMR</i>	<i>TieC</i>	<i>TieS</i>	<i>LBP</i>	<i>AB</i> ³	<i>ABI</i>	<i>ABRP</i>
Infilled Frame	Max. capacity (+ dir)	1.41	1.00	0.98	0.96	1.50	0.50	0.33	1.95	3.07	0.94
	Max. capacity (- dir)	1.91	1.00	0.70	1.00	1.00	0.47	0.35	0.98	3.29	0.97
RC Frame	Column bot. yielding ¹	0.67	0.39	0.64	0.85	0.79	1.07	0.78	0.71	0.67	0.65
	Column top yielding ¹	0.85	1.90	3.12	NA	NA	2.01	2.40	2.55	2.36	1.49
	Beam end yielding ¹	1.16	0.39	0.40	1.56	0.54	0.40	0.49	0.45	0.67	0.44
	Beam end shear crack	-	-	0.35	0.35	0.35	0.5	0.5	-	-	0.35
	Joint shear crack	2.0	2.0	1.0	1.5	1.5	1.0	1.0	2.5	1.0	1.0
	Cover concrete crushing	2.0	2.5	2.5	2.5	2.5	2.0	3.0	2.5	2.5	2.5
	Cover concrete spalling	2.0	3.0	3.5	3.5	3.0	3.0	3.5	3.0	3.0	3.5
	Bar buckling	2.5	3.0	4.0	4.0	4.0	3.5	4.0	NA	-	3.5
Infill Panel	Failure mode ²		SL+DC	DC+CC	CC	SL	SL	SL	DC	DC	CC
	Major wall crack		1.0	1.0	-	1.0	1.5	1.0	0.35	2.5	-
	Plaster spalling		NA	1.5	0.5	NA	NA	1.5	NA	NA	1.5
	Unit peel off	NA	1.0	-	-	1.5	2.0	2.5	-	-	-
	Unit crushing		1.5	2.0	1.5	2.0	2.5	3.0	-	2.5	2.0
	Unit fall off		1.5	2.5	-	2.5	4.0	3.0	-	-	-

¹ According to strain gage measurements placed on longitudinal bars at member ends

² Key: SL – Sliding, DC – Diagonal Compression, CC – Corner Crushing, NA – Not Applicable

³ Test terminated at 3.0% drift

Infill Wall Performance under IP Loading:

Specific points on the normalized experimental force-displacement curve of tested infill walls were correlated with four damage states corresponding to operational, immediate occupation, life safety, and near-collapse performance levels. Damage states DS1 through DS4 were associated with the initial change in elastic lateral stiffness of the IF, the attainment of maximum strength, and a 50% reduction and a 80% reduction in maximum strength of the wall, respectively. The average drift limit values for each DS are described in Table 7.3 below.

Table 7.3. IDR (%) corresponding to proposed DLS's of tested infill walls

<i>Dir.</i>	<i>DLS</i>	<i>CB</i>	<i>CBP</i>	<i>CBMR</i>	<i>TieC</i>	<i>TieS</i>	<i>LBP</i>	<i>AB</i>	<i>ABI</i>	<i>ABRP</i>	<i>Ave.</i>
Push	DLS2	0.35	0.76	0.33	0.35	0.35	0.35	1.96	3.02	0.32	0.40
	DLS3	1.73	1.80	1.33	1.46	1.89	1.04	2.45	NA	1.30	1.51
	DLS4	2.38	2.17	2.87	3.34	NA	2.55	-	NA	2.18	2.58
Pull	DLS2	-0.67	-0.35	-0.26	-0.32	-0.33	-0.34	-0.95	-3.28	-0.32	-0.37
	DLS3	-1.42	-1.55	-1.46	-1.92	-2.07	-0.60	-2.00	NA	-1.53	-1.51
	DLS4	-1.94	-2.36	NA	NA	-3.48	-1.94	-	NA	NA	-2.43

Isolation joints and bilateral mesh reinforcement were found to have the most significant impact on the seismic response of the tested infill wall systems. Both techniques prevented the premature cracking of infill walls, which is the most significant and widespread damage observed in infilled RC frame buildings following moderate earthquakes. The contribution of infill wall to lateral capacity for isolated, bilateral mesh reinforced and continuous horizontal steel plate installed specimens sustained even at deformation demands over 2% drift which is a sign of their accountability during extreme seismic events.

The contribution at large drifts is crucial from the perspective of global structural response considering the prevention of soft story formation that can result from the significant reduction or total dissipation of infill wall resistance at the ground story. Isolation joints are more appropriate for new construction, while mesh overlays and tie systems can be suggested for both new and existing buildings. Both methods can be implemented affordably with readily available materials and equipment without requiring skilled labor.

The suggested strengthening techniques succeed in improving the in-plane and out-of-plane strength of conventional unreinforced infill walls. Additionally, they enable damage management under low drift needs by reducing wall cracking and structural safety under high drift demands by maintaining wall integrity.

Infill Wall Performance under IP+OOP Loading:

The outcomes of parallel experiments showed that infilled frames' OOP capacity is significantly influenced by IP damage. It has been noted that IP drift capacity approximately drops to half when infilled frames are loaded with 33% of their capacity in an OOP direction. This discovery so strongly implies that the relationship between IP and OOP should be taken into account when estimating infilled frame performance.

Mesh overlays or horizontal tie systems were effective in decreasing the reduction in OOP capacity due to previous IP damage.

Limiting IP drift and examining OOP capacity are the traditional methods used in today's earthquake-resistant design guidelines to determine the seismic safety of an infilled frame. Most analytical and experimental research on the seismic behavior of infilled frames examines IP and OOP responses independently. Our experimental findings indicate that interactions between IP and OOP responses have an impact and should be considered when assessing the performance and capacity of infilled RC frames.

Findings in the Light of Recent Earthquakes and Recommendations for Future Earthquakes in Türkiye:

During the course of this study, the author was involved in several post-earthquake damage survey studies after destructive earthquakes in Türkiye as a member of the METU Earthquake Engineering Research Center (EERC), including 2011 Van-Erciş ($M_w=7.2$), 2011 Van-Edremit ($M_w=5.6$), 2020 Elazığ ($M_w=6.5$), 2020 Samos ($M_w=6.9$) and 2023 ($M_w=7.7$ and $M_w=7.6$) Kahramanmaraş earthquakes. All mentioned earthquakes except the latter developed ground accelerations on urban cities below the prescribed design values defined in the corresponding Turkish seismic codes and the final resulted in spectral accelerations above the design level earthquake.

Due to the inherent vulnerabilities of deficient buildings in Türkiye, widespread building damage and collapses have been observed after sizable earthquakes. Generally speaking, buildings with poor compliance to the 1997 Turkish Earthquake Code (ABYYHY 1998) or designed according to previous design regulations can be considered to have poor construction and material quality, poor detailing, low ductility, and a higher chance of heavy damage or collapse in the case of a strong earthquake. In comparison, buildings constructed with strong adherence to the 2007 Turkish Earthquake Code (DBYBHY 2007) and 2018 Turkish Earthquake Code (TBDY 2018) seismic codes can be expected to sustain acceptable damage or satisfy life safety performance after a strong earthquake.

During damage surveys of mentioned earthquakes, the importance of the infill walls to the final performance of framed RC buildings was clearly experienced. A broad evaluation in the light of all damage surveys for the resilient and deficient RC buildings under moderate and strong earthquakes can be made as follows. The structural system of framed RC buildings in Türkiye did not have sufficient lateral stiffness to limit interstory drift demands below acceptable levels (i.e. 0.5%) and infill walls were inevitably and widely damaged.

Türkiye is one of the most seismically prone countries in the world. Millions of people living and working in residential, public and commercial buildings in metropolitan cities face seismic risk. The majority of RC frame buildings in Türkiye use infill walls at the facades and within the plan. These walls existing in deficient buildings pose an essential potential for feasible and efficient seismic upgrading. Developing and implementing viable and innovative improvement techniques for infill walls on a large scale could prevent the collapse of such buildings.

Considering the social, psychological and economic impact of infill wall damage after moderate as well as strong earthquakes, the interaction between the infill walls and RC frame should be eliminated by isolation joints or improved systems needs to be implemented for wall construction to mitigate the damage for new construction. Construction guidelines for infill walls should be implemented in seismic regulations to prevent infill induced irregularities in the structural system. Improved infill wall systems should be promoted and design and construction guidelines should be developed for them.

REFERENCES

- Abdul-kadir, Mohammed Raouf. 1974. "The Structural Behaviour of Masonry Infill Panels in Framed Structures." Doctor of Philosophy, University of Edinburg.
- ABYBHY. 1975. *Afet Bölgelerinde Yapılacak Yapılar Hakkında Yönetmelik*. Ankara: Bayındırlık ve İskan Bakanlığı.
- ABYYHY. 1998. *Afet Bölgelerinde Yapılacak Yapılar Hakkında Yönetmelik*. Edited by Mehmet Nuray Aydınoglu. Ankara: Bayındırlık ve İskan Bakanlığı.
- ACI530-13. 2013. *Building Code Requirements and Specification for Masonry Structures, ACI530/530.1-13*. American Concrete Institute, Structural Engineering Institute of the American Society of Civil Engineers, The Masonry Society.
- Acun, Bora, and Haluk Sucuoğlu. 2006. "Strengthening of Masonry Infill Walls in Reinforced Concrete Frames with Wire Mesh Reinforcement." *8th US National Conference on Earthquake Engineering 2006* 10 (1852): 6022–31.
- Adham, S.A. 1985. "Static and Dynamic Out-of-Plane Response of Brick Masonry Walls." In *3rd North American Masonry Conference*, 1–14. Boulder.
- AI-Chaar, G., G. E. Lamb, and M. A. Lssa. 2003. "Effect of Openings on Structural Performance of Unreinforced Masonry Infilled Frames." *American Concrete Institute, ACI Special Publication SP-211*: 247–61. <https://doi.org/10.14359/12593>.
- AKG Gazbeton. 2017. "Gazbeton Yapı Malzemeleri Ürün Kataloğu," 2017. <http://www.akg-gazbeton.com/Pdf/kapsamli-turkce-subat-2017.pdf>.
- Akhoundi, F., G. Vasconcelos, P. Lourenco, and L. Silva. 2016. "Out-of-Plane Response of Masonry Infilled RC Frames: Effect of Workmanship and Opening." *Brick and Block Masonry: Trends, Innovations and Challenges - Proceedings of the 16th International Brick and Block Masonry Conference, IBMAC 2016*, 1147–54. <https://doi.org/10.1201/b21889-143>.
- Akhoundi, Farhad, Graça Vasconcelos, and Paulo Lourenço. 2020. "Experimental Out-Of-Plane Behavior of Brick Masonry Infilled Frames." *International Journal of Architectural Heritage* 14 (2): 221–37. <https://doi.org/10.1080/15583058.2018.1529207>.
- Akhoundi, Farhad, Graça Vasconcelos, Paulo Lourenço, Luis M. Silva, Fernando Cunha, and Raúl Fanguero. 2018. "In-Plane Behavior of Cavity Masonry

- Infills and Strengthening with Textile Reinforced Mortar.” *Engineering Structures* 156 (December 2017): 145–60. <https://doi.org/10.1016/j.engstruct.2017.11.002>.
- Akin, Lili Anne. 2006. “Behaviour of Reinforced Concrete Frames with Masonry Infills in Seismic Regions.” PhD, Purdue University.
- Akin, E., E. Canbay, B. Binici, and G. Özcebe. 2011. “Testing and Analysis of Infilled Reinforced Concrete Frames Strengthened with CFRP Reinforcement.” *Journal of Reinforced Plastics and Composites* 30 (19): 1605–20. <https://doi.org/10.1177/0731684411424631>.
- Aktaş, Saime Selin. 2023. “Out-of-Plane Seismic Behavior of Brick and Pumice Concrete Infill Walls Built into the RC Frame.” Master of Science, Ankara: Middle East Technical University.
- Al-chaar, Ghassan. 1998. “Non-Ductile Behavior of Reinforced Concrete Frames with Masonry Infill Panels Subjected to In-Plane Loading.” [https://doi.org/10.1061/\(ASCE\)0733-9445\(2002\)128](https://doi.org/10.1061/(ASCE)0733-9445(2002)128).
- Aliaari, Mohammad, and Ali M. Memari. 2007. “Experimental Evaluation of a Sacrificial System for Masonry Infill Walls.” *Journal Architectural Engineering National Conference* 13 (2): 111–25. [https://doi.org/10.1061/\(ASCE\)1076-0431\(2007\)13:2\(111\)](https://doi.org/10.1061/(ASCE)1076-0431(2007)13:2(111)).
- Almusallam, Tarek H., and Yousef A. Al-Salloum. 2007. “Behavior of FRP Strengthened Masonry Walls under Out-of-Plane Seismic Loading.” *Journal of Composites for Construction* 11 (3): 308–18. [https://doi.org/10.1061/\(ASCE\)1090-0268\(2007\)11:3\(308\)](https://doi.org/10.1061/(ASCE)1090-0268(2007)11:3(308)).
- Al-Nimry, Hanan S. 2014. “Quasi-Static Testing of Rc Infilled Frames and Confined Stone-Concrete Bearing Walls.” *Journal of Earthquake Engineering* 18 (1): 1–23. <https://doi.org/10.1080/13632469.2013.835292>.
- Altin, Sinan, Özgür Anil, M. Emin Kara, and Mustafa Kaya. 2008. “An Experimental Study on Strengthening of Masonry Infilled RC Frames Using Diagonal CFRP Strips.” *Composites Part B: Engineering* 39 (4): 680–93. <https://doi.org/10.1016/j.compositesb.2007.06.001>.
- Altin, Sinan, Ugur Ersoy, and Tugrul Tankut. 1992. “Hysteretic Response of Reinforced-Concrete Infilled Frames.” *Journal of Structural Engineering* 118 (8): 2133–50. [https://doi.org/10.1061/\(asce\)0733-9445\(1992\)118:8\(2133\)](https://doi.org/10.1061/(asce)0733-9445(1992)118:8(2133)).
- Alwashali, Hamood, Debasish Sen, Masaki Maeda, and Matsutaro Seki. 2020. “Advantages and Limitations of Retrofitting Masonry Infilled RC Frames by

Ferro-Cement Based on Experimental Observations Advantages and Limitations of Retrofitting Masonry Infilled RC Frames by Ferro-Cement Based on Experimental Observations.” *17th World Conference on Earthquake Engineering*, no. September.

Alwashali, Hamood, Yuta Torihata, Kiwoong Jin, and Masaki Maeda. 2018. “Experimental Observations on the In-Plane Behaviour of Masonry Wall Infilled RC Frames; Focusing on Deformation Limits and Backbone Curve.” *Bulletin of Earthquake Engineering* 16 (3): 1373–97. <https://doi.org/10.1007/s10518-017-0248-x>.

Andreas, U., M. Cerone, P. D’Asdia, and F. Iannozzi. 1985. “A Finite Element Model for the Analysis of Masonry Structures under Cyclic Actions.” In *7th International Brick Masonry Conference*.

Angel, Richard. 1994. “Behavior of Reinforced Concrete Frames With Masonry Infills.” Doctor of Philosophy, University of Illinois at Urbana-Champaign.

Anić, Filip, Davorin Penava, Lars Abrahamczyk, and Vasilis Sarhosis. 2020. *A Review of Experimental and Analytical Studies on the Out-of-Plane Behaviour of Masonry Infilled Frames. Bulletin of Earthquake Engineering*. Vol. 18. Springer Netherlands. <https://doi.org/10.1007/s10518-019-00771-5>.

Anic, Filip, Davorin Penava, Ivica Gulja, Vasilis Sarhosis, and Lars Abrahamczyk. 2021. “Out-of-Plane Cyclic Response of Masonry Infilled RC Frames : An Experimental Study.” *Engineering Structures* 238 (November 2020). <https://doi.org/10.1016/j.engstruct.2021.112258>.

Arslan, Mehmet Emin, Elif Agcakoca, and Merve Şentürk. 2020. “Effects of Plaster Thicknesses on Cyclic Behavior of Infill Walls with Different Materials.” *Periodica Polytechnica Civil Engineering* 64 (3): 678–89. <https://doi.org/10.3311/PPci.15555>.

Arteta, Carlos A., Julian Carrillo, Jorge Archbold, Daniel Gaspar, Cesar Pajaro, Gustavo Araujo, Andres Torregroza, et al. 2019. “Response of Mid-Rise Reinforced Concrete Frame Buildings to the 2017 Puebla Earthquake.” *Earthquake Spectra* 35 (4): 1763–93. <https://doi.org/10.1193/061218EQS144M>.

ASCE7-16. 2016. *Minimum Design Loads for Buildings and Other Structures ASCE7-16. ASCE Standard*. <https://doi.org/10.1061/9780784412916>.

ASCE41-17. 2017. *Seismic Evaluation and Retrofit of Existing Buildings. Seismic Evaluation and Retrofit of Existing Buildings*. <https://doi.org/10.1061/9780784414859>.

- Asteris, P. G., S. T. Antoniou, D. S. Sophianopoulos, and C. Z. Chrysostomou. 2011. "Mathematical Macromodeling of Infilled Frames: State of the Art." *Journal of Structural Engineering* 137 (12): 1508–17. [https://doi.org/10.1061/\(asce\)st.1943-541x.0000384](https://doi.org/10.1061/(asce)st.1943-541x.0000384).
- Asteris, P. G., D. M. Cotsovos, C. Z. Chrysostomou, A. Mohebkah, and G. K. Al-Chaar. 2013. "Mathematical Micromodeling of Infilled Frames: State of the Art." *Engineering Structures* 56 (December): 1905–21. <https://doi.org/10.1016/j.engstruct.2013.08.010>.
- ASTM A370-21. 2021. "A370: Standard Test Methods and Definitions for Mechanical Testing of Steel Products." *ASTM International*. <https://doi.org/10.1520/A0370-21>.
- ASTM C39-21. 2021. *Standard Test Method for Compressive Strength of Cylindrical Concrete Specimens*. *ASTM Standard Book*. https://doi.org/10.1520/C0039_C0039M-21.
- ASTM C109-13. 2013. "Standard Test Method for Compressive Strength of Hydraulic Cement Mortars (Using 2-in. or [50-Mm] Cube Specimens)." *ASTM* i: 1–6. <https://doi.org/10.1520/C0109>.
- ASTM C348-14. 2014. "Standard Test Method for Flexural Strength of Hydraulic-Cement Mortars." *ASTM*. <https://doi.org/10.1520/C0348-14.2>.
- ASTM C349-14. 2014. "C349-97. Standard Test Method for Compressive Strength of Hydraulic-Cement Mortars (Using Portions of Prisms Broken in Flexure)." *ASTM*. <https://doi.org/10.1520/C0349-97>.
- ASTM C469-14. 2014. "Standard Test Method for Static Modulus of Elasticity and Poisson's Ratio of Concrete in Compression." *ASTM*. <https://doi.org/10.1520/C0469>.
- ASTM C496/C496M-17. 2017. "Standard Test Method for Splitting Tensile Strength of Cylindrical Concrete Specimens." https://doi.org/10.1520/C0496_C0496M-17.
- ASTM C1314-14. 2014. "Standard Test Method for Compressive Strength of Masonry Prisms." *ASTM*. <https://doi.org/10.1520/C1314-14.2>.
- ASTM C1437-13. 2013. "Standard Test Method for Flow of Hydraulic Cement Mortar." *ASTM*. <https://doi.org/10.1520/C1437-13.2>.

- ASTM E518-15. 2015. "Standard Test Methods for Flexural Bond Strength of Masonry." <https://doi.org/10.1520/C1072-11.1.2>.
- ASTM E519-10. 2010. "Standard Test Method for Diagonal Tension (Shear) in Masonry Assemblages." *ASTM*. <https://doi.org/10.1520/E0519>.
- Ay, B Ö, T Eroğlu Azak, and M A Erberik. 2016. "Evaluation of Changing Building Characteristics in Turkey." *12th International Congress on Advances in Cibil Engineering*, 1–7.
- Aydin, Beyazit Bestami. 2022. "A Lattice Modelling Framework With Applications on Reinforced Concrete and Autoclaved Aerated Concrete Masonry Infill Walls." Doctor of Philosophy, Ankara: Middle East Technical University.
- Aydinoğlu, Mehmet Nuray. 2007. "From Seismic Coefficient To Performance Based Design: 40 Years Of Earthquake Engineering From An Engineer's Viewpoint." In *Sixth National Conference on Earthquake Engineering*, 15–41. İstanbul.
- Aykac, Sabahattin, Eray Ozbek, Bengi Aykac, and Ilker Kalkan. 2016. "Influence of Strengthening the Infill Walls with Perforated Steel Plates on the Behavior of RC Frames." *Athens Journal of Technology & Engineering* 3 (2): 133–52. <https://doi.org/10.30958/ajte.3-2-2>.
- Baggio, C., A. Bernardini, R. Colozza, L. Corazza, M. Bella, G. Di Pasquale, M. Dolce, et al. 2007. *Field Manual for Post-Earthquake Damage and Safety Assessment and Short Term Countermeasures (AeDES)*. Edited by Artur V. Pinto and Fabio Taucer. Luxembourg: JRC Scientific and Thechnical Reports.
- Bal, I. Engin, Helen Crowley, Rui Pinho, and F. Gülten Gülay. 2008. "Detailed Assessment of Structural Characteristics of Turkish RC Building Stock for Loss Assessment Models." *Soil Dynamics and Earthquake Engineering* 28 (10–11): 914–32. <https://doi.org/10.1016/j.soildyn.2007.10.005>.
- Baran, Mehmet, and Tugce Sevil. 2010. "Analytical and Experimental Studies on Infilled RC Frames." *International Journal of Physical Sciences* 5 (13): 1981–98.
- Basha, Syed Humayun, and Hemant B. Kaushik. 2016. "Behavior and Failure Mechanisms of Masonry-Infilled RC Frames (in Low-Rise Buildings) Subject to Lateral Loading." *Engineering Structures* 111: 233–45. <https://doi.org/10.1016/j.engstruct.2015.12.034>.
- Basha, Syed Humayun, and Hemant B. Kaushik. 2019. *Investigation on Improving the Shear Behavior of Columns in Masonry Infilled RC Frames under Lateral*

- Loads. Bulletin of Earthquake Engineering*. Vol. 17. Springer Netherlands. <https://doi.org/10.1007/s10518-019-00622-3>.
- Bayrak, Oguzhan. 1998. "Seismic Performance of Rectilinearly Confined High Strength Concrete Columns." *PhD Thesis, Department of Civil Engineering, University of California at Toronto, Ontario, Toronto, Canada*, no. February: 363.
- Bayülke, Nejat. 2003. "Betonarme Yapinin Dolgu Duvari." *Türkiye Mühendislik Haberleri*, 85–98.
- Benavent-Climent, A., A. Ramírez-Márquez, and S. Pujol. 2018. "Seismic Strengthening of Low-Rise Reinforced Concrete Frame Structures with Masonry Infill Walls: Shaking-Table Test." *Engineering Structures* 165 (March): 142–51. <https://doi.org/10.1016/j.engstruct.2018.03.026>.
- Benjamin, Jack R., and Harry A. Williams. 1958. "The Behavior of One-Story Brick Shear Walls." *Journal of the Structural Division* 84 (4). <https://doi.org/10.1061/JSDEAG.0000263>.
- Bennett, Richard M., Roger D. Flanagan, Samy Adham, William L Fischer, and Michael A. Tenbus. 1996. "Evaluation and Analysis of the Performance of Masonry Infills During the Northridge Earthquake." Tennessee.
- Bergami, Alessandro Vittorio, and Camillo Nuti. 2015. "Experimental Tests and Global Modeling of Masonry Infilled Frames." *Earthquake and Structures* 9 (2): 281–303. <https://doi.org/10.12989/eas.2015.9.2.281>.
- Bergami, Alessandro Vittorio. 2007. "Implementation and Experimental Verification of Models for Nonlinear Analysis of Masonry Infilled RC Frames." PhD, Roma TRE.
- Bertero, Raul D., and Vitelmo V. Bertero. 2002. "Performance-Based Seismic Engineering: The Need for a Reliable Conceptual Comprehensive Approach." *Earthquake Engineering and Structural Dynamics* 31 (3): 627–52. <https://doi.org/10.1002/eqe.146>.
- Bertero, Vitelmo, and Steven Brokken. 1983. "Infills in Seismic Resistant Building." *Journal of Structural Engineering* 109 (6): 1337–61. [https://doi.org/10.1061/\(asce\)0733-9445\(1983\)109:6\(1337\)](https://doi.org/10.1061/(asce)0733-9445(1983)109:6(1337)).
- Bikçe, M., E. Emsen, M. M. Erdem, and O. F. Bayrak. 2021. "An Investigation on Behavior of RC Frames with Non-Interacting Infill Wall." *Engineering Structures* 245 (November 2020): 112920. <https://doi.org/10.1016/j.engstruct.2021.112920>.

- Bikçe, Murat, and Musab Erdem. 2019. "Investigation of Effective Relative Story Drift Limits According to TEC 2018." In *5. Uluslararası Deprem Mühendisliği ve Sismoloji Konferansı*, 9. Ankara.
- Binici, Baris, Erdem Canbay, Alper Aldemir, Ismail Ozan Demirel, Ugur Uzgan, Zafer Eryurtlu, Koray Bulbul, and Ahmet Yakut. 2019. "Seismic Behavior and Improvement of Autoclaved Aerated Concrete Infill Walls." *Engineering Structures* 193 (August): 68–81. <https://doi.org/10.1016/j.engstruct.2019.05.032>.
- Binici, Baris, Guney Ozcebe, and Ramazan Ozcelik. 2007. "Analysis and Design of FRP Composites for Seismic Retrofit of Infill Walls in Reinforced Concrete Frames." *Composites Part B: Engineering* 38 (5–6): 575–83. <https://doi.org/10.1016/j.compositesb.2006.08.007>.
- Blasi, Gianni, Flavia De Luca, and Maria Antonietta Aiello. 2018. "Brittle Failure in RC Masonry Infilled Frames: The Role of Infill Overstrength." *Engineering Structures* 177 (March): 506–18. <https://doi.org/10.1016/j.engstruct.2018.09.079>.
- Blasi, Gianni, Flavia De Luca, Daniele Perrone, Antonella Greco, and Maria Antonietta Aiello. 2021. "MID 1.1: Database for Characterization of the Lateral Behavior of Infilled Frames." *Journal of Structural Engineering* 147 (10): 04721007. [https://doi.org/10.1061/\(ASCE\)ST.1943-541X.0003117](https://doi.org/10.1061/(ASCE)ST.1943-541X.0003117).
- Bob, Corneliu, Sorin Mărginean, and Adriana Scurt. 2016. "Theoretical/Experimental Study of Reinforced-Concrete Frame with Masonry Infill." *Proceedings of the Institution of Civil Engineers: Structures and Buildings* 169 (11): 825–39. <https://doi.org/10.1680/jstbu.15.00051>.
- Bose, Supratik, and Durgesh C. Rai. 2016. "Lateral Load Behavior of an Open-Ground-Story RC Building with AAC Infills in Upper Stories." *Earthquake Spectra* 32 (3): 1653–74. <https://doi.org/10.1193/121413EQS295M>.
- Brokken, S. T., and V. V. Bertero. 1981. "Studies on Effects of Infills in Seismic Resistant R/C Construction." California. <https://nehrpsearch.nist.gov/static/files/NSF/PB82166190.pdf>.
- Buonopane, S. G., and R. N. White. 1999. "Pseudodynamic Testing of Masonry Infilled Reinforced Concrete Frame." *Journal of Structural Engineering* 125.
- Butenweg, Christoph, Marko Marinković, and Ratko Salatić. 2019. "Experimental Results of Reinforced Concrete Frames with Masonry Infills under Combined Quasi-Static in-Plane and out-of-Plane Seismic Loading." *Bulletin of*

- Earthquake Engineering* 17 (6): 3397–3422. <https://doi.org/10.1007/s10518-019-00602-7>.
- Cai, Gaochuang, and Qiwang Su. 2019. “Effect of Infills on Seismic Performance of Reinforced Concrete Frame Structures -A Full-Scale Experimental Study.” *Journal of Earthquake Engineering* 23 (9): 1531–59. <https://doi.org/10.1080/13632469.2017.1387194>.
- Calvi, G. Michele, Davide Bolognini, and Andrea Penna. 2004. “Seismic Performance of Masonry-Infilled R.C. Frames: Benefits of Slight Reinforcements.” *6th Portuguese Congress on Seismology and Earthquake Engineering*, 253–76.
- Calvi, Gian Michele, and Davide Bolognini. 2001. “Seismic Response of Reinforced Concrete Frames Infilled with Weakly Reinforced Masonry Panels.” *Journal of Earthquake Engineering* 5 (2): 153–85. <https://doi.org/10.1080/13632460109350390>.
- Cardone, Donatello, and Giuseppe Perrone. 2015. “Developing Fragility Curves and Loss Functions for Masonry Infill Walls.” *Earthquake and Structures* 9 (1): 257–79. <https://doi.org/10.12989/eas.2015.9.1.257>.
- Carter, C, and B Staffard Smith. 1967. “Structural Behavior of Masonry Infilled Frames Subjected to Racking Loads.” In *1st International Brick and Block Masonry Conference*, 226–33. Austin, Texas.
- Cavaleri, L., M. Fossetti, and M. Papia. 2005. “Infilled Frames: Developments in the Evaluation of Cyclic Behaviour under Lateral Loads.” *Structural Engineering and Mechanics* 21 (4): 469–94. <https://doi.org/10.12989/sem.2005.21.4.469>.
- Cavaleri, Liborio, and Fabio Di Trapani. 2014. “Cyclic Response of Masonry Infilled RC Frames: Experimental Results and Simplified Modeling.” *Soil Dynamics and Earthquake Engineering* 65: 224–42. <https://doi.org/10.1016/j.soildyn.2014.06.016>.
- Centeno, Jose, Carlos Ventura, Simon Foo, and Otton Lara. 2008. “Seismic Performance Of Gravity Load Designed Reinforced Concrete Frames with Unreinforced Masonry Infill Walls.” In *Structural Congress 2008*.
- Chadwell, C. B., and R. A. Imbsen. 2004. “XTRACT: A Tool for Axial Force - Ultimate Curvature Interactions.” In *Structures 2004*, 1–9. Reston, VA: American Society of Civil Engineers. [https://doi.org/10.1061/40700\(2004\)178](https://doi.org/10.1061/40700(2004)178).

- Cheng, Shao Ge, Yi Xiu Zhu, and Wei Ping Zhang. 2021. "Seismic Performance of RC Frames Strengthened by RC Infill Walls." *Advances in Structural Engineering* 24 (10): 2267–81. <https://doi.org/10.1177/1369433221997726>.
- Chiou, Tsung-Chih, and Shyh-Jiann Hwang. 2015. "Tests on Cyclic Behavior of Reinforced Concrete Frames with Brick Infil." *Earthquake Engineering & Structural Dynamics* 44: 1939–58.
- Chiou, Yaw-Jeng, Jyh-Cherng Tzeng, and Yuh-Wehn Liou. 1999. "Experimental and Analytical Study of Masonry Infilled Frames." *Journal of Structural Engineering* 125 (October): 1109–17.
- Chiozzi, Andrea, and Eduardo Miranda. 2017. "Fragility Functions for Masonry Infill Walls with In-Plane Loading." *Earthquake Engineering and Structural Dynamics* 46 (15): 2831–50. <https://doi.org/10.1002/eqe.2934>.
- Chrysostomou, Christis Zenon. 1991. "Effects of Degrading Infill Walls on the Nonlinear Seismic Response of Two-Dimensional Steel Frames." PhD, Cornell University.
- Colangelo, F. 2005. "Pseudo-Dynamic Seismic Response of Reinforced Concrete Frames Infilled with Non-Structural Brick Masonry." *Earthquake Engineering and Structural Dynamics* 34 (10): 1219–41. <https://doi.org/10.1002/eqe.477>.
- Colangelo, Felice. 2013. "Drift-Sensitive Non-Structural Damage to Masonry-Infilled Reinforced Concrete Frames Designed to Eurocode 8." *Bulletin of Earthquake Engineering* 11 (6): 2151–76. <https://doi.org/10.1007/s10518-013-9503-y>.
- Corte, Gaetano Della, Luigi Fiorino, and Federico Massimo Mazzolani. 2008. "Lateral-Loading Tests on a Real RC Building Including Masonry Infill Panels with and without FRP Strengthening." *Journal of Materials in Civil Engineering* 20 (6): 419–31. [https://doi.org/10.1061/\(asce\)0899-1561\(2008\)20:6\(419\)](https://doi.org/10.1061/(asce)0899-1561(2008)20:6(419)).
- Crisafulli, Francisco J. 1997. "Seismic Behaviour of Reinforced Concrete Structures with Masonry Infills." PhD, University of Canterbury. <http://hdl.handle.net/10092/1221>.
- Crisafulli, Francisco J., Athol J. Carr, and Robert Park. 2005. "Experimental Response of Framed Masonry Structures Designed with New Reinforcing Details." *Bulletin of the New Zealand Society for Earthquake Engineering*.
- Dautaj, Arton D., Qani Kadiri, and Naser Kabashi. 2018. "Experimental Study on the Contribution of Masonry Infill in the Behavior of RC Frame under Seismic

- Loading.” *Engineering Structures* 165 (March): 27–37.
<https://doi.org/10.1016/j.engstruct.2018.03.013>.
- Dautaj, Arton D., Ali Muriqi, Cene Krasniqi, and Burbuqe Shatri. 2019. “Shear Resistance of Masonry Panel in Infilled RC Frames.” *International Journal of Advanced Structural Engineering* 11 (2): 165–77.
<https://doi.org/10.1007/s40091-019-0223-7>.
- Dawe, J. L., and C. K. Seah. 1989. “Out-of-Plane Resistance of Concrete Masonry Infilled Panels.” *Canadian Journal of Civil Engineering* 16 (6): 854–64.
<https://doi.org/10.1139/189-128>.
- DBYBHY. 2007. *Deprem Bölgelerinde Yapılacak Binalar Hakkında Yönetmelik*. Ankara: Bayındırlık ve İskan Bakanlığı.
- Dehghani, Ayoub, Fariborz Nateghi-Alahi, and Gregor Fischer. 2015. “Engineered Cementitious Composites for Strengthening Masonry Infilled Reinforced Concrete Frames.” *Engineering Structures* 105: 197–208.
<https://doi.org/10.1016/j.engstruct.2015.10.013>.
- Demirel, Ismail Ozan, Ahmet Yakut, and Baris Binici. 2022. “Seismic Performance of Mid-Rise Reinforced Concrete Buildings in Izmir Bayrakli after the 2020 Samos Earthquake.” *Engineering Failure Analysis* 137 (March): 106277.
<https://doi.org/10.1016/j.engfailanal.2022.106277>.
- Dhanasekar, M., and A. W. Page. 1986. “Influence of Brick Masonry Infill Properties on the Behaviour of Infilled Frames.” *Proceedings of the Institution of Civil Engineers (London)* 81 (pt 2): 593–605.
<https://doi.org/10.1680/iicep.1986.463>.
- Dizhur, Dmytro, Kevin Walsh, Ivan Giongo, Hossein Derakhshan, and Jason Ingham. 2018. “Out-of-Plane Proof Testing of Masonry Infill Walls.” *Structures* 15 (November 2017): 244–58.
<https://doi.org/10.1016/j.istruc.2018.07.003>.
- Dolšek, Matjaž, and Peter Fajfar. 2001. “Soft Storey Effects in Uniformly Infilled Reinforced Concrete Frames.” *Journal of Earthquake Engineering* 5 (1): 12.
<https://doi.org/10.1080/13632460109350383>.
- Dolšek, Matjaž, and Peter Fajfar. 2008. “The Effect of Masonry Infills on the Seismic Response of a Four Storey Reinforced Concrete Frame—a Probabilistic Assessment.” *Engineering Structures* 30 (11): 3186–92.
<https://doi.org/10.1016/j.engstruct.2008.04.031>.

- Domenico, Mariano Di, Paolo Ricci, and Gerardo M. Verderame. 2019. *Experimental Assessment of the Out-of-Plane Strength of URM Infill Walls with Different Slenderness and Boundary Conditions*. *Bulletin of Earthquake Engineering*. Vol. 17. Springer Netherlands. <https://doi.org/10.1007/s10518-019-00604-5>.
- Domenico, Mariano Di, Paolo Ricci, and Gerardo M. Verderame. 2020. "Experimental Assessment of the Influence of Boundary Conditions on the Out-of-Plane Response of Unreinforced Masonry Infill Walls." *Journal of Earthquake Engineering* 24 (6): 881–919. <https://doi.org/10.1080/13632469.2018.1453411>.
- Domenico, Mariano Di, Maria Teresa De Risi, Paolo Ricci, Gerardo M. Verderame, and Gaetano Manfredi. 2021. "Empirical Prediction of the In-Plane/out-of-Plane Interaction Effects in Clay Brick Unreinforced Masonry Infill Walls." *Engineering Structures* 227 (August 2020): 111438. <https://doi.org/10.1016/j.engstruct.2020.111438>.
- Dorji, Sonam, Hossein Derakhshan, Tatheer Zahra, David P Thambiratnam, and Alireza Mohyeddin. 2020a. "A Review of Experimental and Analytical Studies on Masonry Infilled-Frames Subjected to Lateral Loads." In *Australian Earthquake Engineering Society Virtual Conference*.
- Dorji, Sonam, Hossein Derakhshan, Tatheer Zahra, David P. Thambiratnam, and Alireza Mohyeddin. 2020b. "Seismic Design of Masonry-Infilled Frames: A Review of Codified Approaches." *Proceedings of International Structural Engineering and Construction* 7 (2): STR-48-1-STR-48-6. [https://doi.org/10.14455/ISEC.2020.7\(2\).STR-48](https://doi.org/10.14455/ISEC.2020.7(2).STR-48).
- Doudoumis, I. N., and E. N. Mitsopoulou. 1986. "Non-Linear Analysis of Multistorey Infilled Frames for Unilateral Contact Conditions." In *8th European Conference on Earthquake Engineering*. İstanbul.
- El-Dakhakhni, Wael W., Mohamed Elgaaly, and Ahmad A. Hamid. 2003. "Three-Strut Model for Concrete Masonry-Infilled Steel Frames." *Journal of Structural Engineering* 129 (2): 177–85. [https://doi.org/10.1061/\(ASCE\)0733-9445\(2003\)129:2\(177\)](https://doi.org/10.1061/(ASCE)0733-9445(2003)129:2(177)).
- EN 1052-3. 2002. "Methods of Test for Masonry - Part 3: Determination of Initial Shear Strength."
- EN1998-1. 2004. *Eurocode 8: Design of Structures for Earthquake Resistance - Part 1: General Rules, Seismic Actions and Rules for Buildings*. Vol. 3. <https://doi.org/10.1680/cien.144.6.55.40618>.

- EN1998-3. 2005. *Eurocode 8: Design of Structures for Earthquake Resistance - Part 3: Assessment and Retrofitting of Buildings*.
- Erdem, M.M., E. Emsen, and M. Bikçe. 2021. “Experimental and Numerical Investigation of New Flexible Connection Elements between Infill Walls-RC Frames.” *Construction and Building Materials* 296: 123605. <https://doi.org/10.1016/j.conbuildmat.2021.123605>.
- Erol, Gulseren, and H. Faruk Karadogan. 2016. “Seismic Strengthening of Infilled Reinforced Concrete Frames by CFRP.” *Composites Part B: Engineering* 91: 473–91. <https://doi.org/10.1016/j.compositesb.2016.01.025>.
- Faconi, Luca, and Fausto Minelli. 2020. “Retrofitting RC Infills by a Glass Fiber Mesh Reinforced Overlay and Steel Dowels: Experimental and Numerical Study.” *Construction and Building Materials* 231: 117133. <https://doi.org/10.1016/j.conbuildmat.2019.117133>.
- Faconi, Luca, Fausto Minelli, and Ezio Giuriani. 2018. “Response of Infilled RC Frames Retrofitted with a Cementitious Fiber-Mesh Reinforced Coating in Moderate Seismicity Areas.” *Construction and Building Materials* 160: 574–87. <https://doi.org/10.1016/j.conbuildmat.2017.11.033>.
- Fardis, M. N., S. N. Bousias, G. Franchioni, and T. B. Panagiotakos. 1999. “Seismic Response and Design of RC Structures with Plan-Eccentric Masonry Infills.” *Earthquake Engineering and Structural Dynamics* 28 (2): 173–91. [https://doi.org/10.1002/\(SICI\)1096-9845\(199902\)28:2<173::AID-EQE810>3.0.CO;2-1](https://doi.org/10.1002/(SICI)1096-9845(199902)28:2<173::AID-EQE810>3.0.CO;2-1).
- Federal Emergency Management Agency. 2018. “With Additional Commentary for ASCE/ SEI 41-17,” no. June.
- Fiorato, Anthony Emil. 1971. “An Investigation of the Interaction of Reinforced Concrete Frames with Masonry Filler Walls.” Doctor of Philosophy, University of Illinois, Urbana.
- Flanagan, Roger D., and Richard M. Bennett. 1999. “In-Plane Behavior of Structural Clay Tile Infilled Frames.” *Journal of Structural Engineering* 125 (6): 590–99. [https://doi.org/10.1061/\(ASCE\)0733-9445\(1999\)125:6\(590\)](https://doi.org/10.1061/(ASCE)0733-9445(1999)125:6(590)).
- Fowler, Joele Johnston. 1994. “Analysis of Dynamic Testing Performed on Structural Clay Tile Infilled Frames.” Master of Science, University of Tennessee.

- Francisco J. Crisafulli, and Athol J. Carr. 2007. "Proposed Macro-Model for the Analysis of Infilled Frame Structures." *Bulletin of the New Zealand Society for Earthquake Engineering* 40 (2): 69–77.
- Furtado, André, and Maria Teresa De Risi. 2020. "Recent Findings and Open Issues Concerning the Seismic Behaviour of Masonry Infill Walls in RC Buildings." *Advances in Civil Engineering* 2020. <https://doi.org/10.1155/2020/9261716>.
- Furtado, André, Hugo Rodrigues, António Arêde, José Melo, and Humberto Varum. 2021. "The Use of Textile-Reinforced Mortar as a Strengthening Technique for the Infill Walls out-of-Plane Behaviour." *Composite Structures* 255 (September 2020). <https://doi.org/10.1016/j.compstruct.2020.113029>.
- Furtado, André, Hugo Rodrigues, António Arêde, and Humberto Varum. 2015. "Influence of the in Plane and Out-of-Plane Masonry Infill Walls' Interaction in the Structural Response of RC Buildings." *Procedia Engineering* 114: 722–29. <https://doi.org/10.1016/j.proeng.2015.08.016>.
- Furtado, André, Hugo Rodrigues, António Arêde, and Humberto Varum. 2016a. "Experimental Evaluation of Out-of-Plane Capacity of Masonry Infill Walls." *Engineering Structures* 111: 48–63. <https://doi.org/10.1016/j.engstruct.2015.12.013>.
- Furtado, André, Hugo Rodrigues, António Arêde, and Humberto Varum. 2016b. "Simplified Macro-Model for Infill Masonry Walls Considering the out-of-Plane Behaviour." *Earthquake Engineering & Structural Dynamics* 45 (4): 507–24. <https://doi.org/10.1002/eqe.2663>.
- Furtado, André, Hugo Rodrigues, António Arêde, and Humberto Varum. 2020a. "Effect of the Panel Width Support and Columns Axial Load on the Infill Masonry Walls Out-Of-Plane Behavior." *Journal of Earthquake Engineering* 24 (4): 653–81. <https://doi.org/10.1080/13632469.2018.1453400>.
- Furtado, André, Hugo Rodrigues, António Arêde, and Humberto Varum. 2020b. "Experimental Tests on Strengthening Strategies for Masonry Infill Walls: A Literature Review." *Construction and Building Materials* 263. <https://doi.org/10.1016/j.conbuildmat.2020.120520>.
- Furtado, André, Hugo Rodrigues, Antonio Arede, and Humberto Varum. 2021. "Experimental Investigation on the Possible Effect of Previous Damage, Workmanship and Test Setup on the Out-of-Plane Behaviour of Masonry Infill Walls." *Journal of Earthquake Engineering* 00 (00): 1–32. <https://doi.org/10.1080/13632469.2021.1882359>.

- Furtado, André, Hugo Rodrigues, António Arêde, Humberto Varum, Marin Grubišić, and Tanja Kalman Šipoš. 2018. "Prediction of the Earthquake Response of a Three-Storey Infilled RC Structure." *Engineering Structures* 171 (December 2017): 214–35. <https://doi.org/10.1016/j.engstruct.2018.05.054>.
- Gao, Xuan. 2021. "Experimental and Numerical Assessment of the Seismic Performance of an Innovative Retrofit Scheme for Infilled RC Frames." Doctor of Philosophy, University at Buffalo. <https://doi.org/10.13140/RG.2.2.23463.06561>.
- Gaudio, Carlo Del, Maria Teresa De Risi, Paolo Ricci, and Gerardo Mario Verderame. 2019. "Empirical Drift-Fragility Functions and Loss Estimation for Infills in Reinforced Concrete Frames under Seismic Loading." *Bulletin of Earthquake Engineering* 17 (3): 1285–1330. <https://doi.org/10.1007/s10518-018-0501-y>.
- Gazic, Goran, and Vladimir Sigmund. 2016. "Cyclic Testing of Single-Span Weak Frames with Masonry Infill." *Gradjevinar* 68 (8): 617–33. <https://doi.org/10.14256/JCE.1614.2016>.
- GB50011-2010. 2010. *Code for Seismic Design of Buildings*. Beijing: Ministry of Construction of the People's Republic of China.
- Govindan, P., M. Lakshmi pathy, and A.R. Santhakumar. 1986. "Ductility of Infilled Frames." *ACI Journal Proceedings* 83 (4). <https://doi.org/10.14359/10450>.
- Griffith, M. C., J. Vaculi, N.T.K. Lam, J. Wilson, and E. Lumantarna. 2007. "Cyclic Testing of Unreinforced Masonry Walls in Two-Way Bending." *Earthquake Engineering & Structural Dynamics* 36: 801–21. <https://doi.org/10.1002/eqe.654>.
- Griffith, Mike. 2008. "Seismic Retrofit of RC Frame Buildings with Masonry Infill Walls: Literature Review and Preliminary Case Study." *JRC Publication and Technical Reports*, 72.
- Gu, Xiaoming, and Yong Lu. 2005. "A Fuzzy-Random Analysis Model for Seismic Performance of Framed Structures Incorporating Structural and Non-Structural Damage." *Earthquake Engineering and Structural Dynamics* 34 (10): 1305–21. <https://doi.org/10.1002/eqe.481>.
- Guljaš, Ivica, Davorin Penava, Lucas Laughery, and Santiago Pujol. 2020. "Dynamic Tests of a Large-Scale Three-Story RC Structure with Masonry Infill Walls." *Journal of Earthquake Engineering* 24 (11): 1675–1703. <https://doi.org/10.1080/13632469.2018.1475313>.

- Gulkan, Polat. 2000. "1999 Kocaeli, Turkey Earthquake Reconnaissance Report - Building Code Enforcement Prospects: The Failure of Public Policy." *Earthquake Spectra*, no. 1: 351–74.
- Gülkan, Polat, Baris Binici, Haluk Sucuoglu, Armin Taghipour, Ismail Ozan Demirel, Sadun Tanışer, Oguz Güneş, et al. 2015. "An Innovative Tie System for Improving the Monolithic Behavior of Masonry In-Filled Reinforced Concrete Frames (INFILTIE)." In *3.TDMSK - 3. Türkiye Deprem Mühendisliği ve Sismoloji Konferansı*. İzmir. https://www.researchgate.net/publication/310509988_An_Innovative_Tie_System_for_Improving_the_Monolithic_Behavior_of_Masonry_In-filled_Reinforced_Concrete_Frames_INFILTIE.
- Günay, S., M. Korolyk, D. Mar, K.M. Mosalam, and J. Rodgers. 2009. "Infill Walls as A Spine To Enhance The Seismic Performance Of Non-Ductile Reinforced Concrete Frames." In *ATC & SEI 2009 - Conference on Improving the Seismic Performance of Existing Buildings and Other Structures 1093*, 1093–1104.
- Haider, Sarah. 1995. "In-Plane Cyclic Response of Reinforced Concrete Frames With Unreinforced Masonry Infills." Master of Science, Rice University. <https://scholarship.rice.edu/handle/1911/13956>.
- Hak, Sanja, Paolo Morandi, and Guido Magenes. 2013. "Evaluation of Infill Strut Properties Based on In-Plane Cyclic Tests." *Gradjevinar* 65 (6): 509–21. <https://doi.org/10.14256/jce.868.2013>.
- Harris, Harry G., and Gajanan M. Sabnis. 1999. *Structural Modeling and Experimental Techniques*. CRC Press.
- Hashemi, Alidad, and Khalid M. Mosalam. 2006. "Shake-Table Experiment on Reinforced Concrete Structure Containing Masonry Infill Wall." *Earthquake Engineering & Structural Dynamics* 35 (14): 1827–52. <https://doi.org/10.1002/eqe.612>.
- Henderson, Robert Craig. 1994. "Experimental and Analytical Investigation of Out-of-Plane and In-Plane Seismic Drift in Unreinforced Masonry Infilled Frames." Doctor of Philosophy, The University of Tennessee.
- Hermanns, Lutz, Alberto Fraile, Enrique Alarcón, and Ramón Álvarez. 2014. "Performance of Buildings with Masonry Infill Walls during the 2011 Lorca Earthquake." *Bulletin of Earthquake Engineering* 12 (5): 1977–97. <https://doi.org/10.1007/s10518-013-9499-3>.

- Holmes, Malcolm. 1961. "Steel Frames with Brickwork and Concrete Infilling." *Proceedings of the Institution of Civil Engineers* 19 (4): 473–78. <https://doi.org/10.1680/iicep.1961.11305>.
- Huang, Honglan, and Henry V. Burton. 2020. "A Database of Test Results from Steel and Reinforced Concrete Infilled Frame Experiments." *Earthquake Spectra* 36 (3): 1525–48. <https://doi.org/10.1177/8755293019899950>.
- Huang, M., and K. Simonen. 2018. "Background Document Methodology for Environmental Impact Assessment."
- Huang, Qunxian, Zixiong Guo, and J. S. Kuang. 2016. "Designing Infilled Reinforced Concrete Frames with the 'strong Frame-Weak Infill' Principle." *Engineering Structures* 123: 341–53. <https://doi.org/10.1016/j.engstruct.2016.05.024>.
- IBC2018. 2018. *2018 International Building Code*.
- Imran, Iswandi, and Aris Aryanto. 2009. "Behavior of Reinforced Concrete Frames In-Filled with Lightweight Materials Under Seismic Loads." *Civil Engineering Dimension* 11 (2): 69–77. <https://doi.org/10.9744/ced.11.2.pp.69-77>.
- Jiang, Huanjun, Xiaojuan Liu, and Junjie Mao. 2015. "Full-Scale Experimental Study on Masonry Infilled RC Moment-Resisting Frames under Cyclic Loads." *Engineering Structures* 91: 70–84. <https://doi.org/10.1016/j.engstruct.2015.02.008>.
- Jin, Kiwoong, Ho Choi, and Yoshiaki Nakano. 2016. "Experimental Study on Lateral Strength Evaluation of Unreinforced Masonry-Infilled RC Frame." *Earthquake Spectra* 32 (3): 1725–47. <https://doi.org/10.1193/100714EQS152M>.
- Jin, Wei, Changhai Zhai, Jingchang Kong, Wen Liu, and Maohua Zhang. 2021. "In-Plane and out-of-Plane Quasi-Static Tests on RC Frames with a New Type of Frame-Isolated Infills." *Engineering Structures* 246 (March): 113079. <https://doi.org/10.1016/j.engstruct.2021.113079>.
- Ju, Ruey Shyang, Hung Jen Lee, Cheng Cheng Chen, and Chi Chun Tao. 2012. "Experimental Study on Separating Reinforced Concrete Infill Walls from Steel Moment Frames." *Journal of Constructional Steel Research* 71: 119–28. <https://doi.org/10.1016/j.jcsr.2011.10.004>.
- Kadysiewski, Stephen, and Khalid M. Mosalam. 2009. "Modeling of Unreinforced Masonry Infill Walls Considering In-Plane and out-of-Plane Interaction." *Pacific Earthquake Engineering Research Center*.

http://peer.berkeley.edu/publications/peer_reports/reports_2008/web_PEER8102_Kadysiewski_Mosalam_R.pdf.

- Kakaletsis, D. J., K. N. David, and C. G. Karayannis. 2011. "Effectiveness of Some Conventional Seismic Retrofitting Techniques for Bare and Infilled R/C Frames." *Structural Engineering and Mechanics* 39 (4): 499–520. <https://doi.org/10.12989/sem.2011.39.4.499>.
- Kakaletsis, D. J., and C. G. Karayannis. 2008. "Influence of Masonry Strength and Openings on Infilled R/C Frames under Cycling Loading." *Journal of Earthquake Engineering* 12 (2): 197–221. <https://doi.org/10.1080/13632460701299138>.
- Kalman Šipoš, Tanja, Vladimir Sigmund, and Marijana Hadzima-Nyarko. 2013. "Earthquake Performance of Infilled Frames Using Neural Networks and Experimental Database." *Engineering Structures* 51: 113–27. <https://doi.org/10.1016/j.engstruct.2012.12.038>.
- Kasapgil, Sema Melek, Baris Binici, and Erdem Canbay. 2021. "Seismic Behavior of AAC Infill Walls Insulated with Cementitious Lightweight Panels in Reinforced Concrete Frames." *Engineering Structures* 248 (August): 113215. <https://doi.org/10.1016/j.engstruct.2021.113215>.
- Kassem, Nesreen, Ahmed Atta, and Emad Etman. 2017. "Structural Behavior of Strengthening Masonry In-Filled Frames Subjected to Lateral Load Using Bonded and Un-Bonded CFRP." *KSCE Journal of Civil Engineering* 21 (3): 818–28. <https://doi.org/10.1007/s12205-016-1389-1>.
- Kaushik, Hemant B., Durgesh C. Rai, and Sudhir K. Jain. 2006. "Code Approaches to Seismic Design of Masonry-Infilled Reinforced Concrete Frames: A State-of-the-Art Review." *Earthquake Spectra* 22 (4): 961–83. <https://doi.org/10.1193/1.2360907>.
- Kaya, Fatih, Hamide Tekeli, and Özgür Anil. 2018. "Experimental Behavior of Strengthening of Masonry Infilled Reinforced Concrete Frames by Adding Rebar-Reinforced Stucco." *Structural Concrete* 19 (6): 1792–1805. <https://doi.org/10.1002/suco.201700210>.
- Khalid Mahmoud Aly Mosalam. 1996. "Experimental and Computational Strategies for the Seismic Behavior Evaluation of Frames with Infill Walls." Doctor of Philosophy, Cornell University.
- Khelfi, Mebarek, Nouredine Bourahla, and Mustapha Remki. 2021. "Performance Evaluation of Masonry Infilled RC Frame Structures under Lateral Loads." *Gradjevinar* 73 (3): 219–34. <https://doi.org/10.14256/JCE.2647.2019>.

- Khoshnoud, Hamid Reza, and Kadir Marsono. 2016. "Experimental Study of Masonry Infill Reinforced Concrete Frames with and without Corner Openings." *Structural Engineering and Mechanics* 57 (4): 641–56. <https://doi.org/10.12989/sem.2016.57.4.641>.
- Klingner, Richard E., and Vitelmo V. Bertero. 1976. "Infilled Frames in Earthquake Resistant Construction." California.
- Komaraneni, S., Durgesh C. Rai, and Vaibhav Singhal. 2011. "Seismic Behavior of Framed Masonry Panels with Prior Damage When Subjected to Out-of-Plane Loading." *Earthquake Spectra* 27 (4): 1077–1103. <https://doi.org/10.1193/1.3651624>.
- Koutas, L., S. N. Bousias, and T. C. Triantafillou. 2015. "Seismic Strengthening of Masonry-Infilled RC Frames with TRM: Experimental Study." *Journal of Composites for Construction* 19 (2): 04014048. [https://doi.org/10.1061/\(asce\)cc.1943-5614.0000507](https://doi.org/10.1061/(asce)cc.1943-5614.0000507).
- Koutas, Lampros N., and Dionysios A. Bournas. 2019. "Out-of-Plane Strengthening of Masonry-Infilled RC Frames with Textile-Reinforced Mortar Jackets." *Journal of Composites for Construction* 23 (1): 1–13. [https://doi.org/10.1061/\(asce\)cc.1943-5614.0000911](https://doi.org/10.1061/(asce)cc.1943-5614.0000911).
- Koutromanos, Ioannis, Marios Kyriakides, Andreas Stavridis, Sarah Billington, and P. Benson Shing. 2013. "Shake-Table Tests of a 3-Story Masonry-Infilled RC Frame Retrofitted with Composite Materials." *Journal of Structural Engineering* 139 (8): 1340–51. [https://doi.org/10.1061/\(asce\)st.1943-541x.0000689](https://doi.org/10.1061/(asce)st.1943-541x.0000689).
- Kumar, Mukesh, Muhammad Haider, and Sarosh Hashmat Lodi. 2016. "Response of Low-Quality Solid Concrete Block Infilled Frames." *Proceedings of the Institution of Civil Engineers: Structures and Buildings* 169 (9): 669–87. <https://doi.org/10.1680/jstbu.15.00068>.
- Kurt, Efe G., Barış Binici, Özgür Kurç, Erdem Canbay, Akpinara, and Güney Özcebe. 2011. "Seismic Performance of a Deficient Reinforced Concrete Test Frame with Infill Walls." *Earthquake Spectra* 27 (3): 817–34. <https://doi.org/10.1193/1.3609876>.
- Kwan, Albert Hung Kwok. 1982. "Nonlinear and Cyclic Behaviour of Infilled Frames." Doctor of Philosophy, University of Hong Kong.
- Kyriakides, M. A., and S. L. Billington. 2014. "Cyclic Response of Nonductile Reinforced Concrete Frames with Unreinforced Masonry Infills Retrofitted

- with Engineered Cementitious Composites.” *Journal of Structural Engineering* 140 (2): 04013046. [https://doi.org/10.1061/\(asce\)st.1943-541x.0000833](https://doi.org/10.1061/(asce)st.1943-541x.0000833).
- Lee, Han-seon, and Sung-woo Woo. 2002. “Effect of Masonry Infills on Seismic Performance of a 3-Storey RC Frame with Non-Seismic Detailing.” *Earthquake Engineering & Structural Dynamics* 378 (January 2001): 353–78. <https://doi.org/10.1002/eqe.112>.
- Leeanansaksiri, Anuchat, Phaiboon Panyakapo, and Anat Ruangrassamee. 2018. “Seismic Capacity of Masonry Infilled RC Frame Strengthening with Expanded Metal Ferrocement.” *Engineering Structures* 159 (December 2017): 110–27. <https://doi.org/10.1016/j.engstruct.2017.12.034>.
- Leuchars, J. M., and J. C. Scrivener. 1976. “Masonry Panels Subjected to Cyclic In-Plane Loading.” *Bulletin of the New Zealand Society for Earthquake Engineering* 9 (2): 122–31.
- Liauw, T.C., and A. K. H. Kwan. 1992. “Experimental Study of Shear Wall and Infilled Frame on Shake-Table.” In *10th World Conference on Earthquake Engineering*, 2659–63. Rotterdam.
- Liberatore, Laura, Fabrizio Noto, Fabrizio Mollaioli, and Paolo Franchin. 2018. “In-Plane Response of Masonry Infill Walls: Comprehensive Experimentally-Based Equivalent Strut Model for Deterministic and Probabilistic Analysis.” *Engineering Structures* 167 (November 2017): 533–48. <https://doi.org/10.1016/j.engstruct.2018.04.057>.
- Lin, Kun, Yuri Zarevich Totoev, Hongjun Liu, and Tianyou Guo. 2016. “In-Plane Behaviour of a Reinforcement Concrete Frame with a Dry Stack Masonry Panel.” *Materials* 9 (2): 1–17. <https://doi.org/10.3390/ma9020108>.
- Liu, Yi, and Sandra Soon. 2012. “Experimental Study of Concrete Masonry Infills Bounded by Steel Frames.” *Canadian Journal of Civil Engineering* 39 (2): 180–90. <https://doi.org/10.1139/L11-122>.
- Lourenço, Paulo B., João M. Leite, Manuel F. Paulo-Pereira, A. Campos-Costa, P. X. Candeias, and P. X. Candeias. 2016. “Shaking Table Testing for Masonry Infill Walls: Unreinforced versus Reinforced Solutions.” *Earthquake Engineering & Structural Dynamics* 45: 2241–2260. <https://doi.org/10.1002/eqe.2756>.
- Lu, Xiao, and Zijuan Yan. 2021. “Development and Validation of a Modified Equivalent Strut Model of Lightweight Masonry Block Infill Walls for Quasi-Static In-Plane Cyclic Analysis.” *Journal of Earthquake Engineering* 00 (00): 1–20. <https://doi.org/10.1080/13632469.2021.1988762>.

- Lu, Xiao, and Shumin Zha. 2021. "Full-Scale Experimental Investigation of the in-Plane Seismic Performance of a Novel Resilient Infill Wall." *Engineering Structures* 232 (December 2020): 111826. <https://doi.org/10.1016/j.engstruct.2020.111826>.
- Lu, Y., E. Vintzileou, G. F. Zhang, and T. P. Tassios. 1999. "Reinforced Concrete Scaled Columns under Cyclic Actions." *Soil Dynamics and Earthquake Engineering* 18 (2): 151–67. [https://doi.org/10.1016/S0267-7261\(98\)00037-2](https://doi.org/10.1016/S0267-7261(98)00037-2).
- Luca, Flavia De, Gerardo M. Verderame, Fernando Gómez-Martínez, and Agustín Pérez-García. 2014. "The Structural Role Played by Masonry Infills on RC Building Performances after the 2011 Lorca, Spain, Earthquake." *Bulletin of Earthquake Engineering* 12 (5): 1999–2026. <https://doi.org/10.1007/s10518-013-9500-1>.
- Lunn, Dillon S., and Sami H. Rizkalla. 2011. "Strengthening of Infill Masonry Walls with FRP Materials." *Journal of Composites for Construction* 15 (2): 206–14. [https://doi.org/10.1061/\(asce\)cc.1943-5614.0000088](https://doi.org/10.1061/(asce)cc.1943-5614.0000088).
- Maidiawati, and Yasushi Sanada. 2017. "R/C Frame–Infill Interaction Model and Its Application to Indonesian Buildings." *Earthquake Engineering and Structural Dynamics* 46 (2): 221–41. <https://doi.org/10.1002/eqe.2787>.
- Maidiawati, Yasushi Sanada, and Jafril Tanjung. 2018. "The Behaviours of the Brick-Masonry Infilled RC Frame Structure under Reversed Cyclic Lateral Loading." *International Journal on Advanced Science, Engineering and Information Technology* 8 (6): 2428–34. <https://doi.org/10.18517/ijaseit.8.6.7196>.
- Maidiawati, Jafril Tanjung, Yulia Hayati, Agus, and Hamdeni Medriosa. 2019. "Experimental Investigation of Seismic Performance of Reinforced Brick Masonry Infilled Reinforced Concrete Frames with a Central Opening." *International Journal of GEOMATE* 16 (57): 35–41. <https://doi.org/10.21660/2019.57.4592>.
- Mainstone, R.J. 1971. "On the Stiffness and Strengths of Infilled Frames." *Proceedings of the Institution of Civil Engineers* 49 (2): 230. <https://doi.org/10.1680/iicep.1971.6267>.
- Mainstone, R.J., and G.A Weeks. 1970. "The Influence of Bounding Frame on the Racking Stiffness and Strength of Brick Walls." In *Proceedings of the 2nd International Brick Masonry Conference, Building Research Establishment, Watford, England*, 165–71. Stoke-on-Trent.

- Maio, Nina Avramidou. 1979. "Dynamic Behavior of Brick Structural Elements Infilled to Strengthen R . C . Structures." In *5th International Brick Masonry Conference*, 294–301. Washington.
- Mallick, D. V., and R. T. Severn. 1967. "The Behaviour of Infilled Frames under Static Loading." *Proceedings of the Institution of Civil Engineers* 38 (4): 639–56.
- Mander, J.B., B. Nair, K. Wojtkowski, and J. Ma. 1993. "An Experimental Study on the Seismic Performance of Brick - Infilled Steel Frames with and without Retrofit." New York.
- Mansouri, Ali, Mohammad S. Marefat, and Mohammad Khanmohammadi. 2014. "Experimental Evaluation of Seismic Performance of Low-Shear Strength Masonry Infills with Openings in Reinforced Concrete Frames with Deficient Seismic Details." *The Structural Design of Tall and Special Buildings* 23: 1190–1210. <https://doi.org/10.1002/tal.1115>.
- Marinković, M., and Christoph Butenweg. 2019. "Innovative Decoupling System for the Seismic Protection of Masonry Infill Walls in Reinforced Concrete Frames." *Engineering Structures* 197 (June): 109435. <https://doi.org/10.1016/j.engstruct.2019.109435>.
- Markulak, Damir, Ivan Radić, and Vladimir Sigmund. 2013. "Cyclic Testing of Single Bay Steel Frames with Various Types of Masonry Infill." *Engineering Structures* 51: 267–77. <https://doi.org/10.1016/j.engstruct.2013.01.026>.
- Marx, Karl. 1867. *Capital - A Critique of Political Economy. Volume I: The Process of Capitalist Production*. Edited by Friedrich Engels. Hamburg: Verlag von Otto Meisner.
- Mehrabi, Armin B. 1994. "Behaviour of Masonry-Infilled Reinforced Concrete Frames Subjected to Lateral Loadings." Doctor of Philosophy, University of Colorado.
- Mehrabi, B. Armin, P. Benson Shing, P. Schuller Michael, and L. Noland James. 1996. "Experimental Evaluation of Masonry-Infilled RC Frames." *Journal of Structural Engineering* 122 (3): 228–37. [https://doi.org/http://dx.doi.org/10.1061/\(ASCE\)0733-9445\(1996\)122:3\(228\)](https://doi.org/http://dx.doi.org/10.1061/(ASCE)0733-9445(1996)122:3(228)).
- Milanesi, R. R., P. Morandi, C. F. Manzini, L. Albanesi, and G. Magenes. 2022. "Out-of-Plane Response of an Innovative Masonry Infill with Sliding Joints from Shaking Table Tests." *Journal of Earthquake Engineering* 26 (4): 1789–1823. <https://doi.org/10.1080/13632469.2020.1739173>.

- Milanesi, Riccardo R., Paolo Morandi, Sanja Hak, and Guido Magenes. 2021. "Experiment-Based out-of-Plane Resistance of Strong Masonry Infills for Codified Applications." *Engineering Structures* 242 (March): 112525. <https://doi.org/10.1016/j.engstruct.2021.112525>.
- Milijaš, Aleksa, Bogdan Šakić, Marko Marinković, Christoph Butenweg, and Sven Klinkel. 2021. "Experimental Investigation of Behaviour of Masonry Infilled Rc Frames Under Out-of-Plane Loading." *8th International Conference on Computational Methods in Structural Dynamics and Earthquake Engineering Methods in Structural Dynamics and Earthquake Engineering*, 829–46. <https://doi.org/10.7712/120121.8528.18914>.
- Ming, Liu, Cheng Yun, and Liu Xiaowei. 2011. "Shaking Table Test on Out-of-Plane Stability of Infill Masonry Wall." *Transactions of Tianjin University* 17 (2): 125–31. <https://doi.org/10.1007/s12209-011-1534-3>.
- Minotto, Massimiliano, Nicolò Verlato, Marco Donà, and Francesca da Porto. 2020. "Strengthening of In-Plane and Out-of-Plane Capacity of Thin Clay Masonry Infills Using Textile- and Fiber-Reinforced Mortar." *Journal of Composites for Construction* 24 (6): 04020059. [https://doi.org/10.1061/\(asce\)cc.1943-5614.0001067](https://doi.org/10.1061/(asce)cc.1943-5614.0001067).
- Misir, I. Serkan, Ozgur Ozcelik, Sadik Can Girgin, and Serap Kahraman. 2012. "Experimental Work on Seismic Behavior of Various Types of Masonry Infilled RC Frames." *Structural Engineering and Mechanics* 44 (6): 763–74. <https://doi.org/10.12989/sem.2012.44.6.763>.
- Misir, Ibrahim Serkan. 2015. "Potential Use of Locked Brick Infill Walls to Decrease Soft-Story Formation in Frame Buildings." *Journal of Performance of Constructed Facilities* 29 (5): 1–10. [https://doi.org/10.1061/\(ASCE\)CF.1943-5509.0000633](https://doi.org/10.1061/(ASCE)CF.1943-5509.0000633).
- Misir, Ibrahim Serkan, Ozgur Ozcelik, Sadik Can Girgin, and Umut Yucel. 2016. "The Behavior of Infill Walls in RC Frames Under Combined Bidirectional Loading." *Journal of Earthquake Engineering* 20 (4): 559–86. <https://doi.org/10.1080/13632469.2015.1104748>.
- Moghaddam, Hassan Alijani. 1988. "Seismic Behaviour of Brick Infilled Frames." Doctor of Philosophy, Imperial College of Science and Technology.
- Mohammadi, M., V. Akrami, and R. Mohammadi-Ghazi. 2011. "Methods to Improve Infilled Frame Ductility." *Journal of Structural Engineering* 137 (6): 646–53. [https://doi.org/10.1061/\(asce\)st.1943-541x.0000322](https://doi.org/10.1061/(asce)st.1943-541x.0000322).

- Morandi, Paolo, Sanja Hak, and Guido Magenes. 2018a. "Mechanical Characterization and Force-Displacement Hysteretic Curves from in-Plane Cyclic Tests on Strong Masonry Infills." *Data in Brief* 16: 886–904. <https://doi.org/10.1016/j.dib.2017.12.015>.
- Morandi, Paolo, Sanja Hak, and Guido Magenes. 2018b. "Performance-Based Interpretation of in-Plane Cyclic Tests on RC Frames with Strong Masonry Infills." *Engineering Structures* 156 (December 2017): 503–21. <https://doi.org/10.1016/j.engstruct.2017.11.058>.
- Morandi, Paolo, R. R. Milanesi, and G. Magenes. 2018. "Innovative Solution for Seismic-Resistant Masonry Infills with Sliding Joints: In-Plane Experimental Performance." *Engineering Structures* 176 (September): 719–33. <https://doi.org/10.1016/j.engstruct.2018.09.018>.
- Mosalam, Khalid M., and Selim Günay. 2015. "Progressive Collapse Analysis of Reinforced Concrete Frames with Unreinforced Masonry Infill Walls Considering In-Plane/out-of-Plane Interaction." *Earthquake Spectra* 31 (2): 921–43. <https://doi.org/10.1193/062113EQS165M>.
- Moşoarcă, M., C. Petruş, V. Stoian, and A. Anastasiadis. 2016. "Behaviour of Masonry Infills Subjected to out of Plane Seismic Actions. Part 1: Theoretical Analysis." *Brick and Block Masonry: Trends, Innovations and Challenges - Proceedings of the 16th International Brick and Block Masonry Conference, IBMAC 2016*, no. June: 1283–92. <https://doi.org/10.1201/b21889-159>.
- Murty, C V R, and Sudhir K Jain. 2000. "Beneficial Influence of Masonry Infill Walls on Seismic Performance of Rc Frame Buildings." *Twelfth World Conference on Earthquake Engineering (12WCEE)*, no. 1764: 1–6.
- Negro, Paolo, and Guido Verzeletti. 1996. "Effect of Infills on The Global Behaviour of R/C Frames: Energy Considerations From Pseudodynamic Tests." *Earthquake Engineering and Structural Dynamics* 25 (February): 753–73.
- Nicola, Tarque, Candido Leandro, Camata Guido, and Spacone Enrico. 2015. "Masonry Infilled Frame Structures: State-of-the-Art Review of Numerical Modelling." *Earthquake and Structures* 8 (3): 733–59. <https://doi.org/10.12989/eas.2015.8.3.733>.
- NZSEE – Part C7. 2017. *The Seismic Assessment of Existing Buildings Part C7: Moment Resisting Frames with Infill Panels*. New Zealand. <https://www.building.govt.nz/assets/Uploads/building-code-compliance/b-stability/b1-structure/seismic-assessment/c7-moment-resisting-frames-infill-panels.pdf>.

- Ockleston, A. J. 1955. "Load Tests on a Three Storey Reinforced Concrete Building in Johannesburg." *The Structural Engineer* 33 (10): 304–22. <http://scholar.google.com/scholar?hl=en&btnG=Search&q=intitle:Load+Tests+on+a+Three+Storey+Reinforced+Concrete+Building+in+Johannesburg#0>.
- Onat, Onur, António A. Correia, Paulo B. Lourenço, and Ali Koçak. 2018. "Assessment of the Combined In-Plane and out-of-Plane Behavior of Brick Infill Walls within Reinforced Concrete Frames under Seismic Loading." *Earthquake Engineering and Structural Dynamics* 47 (14): 2821–39. <https://doi.org/10.1002/eqe.3111>.
- O'Reilly, Gerard J., and Gian Michele Calvi. 2021. "A Seismic Risk Classification Framework for Non-Structural Elements." *Bulletin of Earthquake Engineering* 19 (0123456789): 5471–94. <https://doi.org/10.1007/s10518-021-01177-y>.
- Ozcebe, Guney, Ugur Ersoy, Tugrul Tankut, Ugurhan Akyuz, and Emrah Erduran. 2004. "Rehabilitation of Existing Reinforced Concrete Structures Using CFRP Fabrics." *13th World Conference on Earthquake Engineering*, no. 1393.
- Ozden, Sevket, Umut Akguzel, and Turan Ozturan. 2011. "Seismic Strengthening of Infilled Reinforced Concrete Frames by CFRP." *ACI Structural Journal* 108 (4): 1–9.
- Özmen, Bülent. 2012. "Türkiye Deprem Bölgeleri Haritalarının Tarihsel Gelişimi." *Türkiye Jeoloji Bülteni* 55 (1): 43–55.
- Pachappoyil, Nidhin S, and Pankaj Agarwal. 2021. "Performance Evaluation of the Energy Dissipating Hysteretic Infill Wall Frame Considering Opening under In-Plane and out-of-Plane Loading." *Engineering Structures* 249 (March): 113329. <https://doi.org/10.1016/j.engstruct.2021.113329>.
- Palieraki, Vasiliki, Christos Zeris, Elizabeth Vintzileou, and Chrissy Elpida Adami. 2018. "In-Plane and out-of Plane Response of Currently Constructed Masonry Infills." *Engineering Structures* 177 (December 2017): 103–16. <https://doi.org/10.1016/j.engstruct.2018.09.047>.
- Pallarés, Francisco J., Antonio Davia, Wael M. Hassan, and Luis Pallarés. 2021. "Experimental and Analytical Assessment of the Influence of Masonry Façade Infills on Seismic Behavior of RC Frame Buildings." *Engineering Structures* 235 (January). <https://doi.org/10.1016/j.engstruct.2021.112031>.
- Pallarés, Francisco J., and Luis Pallarés. 2016. "Experimental Study on the Response of Seismically Isolated Masonry Infilled Steel Frames during the Initial Stages of a Seismic Movement." *Engineering Structures* 129: 44–53. <https://doi.org/10.1016/j.engstruct.2016.09.019>.

- Pantò, B., L. Silva, G. Vasconcelos, and P. B. Lourenço. 2019. “Macro-Modelling Approach for Assessment of out-of-Plane Behavior of Brick Masonry Infill Walls.” *Engineering Structures* 181 (August 2018): 529–49. <https://doi.org/10.1016/j.engstruct.2018.12.019>.
- Paulay, T., and M. J. N. Priestley. 1992. *Seismic Design of Reinforced Concrete and Masonry Buildings*. John Wiley & Sons.
- Peng, Quanmin, Xiaojie Zhou, and Chenghao Yang. 2018. “Influence of Connection and Constructional Details on Masonry-Infilled RC Frames under Cyclic Loading.” *Soil Dynamics and Earthquake Engineering* 108 (February): 96–110. <https://doi.org/10.1016/j.soildyn.2018.02.009>.
- Penna, Andrea, Guido Magenes, and Gian Michele Calvi. 2008. “Seismic Performance of AAC Infill and Bearing Walls with Different Reinforcement Solutions.” In *14th International Brick and Block Masonry Conference*. Sydney.
- Pereira, M. F. Paulo, M. F. Neto Pereira, J. E. Dias Ferreira, and P. B. Lourenço. 2011. “Behavior of Damaged Masonry Infill Panels in RC Frames Subjected to out of Plane Loads.” In *7th International Conference on Analytical Models and New Concepts in Concrete and Masonry Structures*. Krakow.
- Pires, Felicita. 1991. “Behaviour Under Horizontal Actions of Reinforced Concrete Frames Infilled with Brick Masonry.” In *9th International Brick and Block Masonry Conference*, 528–35. Berlin.
- Pires, Felicita, and E. Cansado Carvalho. 1994. “Cyclic Behaviour of Reinforced Concrete Frames Infilled with Brick Masonry Walls.” In *10th International Brick and Block Masonry Conference*, edited by N. G. Shrive and A. Huizer, 303–12. Calgary.
- Polyakov, S.V. 1956. “Masonry in Framed Buildings.” *Gosudarstvennoe Izdatel'stvo Literatury Po Stroitel'stvu Arkhitektue* Translated (Moscow, Russia).
- Polyakov, S.V.. 1960. “On the Interaction between Masonry Filler Walls and Enclosing Frame When Loaded in the Plane of the Wall.” *Translation in Earthquake Engineering, Earthquake Engineering Research Institute (EERI)*, 36–42.
- Porto, F. Da, N. Verlato, G. Guidi, and C. Modena. 2016. “The INSYSME Project: Innovative Construction Systems for Earthquake Resistant Masonry Infill Walls.” *Brick and Block Masonry: Trends, Innovations and Challenges* -

Proceedings of the 16th International Brick and Block Masonry Conference, IBMAC 2016, 1173–78. <https://doi.org/10.1201/b21889-146>.

- Porto, Francesca da, Marco Donà, Nicolò Verlato, and Giovanni Guidi. 2020. “Experimental Testing and Numerical Modeling of Robust Unreinforced and Reinforced Clay Masonry Infill Walls, With and Without Openings.” *Frontiers in Built Environment* 6 (December). <https://doi.org/10.3389/fbuil.2020.591985>.
- Porto, Francesca da, Giovanni Guidi, Massimo Dalla Benetta, and Nicolò Verlato. 2013. “Combined In-Plane/Out-of-Plane Experimental Behaviour of Reinforced and Strengthened Infill Masonry Walls.” *12th Canadian Masonry Symposium*, no. June: 1–11.
- Porto, Francesca da, Giovanni Guidi, Nicolò Verlato, and Claudio Modena. 2015. “Effectiveness of Plasters and Textile Reinforced Mortars for Strengthening Clay Masonry Infill Walls Subjected to Combined In-Plane/out-of-Plane Actions / Wirksamkeit von Putz Und Textilbewehrtem Mörtel Bei Der Verstärkung von Ausfachungswänden Aus Ziegel.” *Mauerwerk* 19 (5): 334–54. <https://doi.org/10.1002/dama.201500673>.
- Pradhan, Bharat, Maria Zizzo, Vasilis Sarhosis, and Liborio Cavaleri. 2021. “Out-of-Plane Behaviour of Unreinforced Masonry Infill Walls: Review of the Experimental Studies and Analysis of the Influencing Parameters.” *Structures* 33 (February): 4387–4406. <https://doi.org/10.1016/j.istruc.2021.07.038>.
- Preti, M., N. Bettini, and G. Plizzari. 2012. “Infill Walls with Sliding Joints to Limit Infill-Frame Seismic Interaction: Large-Scale Experimental Test.” *Journal of Earthquake Engineering* 16 (1): 125–41. <https://doi.org/10.1080/13632469.2011.579815>.
- Preti, Marco, and Valentino Bolis. 2017. “Masonry Infill Construction and Retrofit Technique for the Infill-Frame Interaction Mitigation: Test Results.” *Engineering Structures* 132: 597–608. <https://doi.org/10.1016/j.engstruct.2016.11.053>.
- Preti, Marco, Laura Migliorati, and Ezio Giuriani. 2015. “Experimental Testing of Engineered Masonry Infill Walls for Post-Earthquake Structural Damage Control.” *Bulletin of Earthquake Engineering* 13 (7): 2029–49. <https://doi.org/10.1007/s10518-014-9701-2>.
- Pujol, S., and D. Fick. 2010. “The Test of a Full-Scale Three-Story RC Structure with Masonry Infill Walls.” *Engineering Structures* 32 (10): 3112–21. <https://doi.org/10.1016/j.engstruct.2010.05.030>.
- Ricci, Paolo, Mariano Di Domenico, and Gerardo M. Verderame. 2018a. “Experimental Assessment of the In-Plane/out-of-Plane Interaction in

- Unreinforced Masonry Infill Walls.” *Engineering Structures* 173 (July): 960–78. <https://doi.org/10.1016/j.engstruct.2018.07.033>.
- Ricci, Paolo, Mariano Di Domenico, and Gerardo M. Verderame. 2018b. “Experimental Investigation of the Influence of Slenderness Ratio and of the In-Plane/out-of-Plane Interaction on the out-of-Plane Strength of URM Infill Walls.” *Construction and Building Materials* 191: 507–22. <https://doi.org/10.1016/j.conbuildmat.2018.10.011>.
- Risi, Maria Teresa De, Mariano Di Domenico, Paolo Ricci, Gerardo Mario Verderame, and Gaetano Manfredi. 2019. “Experimental Investigation on the Influence of the Aspect Ratio on the In-Plane/out-of-Plane Interaction for Masonry Infills in RC Frames.” *Engineering Structures* 189 (September 2018): 523–40. <https://doi.org/10.1016/j.engstruct.2019.03.111>.
- Risi, Maria Teresa De, Carlo Del Gaudio, Paolo Ricci, and Gerardo Mario Verderame. 2018. “In-Plane Behaviour and Damage Assessment of Masonry Infills with Hollow Clay Bricks in RC Frames.” *Engineering Structures* 168 (October 2017): 257–75. <https://doi.org/10.1016/j.engstruct.2018.04.065>.
- Rodrigues, H., H. Varum, and A. Costa. 2008. “A Non-Linear Masonry Infill Macro-Model to Represent the Global Behaviour of Buildings under Cyclic Loading.” *International Journal of Mechanics and Materials in Design* 4 (2): 123–35. <https://doi.org/10.1007/s10999-008-9070-6>.
- Roosta, Soraya, and Yi Liu. 2021. “Behavior of Concrete Masonry Infills Bounded by Masonry Frames Subjected to In-Plane Lateral Loading – Experimental Study.” *Engineering Structures* 247 (April): 113153. <https://doi.org/10.1016/j.engstruct.2021.113153>.
- Rossetto, T., and A. Elnashai. 2003. “Derivation of Vulnerability Functions for European-Type RC Structures Based on Observational Data.” *Engineering Structures* 25 (10): 1241–63. [https://doi.org/10.1016/S0141-0296\(03\)00060-9](https://doi.org/10.1016/S0141-0296(03)00060-9).
- Rossetto, Tiziana. 2004. “Vulnerability Curves for the Seismic Assessment of Reinforced Concrete Building Populations.” Doctor of Philosophy, University of London.
- Rossi, Andrea, Paolo Morandi, Riccardo R Milanese, Guido Magenes, Iuss Pavia, and Emilia Re. 2021. “Influence of The Infill Typology in the Evaluation of the Annual Losses of RC Structures Through the Application of a New Method.” In *8th ECCOMAS Thematic Conference on Computational Methods in Structural Dynamics and Earthquake Engineering*, 886–98.

- Saatcioglu, Murat, Fabio Serrato, and Simon Foo. 2005. "Seismic Performance of Masonry Infill Walls Retrofitted with CFRP Sheets." In *7th Int. Symp. on Fiber-Reinforced (FRP) Polymer Reinforcement for Concrete Structures*, edited by Carol K. Shield, John P. Busel, Stephanie L. Walkup, and Doug D. Gremel, 341–53. American Concrete Institute.
- Sagar, S. Lalit, Vaibhav Singhal, and Durgesh C. Rai. 2019. "In-Plane and Out-of-Plane Behavior of Masonry-Infilled RC Frames Strengthened with Fabric-Reinforced Cementitious Matrix." *Journal of Composites for Construction* 23 (1): 04018073. [https://doi.org/10.1061/\(asce\)cc.1943-5614.0000905](https://doi.org/10.1061/(asce)cc.1943-5614.0000905).
- Santarsiero, Giuseppe, Alessandra De Angelis, Vincenzo Manfredi, Francesco Santamato, Angelo Masi, and Marisa Pecce. 2021. "Out-of-Plane Ambient Vibration Tests of an Infill Wall in RC Frame Subjected to Previous In-Plane Damage." In *Civil Structural Health Monitoring*, 205–18. Springer International Publishing. https://doi.org/10.1007/978-3-030-74258-4_14.
- Saouma, By Victor E, Jerry J Broz, Eugene Briihwiler, and Howard L Boggs. 1991. "Effect of Aggregate and Specimen Size on Fracture Properties of Dam Concrete." *Journal of Materials in Civil Engineering* 3 (3): 204–18.
- Sarno, Luigi Di, Jing-Ren Wu, Fabio Freddi, Mario D’Aniello, Stathis Bousias, Fernando Gutiérrez-Urzúa, Raffaele Landolfo, and Nikolaos Stathas. 2021. "Numerical Modelling of Masonry Infill Walls in Existing Steel Frames." In *8th International Conference on Computational Methods in Structural Dynamics and Earthquake Engineering Methods in Structural Dynamics and Earthquake Engineering*, 1519–31. Athens. <https://doi.org/10.7712/120121.8577.18872>.
- Sassun, Kathy, Timothy J. Sullivan, Paolo Morandi, and Donatello Cardone. 2016. "Characterising the In-Plane Seismic Performance of Infill Masonry." *Bulletin of the New Zealand Society for Earthquake Engineering* 49 (1): 98–115. <https://doi.org/10.5459/bnzsee.49.1.98-115>.
- Schwarz, S., A. Hanaor, and D. Z. Yankelevsky. 2015. "Experimental Response of Reinforced Concrete Frames With AAC Masonry Infill Walls to In-Plane Cyclic Loading." *Structures* 3: 306–19. <https://doi.org/10.1016/j.istruc.2015.06.005>.
- Seki, Matsutaro, Viorel Popa, Eugen Lozinca, Andreea Dutu, and Andrei Papurcu. 2018. "Experimental Study on Retrofit Technologies for Rc Frames With Infilled Brick Masonry Walls in Developing Countries." In *16th European Conference on Earthquake Engineering*, 1–12. Thessaloniki.

- Sen, Debasish, Hamood Alwashali, Md Shafiul Islam, Matsutaro Seki, and Masaki Maeda. 2021. "Lateral Strength Evaluation of Ferrocement Strengthened Masonry Infilled RC Frame Based on Experimentally Observed Failure Mechanisms." <https://doi.org/10.21203/rs.3.rs-422754/v1>.
- Sezen, H., A. S. Whittaker, K. J. Elwood, and K. M. Mosalam. 2003. "Performance of Reinforced Concrete Buildings during the August 17, 1999 Kocaeli, Turkey Earthquake, and Seismic Design and Construction Practise in Turkey." *Engineering Structures* 25 (1): 103–14. [https://doi.org/10.1016/S0141-0296\(02\)00121-9](https://doi.org/10.1016/S0141-0296(02)00121-9).
- Shah, Syed Azmat Ali, Asfandyar Ahmed, Khan Shahzada, Syed Muhammad Ali, Akhtar Naeem Khan, and Akhter Gul. 2021. "Experimental and Numerical Assessment of Masonry Infill on Seismic Performance of RC Frame Structure." *Journal of Engineering and Applied Sciences* 40 (1). <https://doi.org/10.17582/journal.jeas/40.1.24.36>.
- Shah, Syed Azmat Ali, Junaid Shah Khan, Syed Muhammad Ali, Khan Shahzada, Waqar Ahmad, Junaid Shah, and Maria T. De Risi. 2019. "Shake Table Response of Unreinforced Masonry and Reinforced Concrete Elements of Special Moment Resisting Frame." *Advances in Civil Engineering* 2019. <https://doi.org/10.1155/2019/7670813>.
- Shah, Syed Azmat Ali, Khan Shahzada, Bora Gencturk, Qazi Sami Ullah, Zawar Hussain, and Muhammad Javed. 2021. "In-Plane Quasi-Static Cyclic Load Tests on Reinforced Concrete Frame Panels with and without Brick Masonry Infill Walls." *Journal of Earthquake Engineering* 00 (00): 1–25. <https://doi.org/10.1080/13632469.2021.1884147>.
- Shing, P Benson, and Armin B Mehrabi. 2002. "Behaviour and Analysis of Masonry-Infilled Frames." *Progress in Structural Engineering and Materials* 4 (3): 320–31. <https://doi.org/10.1002/pse.122>.
- Sigmund, V., and D. Penava. 2014. "Influence of Openings, with and without Confinement, on Cyclic Response of Infilled R-C Frames - An Experimental Study." *Journal of Earthquake Engineering* 18 (1): 113–46. <https://doi.org/10.1080/13632469.2013.817362>.
- Silva, L., G. Vasconcelos, P. Lourenço, and F. Akhoundi. 2016. "Experimental Evaluation of a Constructive System for Earthquake Resisting Masonry Enclosure Walls." *Brick and Block Masonry: Trends, Innovations and Challenges - Proceedings of the 16th International Brick and Block Masonry Conference, IBMAC 2016* 2003: 1333–40. <https://doi.org/10.1201/b21889-165>.

- Silva, Luis M., Graça Vasconcelos, and Paulo B. Lourenço. 2021. "Innovative Systems for Earthquake-Resistant Masonry Infill Walls: Characterization of Materials and Masonry Assemblages." *Journal of Building Engineering* 39 (December 2020): 102195. <https://doi.org/10.1016/j.jobbe.2021.102195>.
- "Sketch-Up." 2016. California, USA: Trimble Inc.
- Smith, B. Stafford, and C. Carter. 1969. "A Method of Analysis for Infilled Frames." In *Proceedings of the Institution of Civil Engineers*, 31–48. London: Institute of Civil Engineers. <https://doi.org/10.1680/iicep.1970.6801>.
- Sousa, Luis, and Ricardo Monteiro. 2018. "Seismic Retrofit Options for Non-Structural Building Partition Walls: Impact on Loss Estimation and Cost-Benefit Analysis." *Engineering Structures* 8 (27): 8–27. <https://doi.org/10.1016/j.engstruct.2018.01.028>.
- Stavridis, Andreas. 2009. "Analytical and Experimental Study of Seismic Performance of Reinforced Concrete Frames Infilled with Masonry Walls." PhD, University of California.
- Stavridis, Andreas, Ioannis Koutromanos, and P. Benson Shing. 2011. "Shake-Table Tests of a Three-Story Reinforced Concrete Frame with Masonry Infill Walls." *Earthquake Engineering & Structural Dynamics*.
- Stylianidis, C. K. 2012. "Experimental Investigation of Masonry Infilled R/C Frames." *The Open Construction and Building Technology Journal* 6 (1): 194–212. <https://doi.org/10.2174/1874836801206010194>.
- Su, Qiwang, and Gaochuang Cai. 2017. "Seismic Behaviour of Full-Scale Hollow Bricks-Infilled RC Frames under Cyclic Loads." *Bulletin of Earthquake Engineering* 15 (7): 2981–3012. <https://doi.org/10.1007/s10518-016-0074-6>.
- Sucuoglu, Haluk. 2013. "Implications of Masonry Infill and Partition Damage in Performance Perception in Residential Buildings after a Moderate Earthquake." *Earthquake Spectra* 29 (2): 661–67. <https://doi.org/10.1193/1.4000147>.
- Sucuoglu, Haluk, and Umair A. Siddiqui. 2014. "Pseudo-Dynamic Testing and Analytical Modeling of AAC Infilled RC Frames." *Journal of Earthquake Engineering* 18 (8): 1281–1301. <https://doi.org/10.1080/13632469.2014.932723>.
- Suzuki, Tomomi, Ho Choi, Yasushi Sanada, Yoshiaki Nakano, Kazuto Matsukawa, Devjyoti Paul, Polat Gülkan, and Baris Binici. 2017. "Experimental Evaluation of the In-Plane Behaviour of Masonry Wall Infilled RC Frames." *Bulletin of*

Earthquake Engineering 15 (10): 4245–67. <https://doi.org/10.1007/s10518-017-0139-1>.

Tanjung, Jafril, Febrin Anas Ismail, Maidiawati, and Rudiansyah Putra. 2020. “A Simple Method for Strengthening the Brick Masonry Infilled in the Reinforced Concrete Frame Structure.” *International Journal of GEOMATE* 18 (66): 118–23. <https://doi.org/10.21660/2020.66.9488>.

Tasligedik, Ali Sahin, and Stefano Pampanin. 2017. “Rocking Cantilever Clay Brick Infill Wall Panels: A Novel Low Damage Infill Wall System.” *Journal of Earthquake Engineering* 21 (7): 1023–49. <https://doi.org/10.1080/13632469.2016.1190797>.

Tasnimi, A. A., and A. Mohebkah. 2011. “Investigation on the Behavior of Brick-Infilled Steel Frames with Openings, Experimental and Analytical Approaches.” *Engineering Structures* 33 (3): 968–80. <https://doi.org/10.1016/j.engstruct.2010.12.018>.

Tawfik Essa, Ahmed Sayed Ahmed, Mohamed Ragai Kotp Badr, and Ashraf Hasan El-Zanaty. 2014. “Effect of Infill Wall on the Ductility and Behavior of High Strength Reinforced Concrete Frames.” *HBRC Journal* 10 (3): 258–64. <https://doi.org/10.1016/j.hbrcj.2013.12.005>.

TBDY. 2018. *Türkiye Bina Deprem Yönetmeliği*. Ankara: Çevre ve Şehircilik Bakanlığı.

Teguh, Mochamad. 2017. “Experimental Evaluation of Masonry Infill Walls of RC Frame Buildings Subjected to Cyclic Loads.” *Procedia Engineering* 171: 191–200. <https://doi.org/10.1016/j.proeng.2017.01.326>.

Tekeli, H., and A. Aydin. 2017. “An Experimental Study of the Seismic Behavior of Infilled RC Frames with Opening.” *Scientia Iranica* 24 (5): 2271–82. <https://doi.org/10.24200/sci.2017.4150>.

Todorovic, Lana. 2019. “Out of Plane Seismic Performance of AAC Infill Walls with Openings.” Master of Science, Middle East Technical University.

Tsantilis, Aristomenis V., and Thanasis C. Triantafillou. 2018. “Innovative Seismic Isolation of Masonry Infills Using Cellular Materials at the Interface with the Surrounding RC Frames.” *Engineering Structures* 155 (November 2017): 279–97. <https://doi.org/10.1016/j.engstruct.2017.11.025>.

Tu, Yi Hsuan, Tsung Hua Chuang, Pai Mei Liu, and Yuan Sen Yang. 2010. “Out-of-Plane Shaking Table Tests on Unreinforced Masonry Panels in RC Frames.”

- Turgay, Tahsin, Meril Cigdem Durmus, Baris Binici, and Guney Ozcebe. 2014. “Evaluation of the Predictive Models for Stiffness, Strength, and Deformation Capacity of RC Frames with Masonry Infill Walls.” *Journal of Structural Engineering* 140 (10): 06014003. [https://doi.org/10.1061/\(asce\)st.1943-541x.0001069](https://doi.org/10.1061/(asce)st.1943-541x.0001069).
- Umar, Zeeshan, Syed Azmat Ali Shah, Tayyaba Bibi, Khan Shahzada, and Asfandyar Ahmad. 2021. “Innovative Seismic Isolation of Masonry Infills Using Cellular Material at the Interface with the Surrounding RC Frame.” *Journal of Building Engineering* 40 (May): 102736. <https://doi.org/10.1016/j.jobbe.2021.102736>.
- Van, Tze Che, and Tze Liang Lau. 2021. “Experimental Evaluation of Reinforced Concrete Frames with Unreinforced Masonry Infills under Monotonic and Cyclic Loadings.” *International Journal of Civil Engineering* 19 (4): 401–19. <https://doi.org/10.1007/s40999-020-00576-7>.
- Verderame, G. M., P. Ricci, C. del Gaudio, and M. T. de Risi. 2016. “Experimental Tests on Masonry Infilled Gravity- and Seismic-Load Designed RC Frames.” *Brick and Block Masonry: Trends, Innovations and Challenges - Proceedings of the 16th International Brick and Block Masonry Conference, IBMAC 2016*, 1349–58. <https://doi.org/10.1201/b21889-167>.
- Verderame, Gerardo M., Paolo Ricci, Maria Teresa De Risi, and Carlo Del Gaudio. 2019. “Experimental Assessment and Numerical Modelling of Conforming and Non-Conforming RC Frames with and without Infills.” *Journal of Earthquake Engineering* 00 (00): 1–42. <https://doi.org/10.1080/13632469.2019.1692098>.
- Verlato, N., G. Guidi, F. da Porto, and C. Modena. 2016. “Innovative Systems for Masonry Infill Walls Based on the Use of Rubber Joints: Finite Element Modelling and Comparison with in-Plane Tests.” *Brick and Block Masonry: Trends, Innovations and Challenges - Proceedings of the 16th International Brick and Block Masonry Conference, IBMAC 2016*, 1155–62. <https://doi.org/10.1201/b21889-144>.
- Vicente, Romeu Silva, Hugo Rodrigues, Humberto Varum, Anibal Costa, and José António Raimundo Mendes da Silva. 2012. “Performance of Masonry Enclosure Walls: Lessons Learned from Recent Earthquakes.” *Earthquake Engineering and Engineering Vibration* 11 (1): 23–34. <https://doi.org/10.1007/s11803-012-0095-3>.

- Walsh, Kevin, Dmytro Dizhur, Ivan Giongo, Hossein Derakhshan, and Jason Ingham. 2018. "Predicted Versus Experimental Out-of-Plane Force-Displacement Behaviour of Unreinforced Masonry Walls." *Structures* 15 (July): 292–306. <https://doi.org/10.1016/j.istruc.2018.07.012>.
- Walsh, Kevin Q., Dmytro Y. Dizhur, Jalil Shafaei, Hossein Derakhshan, and Jason M. Ingham. 2015. "In Situ Out-of-Plane Testing of Unreinforced Masonry Cavity Walls in as-Built and Improved Conditions." *Structures* 3: 187–99. <https://doi.org/10.1016/j.istruc.2015.04.005>.
- Wang, Fei, Kaozhong Zhao, Jianwei Zhang, and Kai Yan. 2021. "Influence of Different Types of Infill Walls on the Hysteretic Performance of Reinforced Concrete Frames." *Buildings* 11 (7): 1–18. <https://doi.org/10.3390/buildings11070310>.
- Wararuksajja, Wongsas, Jarun Srechai, and Sutat Leelataviwat. 2020. "Seismic Design of RC Moment-Resisting Frames with Concrete Block Infill Walls Considering Local Infill-Frame Interactions." *Bulletin of Earthquake Engineering*, no. 0123456789. <https://doi.org/10.1007/s10518-020-00942-9>.
- Wu, Jian, Li Dan Zhang, Qing Yu, and Bo Wang. 2020. "Out-of-Plane Shaking Table Tests on Seismic Response of RC Frame Infilled with a New Type of Shale Fired Heat-Insulation Blocks." *Advances in Materials Science and Engineering* 2020. <https://doi.org/10.1155/2020/5091707>.
- Xie, Xianxin, Zhe Qu, Haoran Fu, and Lingxin Zhang. 2021. "Effect of Prior In-Plane Damage on the out-of-Plane Behavior of Masonry Infill Walls." *Engineering Structures* 226 (September 2020): 111380. <https://doi.org/10.1016/j.engstruct.2020.111380>.
- Yoon, Rokhyun, Yasushi Sanada, and Takumi Akahori. 2017. "Seismic Performance Evaluation of RC Moment-Resisting Frames with Typical Non-Structural Walls in Japan." *Journal of Advanced Concrete Technology* 15 (9): 544–57. <https://doi.org/10.3151/jact.15.544>.
- Yorulmaz, M., and M. A Sozen. 1968. "Behavior of Single-Story Reinforced Concrete Frames with Filler Walls."
- Yu, You Sheng, Ya Nan Guo, and Can Mei. 2021. "Mechanical Behavior of CCA Wall Infilled Steel Frames with Preset Vertical Slits." *KSCE Journal of Civil Engineering* 25 (10): 3852–65. <https://doi.org/10.1007/s12205-021-2166-3>.
- Yuen, Terry Y.P., Han hui Zhang, J. S. Kuang, and Qunxian Huang. 2018. "Shake Table Tests on RC Frame Infilled by Slitted Masonry Panels." *Bulletin of*

- Earthquake Engineering* 16 (9): 4027–52. <https://doi.org/10.1007/s10518-018-0339-3>.
- Yuksel, E., H. Ozkaynak, O. Buyukozturk, C. Yalcin, A. A. Dindar, M. Surmeli, and D. Tastan. 2010. “Performance of Alternative CFRP Retrofitting Schemes Used in Infilled RC Frames.” *Construction and Building Materials* 24 (4): 596–609. <https://doi.org/10.1016/j.conbuildmat.2009.09.005>.
- Yuksel, E., and P. Teymur. 2011. “Earthquake Performance Improvement of Low Rise RC Buildings Using High Strength Clay Brick Walls.” *Bulletin of Earthquake Engineering* 9 (4): 1157–81. <https://doi.org/10.1007/s10518-010-9242-2>.
- Zahura, Fatema, Debasish Sen, Rishat Sabrin, Anik Das, M Jobaer Uddin, Zasiah Tafheem, Farzana Khanam, Hamood Alwashali, and Masaki Maeda. 2020. “In-Plane Seismic Performance of Masonry Infilled RC Frame with and without Ferrocement Overlay.” *17th World Conference on Earthquake Engineering*, no. September.
- Zarnic, R., and M. Tomazevic. 1985. “Study of the Behaviour of Masonry Infilled Reinforced Concrete Frames Subjected to Seismic Loading.” In *Proceedings of the 7th International Conference on Brick Masonry*, 1315–26. Melbourne.
- Žarnić, Roko, Samo Gostič, Adam J. Crewe, and Colin A. Taylor. 2001. “Shaking Table Tests of 1:4 Reduced-Scale Models of Masonry Infilled Reinforced Concrete Frame Buildings.” *Earthquake Engineering and Structural Dynamics* 30 (6): 819–34. <https://doi.org/10.1002/eqe.39>.
- Zhai, Changhai, Jingchang Kong, Xiaoming Wang, and Zhi Qiang Chen. 2016. “Experimental and Finite Element Analytical Investigation of Seismic Behavior of Full-Scale Masonry Infilled RC Frames.” *Journal of Earthquake Engineering* 20 (7): 1171–98. <https://doi.org/10.1080/13632469.2016.1138171>.
- Zhang, H H, and J S Kuang. 2014. “Shake Table Tests of Infilled Rc Frames With Different Column-To-Infill Connections.” In *2nd European Conference on Earthquake Engineering*, 1–10. İstanbul.
- Zovkic, Jurko, Vladimir Sigmund, and Ivica Guljas. 2013. “Cyclic Testing of a Single Bay Reinforced Concrete Frames with Various Types of Masonry Infill.” *Earthquake Engineering & Structural Dynamics*, no. 42: 1131–49. <https://doi.org/10.1002/eqe.2263>.

APPENDICES

A. Database of Previous Experimental Studies

Appendix A - Database of Previous Experimental Studies

#	Author	Dir.	Load	Scale	Brick Unit	Frame	# of tests	Major variables under study
1	Ockleston (1955)	IP	M	1/1	SCB	RC	2	Presence of infill
2	Polyakov (1956)	IP	M	1/2	SCB	S	5	Presence of infill
3	Benjamin & Williams	IP	M	1/1	SCB	S	24	Frame strength, aspect ratio, scaling, openings
4	Polyakov (1960)	IP	M	1/4		S	1	Presence of infill
5	Holmes (1961)	IP	M	1/1	CMU	S	13	Brick type, frame geometry
6	Carter & Smith (1967)	IP	M	1/2	SCB	S	1	Presence of infill
7	Yorulmaz & Sozen	IP	M	1/8	HCB	RC	10	Frame reinforcement ratio
8	Mainstone & Weeks	IP	M	1/1	SCB	S	6	Infill to frame strength
9	Fiorato (1971)	IP	M	1/8	HCB	RC	26	Frame reinforcement, vertical load,
10	Klingner & Bertero	IP	C	1/3	SCB, CMU	RC	4	Brick type
11	Leuchars & Scrivener	IP	M	1/2	HCB	RC	3	Vertical reinforcement of panel
12	Maio (1979)	IP	M	1/1	HCB	RC	5	Brick type, openings
13	Brokken & Bertero	IP	M+C	1/3	SCB, HCB, CMU	RC	18	Steel mesh overlay, brick units
14	Kwan (1982)	IP	M+C	1/8	WP	S	14	Interface connector, isolation gap,
15	Zarnic & Tomazevic	IP	C	1/2	SCB	RC	4	Horizontal reinforcement of panel
16	Govindan et al. (1986)	IP	C	1/4	SCB	RC	2	Presence of infill
17	Dawe & Seah (1989)	OOP	M _{AirB}	1/1	CMU	S	9	Boundary conditions, openings,
18	Pires (1991)	IP	C	2/3	HCB	RC	7	Frame reinf, confined masonry, steel
19	Altin et al. (1992)	IP	C	1/3	CWP	RC	14	Frame reinforcement, confined
20	Liauw & Kwan (1992)	IP	ShkT	1/3	SCB	RC	2	Presence of infill
21	Mander et al. (1993)	IP	C	1/1	SCB	S	4	Retrofit: Steel mesh overlay
22	Angel (1994)	IP+OOP	C+M _{AirB}	1/1	SCB, CMU	RC	8	Slenderness of wall, mortar & brick
23	Fowler (1994)	IP+OOP	ShkT	1/1	HCB	S	2	Presence of infill
24	Henderson (1994)	IP+OOP	C	1/1	CMU	S	2	Prior out-of-plane loading of frame
25	Mehrabi (1994)	IP	M+C	1/2	HCB, SCB	RC	14	Panel to frame strength, aspect ratio,
26	Pires & Carvalho	IP	C	1/1	HCB	RC	9	Openings, frame ductility, confined

Appendix A (continued)- Database of Previous Experimental Studies

#	Author	Dir.	Load	Scale	Brick Unit	Frame	# of tests	Major variables under study
27	Haider (1995)	IP	C	1/1.2	HCB	RC	6	Panel to frame strength, aspect
28	Khalid M.A. Mosalam (1996)	IP	C+PsD	1/3	HCB	S	6	Wall strength, openings, # of bays
29	Negro and Verzeletti (1996)	IP	PsD	1/1	HCB	RC	3	Infill pattern (i.e. soft story)
30	Crisafulli (1997)	IP	C	3/4	SCB	RC	2	Tapered frame joint
31	Al-chaar (1998)	IP	M	1/2	SCB+CMU	RC	5	Number of bays, brick type
32	Buonopane and White (1999)	IP	PsD	1/2	CMU	RC	1	Intensity of loading
33	Chiou, Tzeng, and Liou (1999)	IP	M	1/1	SCB	RC	3	Openings
34	Fardis et al. (1999)	IP+OOP	ShkT	1/1	HCB	RC	2	Infill pattern
35	Flanagan and Bennett (1999)	IP	C	1/1.2	HCB	S	9	Panel to frame strength, wall thickness
36	Murty and Jain (2000)	IP	C	1/2.7	SCB	RC	12	Horizontal reinforcement, brick scale
37	Calvi and Bolognini (2001)	IP+OOP	C+M4pt	1/1	HCB	RC	9	Mesh overlay and horizontal reinf.
38	Žarnić et al. (2001)	IP+OOP	ShkT	1/4	SCB	RC	2	# of story, plan geometry
39	Dolšek and Fajfar (2001)	IP	PsD	1/1	HCB	RC	1	Ground motion intensity
40	Lee and Woo (2002)	IP	ShkT	1/5	SCB	RC	2	Infill pattern
41	Al-Chaar et al. (2003)	IP	C	1/2	CMU	RC	2	Openings
42	El-Dakhkhid et al. (2003)	IP	C	1/1	CMU	S	6	FRP strengthening, openings
43	Ozcebe et al. (2004)	IP	C	1/3	HCB	RC	7	FRP strengthening, connection detail
44	Cavaleri et al. (2005)	IP	C	1/2	SCB, HCB	RC	10	Isolation joint, wall type, tapered joint
45	Colangelo (2005)	IP	PsD	1/2	HCB	RC	13	Frame aspect ratio, reinforcement ratio
46	Crisafulli et al. (2005)	IP	C	3/4	SCB	RC	2	Panel to frame strength
47	Saatcioglu et al. (2005)	IP	C	1/2	CMU	RC	2	FRP strengthening
48	Acun and Sucuoglu (2006)	IP	C	1/2	HCB	RC	4	FRP strengthening, plaster strength
49	Hashemi and Mosalam (2006)	IP	ShkT	3/4	SCB	RC	1	Presence of infill
50	Aliaari and Memari (2007)	IP	M	1/4	SCB	S	11	Isolation gap with fuse elements
51	Almusallam & Al-Salloum	IP	C	1/1.7	CMU	RC	3	FRP strengthening
52	Bergami (2007)	IP	C	1/2	HCB	RC	3	Mortar type

Appendix A (continued)- Database of Previous Experimental Studies

#	Author	Dir.	Load	Scale	Brick Unit	Frame	# of tests	Major variables under study
53	Griffith et al. (2007)	OOP	CAirB	1/1	SCB	RC	8	Openings, precompression
54	Altin et al. (2008)	IP	C	1/3	HCB	RC	10	FRP strengthening, arrangement type
55	Centeno et al. (2008)	IP	M+ShkT	1/2	CMU	RC	2	Load type (dynamic vs static)
56	Della Corte et al. (2008)	IP	C	1/1	SCB	RC	2	FRP strengthening, real building test
57	Kakaletsis&Karayannis(IP	C	1/3	HCB	RC	7	Brick type, openings
58	Penna et al. (2008)	IP	C	1/1	ACB	RC	5	Horizontal reinf. of panel, tie beam
59	Imran and Aryanto (2009)	IP	C	1/2	SCB-ACB	RC	2	Brick type
60	Stavridis (2009)	IP	C+ShkT	2/3	SCB	RC	5	Openings
61	Baran and Sevil (2010)	IP	C	1/3	HCB	RC	9	Number of story, axial load ratio
62	Pujol and Fick (2010)	IP	C	1/1	SCB	RC	2	Presence of infill
63	Tu et al. (2010)	OOP	ShkT	1/1	SCB	RC	4	Confined infill, slenderness
64	Yuksel et al. (2010)	IP	C	1/3	HCB	RC	6	FRP strengthening
65	Akin et al. (2011)	IP	C	1/3	HCB	RC	8	FRP strengthening, aspect ratio
66	Asteris et al. (2011)	IP	C	1/3	SCB	RC	10	Openings
67	Kakaletsis et al. (2011)	IP	C	1/3	HCB	RC	3	Brick type, repair
68	Komaraneni et al. (2011)	IP+OOP	C+ShkT	1/2	SCB	RC	3	Slenderness ratio, tie beam and column
69	Kurt et al. (2011)	IP	PsD	1/2	HCB	RC	1	Intensity of earthquake
70	Lunn and Rizkalla (2011)	OOP	M	1/1	SCB	RC	14	Aspect ratio, FRP strengthening, # of whytes
71	Ming et al. (2011)	OOP	ShkT	1/3	CMU	RC	2	Connection detail (i.e. wedge brick vs tie bar)
72	Mohammadi et al. (2011)	IP	C	2/3	SCB	S	6	Retrofit (cornerless infill, hor. sliding joint)
73	Orden et al. (2011)	IP	C	1/3	HCB	RC	5	FRP strengthening, arrangement type
74	Pereira et al. (2011)	IP+OOP	C+C4pt	1/15	HCB	RC	3	Presence of plaster, mesh and horizontal reinf.
75	Stavridis et al. (2011)	IP	ShkT	2/3	SCB	RC	1	Ground motion intensity
76	Tasnimi & Mohebbkhal	IP	C	1/15	SCB	S	6	Openings
77	Yuksel and Teymur (2011)	IP	C	1/2	SCB	RC	3	Connection detail
78	Ju et al. (2012)	IP	C	4/5	CWP	S	4	Isolation gap

Appendix A (continued)- Database of Previous Experimental Studies

#	Author	Dir.	Load	Scale	Brick Unit	Frame	# of tests	Major variables under study
79	Liu and Soon (2012)	IP	M	1/3	CMU	S	11	Panel to frame strength, aspect ratio, openings
80	Misir et al. (2012)	IP	C	1/2	HCB	RC	3	Dry sliding joints
81	Preti et al. (2012)	IP	C	1/1	HCB+Adobe	S	5	Brick type, sliding joints
82	Stylianidis (2012)	IP	C	1/3	HCB	RC	38	Aspect ratio, frame reinf., axial load, mortar
83	Da Porto et al. (2013)	IP+OOP	C+M4pt	1/1	HCB	RC	7	Slenderness, steel and fiber mesh overlay
84	Koutromanos et al. (2013)	IP	ShkT	1/1.5	SCB	RC	1	Steel mesh overlay
85	Markulak et al. (2013)	IP	C	1/2	HCB+ACB	S	10	Brick type
86	Zovkic et al. (2013)	IP	C	1/2.5	HCB+ACB	RC	10	Brick type
87	Al-Nimry (2014)	IP	C	1/3	CMU	RC	5	Openings, axial load, tie members at interface
88	Cavaleri&Di Trapani	IP	C	1/1.5	SCB, HCB, CMU	RC	12	Panel to frame strength, brick type
89	Zhang and Kuang (2014)	IP	ShkT	1/3	SCB	RC	2	Isolation gap
90	Kyriakides &	IP	C	1/5	SCB	RC	4	External strengthening (i.e. ECC)
91	Mansouri et al. (2014)	IP	C	1/2	SCB	RC	6	Openings
92	Sigmund and Penava (2014)	IP	C	1/2.5	HCB	RC	10	Openings, tie columns
93	Sucuoglu & Siddiqui	IP	PsD	1/2	ACB	RC	2	Presence of infill
94	Tawfik Essa et al. (2014)	IP	C	1/2	HCB, CMU	RC	4	Brick type, wall thickness
95	Bergami and Nuti (2015)	IP	C	1/2	HCB	RC	3	Presence of infill
96	Chiou and Hwang (2015)	IP	C	1/1	SCB	RC	4	Aspect ratio, mortar strength
97	da Porto et al. (2015)	IP+OOP	C+M4pt	1/1	HCB	RC	8	TRM strengthening
98	Dehghani et al. (2015)	IP	C	1/2	SCB	RC	3	ECC overlay
99	Furtado et al. (2015)	IP+OOP	C+HC8pt	1/1	HCB	RC	3	Prior IP damage level
100	Jiang et al. (2015)	IP	C	1/1	ACB	RC	7	Isolation joint, tie column
101	Koutas et al. (2015)	IP	C	2/3	HCB	RC	2	TRM strengthening
102	Preti et al. (2015)	IP+OOP	C+HC8pt	1/1	HCB	S	2	Openings on retrofitted panel
103	Schwarz (2015)	IP	C	1/2	ACB	RC	9	Aspect ratio, confined masonry, prestress
104	Walsh et al. (2015)	OOP	M	1/1	SCB	RC	10	Boundary conditions, ties between wythes

Appendix A (continued)- Database of Previous Experimental Studies

#	Author	Dir.	Load	Scale	Brick Unit	Frame	# of tests	Major variables under study
105	Akhoundi et al. (2016)	OOP	HCAirB	1/1.5	HCb	RC	3	Workmanship, openings
106	Aykac et al. (2016)	IP	C	1/2	HCb	RC	14	Steel plate overlay, column axial load, tie
107	Basha and Kaushik (2016)	IP	C	1/2	SCB	RC	8	Frame ductility, brick scale
108	Bob et al. (2016)	IP	C	1/2	HCb,CMU, ACB	RC	6	Brick type, tie connection to frame
109	Bose and Rai (2016)	IP	C	1/2.5	ACB	RC	2	Presence of infill
110	Erol and Karadogan (2016)	IP	C	1/2	HCb	RC	5	FRP strengthening
111	Furtado et al. (2016a)	IP+OOP	C+HCAirB	1/1	HCb	RC	3	Prior in-plane damage
112	Gazic and Sigmund (2016)	IP	C	1/2	HCb, SCB	RC	14	Frame reinf., column size, wall materials
113	Huang et al. (2016)	IP	C	1/2	CMU,SCB, ACB	RC	5	Brick type
114	Jin et al. (2016)	IP	C	1/4	CMU	RC	4	Beam strength, strain distribution on infill
115	Khoshnoud&Marsono	IP	M	1/4	SCB	RC	2	Panel compression corner cut
116	Kumar et al. (2016)	IP	C	1/1	CMU	RC	3	Presence of infill
117	Lin et al. (2016)	IP	C	1/1	SCB	RC	2	Horizontal slip joints (i.e. dry joint)
118	Loureço et al. (2016)	IP+OOP	ShkT	1/1.5	HCb	RC	3	Mesh overlay, horizontal reinforcement
119	Misir et al. (2016)	IP+OOP	C+M4pt	1/1.2	HCb, CMU, ACB	RC	6	Number of whytes, brick type
120	Moşoarcă et al. (2016)	OOP	C	1/1	HCb	S	3	Fiber mesh overlay
121	Pallarés and Pallarés (2016)	IP	C	1/1.5	HCb	S	7	Isolation joint (isolator bricks)
122	Silva et al. (2016)	IP+OOP	C+HCAirB	1/1.5	HCb	RC	4	Vertical reinforcement
123	Verderame et al. (2016)	IP	C	1/2	HCb	RC	4	Frame ductility
124	Verlato et al. (2016)	IP+OOP	C+M8pt	1/1	HCb	RC	4	Horizontal sliding joint, opening
125	Zhai et al. (2016)	IP	C	1/1	CMU	RC	4	Openings
126	Kassem et al. (2017)	IP	M	1/2	HCb	RC	6	FRP strengthening
127	Maidiwati & Sanada	IP	C	1/2.5	SCB	RC	4	Brick scale, presence of plaster
128	Preti and Bolis (2017)	IP+OOP	C+HC8pt	1/1	HCb	S	4	Vertical splitting of infill
129	Su and Cai (2017)	IP	C	1/1	HCb	RC	3	Openings
130	Suzuki et al. (2017)	IP	C	1/4	CMU	RC	5	Stacking pattern, # of bays/stories

Appendix A (continued)- Database of Previous Experimental Studies

#	Author	Dir.	Load	Scale	Brick Unit	Frame	# of tests	Major variables under study
131	Tasligedik& Pampanin	IP	C	1/1	SCB	RC	3	Vertical splitting of infill
132	Teguh (2017)	IP	C	1/1	SCB+	RC	3	Tie beam and column, brick type
133	Tekeli and Aydin (2017)	IP	C	1/3	HCB	RC	10	Openings
134	Yoon et al. (2017)	IP	C	1/2.5	CWP	RC	3	Isolation joint
135	Akhoundi et al. (2018)	IP	C	1/1.8	HCB	RC	7	TRM strengthening, workmanship
136	Alwashali et al. (2018)	IP	C	1/2	SCB	RC	2	Panel to frame strength
137	BenaventCliment et al. (2018)	IP	ShkT	1/2.5	SCB	RC	2	Intensity of ground motion
138	Dautaj et al. (2018)	IP	C	2/3	HCB+SCB	RC	8	Panel to frame strength, brick type
139	Dizhur et al. (2018)	OOP	HCAirB	1/1	SCB	RC	19	In-situ testing
140	Facconi et al. (2018)	IP	C	1/1	HCB	RC	3	Fiber mesh overlay
141	Furtado et al. (2018)	IP	ShkT	1/2.5	CB	RC	1	Ground motion intensity
142	Kaya et al. (2018)	IP	C	1/3	HCB	RC	11	Steel mesh overlay, connection details
143	Leenansaksiri et al. (2018)	IP	C	1/1	SCB	RC	3	Steel mesh overlay
144	Maidiawati et al. (2018)	IP	C	1/2.5	SCB	RC	2	Presence of infill
145	Morandi et al. (2018b)	IP	C	1/1	HCB	RC	3	Sliding joints, openings
146	Morandi et al. (2018)	IP+OOP	C	1/1	HCB	RC	3	Openings
147	Onat et al. (2018)	IP+OOP	ShkT	1/1	HCB	RC	2	Bed joint reinforcement
148	Palieraki et al. (2018)	IP+OOP	C+HC6pt	1/1	HCB	RC	3	Prior in-plane damage
149	Peng et al. (2018)	IP	C	1/2	CMU	RC	5	Isolation joint, tie column
150	Ricci et al. (2018b)	IP+OOP	C+M4pt	2/3	HCB	RC	8	Prior in-plane damage, slenderness
151	Ricci et al. (2018)	IP+OOP	C+M4pt	2/3	HCB	RC	3	Prior in-plane damage level
152	Seki et al. (2018)	IP	C	1/2	SCB	RC	5	Steel mesh overlay, timber framed panel
153	Tsantilis&Triantafillou	IP	C	1/3	HCB	RC	5	Isolation joint, openings
154	K. Walsh et al. (2018)	OOP	MAirB	1/1	SCB	RC	19	Boundary conditions, geometry, infill strength
155	Yuen et al. (2018)	IP	ShkT	1/3	SCB	RC	5	Isolation joint, steel ties, vertical split
156	Alwashali et al. (2018)	IP	C	1/2	SCB	RC	3	Column, beam and mortar strength

Appendix A (continued)- Database of Previous Experimental Studies

#	Author	Dir.	Load	Scale	Brick Unit	Frame	# of tests	Major variables under study
157	Basha and Kaushik (2019)	IP	C	1/2	SCB	RC	7	Column dimension, brick type, tie beam
158	Binici et al. (2019)	IP+OOP	C+MAirB	1/2	HCB	RC	6	Prior in-plane damage, isolation joint
159	Butenweg et al. (2019)	IP+OOP	C+MAirB	1/1	HCB	RC	4	Loading sequence, boundary conditions
160	Cai and Su (2019)	IP	C	1/1	HCB, ACB	RC	4	Brick type
161	Dautaj et al. (2019)	IP	C	2/3	HCB	RC	5	Horizontal slip joint, panel to frame strength
162	De Risi et al. (2019)	IP+OOP	C+M4pt	2/3	HCB	RC	4	Prior in-plane damage level
163	Di Domenico (2019)	OOP	M4pt	2/3	HCB	RC	4	Wall thickness, boundary conditions
164	Koutas and Bournas (2019)	OOP	M4pt	1/1	SCB	RC	6	Number of whytes, TRM overlay
165	Maidiawati et al. (2019)	IP	C	1/4	SCB	RC	6	Openings, horizontal reinf. of panel
166	Marinković&Butenweg(IP+OOP	C+HCAirB	1/1	HCB	RC	4	Isolation gap
167	Pantò et al. (2019)	OOP	AirB	2/3	HCB	RC	4	Vertical and horizontal steel ties
168	Sagar et al. (2019)	IP+OOP	C+ShKT	1/2	SCB	RC	6	Fiber mesh overlay, prior IP damage
169	Shah et al. (2019)	IP+OOP	ShKT	1/2	SCB	RC	1	Intensity of ground motion
170	Verderame et al. (2019)	IP	C	1/2	HCB	RC	4	Frame ductility
171	Akhoundi et al. (2020)	IP+OOP	C+HCAirB	1/2	HCB	RC	6	Previous IP damage, openings, # of whytes
172	Alwashali et al. (2020)	IP	C	1/2	SCB	RC	2	Steel mesh overlay
173	Arslian et al. (2020)	IP	C	1/2	HCB,ACB,CMU	S	9	Brick type, presence and thickness of plaster
174	da Porto et al. (2020)	IP+OOP	C+M4pt	1/1	HCB	RC	9	Prior IP damage, openings, panel reinf.
175	Di Domenico (2020)	OOP	M4pt	2/3	HCB	RC	3	Boundary conditions
176	Facconi and Minelli (2020)	IP	C	1/1	HCB	RC	4	TRM strengthening, connection to frame
177	Furtado et al. (2020a)	OOP	HCAirB	1/1	HCB	RC	2	Boundary conditions, column axial load
178	Guljaš et al. (2020)	IP+OOP	ShKT	1/2.5	HCB, SCB	RC	2	Brick type, tie columns
179	Minotto et al. (2020)	IP+OOP	C+M8pt	1/1	HCB	RC	8	TRM strengthening
180	Tanjung et al. (2020)	IP	C	1/4	SCB	RC	4	Fiber and steel mesh overlay
181	Wararuksaja (2020)	IP	C	1/1	CMU	RC	2	Frame reinforcement
182	Wu et al. (2020)	OOP	ShKT	1/1	HCB	RC	4	Isolation joint, tie beam

Appendix A (continued)- Database of Previous Experimental Studies

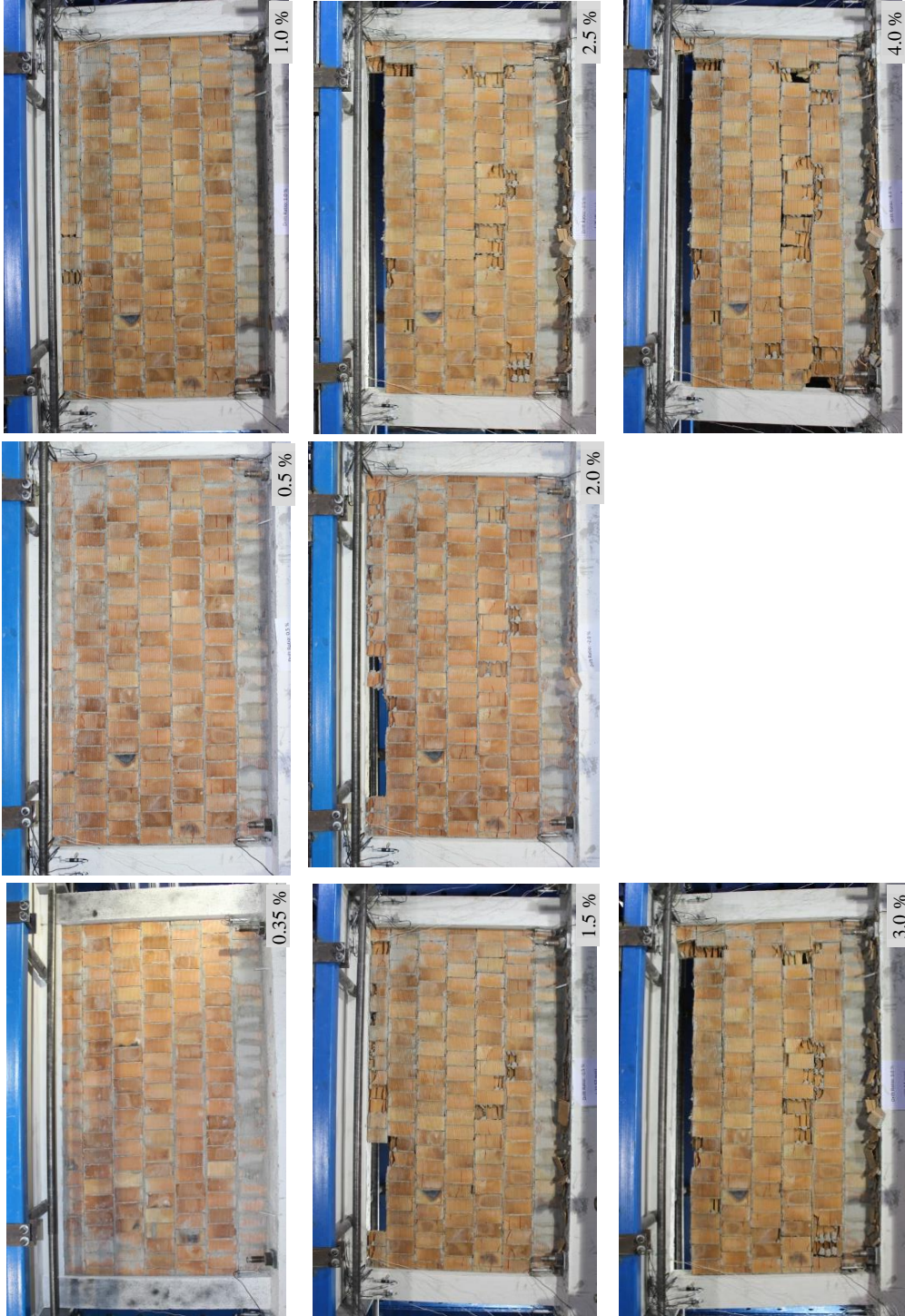
#	Author	Dir.	Load	Scale	Brick Unit	Frame	# of tests	Major variables under study
183	Zahura et al. (2020)	IP	C	1/2	SCB	RC	2	Steel mesh overlay
184	Anic et al. (2021)	OOP	C	1/2	HCB	RC	6	Openings
185	Bikçe et al. (2021)	IP	C	2/3	ACB	RC	3	Isolation joint
186	Cheng et al. (2021)	IP+OOP	ShkT	1/5	SCB	RC	2	Intensity of ground motion
187	Di Domenico et al. (2021)	IP+OOP	C+M4pt	2/3	HCB	RC	3	Prior in-plane damage level
188	Di Sarno et al. (2021)	IP	PsD	3/4	HCB	S	1	Presence of infill
189	Erdem et al. (2021)	IP	C	2/3	ACB	RC	5	Isolation joint
190	Furtado et al. (2021)	OOP	HC28pt	1/1	HCB	RC	5	TRM strengthening, prior in-plane damage
191	Furtado et al. (2021)	IP+OOP	HC22pt	1/1	HCB	RC	3	Prior in-plane damage, openings
192	Furtado et al. (2021)	IP+OOP	HC28pt	1/1	HCB	RC	4	Prior IP damage, workmanship
193	Jin et al. (2021)	IP	C	2/3	SCB	RC	4	Sliding joints
194	Gao (2021)	IP+OOP	C+M4pt	1/2	SCB	RC	6	Isolation joint, tie column
195	Kasapgil et al. (2021)	IP+OOP	C+MAirB	1/2	ACB	RC	8	OOP load ratio, insulation panel overlay
196	Khelifi et al. (2021)	IP	C	3/4	SCB	RC	2	Tapered beam-column joint
197	Lu and Zha (2021)	IP	C	1/1	CMU	RC	2	Resilient infill (vertical splitting)
198	Milanesi et al. (2021)	OOP	HC16pt	1/1	HCB	RC	2	Boundary conditions, load type
199	Milijaš et al. (2021)	OOP	HCAirB	1/1	HCB	RC	2	Brick type, boundary conditions
200	Pachappoyl&Agarwl	IP+OOP	C+CAirB	1/1	SCB, CMU	RC	6	Energy dissip. device, openings, brick type
201	Pallarés et al. (2021)	IP	C	1/1	HCB	RC	2	Presence of infill
202	Roosta and Liu (2021)	IP	M+C	1/3	CMU	RC	4	Isolation gap, openings
203	Santarsiero et al. (2021)	IP	C	1/1	HCB	RC	4	Presence of infill, prior IP damage
204	Sen et al. (2021)	IP	C	1/2	SCB	RC	2	Steel mesh overlay, mesh reinf. ratio
205	Shah et al. (2021)	IP	C	1/1	SCB	RC	4	Openings
206	Shah et al. (2021)	IP	C	1/1	SCB	RC	2	Presence of infill
207	Umar et al. (2021)	IP	C	1/1	SCB	RC	2	Isolation joint
208	Van and Lau (2021)	IP	M+C	1/2	SCB	RC	6	Load type, aspect ratio

Appendix A (continued)- Database of Previous Experimental Studies

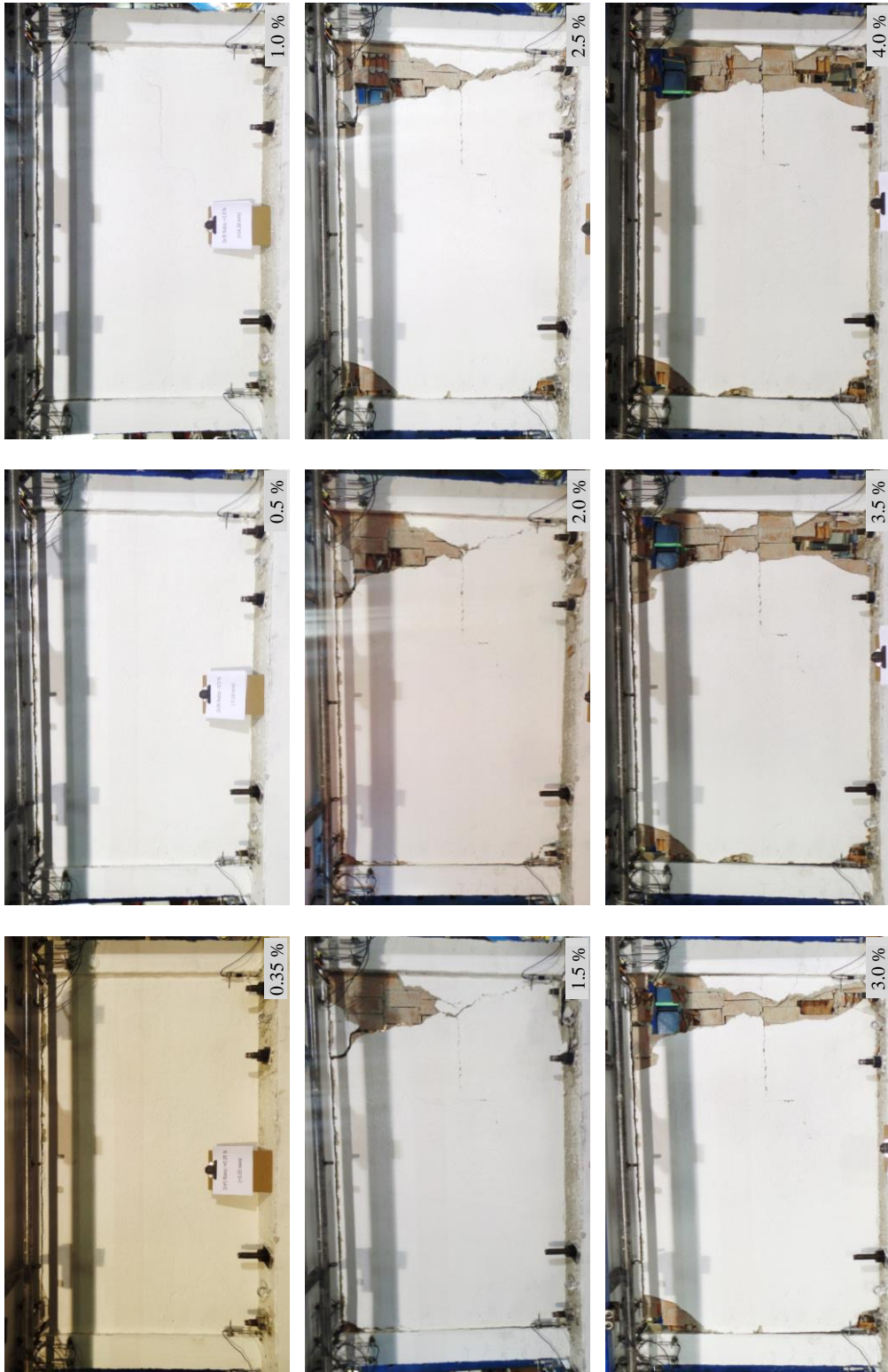
#	Author	Direction	Load	Scale	Brick Unit	Frame	# of tests	Major variables under study
209	Wang et al. (2021)	IP	C	1/2	HCB, ACB	RC	3	Brick type
210	Xie et al. (2021)	IP+OOP	C+MAirB	1/1	CMU	RC	7	Prior in-plane damage level, tie bars
211	Yu, Guo et al. (2021)	IP	C	1/2	WP	S	4	Vertical splitting of panel
212	Aydin et al. (2022)	IP	C	1/2	ACB	RC	2	Openings
213	Souza et al., 2022	IP	C	2/3	HCB, WP	RC	3	Strengthening with wall panels
214	Milanesi et al. (2022)	IP+OOP	ShkT	1/1	HCB	RC	2	Sliding joints, openings

B. Infill Damage vs Drift for Frame Specimens Tested under IP Load

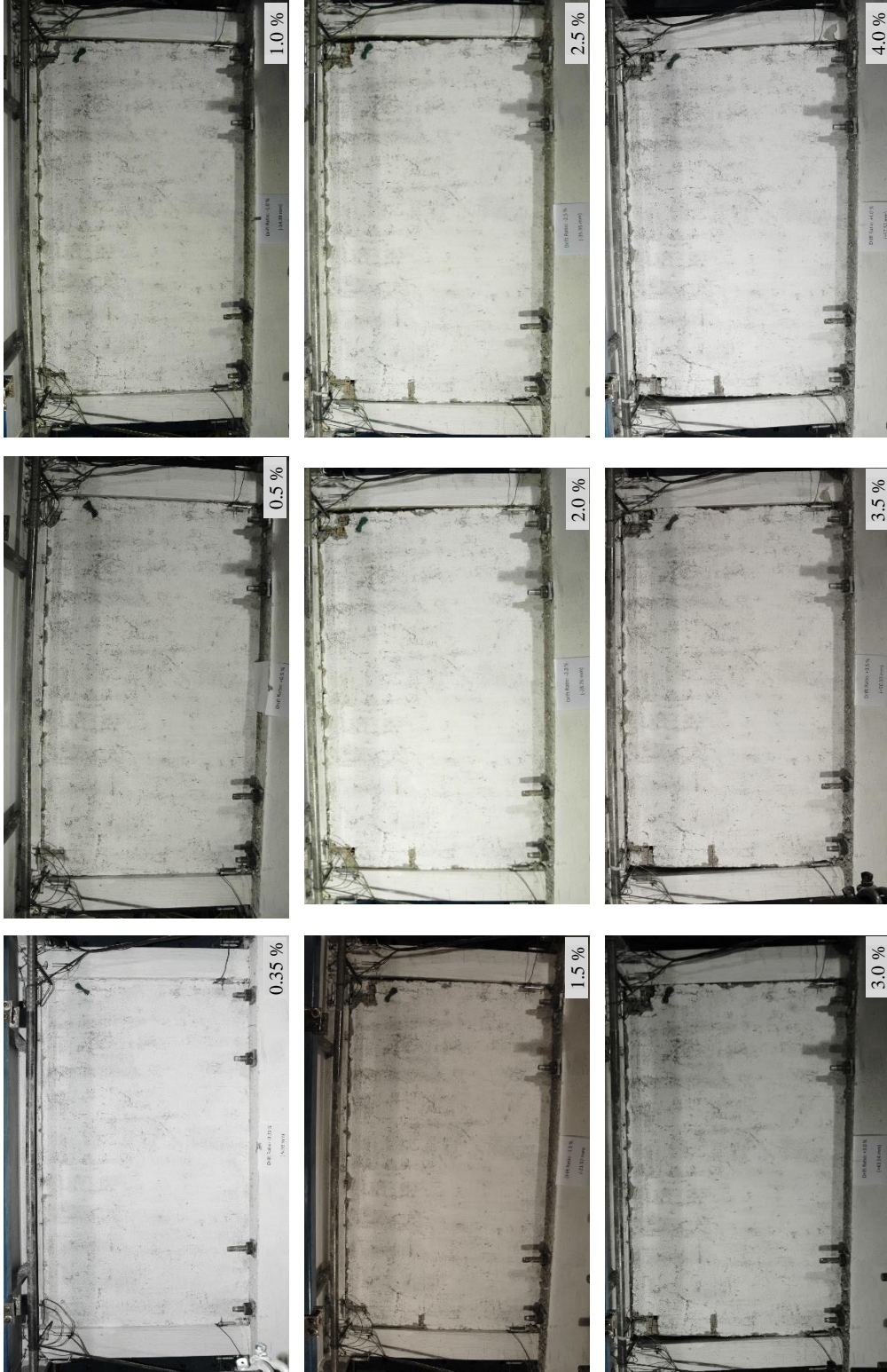
B.1. Hollow Clay Brick Infilled Frame (CB)



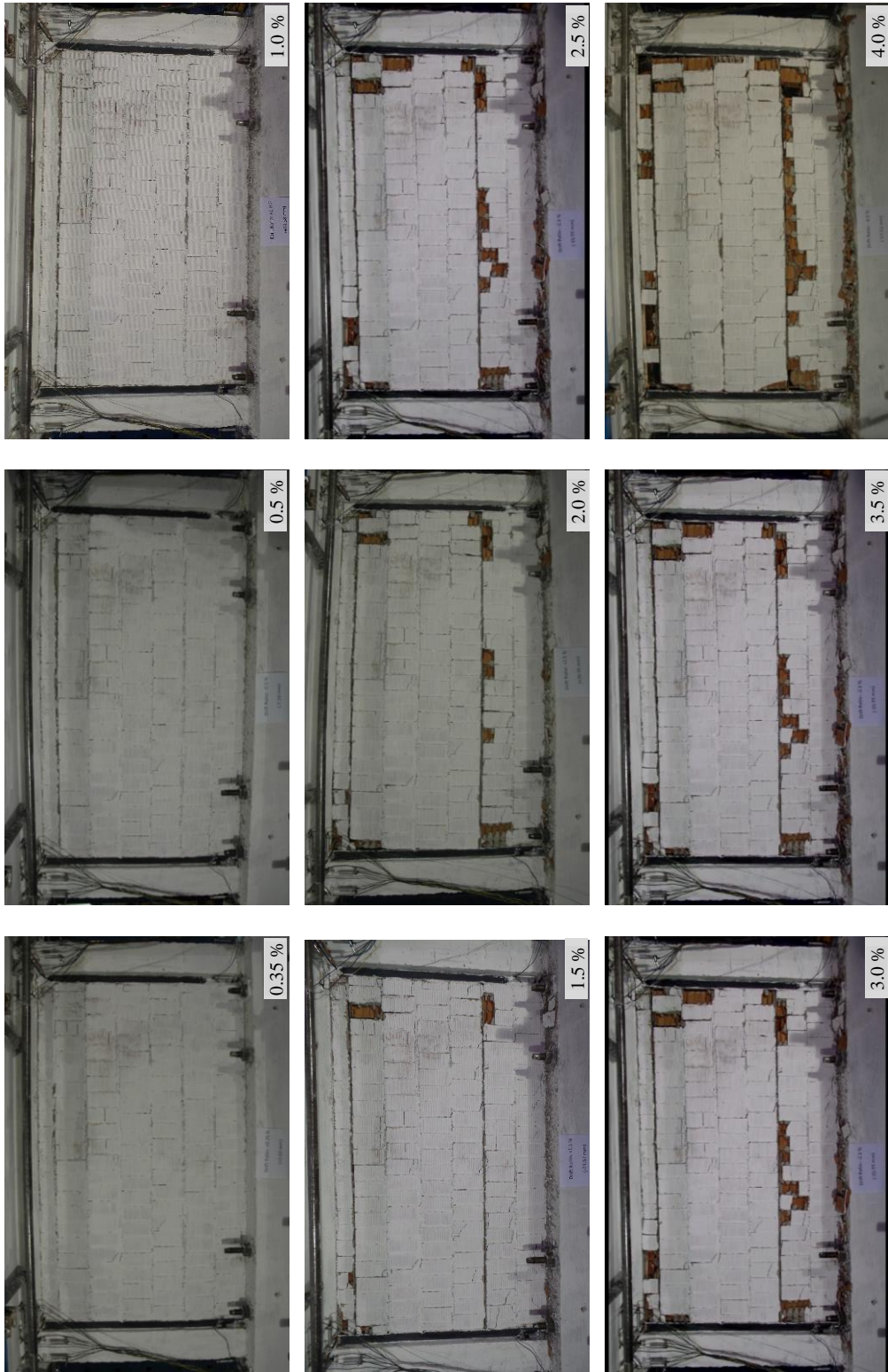
B.2. Hollow Clay Brick Infilled Frame with Plaster (CBP)



B.3. Hollow Clay Brick Infilled Frame with Bilateral Steel Mesh Reinforcement and Plaster (CBMR)



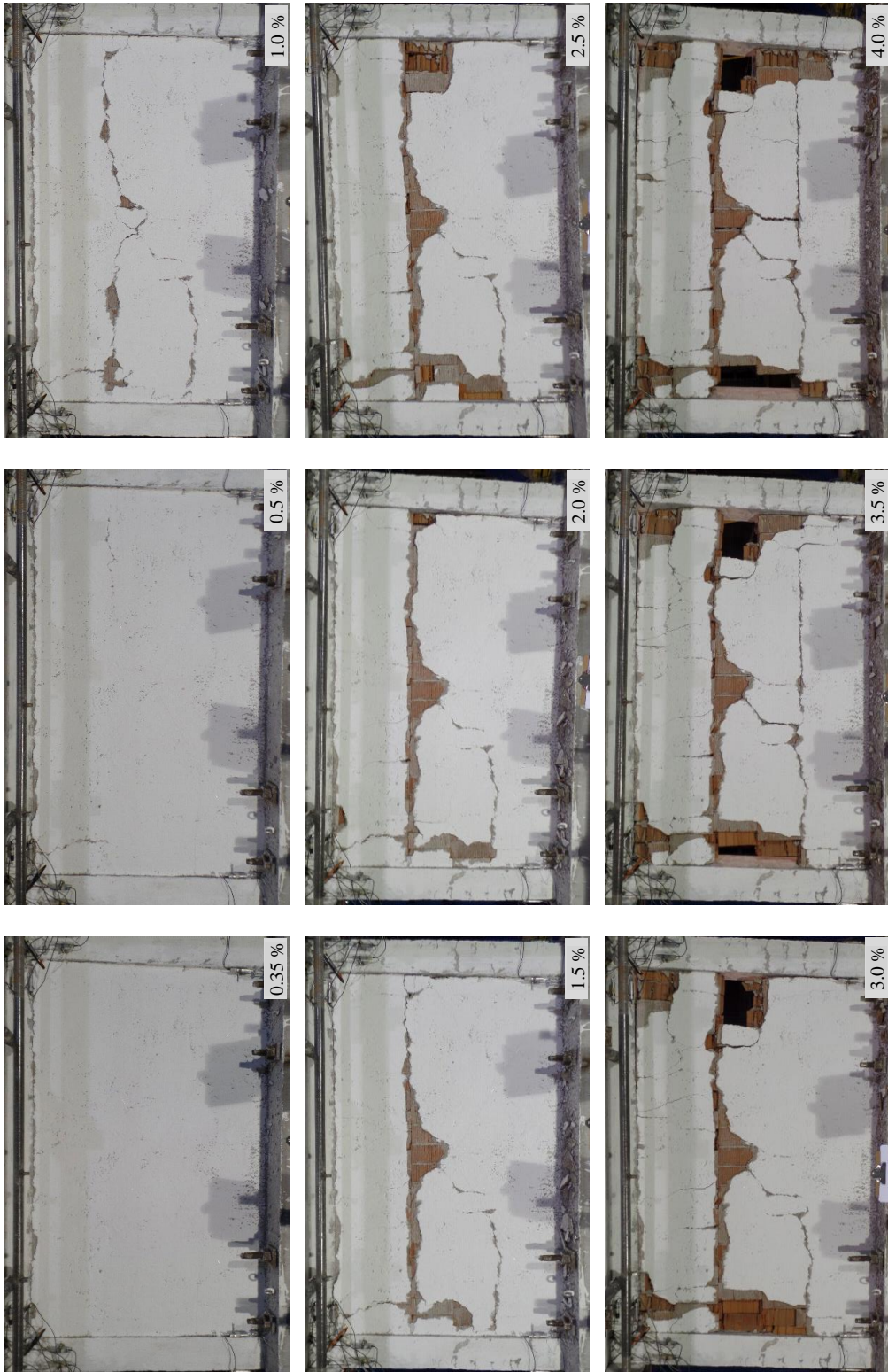
B.4. Hollow Clay Brick Infilled Frame with Continuous Horizontal Steel Ties (TieC)



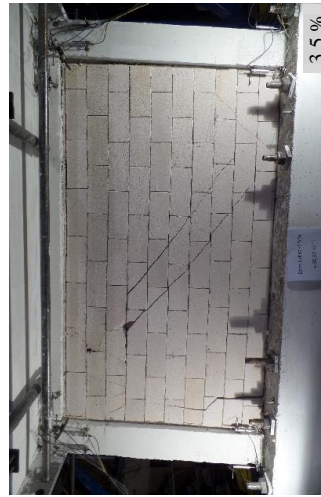
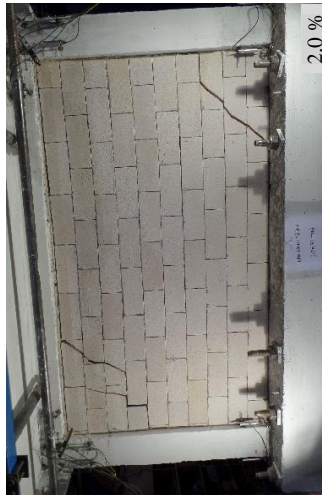
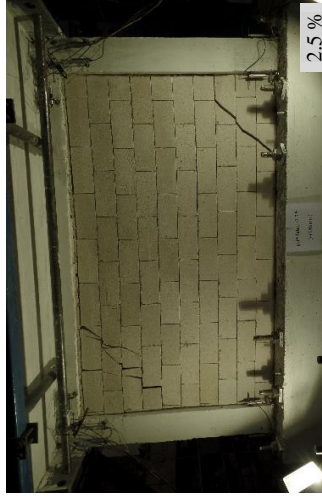
B.5. Hollow Clay Brick Infilled Frame with Staggered Horizontal Steel Ties (TieS)



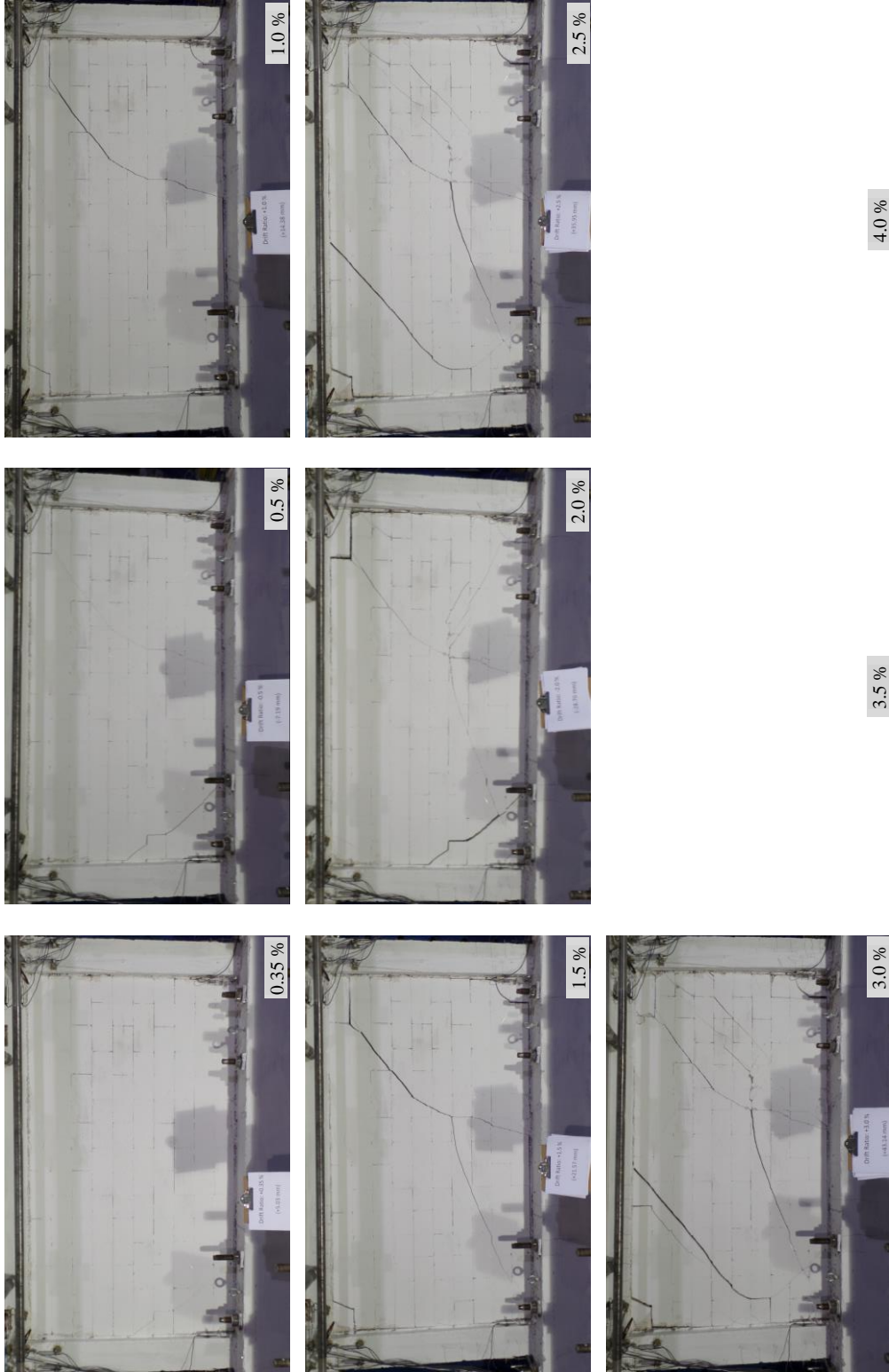
B.6. Locking Clay Brick Infilled Frame with Plaster (LBP)



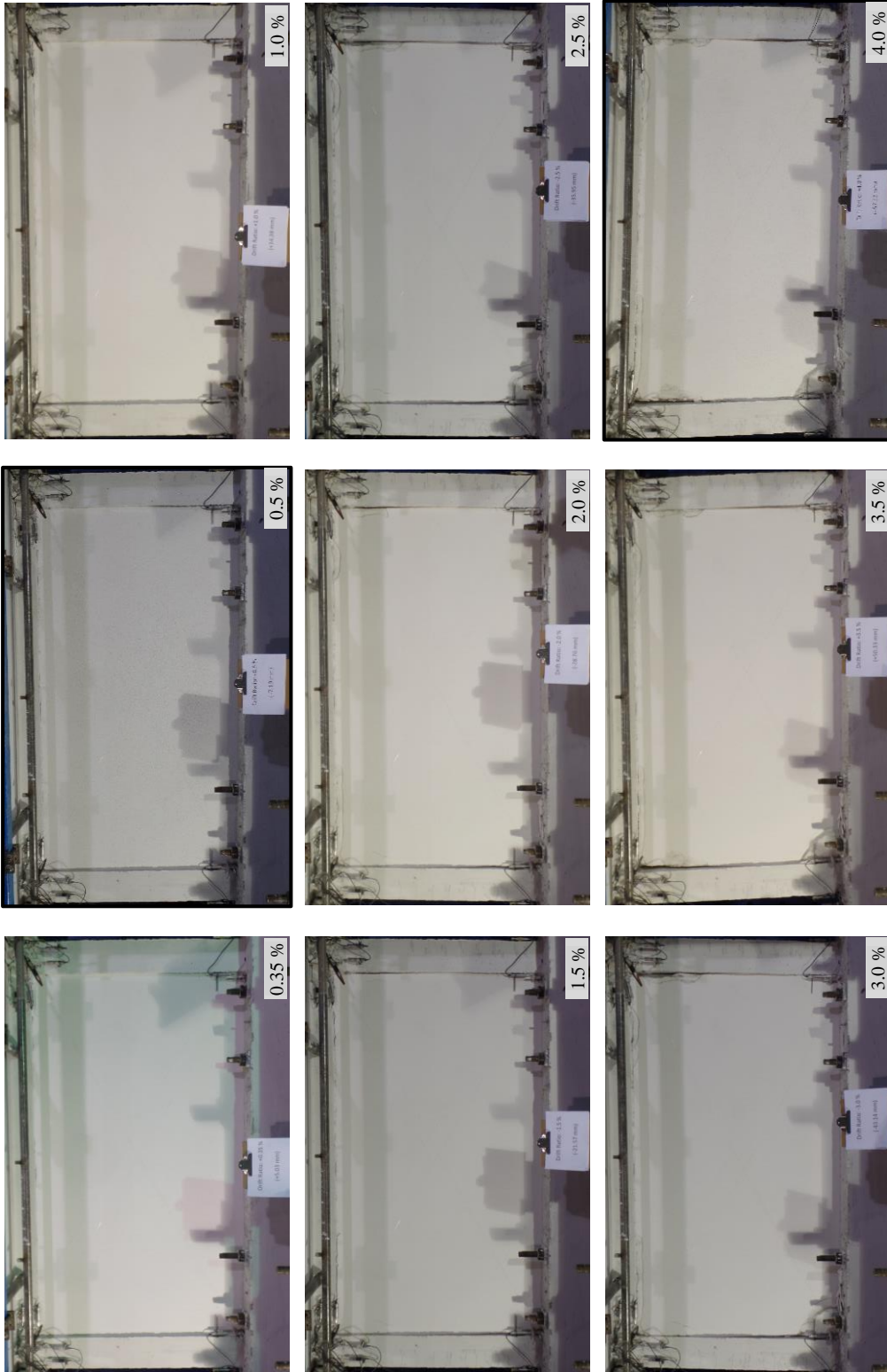
B.7. Aerated Concrete Block Infilled Frame with 2cm Isolation Joints at Contact Surfaces (ABI)



B.8. Aerated Concrete Block Infilled Frame with 2cm Isolation Joint under the Upper Beam (AB)



B.9. Aerated Concrete Block Infilled Frame with Fiber Reinforced Plaster (ABRP)



CURRICULUM VITAE

Surname, Name: Demirel, İsmail Ozan
E-mail: ismailozandemirel@gmail.com



EDUCATION

- 2011 - 2023 Middle East Technical University, Ph.D.
Title: Infilled Reinforced Concrete Frame
Performance Under Seismic Actions
Civil Engineering Department
Advisor: Prof. Ahmet Yakut
- 2007 - 2010 Middle East Technical University, M.Sc.
Title: A Nonlinear Equivalent Frame Model for
Displacement Based Analysis of Unreinforced
Brick Masonry Buildings
Civil Engineering Department
Advisor: Prof. Haluk Sucuoğlu
- 2003 - 2007 Middle East Technical University, B.A.
Civil Engineering Department
Structural Mechanics Division

EMPLOYMENT

- 2022 - 2023 Individual Structural Consultant
MoEUCC
SREEPB Project
- 2017 - 2023 Instructor
Bilkent University
Department of Architecture
- 2007 - 2017 Teaching Assistant
Middle East Technical University
Civil Engineering Department

RESEARCH INTERESTS

Simplified nonlinear modeling of unreinforced masonry buildings.

In-plane and out-of-plane testing of infilled reinforced concrete frames.

Seismic performance assessment and strengthening of RC and masonry structures.

Earthquake reconnaissance survey and building damage assessment.

Dry joint masonry arch bridges.

PUBLICATIONS

A. PEER-REVIEWED JOURNAL ARTICLES

1. Akkar, S., Aldemir, A., Askan, A., Bakir, S., Canbay, E., **Demirel, I. O.**, Erberik, M. A., Gulerce, Z., Gulkan, P., Kalkan, E., Prakash, S., Sandikkaya, M. A., Sevilgen, V., Ugurhan, B., Yenier, E., Gülerce, Z., Gülkan, P., Kalkan, E., Prakash, S., Yenier, E. (2011). 8 March 2010 Elazig-Kovancilar (Turkey) Earthquake: Observations on Ground Motions and Building Damage. *Seismological Research Letters*, 82(1), 42–58. <https://doi.org/10.1785/gssrl.82.1.42>
2. Aldemir, A., Erberik, M. A., **Demirel, I. O.**, & Sucuoglu, H. (2013). Seismic performance assessment of unreinforced masonry buildings with a hybrid modeling approach. *Earthquake Spectra*, 29(1). <https://doi.org/10.1193/1.4000102>
3. Yakut, A., & **Demirel, I. O.** (2013). Influence of Clay Tile Brick Infill Walls on Seismic Response of Buildings. *Advanced Materials Research*, 747, 273–276. <https://doi.org/10.4028/www.scientific.net/amr.747.273>
4. Cobanoglu, B., Aldemir, A., **Demirel, I. O.** I. O., Binici, B., Canbay, E., & Yakut, A. (2017). Seismic Performance Assessment of Masonry Buildings Using in Situ Material Properties. *Journal of Performance of Constructed Facilities*, 31(4), 04017033. [https://doi.org/10.1061/\(asce\)cf.1943-5509.0001030](https://doi.org/10.1061/(asce)cf.1943-5509.0001030)
5. **Demirel, İ. O.**, Yakut, A., & Binici, B. (2018). Dolgu Duvarların Düzlem Dışı Yönde Hava Yastığı ile Deneyi. *Anadolu Üniversitesi*

Bilim Ve Teknoloji Dergisi - B Teorik Bilimler, 6, 133–140.
<https://doi.org/10.20290/aubtdb.489940>

6. Binici, B., Canbay, E., Aldemir, A., **Demirel, I. O.**, Uzgan, U., Eryurtlu, Z., Bulbul, K., & Yakut, A. (2019). Seismic behavior and improvement of autoclaved aerated concrete infill walls. *Engineering Structures*, 193, 68–81. <https://doi.org/10.1016/j.engstruct.2019.05.032>
7. Todorovic, L., **Demirel, I. O.**, & Binici, B. (2020). Effect of openings on the seismic response of AAC infilled frames and an innovative method to improve performance. *International Journal of Masonry Research and Innovation*, 5(2), 226–247. <https://doi.org/10.1504/ijmri.2020.106333>
8. **Demirel, I. O.**, Yakut, A., Akyuz, U., Yigin, H., & Dikbayir, H. E. (2021). Kashiřskaya AVM Projesindeki Cam Korkulukların Detaylı İncelenmesi. *Teknik Dergi*, 10565–10576. <https://doi.org/10.18400/tekderg.569821>
9. **Demirel, I. O.**, & Aldemir, A. (2021). Simplified Approach for Seismic Performance Assessment of Dry-Joint Masonry Arch Bridges. *Buildings*, 11(7), 313. <https://doi.org/10.3390/buildings11070313>
10. Erduran, D. Ü., **Demirel, I. O.**, & Elias-ozkan, S. T. (2021). Kâgir duvar atıklarının yeniden kullanım için analizi. *Journal of the Faculty of Engineering and Architecture of Gazi University*, 36(4), 1923–1938. <https://doi.org/10.17341/gazimmfd.624512>
11. **Demirel, I.O.**, Yakut, A., Binici, B. (2022). Seismic Performance of Mid-rise Reinforced Concrete Buildings in Izmir Bayraklı after the 2020 Samos Earthquake. *Engineering Failure Analysis*, 137 (2022). <https://doi.org/10.1016/j.engfailanal.2022.106277>
12. **Demirel, I.O.**, Binici, B., Yakut, A. (2023). In-plane Seismic Performance of Different Infill Wall Systems in Ductile Reinforced Concrete Frames. *Bulletin of Earthquake Engineering* (2023). <https://doi.org/10.1007/s10518-023-01663-5>

B. CONFERENCE PRESENTATIONS (INTERNATIONAL)

1. **Demirel, I.O.**, Aldemir, A. and Erberik, M.A. (2012), “A New Computational Method for the Assessment of URM Buildings”, *10th International Congress on Advances in Civil Engineering*, 17 - 19 October, Ankara, Turkey.
2. Aldemir, A., Erdil, B., **Demirel, I.O.**, Yakut, A. and Binici, B. (2014), “Damage from Two Consecutive Earthquakes at City of Van (Turkey)”, *10th National Conference on Earthquake Engineering*, 21

– 25 July, Alaska, USA.

3. **Demirel, I.O.**, Aldemir, A., Yakut, A. and Binici, B. (2014). “Comparison of Analytical and Observed Damages on a Commercial RC Building”, *10th National Conference on Earthquake Engineering*, 21 – 25 July, Alaska, USA.
4. **Demirel, I.O.**, Yakut, A., Binici, B. and Canbay, E. (2015), “Experimental Investigation of Infill Behaviour in RC Frames”, *9th Pacific Conference on Earthquake Engineering*, 6-8 November, Sydney, Australia.
5. **Demirel, I.O.**, Yakut, A. and Binici, B. (2016), “Influence of Infill Wall System on Seismic Behavior of RC Frames”, *12th International Congress on Advances in Civil Engineering*, 21 - 23 September, İstanbul, Turkey.
6. **Demirel, I.O.**, Yakut, A. and Binici, B. (2016), “An Experimental Study on In-plane Seismic Performance of Infilled RC Frames”, *11th fib International PhD Symposium in Civil Engineering*, 29 - 31 August, Tokyo, Japan.
7. **Demirel, I.O.**, Yakut, A. and Binici, B. (2017), “Seismic Behaviour of RC Frames Infilled with Different Techniques”, *16th World Conference on Earthquake Engineering*, 9 - 13th January, Santiago, Chile.
8. **Demirel, I.O.**, Yakut, A. and Metin, H. (2017), “Infilled Frame Response Under Seismic Excitation”, *17th International Scientific Conference VSU'2017*, 8 - 9th June, Sofia, Bulgaria.
9. Binici, B., **Demirel, I.O.**, Aldemir, A., Canbay, E., Yakut, A. (2017), “Behaviour of AAC Infilled RC Frames under In Plane and Out of Plane Seismic Demands”, *Australian Earthquake Engineering Society 2017 Conference*, Nov 24-26, Canberra, Australia.
10. **Demirel, I.O.**, Yakut, A. and Binici, B. (2017), “Experimental Testing of Infill Walls In Out- of-Plane Direction with Airbag”, *4th International Earthquake Engineering and Seismology Conference*, 11-13th October 2017, Eskişehir, Türkiye.
11. **Demirel, I.O.**, Yakut, A., Binici, B. (2018) “Strengthening Infilled RC Frames Against Biaxial Seismic Action”, *12th fib International PhD Symposium in Civil Engineering*, 29- 31th August 2018, Prague, Czech Republic.
12. Binici, B., Canbay, E., Aldemir, A., **Demirel, I.O.**, Uzgan, U., Eryurtlu, Z., Bulbul, K., Yakut A. (2018) “Behavior of Autoclaved Aerated Concrete Infill Walls under combined In-Plane and Out-of-

Plane Actions”, *13th International Congress on Advances in Civil Engineering*, 12-14 September 2018, İzmir, Turkey.

13. Binici, B., Canbay, E., **Demirel, I.O.**, Aldemir, A., Uzgan, U., Eryurtlu, Z., Yakut A. (2018) “Seismic Response of Autoclaved Aerated Concrete Masonry Infill Walls under In-Plane and Out-of-Plane Seismic Demands”, *6th International Conference on Autoclaved Aerated Concrete*, 4-6 September 2018, Potsdam, Germany.
14. Canbay, E., Binici, B., **Demirel, I.O.**, Aldemir, A., Uzgan, U., Eryurtlu, Z., Bubul K. (2018) “DEGAS: An Innovative Earthquake Proof AAC Wall System”, *6th International Conference on Autoclaved Aerated Concrete*, 4-6 September 2018, Potsdam, Germany.
15. Binici, B., Canbay, E., Aldemir, A., **Demirel, I.O.**, Uzgan, U., Eryurtlu, Z., Yakut A. (2018) “An Innovative System for the Protection of Autoclaved Aerated Concrete Infill Walls Subjected to Seismic Demands”, *4th Australasia and South-East Asia Structural Engineering and Construction Conference*, 3-5 December 2018, Queensland, Australia.
16. **Demirel, I.O.**, Yakut, A. and Binici, B., Canbay, E. (2018), “Performance Based Limit States for Infill Walls in RC Frames”, *16th European Conference on Earthquake Engineering*, 18-21th June 2018, Thessaloniki, Greece.
17. Todorovic, L., **Demirel, I.O.**, Binici, B. (2019), “Effect of Openings on the Seismic Response of AAC Infilled Frames”, *5th International Earthquake Engineering and Seismology Conference*, 8-11th October 2019, Ankara, Türkiye.

C. CONFERENCE PRESENTATIONS (NATIONAL)

1. **Demirel, İ.O.**, Erberik, M.A. ve Sucuoğlu, H. (2011), “Tuğla Yığma Yapıların Performans Esaslı Değerlendirilmesi İçin Doğrusal Olmayan Çerçeve Modeli”, *1. Türkiye Deprem Mühendisliği ve Sismoloji Konferansı*, 11 - 14 Ekim, Ankara, Türkiye.
2. **Demirel, İ.O.**, Akansel, V.H., Bankir, Ş., Geneş, M.C., Erberik, M.A., Yakut, A. (2013), “Antakya'daki Yığma Binaların Özelliklerinin Deprem Performansı Açısından Analitik Olarak Değerlendirilmesi”, *2. Türkiye Deprem Mühendisliği ve Sismoloji Konferansı*, 25 – 27 Eylül, Hatay, Türkiye.
3. Yakut, A., Binici, B., **Demirel, İ.O.**, Özcebe, G. (2013), “Dolgu Duvarların Deprem Davranışına Etkisi”, *2. Türkiye Deprem Mühendisliği ve Sismoloji Konferansı*, 25 – 27, Hatay, Türkiye.

4. **Demirel, İ.O.**, Yakut, A., Binici, B., Canbay, E. (2015), “Betonarme Çerçeveselerde Dolgu Duvar Etkisinin İncelenmesi Üzerine Deneysel Çalışma”, 3. *Türkiye Deprem Mühendisliği ve Sismoloji Konferansı*, 14-16 Ekim, İzmir, Türkiye.
5. **Demirel, İ.O.**, Canbay, E., Binici, B., Yakut, A., Eryurtlu, Z. (2015), “Gazbeton Dolgulu Betonarme Çerçeveselerin Deprem Performansı Üzerine Deneysel Çalışma”, 3. *Türkiye Deprem Mühendisliği ve Sismoloji Konferansı*, 14-16 Ekim, İzmir, Türkiye.
6. Gülkan, P., Binici, B., Sucuoğlu, H., Taghipour, A., **Demirel, İ.O.**, Tanışer, S., Güneş, O., Ismail, M., Fehling, E., Nakano, Y., Sanada Y., Choi, H. (2015), “An Innovative Tie System for Improving the Monolithic Behavior of Masonry In-filled Reinforced Concrete Frames (INFILTIE)”, 3. *Türkiye Deprem Mühendisliği ve Sismoloji Konferansı*, 14-16 Ekim, İzmir, Türkiye.

BOOKS

Demirel, İ.O., (2011), “Equivalent Frame Approach for Nonlinear Modeling of Masonry Buildings; Basics, Verifications, Applications”, Lab Lambert Academic Publishing, ISBN: 978-3-8465-0420-8.

<https://www.lap-publishing.com/catalog/details/store/gb/book/978-3-8465-0420-8/equivalent-frame-approach-for-nonlinear-modeling-of-masonry-buildings>

POST-EARTHQUAKE RECONNAISSANCE REPORTS

1. Bakır, S., Canbay, E., Erberik, M.A., Gülerce, Z., Aldemir, A. ve **Demirel, İ.O.** (2010), “8 Mart 2010 Başyurt-Karakoçan (Elazığ) Depremi Ön İnceleme Raporu”, Rapor No: METU/EERC 2011-02, Deprem Mühendisliği Araştırma Merkezi, Orta Doğu Teknik Üniversitesi.
2. Yakut, A., Binici, B., Canbay, C., Erberik, A., Askan, A., Caner, A., Sarıtaş, A., Aldemir, A., **Demirel, İ.O.**, Erdil, B., Ay, Ö., Özçelik, R., Akansel, V.H., Kale, Ö., Okuyucu, D. (2011), “23 Ekim 2011 Mw 7.2 Van Depremi Sismik Ve Yapısal Hasara İlişkin Saha Gözlemleri”, Rapor No: METU/EERC 2011-04, Deprem Mühendisliği Araştırma Merkezi, Orta Doğu Teknik Üniversitesi.
3. Binici, B., Canbay, C., Özcebe, G., Yakut, A., Aldemir, A., **Demirel, İ.O.**, Erdil, B., Kale, Ö. (2012), “9 Kasım 2011 Mw 5.6 Van - Edremit

Depremi Sismik ve Yapısal Hasara İlişkin Gözlemler”, Rapor No: METU-EERC / İMO 2012-01, Deprem Mühendisliği Araştırma Merkezi, Orta Doğu Teknik Üniversitesi.

4. Ay, Ö., Binici,B., Canbay,C., Yakut, A., **Demirel, İ.O.**, Aktaş., S.S., Aydın., B.B., Türksönmez., B., Çelik., O.C., Caner, A. (2020), “30 Ekim 2020 Mw 6.6 Sisam Adası (İzmir-Seferihisar Açıkları) Depremi Sismik ve Yapısal Hasara İlişkin Saha Gözlemleri”, Rapor No: ODTÜ / DMAM 2020-03, Deprem Mühendisliği Araştırma Merkezi, Orta Doğu Teknik Üniversitesi.
5. Ajobiewe, T., Akbaş, B., Akdede, N., Akın, M., ..., **Demirel, İ.O.**, ... , Yeşil, S.T., Yılmaz, S., Yılmaz, S. (2023), “6 Şubat 2023 Kahramanmaraş-Pazarcık Mw=7.7 ve Elbistan Mw=7.6 Depremleri Ön Değerlendirme Raporu”, Rapor No: ODTÜ / DMAM 2023-01, Deprem Mühendisliği Araştırma Merkezi, Orta Doğu Teknik Üniversitesi.

PARTICIPATED RESEARCH PROJECTS

1. IntenC “Empirical and Analytical Assessment of Masonry Structures under Seismic Action”, International Bureau of the BMBF, 2013-2014.
2. CONCERT-Japan “Performance of Infill Walls and Improving Their Performance for Earthquake Resilience”, Japan Science and Technology Council, 2013-2015.
3. INSYSME-EU “Innovative Systems for the Earthquake Resistant Masonry Enclosures in RC Buildings”, European Commission grant FP7-SME-2013-2-GA606229, 2013-2016.

TEACHING EXPERIENCE

2017 - 2023	Bilkent University (Instructor) Department of Architecture ARCH 231 - Statics and Strength of Materials ARCH 331 - Structural Design I ARCH 332 - Structural Design II
2007 - 2017	Middle East Technical University (TA) Civil Engineering Department CE224 - Mechanics of Materials CE383 - Structural Analysis CE529 - Structural Dynamics